COMPARING THE RADIOLOGICAL ANATOMY, ELECTROPHYSIOLOGY, AND BEHAVIORAL ROLES OF THE PEDUNCULOPONTINE AND SUBTHALAMIC NUCLEI IN THE NORMAL AND PARKINSONIAN BRAIN

Bhooma R. Aravamuthan
Magdalen College
University of Oxford

Dissertation submitted for the degree of
Doctor of Philosophy
Trinity 2008

Department of Physiology, Anatomy, and Genetics
Sherrington Building, Parks Road
Oxford OX1 3PT, UK

Neurophysiological Pharmacology Section
National Institute of Neurological Disorders and Stroke
Building 35, Room 1C 411
Bethesda, MD 20892-3702, USA

This thesis is dedicated to my inspirations:

My uncle,
Dr. AKS Gopalan

And my parents,
Dr. Raja and Lakshmi Aravamuthan

COMPARING THE RADIOLOGICAL ANATOMY, ELECTROPHYSIOLOGY, AND BEHAVIORAL ROLES OF THE PEDUNCULOPONTINE AND SUBTHALAMIC NUCLEI IN THE NORMAL AND PARKINSONIAN BRAIN

Bhooma Aravamuthan, Magdalen College

Dissertation submitted for the degree of Doctor of Philosophy, Trinity 2008

Deep brain stimulation (DBS) of the subthalamic nucleus (STN) and DBS of the pedunculopontine nucleus (PPN) have been shown to be effective surgical therapies for Parkinson's disease (PD). To better understand the PPN and STN as DBS targets for PD, this research compares the anatomy, electrophysiology, and motor control roles of these nuclei. PPN and STN connections were examined *in vivo* in human subjects and in the non-human primate using probabilistic diffusion tractography. Both the PPN and STN were connected with each other and with the motor cortex (M1) and basal ganglia. After studying these anatomical connections in primates, their functional significance was further explored in an anesthetized rat model of PD. Examination of the electrophysiological relationship between the PPN and basal ganglia in the presence of slow cortical oscillatory activity suggested that excitatory input from the STN may normally modulate PPN spike timing but that inhibitory oscillatory input from the basal ganglia output nuclei has a greater effect on PPN spike timing in the parkinsonian brain. To examine transmission and modulation of oscillatory activity between these structures at higher frequencies, LFP activity was recorded from the PPN and STN in PD patients performing simple voluntary movements. Movement-related modulation of oscillatory activity predominantly occurred in the α (8-12 Hz) and low β (12-20 Hz) frequencies in the STN but in the high β (20-35 Hz) frequencies in the PPN, supporting observations from rodent studies suggesting that oscillatory activity is not directly transmitted from the STN to the PPN in PD. Finally, to better understand the roles of the STN and PPN in large-scale movement, the effects of STN and PPN DBS on gait abnormalities in PD patients were studied. DBS of the STN appeared to improve gait by optimising executive gait control while DBS of the PPN appeared to restore autonomic gait control. These results have several implications for DBS patient selection, surgical targeting, and for understanding the mechanisms underlying DBS efficacy.

I. ACKNOWLEDGEMENTS

Prof. Tipu Aziz, Dr. Debbi Bergstrom, Prof. John Stein, and Dr. Judie Walters were amazing supervisors and I owe them much more than this thesis. I cannot thank them enough.

Dr. Heidi Johansen-Berg, Dr. Karla Miller, Jennifer McNab, and Dr. Natalie Voets of the Oxford FMRIB Centre patiently taught me the principles of diffusion tensor imaging and helped me focus my thoughts and analyses from the fanciful to the practical.

Dr. Louise Parr-Brownlie was my first line of defense and a clutch troubleshooter during the electrophysiological recordings in anesthetized rats. Robin (P.S. Buttercup) French and Joe Taylor helped do several of the dopamine cell lesioning procedures in the rats and also aided in data collection and analysis. I also owe P.S. Buttercup and Joe thanks for entertaining me in lab.

Dr. Shouyan Wang was a great teacher and helped me constructively channel pent-up frustration on countless occasions. The local field potential recordings from the STN and PPN in Parkinson's disease patients and the analyses of these recordings were all done under his supervision. Dr. Xuguang Liu was instrumental in helping interpret these results and in pushing us to publish the findings.

Dr. Julie Stebbins and Mr. Tim Theologis were generous with their time and resources. They offered me unlimited access to a state-of-the-art gait lab and to their wide range of expertise in gait pathology. Special thanks to Julie for also giving me unlimited access to the lab stash of tea, coffee, and digestives.

Mary Denyer and the George C. Marshall Commission introduced me to this international adventure. Dr. Michael Lenardo and the NIH-OxBridge Program helped shape it into a salient DPhil. Their praise and encouragement were great motivators.

Finally, I thank my parents for being my most trusted advisors, my brother for providing a listening ear when it counted the most, my grandparents for being my most ardent fans, and my fiancée for his unyielding support. I am lucky to have them in my life.

II. ABBREVIATIONS

6-OHDA	6-hydroxydopamine
ANOVA	Analysis of variance
cm	Centimeters
CT	Computed tomography (scan)
D1	D1 striatal dopamine receptor
D2	D2 striatal dopamine receptor
DCN	Deep cerebellar nuclei
DBS	Deep brain stimulation
dPMC	Dorsal premotor cortex
DS/SS	Ratio of double support duration to single support duration during a gait cycle
DTI	Diffusion tensor imaging
EC	Externally-cued
EPN	Entopeduncular nucleus
ERD	Event-related desynchronization
ERP	Event-related potential
ERS	Event-related synchronization
FDT	FMRIB's diffusion toolbox
FLIRT	FMRIB's linear registration tool
g	Gram(s)
GABA	γ-aminobutyric acid
GP	Globus pallidus
GPe	External segment of the globus pallidus
GPi	Internal segment of the globus pallidus
GPi/SNpr	GPi and/or SNpr, basal ganglia output nuclei
Hz	Hertz
IG	Internally-generated
i.p.	Intraperitoneal
i.v.	Intravenous
kg	Kilogram
L-DOPA	Levodopa
LFP	Local field potential
LL	Lateral lemniscus
M	Molar
M1	Primate primary motor cortex
M1-fore-L	Lower forelimb region of the primate primary motor cortex
M1-fore-U	Upper forelimb region of the primate primary motor cortex
M1-hind	Hindlimb region of the primate primary motor cortex
M1-orof	Orofacial region of the primate primary motor cortex
M1-trunk	Trunk region of the primate primary motor cortex
MCer	Mid-cerebellum (declive and folium)
mg	Milligram
min	Minute(s)

MiTg	Microcellular tegmental nucleus
mL	Milliliter(s)
mm	Millimeter(s)
mM	Millimolar
MNI	Montreal Neurological Institute
MPTP	1-methyl 4-phenyl 1,2,3,6-tetrahydropyridine
MRI	Magnetic resonance image/imaging
msec	Milliseconds
MSN	Medium spiny neuron
mT	Millitesla(s)
mV	Millivolts
n	Number of subjects
NMDA	N-methyl-D-aspartic acid
p	Probability
PAG	Periaqueductal gray
PD	Parkinson's disease
PMC	Premotor cortex
PPN	Pedunculopontine nucleus
PPNc	Pedunculopontine nucleus, pars compacta
PPNd	Pedunculopontine nucleus, pars dissipata
RGB	Red-green-blue (image)
RMS	Root mean square
PPN DBS OFF	Parkinson's disease patient with PPN DBS implants, off stimulation
RN	Red nucleus
rs	Rubrospinal tract
SCD	Superior cerebellar decussation
SD	Standard deviation
SE	Standard error
sec	Seconds(s)
SMA	Supplementary motor area
SN	Substantia nigra
SNpc	Substantia nigra pars compacta
SNpr	Substantia nigra pars reticulata
STN	Subthalamic nucleus
STN DBS OFF	Parkinson's disease patient with STN DBS implants, off stimulation
STWA	Spike-triggered waveform average
T	Tesla(s)
Thal	Thalamus
vPMC	Ventral premotor cortex
xscp	Decussation of the superior cerebellar peduncle
µm	Micrometer(s)
µL	Microliter(s)
µV	Microvolt(s)

III. PUBLICATIONS AND CITABLE ABSTRACTS

PEER-REVIEWED PUBLISHED MANUSCRIPTS:

Aravamuthan BR, Muthusamy KA, Stein JF, Aziz TZ, Johansen-Berg H (2007) Topography of cortical and sub-cortical connections of the human pedunculopontine and subthalamic nuclei. NeuroImage 37:694-705.
(includes results reported in Section 2)

Muthusamy KA, **Aravamuthan BR**, Kringelbach ML, Jenkinson N, Voets NL, Johansen-Berg H, Stein JF, Aziz TZ (2007) Connectivity of the human pedunculopontine nucleus region (PPN) and diffusion tensor imaging in surgical targeting. J Neurosurg 107:814-820.

Aravamuthan BR, McNab JA, Miller KL, Rushworth M, Jenkinson N, Stein JF, Aziz TZ (2008) Organisation of cortical and sub-cortical connections within the primate (*Macaca mulatta*) pedunculopontine nucleus determined using probabilistic diffusion tractography. J Clin Neurosci.
(in press, includes results reported in Section 2)

Aravamuthan BR, Bergstrom DA, French RA, Taylor JJ, Parr-Brownlie LC, Walters JR (2008) The relationship between neuronal activity in the pedunculopontine nucleus and motor cortex is altered in a rodent model of Parkinson's disease.
(in press, includes results reported in Section 3)

MANUSCRIPTS SUBMITTED FOR PEER-REVIEW:

Aravamuthan BR, Wang S, Green A, Stein JF, Aziz TZ, Liu X (2008) The human subthalamic nucleus is differentially involved in controlling both internally generated and visually cued movements in Parkinson's disease.
(includes results reported in Section 4)

SELECTED CITABLE CONFERENCE ABSTRACTS:

Aravamuthan BR, Muthusamy K, Johansen-Berg H, Voets N, Liu X, Stein JF, Aziz TZ (2006) Human pedunculopontine nucleus connections traced using probabilistic diffusion tractography. Society for Neuroscience. Neuroscience Meeting Planner: 882.14/AA19.
(includes results reported in Section 2)

Aravamuthan BR, Wang S, Green A, Stein JF, Aziz TZ, Liu X (2006) The human subthalamic nucleus is differentially involved in controlling both internally generated and visually cued movements in Parkinson's disease. Movement Disorders 21(S15): P1353.
(includes results reported in Section 4)

Aravamuthan BR, Bergstrom DA, French RA, Taylor JJ, Parr-Brownlie LC, Walters JR (2007) The relationship between neuronal activity in the pedunculopontine nucleus and motor cortex is altered in a rodent model of Parkinson's disease. Society for Neuroscience. Neuroscience Meeting Planner: 516.24/UU14.
(includes results reported in Section 3)

IV. TABLE OF CONTENTS

1. Effects of Parkinson's disease on the basal ganglia 1

1.1 Anatomy of the basal ganglia 2

1.1.1 The striatum 4

1.1.2. The substantia nigra pars reticulata (SNpr) 5

1.1.3. The globus pallidus (GP) 6

1.1.4. The subthalamic nucleus (STN) 7

1.1.5. The pedunculopontine nucleus (PPN) 10

1.2 Rate-based and oscillations models of basal ganglia function 15

1.3 Propagation of network oscillations in the basal ganglia 19

1.4 Deep brain stimulation of the STN in Parkinson's disease 22

1.5 Deep brain stimulation of the PPN in Parkinson's disease 23

1.6 Research questions and experiment summaries 24

2. Anatomical comparison of the pedunculopontine and subthalamic nuclei 27

2.1 Anatomy of the human PPN and STN 27

2.1.1 Introduction and rationale 27

2.1.2 Methods 30

2.1.2.1 Subjects and image acquisition 30

2.1.2.2 Image pre-processing 30

2.1.2.3 Determining regions strongly inter-connected to the PPN or STN with probabilistic tractography 31

2.1.2.4 Creating anatomical masks of inter-connected regions 33

2.1.2.5 Determining of the topography of PPN and STN connections 35

2.1.2.6 Determining of the paths of connections between the PPN, STN, and other inter-connected brain regions 36

2.1.3 Results 38

2.1.3.1 Connections and topography of the PPN 38

2.1.3.2 Connections and topography of the STN 43

2.1.4 Discussion 50

2.1.4.1 Methodological considerations 50

2.1.4.2 Human PPN and STN connections largely match connections previously shown in non-human primates 51

2.1.4.3 Human STN topography matches topography previously shown in animals 53

2.1.4.4 Demonstration of the existence of PPN topography in humans 54

2.1.4.5 Functional implications in humans 55

2.1.4.6 Concluding remarks 56

2.2 Anatomy of the PPN and STN in a normal primate (*Macaca mulatta*) brain 57

2.2.1 Introduction and rationale 57

2.2.2 Methods 60

2.2.2.1 Brain extraction and fixation 60

2.2.2.2 Image acquisition 60
2.2.2.3 Image pre-processing and determining regions strongly inter-connected to the PPN 61
2.2.2.4 Creating anatomical masks of inter-connected regions 63
2.2.2.5 Determining the organization of PPN connections 64
2.2.3 Results 68
2.2.3.1 Connections of the PPN 68
2.2.3.2 Organization of PPN connections 68
2.2.4 Discussion 69
2.2.4.1 Monkey PPN anatomy determined using diffusion tractography compared to monkey PPN anatomy described previously 70
2.2.4.2 Monkey PPN anatomy compared to human PPN anatomy using diffusion tractography 72
2.2.4.3 Usefulness for the study of animal neuroanatomy 74
2.2.4.4 Concluding remarks 75
3. Differences in the electrophysiological relationship between the PPN and basal ganglia in the normal and parkinsonian brain 76
3.1 Introduction and rationale 76
3.2 Methods 79
3.2.1 Nigrostriatal lesions and behavioral testing 79
3.2.2 Surgical and recording procedures 80
3.2.3 Data analysis 83
3.3 Results 85
3.3.1 PPN and M1 spike and LFP relationships in the urethane-anesthetized rat 85
3.3.1.1 Effect of dopamine cell lesion on PPN and M1 LFP activity 87
3.3.1.2 Effect of dopamine cell lesion on PPN neuronal activity 88
3.3.1.3 Relationship between PPN spiking and LFP activity in the PPN and M1 90
3.3.2 PPN and M1 spike and LFP relationships in the ketamine-anesthetized rat 95
3.4 Discussion 98
3.4.1 Increased oscillatory PPN activity after dopamine cell lesion in the urethane-anesthetized rat 99
3.4.2 Effect of basal ganglia output on PPN spike timing following dopamine cell lesion in the urethane-anesthetized rat 103
3.4.3 Causes of coherent decreases in M1 and PPN LFP power in the urethane-anesthetized rat 105
3.4.4 Comparison of the neurological effects of urethane and ketamine 107
3.4.5 Relevance to faster oscillations in Parkinson's disease patients 109
4. Modulation of STN and PPN activity during simple voluntary movement 110
4.1 Modulation of STN LFP activity during cued and self-paced voluntary movements 110
4.1.1 Introduction and rationale 110
4.1.2 Methods 112
4.1.2.1 Patients, electrode implantation, and electrode placement confirmation 112

4.1.2.2 Visuomotor paradigms 115
4.1.2.3 LFP and EMG recordings 118
4.1.2.4 Signal processing and analysis 119
4.1.2.5 Statistical analyses 123
4.1.3 Results 127
4.1.3.1 Similarities in STN LFP modulation between EC and IG tasks 129
4.1.3.2 Differences in STN LFP modulation between EC and IG tasks 129
4.1.4 Discussion 132
4.1.4.1 Modulation of STN activity related to motor preparation, selection, and execution 132
4.1.4.2 Greater bilateral STN involvement during externally-cued movement 134
4.1.4.3 Role of the STN in facilitation of movement by an external cue in Parkinson's disease 135
4.1.4.4 STN LFP modulation specific to Parkinson's disease patients 136
4.1.4.5 Concluding remarks 137
4.2 Modulation of PPN LFP activity during cued and self-paced rapid voluntary movements 137
4.2.1 Introduction and rationale 137
4.2.2 Methods 139
4.2.3 Results 141
4.2.3.1 Similarities in PPN LFP modulation between EC and IG tasks 142
4.2.3.2 Differences in PPN LFP modulation between EC and IG tasks 147
4.2.4 Discussion 148
4.2.4.1 High β band modulation in the PPN is related to motor preparation and cue processing 148
4.2.4.2 Role of the PPN in facilitation of movement by an external cue in Parkinson's disease 149
4.2.4.3 PPN LFP modulation specific to Parkinson's disease patients 149
4.2.4.4 Differences between LFP modulation in the PPN and STN 151
4.2.4.5 Concluding remarks 152
5. Effects of STN and PPN stimulation on gait 154
5.1 Introduction and rationale 154
5.2 Methods 158
5.2.1 Subjects 158
5.2.2 Gait task design 158
5.2.3 Data capture and processing 160
5.3 Results 163
5.3.1 Effect of turning on gait performance of healthy control subjects 163
5.3.2 Effects of STN stimulation on gait 165
5.3.2.1 Effects of STN stimulation on gait performance and standing balance 165
5.3.2.2 Effects of STN stimulation on thoracic and pelvic angles during walking 167
5.3.2.3 Effects of STN stimulation on thoracic and pelvic angles during turning 167
5.3.3 Effects of PPN stimulation on gait 169

5.3.3.1 Effects of PPN stimulation on gait performance and standing balance 169
5.3.3.2 Effects of PPN stimulation on thoracic and pelvic angles during walking 171
5.3.3.3 Effects of PPN stimulation on thoracic and pelvic angles during turning 172
5.4 Discussion 175
5.4.1 Differences between PPN and STN DBS 176
5.4.2 Concluding remarks 177
6. Implications for DBS in Parkinson's disease 179
6.1 Summary of results 179
6.1.1 Comparison of PPN and STN anatomy 179
6.1.2 Electrophysiological relationship between the PPN and basal ganglia 181
6.1.3 Modulation of STN and PPN oscillatory activity during simple voluntary movement 182
6.1.4 Effects of STN and PPN DBS on gait 186
6.2 Choosing Parkinson's disease patient candidates for STN and PPN DBS 187
6.3 Optimally targeting the STN and PPN for DBS 189
6.4 Insights into the mechanisms underlying STN and PPN DBS efficacy 190
6.5 The efficacy of dual STN and PPN DBS for Parkinson's disease: Insights and future research 193
7. References 196

1. EFFECTS OF PARKINSON'S DISEASE ON THE BASAL GANGLIA

Parkinson's disease (PD) is the second most common neurodegenerative disorder. Associated with three main symptoms—slowness of movement (bradykinesia), inability to initiate movement (akinesia), and a characteristic 4-5 Hz resting tremor—the effects of PD on mobility are debilitating (Parkinson, 1817).

The primary pathology associated with PD is the loss of dopaminergic neurons in the substantia nigra pars compacta (SNpc). The SNpc is a core part of the basal ganglia, a collection of sub-cortical nuclei important for motor control. Treatments for PD have focused on remedying various pharmacological or electrophysiological imbalances in the basal ganglia associated with SNpc degeneration. One of these therapies is deep brain stimulation (DBS) which involves electrical stimulation of a basal ganglia nucleus thought to fire at an improper, or antikinetic, frequency in the parkinsonian brain. In order to understand the rationale behind the use of various PD therapies including DBS, the functional anatomy of the basal ganglia as well as the effects of PD and DBS on the activity of basal ganglia nuclei are summarized in this section.

1.1 Anatomy of the basal ganglia

The basal ganglia serve as a modulatory conduit for information within functional thalamo-cortical loops that govern a wide range of functions (Parent and Hazrati, 1995a). The striatum and subthalamic nucleus (STN) receive input to the basal ganglia while the internal segment of the globus pallidus (GPi) and the substantia nigra pars reticulata (SNpr) serve as the major output nuclei. Dopaminergic input to the striatum (like that from the SNpc) modulates cortical input to the striatum and facilitates transmission of cortical information through the basal ganglia. Information from the cortex can pass from the striatum to the output nuclei directly or indirectly via other basal ganglia nuclei (the external segment of the globus pallidus (GPe) and the STN). The basal ganglia output nuclei (GPi and SNpr) then send this information to the thalamus where it modulates activity in thalamo-cortical loops (Fig. 1.1A) (Mink, 1996; Wichmann and DeLong, 2003; Hamani *et al.*, 2004; Tisch *et al.*, 2004; DeLong and Wichmann, 2007). Though these thalamo-cortical loops (generally associated with sensorimotor, associative, or limbic functions) were long thought to be maintained independently and in parallel (Alexander *et al.*, 1986; Albin *et al.*, 1989; Alexander and Crutcher, 1990), there is considerable anatomical evidence suggesting integration and convergence of information across these loops in the basal ganglia (Hedreen and DeLong, 1991; Percheron and Filion, 1991; Lynd-Balta and Haber, 1994; Parent *et al.*, 2001).

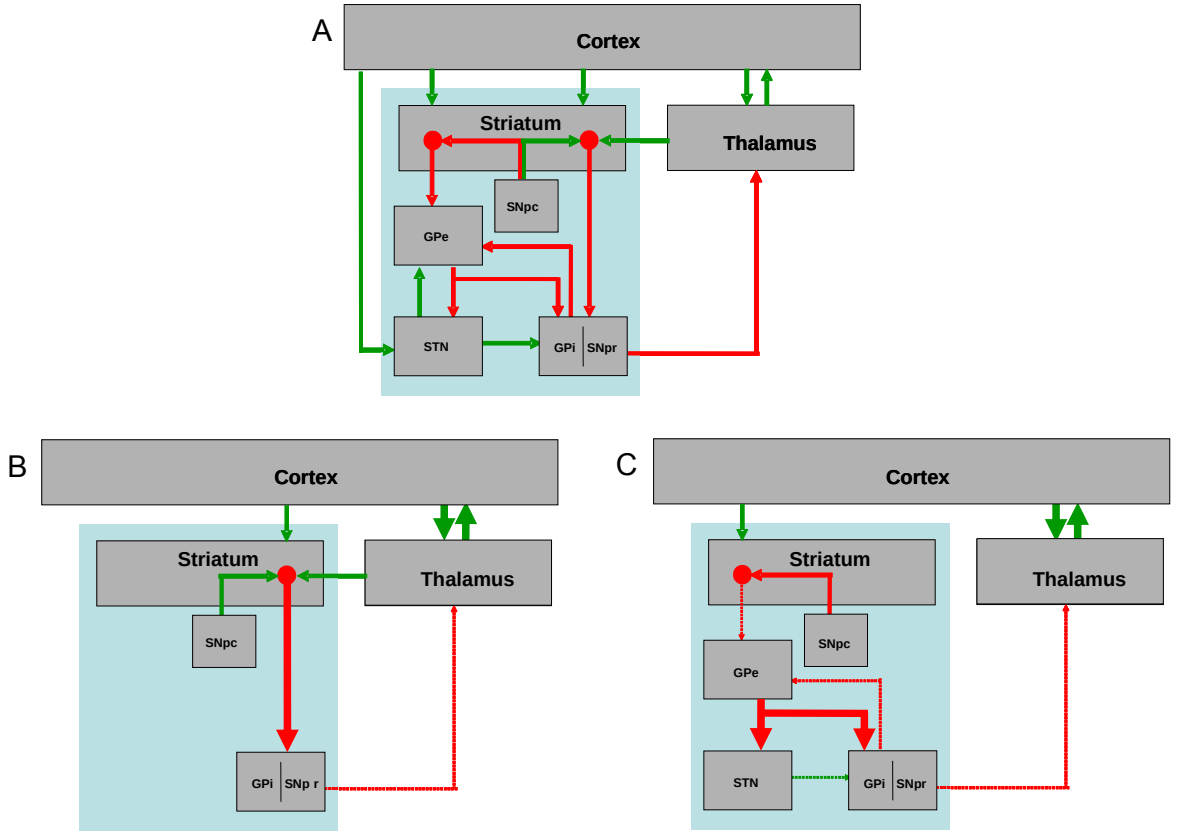

Figure 1.1. Rate-based model of basal ganglia function (adapted from Wichmann and DeLong, 2006). A) Major connections of the basal ganglia-thalamo-cortical circuit. B) Direct pathway in the rat-based model of basal ganglia function. C) Indirect pathway in the rate-based model of basal ganglia function. Arrows between structures indicate direct connections (green: excitatory, red: inhibitory). In (B) and (C), thicker arrows indicate increased activity while thinner broken arrows indicate decreased activity in response to dopamine release in the striatum.

1.1.1 The striatum

The striatum receives two major types of input: excitatory glutamatergic input from various cortical areas (Gerfen, 1984, 1989) and modulatory dopaminergic input from the SNpc and ventral tegmental area (Kaiya and Namba, 1981; Bouyer *et al.*, 1984; Hattori *et al.*, 1991; Karle *et al.*, 1994; Csillag, 1999; Saka *et al.*, 2002), a cluster of dopaminergic neurons that helps govern incentive and reward behavior. The medium spiny neurons (MSNs) in the striatum receive the majority of these cortical and dopaminergic inputs as they comprise 95% of all striatal cells. MSNs arborize extensively within the striatum and also connect to cortical and dopaminergic efferents (Gimenez-Amaya and Graybiel, 1991; Flaherty and Graybiel, 1993). The remaining 5% of striatal cells, striatal interneurons, receive the majority of glutamatergic afferents from the centromedian/parafascicular complex of the thalamus (Apicella *et al.*, 1991, 1996, 1997; Aosaki *et al.*, 1995) in addition to receiving some cortical and dopaminergic input. These interneurons are thus capable of serving complex modulatory roles within the striatum.

Cortical projections from sensorimotor areas (primary motor cortex (M1), somatosensory cortex, premotor cortex (PMC), and supplementary motor area (SMA)), associative areas (frontal, temporal, parietal, preoccipital, and parahippocampal cortices), and limbic areas (limbic cortex, paralimbic cortex, amygdala, and hippocampus) are, to some extent, anatomically segregated in the striatum (Gerfen, 1984, 1989; Flaherty and Graybiel, 1991). Homunclulus-like representations can be found throughout the striatum loosely related to the somatotopy in the corresponding connected cortical areas. The majority of sensorimotor cortical input goes to the putamen of the striatum, though a small

portion of the caudate also receives this input. Most associative cortical input goes to the caudate and most limbic cortical input goes to the ventral caudate and ventral putamen (Somogyi *et al.*, 1981; Dube *et al.*, 1988; Lapper and Bolam, 1992; Smith *et al.*, 1994a). Dopaminergic synapses at the base of the dendritic spine of MSNs (Cheramy *et al.*, 1981; ; Gale and Casu, 1981; Kaiya and Namba, 1981Bouyer *et al.*, 1984; Hattori *et al.*, 1991; Amalric and Koob, 1993; Karle *et al.*, 1994; Saka *et al.*, 2002) are capable of modulating this cortical input to the striatum (Garcia-Munoz *et al.*, 1991; Flores-Hernandez *et al.*, 1997; Calabresi *et al.*, 1999; Plotkin *et al.*, 2005).

In addition to receiving most input to the striatum, MSNs also serve as inhibitory GABAergic striatal efferents and are the primary striatal output neurons (Bolam, 1984; Semba *et al.*, 1987; Gerfen, 1988; Bennett and Bolam, 1994; White *et al.*, 1994). Striatal output goes to the GPe, GPi, (Kemp and Powell, 1971; Fox and Rafols, 1975, 1976; Kim, 1978) and SNpr (Fox and Rafols, 1976; Kim, 1978, 1979; Kitai, 1981; Gerfen, 1985; Amalric and Koob, 1993). A large portion of sensorimotor and associative cortical input that was segregated at the striatal level converges at the level of the SNpr (Somogyi *et al.*, 1981; Gerfen, 1985; Amalric and Koob, 1993) and globus pallidus (GP) (Kemp and Powell, 1971; Fox and Rafols, 1975, 1976; Van der Kooy and Carter, 1981).

1.1.2 The substantia nigra pars reticulata (SNpr)

The SNpr (along with the GPi) serves as a major inhibitory GABAergic output center for the basal ganglia. Input to this midbrain nucleus comes as inhibitory GABAergic efferents from the striatum (Fox and Rafols, 1976; Kim,

1978, 1979; Kitai, 1981; Somogyi *et al.*, 1981; Gerfen, 1984, 1985; Hedreen and DeLong, 1991; Deniau *et al.*, 1996) and the GPe (Kemp and Powell, 1971; Amalric and Koob, 1993; Parent and Hazrati, 1995b) and as excitatory glutamatergic efferents from the STN (Carpenter *et al.*, 1981; Gerfen *et al.*, 1982). The shape and extensive arborization of SNpr dendrites allows for synaptic integration of inputs coming from different structures (Cheramy *et al.*, 1981; Gerfen *et al.*, 1982; Sanderson *et al.*, 1986; Hedreen and DeLong, 1991; Whone *et al.*, 2003). The SNpr sends inhibitory GABAergic projections primarily to the ventroanterior and ventrolateral thalamus (Herkenham, 1979; Sakai and Smith, 1992), but also sends a strong projection to the pedunculopontine nucleus (PPN) (Scarnati *et al.*, 1984, 1986; Spann and Grofova, 1991).

1.1.3 The globus pallidus (GP)

Both the GPe and GPi receive inhibitory GABAergic input from the striatum (both the caudate and putamen), excitatory glutamatergic input from the STN, and reciprocal inhibitory GABAergic input from each other (Chang *et al.*, 1981; Hazrati *et al.*, 1990; Smith *et al.*, 1994b; Shink *et al.*, 1996). Input from the GPe, STN, and striatum synapse on the same cells in the GPi (Chang *et al.*, 1981; Hazrati *et al.*, 1990; Smith *et al.*, 1994b; Shink *et al.*, 1996) with striatal connections making up 70-80% of all synapses (Chang *et al.*, 1981). The primary functional difference between the GPe and GPi is in their output profile (Hazrati and Parent, 1992a). The GPe sends the majority of its inhibitory GABAergic output to the basal ganglia output nuclei (GPi and SNpr) and to the STN (Kim *et al.*, 1976; Parent and De Bellefeuille, 1982; Hazrati and Parent, 1991). The GPi, on the other hand, acts as a basal ganglia output nucleus and

sends the majority of its inhibitory GABAergic efferents to the ventroanterior, ventrolateral, and centromedian / parafascicular complex of the thalamus (Kim *et al.*, 1976; Parent and De Bellefeuille, 1982; Hazrati and Parent, 1991). The GPi sends a strong inhibitory projection to the PPN as well (Rye *et al.*, 1987; Scarnati *et al.*, 1988; Semba and Fibiger, 1992; Shink *et al.*, 1997). It is also interesting to note that the rodent entopeduncular nucleus (EPN) is widely accepted as a homologue of the primate GPi. Both the EPN and GPi receive projections from the striatum, STN, and GPe and send projections to the thalamus and PPN (Joel and Weiner, 2000). These inputs and outputs have similar topographical organization in the EPN and GPi as well (Joel and Weiner, 2000). However, one interesting difference between the rodent EPN and the primate GPi is the possibly stronger functional relationship between the EPN and the control of head and neck movements in rats (Takada *et al.*, 1994). This may underlie basic differences in the roles of the rodent and primate basal ganglia in the control of quadrupedal or bipedal gait.

1.1.4 The subthalamic nucleus (STN)

The STN has come to the forefront in PD research as it has become the most common surgical target for PD therapy. Noting that firing rate and oscillatory activity in the STN are greater in the parkinsonian brain than they are in the normal brain (Hollerman and Grace, 1992; Hassani *et al.*, 1996; Magill *et al.*, 2000; Vila *et al.*, 2000; Ni *et al.*, 2001; Walters *et al.*, 2007), STN lesions (Andy *et al.*, 1963; Bergman *et al.*, 1990; Guridi *et al.*, 1993) and, more recently, high frequency DBS of the STN have been effectively used as therapies for PD (Krack *et al.*, 1997a, 1997b, 2003; Kumar *et al.*, 1998;

Limousin *et al.*, 1998; Burchiel *et al.*, 1999; Stolze *et al.*, 2001; Kleiner-Fisman *et al.*, 2003; Hamel *et al.*, 2003; Rodriguez-Oroz *et al.*, 2005). Due to the behavioral and electrophysiological information that can be garnered by stimulating or recording from DBS electrodes, the STN has become a window into the dysfunctional effects of PD on neuronal activity in the human brain.

A large portion of the STN relates to or is affected by movement. It is estimated that 30-50% of all STN neurons becoming activated with flexion of contralateral joints (DeLong *et al.*, 1984, 1985; Bergman *et al.*, 1994; Wichmann *et al.*, 1994a). Excitation and inhibition of the STN also have distinct effects on motor behaviour. Sufficient pharmacological excitation of the STN can elicit abnormal movements or postural asymmetry (Dybdal and Gale, 2000; Perier *et al.*, 2000, 2002). On the other hand, lesions of the STN can induce ballism, movements characterized by flailing and forceful movements of the limbs (Hammond *et al.*, 1979; Crossman *et al.*, 1980, 1984; Beurrier *et al.*, 1997).

Distinct topography is evident in the STN as brain regions primarily associated with sensorimotor, associative, or limbic functions are segregated. Most of the dorsal STN is connected to motor brain areas, most of the ventral STN is connected to associative brain areas, and the medial tip of the STN is connected to both limbic and associative brain areas (DeLong *et al.*, 1984, 1985; Bergman *et al.*, 1994; Wichmann *et al.*, 1994a; Pahapill and Lozano, 2000; Hamani *et al.*, 2004).

The STN receives two major sources of input: excitatory glutamatergic projections from several cortical areas and inhibitory GABAergic projections from the GPe. Most cortical afferents to the STN come from sensorimotor

regions, namely from M1 (primarily layer V neurons), SMA, pre-SMA, and the dorsal and ventral PMC (dPMC and vPMC) (Carpenter *et al.*, 1981; Jurgens, 1984; Nambu *et al.*, 1996, 1997, 2000, 2002; Inase *et al.*, 1999). Motor and limbic portions of the GPe send projections to segregated areas of the STN, though considerable overlap exists between these projections suggesting that the STN could serve as yet another site of information convergence in the basal ganglia (Kim *et al.*, 1976; Carpenter *et al.*, 1981; Parent and De Bellefeuille, 1982; DeLong *et al.*, 1985; Parent and Hazrati, 1995b). Other sources of input to the STN include glutamatergic efferents from the centromedian/parafascicular complex of the thalamus (Sugimoto *et al.*, 1983; Sugimoto and Hattori, 1983; Sadikot *et al.*, 1992a, 1992b), and both cholinergic and glutamatergic input from the PPN (Edley and Graybiel, 1983; Hammond *et al.*, 1983; Woolf and Butcher, 1986; Lavoie and Parent, 1994c).

The STN is the only basal ganglia nucleus that provides primarily excitatory glutamatergic efferent activity. The STN sends most of this output to the GPe and GPi and these STN efferents extensively arborize throughout both nuclei (Smith *et al.*, 1990; Hazrati and Parent, 1992a; Fujimoto and Kita, 1993; Parent and Hazrati, 1995b). The STN also innervates the other basal ganglia output nucleus, the SNpr, and sends excitatory projections to the SNpc as well (Carpenter *et al.*, 1981; Kita and Kitai, 1987; Smith *et al.*, 1990; Smith and Grace, 1992; Parent and Hazrati, 1995b; Joel and Weiner, 1997). STN projections to the striatum have been described (Kita and Kitai, 1987; Smith *et al.*, 1990), though they are scant and are not as extensively arborized as the projections to the GP and SNpr. Though the role of the STN in motor circuits has been the focus of PD research, the STN is also intimately involved in the

modulation of limbic thalamo-cortical loops via projections to the ventral pallidum, a nucleus in the basal forebrain that is considered to be the major limbic circuit output region (Inglis and Winn, 1995; Turner *et al.*, 2001; Temel *et al.*, 2005). These limbic connections of the STN have garnered increased interest after reports that DBS of the STN can be concomitant with emotional disturbances (Saint-Cyr *et al.*, 2000; Takeshita *et al.*, 2005; Castelli *et al.*, 2006; Temel *et al.*, 2006; Berney *et al.*, 2007).

Other targets of STN output include the PPN (Jackson and Crossman, 1981b, 1983; Kita and Kitai, 1987; Steininger *et al.*, 1992; Parent and Hazrati, 1995b) which, when excited by STN input, is thought to facilitate the modulation of motor activity in the spinal cord (Brudzynski *et al.*, 1986; Rye *et al.*, 1987; Lee *et al.*, 2000; Pahapill and Lozano, 2000). This connection has also received more research attention (Sections 2.1, 3) since the PPN has been demonstrated to be an effective DBS target for PD (Plaha and Gill, 2005; Mazzone *et al.*, 2005; Stefani *et al.*, 2007).

1.1.5 The pedunculopontine nucleus (PPN)

The PPN plays a key role in regulating and relaying motor information from the basal ganglia to lower motor regions via the spinal cord (Grillner, 1981, 2008; Brudzynski *et al.*, 1986; Rye *et al.*, 1987; Lee *et al.*, 2000; Pahapill and Lozano, 2000). In addition to receiving input from the basal ganglia, the PPN also sends efferents to the thalamus, which has led some to consider the PPN as an auxiliary basal ganglia output nucleus (Mena-Segovia *et al.*, 2004). The PPN has been shown to be essential for gait initiation and maintenance (Masdeu *et al.*, 1994; Lee *et al.*, 2000; Pahapill and Lozano, 2000), and

lesioning of the PPN causes akinesia (Kojima *et al.*, 1997; Munro-Davies *et al.*, 1999; Matsumura and Kojima, 2001). Furthermore, the PPN has been linked to the pathogenesis of PD and other movement disorders since the PPN has been shown to degenerate in the late-stages of these diseases (Hirsch *et al.*, 1987). However, the role of PPN in movement and movement disorders is still unclear (Inglis and Winn, 1995; Winn, 2006).

The PPN is a neurochemically heterogenous nucleus located in the brainstem and is comprised of the pars compacta (PPNc) and pars dissipata (PPNd) regions. Cholinergic neurons predominate in the PPNc and also make up a large portion of the PPNd. Glutaminergic neurons are generally localized to the PPNd and are the second most abundant neuronal type in the PPN (Rye *et al.*, 1987; Spann and Grofova, 1992; Lavoie and Parent, 1994b). Several other neuronal sub-types, including dopaminergic, serotonergic, and GABAergic cells, can also be found in the PPN (Rye *et al.*, 1987; Spann and Grofova, 1992; Lavoie and Parent, 1994b).

The PPN can be further subdivided by examining the various electrophysiological properties of PPN neurons. There are three types of neurons in the PPN evident in *in vitro* slice recordings (Kang and Kitai, 1990; Takakusaki and Kitai, 1997). Type I neurons are activated via excitation or inhibition and fire in a bursting manner (10-20 spikes/sec during the burst). Type II neurons respond solely to excitatory stimuli and have a slow, tonic, and repetitive firing pattern (0.5-8 spikes/sec). Type II action potentials are followed by a long period of hyperpolarization. Finally Type III neurons exhibit both Type I and Type II firing patterns. Type I behavior predominates in the PPN, though

up to 25% of PPN neurons exhibit Type II behavior at any given time (Lee *et al.*, 2000; Pahapill and Lozano, 2000).

Information about the somatotopic organization of PPN connections is limited. Until recently (Section 2.1; Aravamuthan *et al.*, 2007), the organization of PPN connections within the nucleus has only been demonstrated for cerebral cortex connections in primates (Matsumura *et al.*, 2000) which showed that more dorsal regions of the primary motor cortex (M1) connected with more lateral areas of the PPN, while ventral regions connected predominantly with the medial PPN. This same relationship was found within sub-regions of M1. For example, dorsal portions of the M1 hindlimb and forelimb regions projected laterally into the PPN while ventral portions of these M1 sub-regions projected to the medial PPN. In animal studies, sub-cortical structures have not been shown to connect preferentially with a specific PPN region, though it has been shown that efferents from the GPi project throughout the entire PPN in the squirrel monkey (Shink *et al.*, 1997). Rodent PPN somatotopy has not been described.

Furthermore, the connections of the PPN differ between rodents and primates. The major inputs to the PPN are the GPi and the SNpr (Shink *et al.*, 1996, 1997) in non-human primates and the STN in rats (Spann and Grofova, 1991), though both the rodent and primate PPN receive input from all three basal ganglia structures. Pallidal outflow to the PPN is GABAergic and is preferentially targeted to the non-cholinergic neurons in the PPNd (Rye *et al.*, 1987; Scarnati *et al.*, 1988; Semba and Fibiger, 1992; Shink *et al.*, 1997). The SNpr also projects to non-cholinergic neurons in the PPNd (Scarnati *et al.*, 1984, 1986; Spann and Grofova, 1991), but it is unknown whether the SNpr

and GP project to the same neurons. The STN sends excitatory glutaminergic projections to the PPN (Jackson and Crossman, 1981b, 1983; Kita and Kitai, 1987; Steininger *et al.*, 1992; Parent and Hazrati, 1995b), but it is not known which cell group is targeted. The PPN also receives input from the deep cerebellar nuclei (DCN) (Hazrati and Parent, 1992b) in primates and from the cervical and lumbar regions of the spinal cord (Spann and Grofova, 1989) in rodents suggesting a role for the PPN as a sensory relay center for the basal ganglia (Fig. 1.2) (Lee *et al.*, 2000; Pahapill and Lozano, 2000; Mena-Segovia *et al.*, 2004). Although, input from the DCN to the PPN has not been observed in rodents and input from spinal cord regions to the PPN has not been observed in primates, these connections are also suspected to exist (Lee *et al.*, 2000; Matsumura *et al.*, 2000; Pahapill and Lozano, 2000). Finally, the PPN has also been shown to receive direct input from M1, the SMA, and the PMC in primates (Matsumura *et al.*, 2000), but these connections have not been demonstrated in rodents.

The efferent connections of the PPN with the basal ganglia are numerous and are more prominent than PPN projections to the spinal cord and lower motor centers in both rodents and primates (Lee *et al.*, 2000; Pahapill and Lozano, 2000). The major ouputs of the PPN are the SNpc and the STN in non-human primates (Lavoie and Parent, 1994a, 1994c) and the GPi (or entepeduncular nucleus) in rodents (Rye *et al.*, 1987; Scarnati *et al.*, 1988), though both the rodent and primate PPN project to all three structures (Scarnati *et al.*, 1984; Gould *et al.*, 1989; Spann and Grofova, 1992; Lavoie and Parent, 1994a, 1994c). Generally, stimulation of the PPN induces excitation of neurons in the STN and GPi and excitation of the dopaminergic neurons in the SNpc

(reviewed in Lee *et al.*, 2000; Pahapill and Lozano, 2000). Descending projections from the rodent and primate are mostly to the medullary reticular formation, a brainstem structure that sends bilateral projections to the spinal cord (Fig. 1.2) (Edley and Graybiel, 1983; Rye *et al.*, 1987; Semba and Fibiger, 1992; Inglis and Winn, 1995). Another major target of PPN outflow is the thalamus (Lavoie and Parent, 1994c), a projection which has, as aforementioned, lead some to consider the PPN as an auxiliary basal ganglia output nucleus (Mena Segovia *et al.*, 2005).

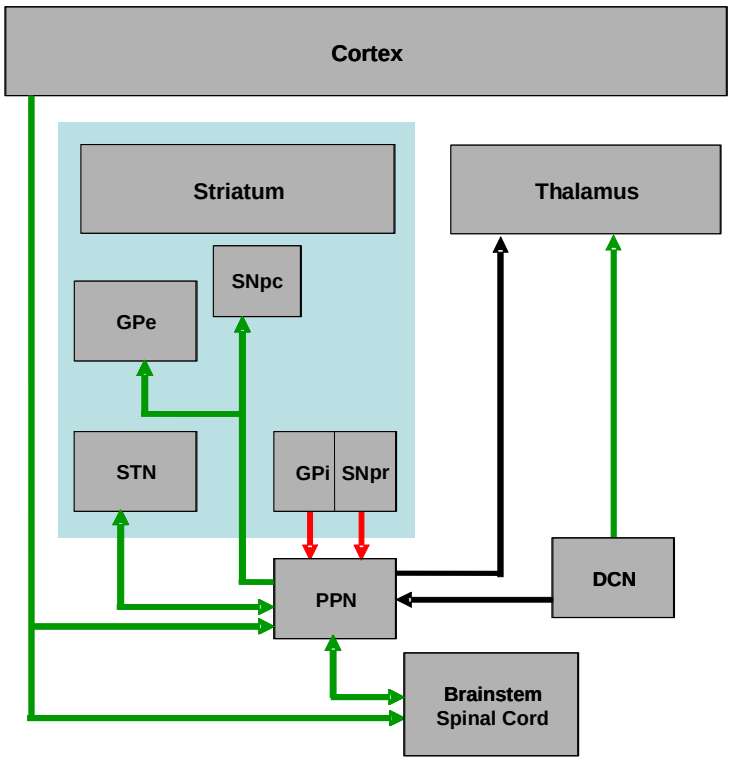

Figure 1.2. Known connections of the PPN in non-human primates determined using conventional anatomical tracing techniques (Lee *et al.*, 2000; Matsumura *et al.*, 2000; Pahapill and Lozano, 2000). Arrows between structures indicate direct connections (green: excitatory, red: inhibitory, black: either inhibitory or excitatory).

The rodent and primate PPN also may differ in their relative motor functions and the rodent PPN has been more closely linked to reward-related behavior (Inlgis and Winn, 1995; Winn, 2006). This may be due to stronger

connections between the PPN and limbic structures. The rodent PPN projects to the amygdala and lateral hypothalamus and receives robust input from the ventral pallidum, the same limbic output structure to which the STN projects (Inglis and Winn, 2006). Although the research presented in the subsequent Sections focuses mainly on the motor roles of the STN and PPN with regards to DBS of these structures in PD patients, it is also interesting to note the indirect connection between the STN and PPN in limbic thalamo-cortical loops as these limbic circuits are also likely to be affected by electrical stimulation of the STN or PPN.

The PPN is the main part of the mesencephalic motor region and has been shown to be involved with locomotion in several studies. Generally, excitation of the PPN is prokinetic while PPN inhibition is akinetic (Lee *et al.*, 2000; Pahapill and Lozano, 2000). Excitation of the PPN can be pharmacologically induced by administration of glutamate agonists (Hammond *et al.*, 1983a; Sanchez and Leonard, 1994). Furthermore, stimulation of the PPN at conventional frequencies used for DBS (>100 Hz) has been shown to induce akinesia while stimulation at various frequencies below 60 Hz has been shown to have prokinetic effects in several studies (reviewed in Lee *et al.*, 2000; Pahapill and Lozano, 2000).

1.2 Rate-based and oscillations models of basal ganglia function

Studies focusing on the anatomy of functionally segregated basal ganglia-thalamo-cortical loops (Parent and Hazrati, 1995a) led to the classical "rate-based" model of basal ganglia function (Albin *et al.*, 1989; DeLong, 1990).

This model was partially developed to help explain how PD pathology could cause parkinsonian motor symptoms (bradykinesia, akinesia, and resting tremor). PD has historically been characterized by degeneration of the dopaminergic neurons in the SNpc which, according to the rate-based model, throws off the balance between the "direct" and "indirect" pathways in the basal ganglia (Fig. 1.1A). The direct pathway refers to the direct connections between the striatum and the basal ganglia output nuclei (GPi/SNpr) while the indirect pathway refers to information flow from the striatum to the GPi/SNpr via the GPe and STN. In the rate-based model, the direct pathway facilitates movement by increasing thalamo-cortical based integration of motor information (Fig. 1.1B). The indirect pathway inhibits this thalamo-cortical interaction (Fig. 1.1C). Dopamine released from the SNpc to the striatum stimulates the direct pathway and inhibits the indirect pathway, thus facilitating coordinated movement overall. Therefore, according to the rate-based model, degeneration of SNpc dopaminergic neurons in PD causes over-activity of the indirect pathway in the basal ganglia and consequent paucity of movement (Tisch *et al.*, 2004).

Treatments for PD have focused on manipulating the basal ganglia with this "rate-based" model in mind. For example, according to the rate-based model, over-activity of the STN in the indirect pathway results in increased GPi activity which in turn increases inhibition of thalamo-cortical pathways. Lesions of the STN in monkeys treated with 1-methyl 4-phenyl 1,2,3,6-tetrahydropyridine (MPTP) lessened parkinsonian symptoms and consequently provided evidence for this hypothesis (Bergman *et al.*, 1990; Aziz *et al.*, 1991, 1992). Eventually, treatments for PD involving lesioning the STN (Guridi *et al.*,

1993) and the GPi (Laitinen *et al.*, 1992) became widely clinically available. When the lesions were properly targeted and not too large as to damage surrounding structures, symptoms were dramatically ameliorated. Yet, the permanence and high risk of lesioning did not make it an ideal treatment option.

In the last decade, high frequency DBS of the GPi and STN, involving chronic implantation of stimulating macroelectrodes in these structures, was shown to be just as effective, if not more effective than lesioning the GPi or STN (Siegfried and Lippitz, 1994; Limousin *et al.*, 1995; Krack *et al.*, 1997b). The efficacy of DBS of the GPi and STN has been attributed to the use of frequencies high enough to induce depolarization block, which would keep stimulated neurons in a hyperpolarized state and thus prevent firing in, or virtually lesion, the stimulated structures (Bennazzouz and Hallett, 2000). However, recent evidence has shown that stimulation of the STN at frequencies too low to induce depolarization block still results in improvement of parkinsonian symptoms (Haslinger *et al.*, 2005). Furthermore, the rate-based model predicts that DBS and lesions would ameliorate only parkinsonian hypokinesia via disinhibition of thalamo-cortical interaction in PD. However, DBS and lesions also facilitate normal movement in PD patients by reducing tremors, an effect that cannot be explained by the rate-based view of basal ganglia function (Kringelbach *et al.*, 2007). Since the clinical introduction of DBS in the mid-1990s, DBS of the STN has now become the most common surgical treatment for PD (Krack *et al.*, 1997a; Brock *et al.*, 1998; Krause *et al.*, 2001). However, the mechanism underlying the efficacy of DBS still remains unknown (Kringelbach *et al.*, 2007).

Based on the DBS paradox, the conventional rate-based model has come under fire. In its place, support for an "oscillation" model is gaining momentum (Brown, 2003; Brown and Williams, 2005). Neural networks are thought to communicate, at least in part, via synchronous firing (Salinas and Sejnowski, 2001; Schnitzler and Gross, 2005). General changes in the synchronization of neuronal firing in a given area can be recorded by measuring local field potentials (LFPs). This is done by placing an electrode in the extracellular space that records change in the potential of the surrounding fluid and thus the net change in the membrane potentials of local neurons. In many cases, neural communication is mediated not only by synchronous firing, but by distinct and often repetitive patterns of increases and decreases in firing rate. These periodic fluctuations, or oscillations, are evident in LFP recordings (Salinas and Sejnowski, 2001; Schnitzler and Gross, 2005). These oscillations in neuronal activity have been studied extensively in the cortex with regards to their role in behavior and cortico-cortical communication (reviewed in Neuper and Pfurtscheller, 2001; Salinas and Sejnowski, 2001; Schnitzler and Gross, 2005). However, unlike the cortex, the normal basal ganglia rarely display oscillatory firing and most structures fire irregularly (reviewed in Bergman *et al.*, 1998a; Murer *et al.*, 2002). In PD, there appears to be increased transmission of oscillatory cortical activity to the basal ganglia (Bergman *et al.*, 1998a; Murer *et al.*, 2002). LFP recordings from DBS electrodes implanted in PD patients display oscillatory activity at tremor (θ, approximately 3-5 Hz) and β frequencies (12-30 Hz) in the GPi and STN (Brown, 2003; Brown and Williams, 2005). However, with dopaminergic treatment, decreases in θ and β oscillatory activity and increases in γ (>60 Hz) oscillations are observed in the basal ganglia of PD

patients (Brown, 2003; Brown and Williams, 2005). It has been suggested that this γ frequency synchrony closely resembles normal “irregular” basal ganglia firing patterns (Schnitzler and Gross, 2005) and is prokinetic while θ and β oscillatory activity is antikinetic (Brown, 2003; Brown and Williams, 2005). The association of different oscillatory frequencies with antikinetic and prokinetic functions has been supported by electrophysiological recordings in several species including rats (Ruskin *et al.*, 1999, 2003; Brown *et al.*, 2002; Sharott *et al.*, 2005b), monkeys (Bergman *et al.*, 1994, 1998b; Wichmann *et al.*, 1999, 2002; Soares *et al.*, 2004), and humans (Levy *et al.*, 2000, 2002; Williams *et al.*, 2002; Brown, 2003, 2004). Since both lesions and DBS of basal ganglia structures would disrupt antikinetic PD oscillations, the oscillation model can account for the efficacy of both these treatments.

1.3 Propagation of network oscillations in the basal ganglia

Several studies have demonstrated an association between sensorimotor activity and the modulation of oscillatory activity in the normal cerebral cortex. For example, motor preparation and execution of both cued and self-paced motor tasks are associated with decreased power in the α and β frequency ranges (<35 Hz) in cortical EEG recorded from healthy human subjects (Klimesch *et al.*, 1993; Pfurtscheller and Neuper, 1994; Pfurtscheller *et al.*, 1997, 2000, 2001; Pfurtscheller and Lopes da Silva, 1999; Neuper and Pfurtscheller, 2001).

The main source of cortical input to the basal ganglia is via the striatum (Section 1.1.1). In the normal striatum, striatal inhibitory interneurons and an

inward rectifying K^+ current tend to keep MSNs, the striatal projection neurons, in a predominantly hyperpolarized state (Nisenbaum *et al.*, 1994, 1996; Nisenbaum and Wilson, 1995; Tepper *et al.*, 2004; Mallet *et al.*, 2005, 2006). MSNs will fire rarely and only with multiple, coincident, excitatory glutamatergic inputs from the cortex (Garcia-Munoz *et al.*, 1991; Plotkin *et al.*, 2005). Since the striatum does not propagate cortical oscillations faithfully to downstream structures, the resultant firing in the basal ganglia, as has been demonstrated in the normal rat (Sanderson *et al.*, 1986; MacLeod *et al.*, 1990; Hollerman and Grace, 1992; Burbaud *et al.*, 1995; Hassani *et al.*, 1996; Murer *et al.*, 1997; Rohlfs *et al.*, 1997; Magill *et al.*, 2000; Tseng *et al.*, 2000, 2001a, 2001b; Vila *et al.*, 2000; Ni *et al.*, 2001; Belluscio *et al.*, 2003; Tai *et al.*, 2003; Walters *et al.*, 2007; Parr-Brownlie *et al.*, 2007) and non-human primate (Karmon and Bergman, 1993; Bergman *et al.*, 1994; Wichmann *et al.*, 1994b; Raz *et al.*, 2000), tends to be tonic and does not tend to oscillate with cortical periods of depolarization. The striatum thus serves as a functional gate, preventing oscillatory cortical activity from invading the downstream basal ganglia (Murer *et al.*, 2002; Walters *et al.*, 2007).

A secondary source of cortical input to the basal ganglia is via the STN (Section 1.1.5). Unlike cells in other basal ganglia nuclei, a portion of STN neurons do fire synchronously with cortical firing. Estimates in the normal urethane-anesthetized rat suggest that 1 out of 4 STN neurons are oscillatory while close to no cells are oscillatory in other basal ganglia nuclei (Walters *et al.*, 2007). It is likely that this subset of STN cells is more influenced by input from cortical neurons via the so-called “hyperdirect” pathway between the cortex and STN (Jackson and Crossman, 1981a; Jurgens, 1984; Rouzaire-

Dubois and Scarnati, 1987; Fujimoto and Kita, 1993; Nambu *et al.*, 1997; Inase *et al.*, 1999) and not as affected by cortical input transmitted via the striatum.

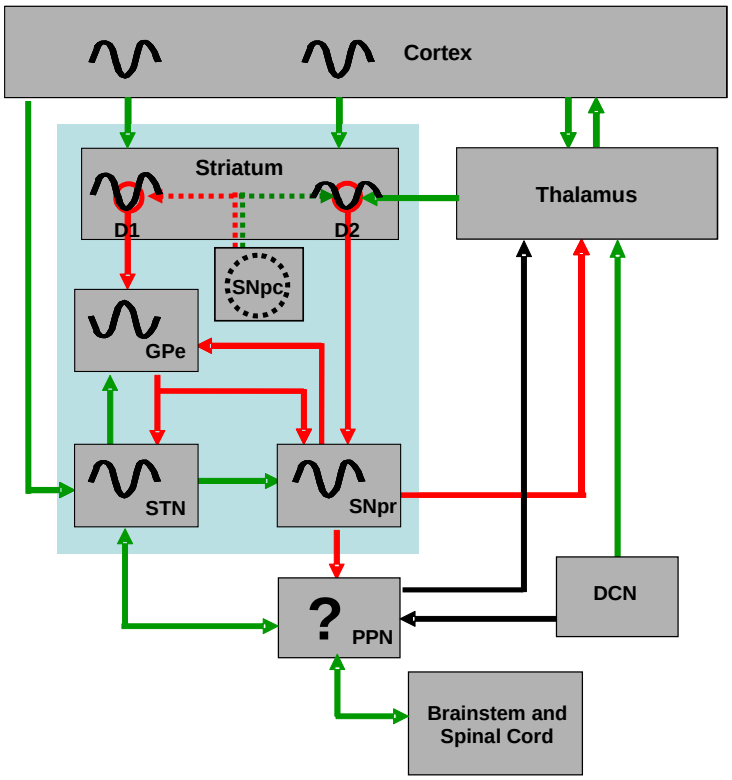

Figure 1.3. Phase relationships between firing in the cortex and firing in the basal ganglia in the urethane-anesthetized 6-OHDA lesioned rat (Walters *et al.*, 2007). Example LFP traces are indicated in each structure as they would appear if recorded simultaneously. Troughs indicate periods of greatest depolarization in the structure while peaks indicate periods of least depolarization. Until recently (Section 3), the phase relationship between firing in the PPN and firing in the cortex was unknown (indicated with a '?' in this figure). Dashed lines around and emerging from the SNpc indicate degeneration of dopamine neurons in the SNpc following 6-OHDA lesion. Arrows between structures indicate direct connections (green: excitatory, red: inhibitory, black: either inhibitory or excitatory).

Depletion of dopamine in the striatum, as in PD, appears to result in opening of the striatal oscillatory gate. As dopaminergic neurons from the SNpc synapse directly on MSNs, dopamine is poised to play a diverse and widespread modulatory role in the striatum (Section 1.1.1). In dopamine-depleted animal models of PD (i.e. the 6-OHDA lesion rat model and the MPTP

lesion primate model), oscillatory activity in the striatum and basal ganglia is greatly increased compared to oscillatory activity in normal control animals and is synchronous with oscillatory activity in the cortex (Sanderson *et al.*, 1986; MacLeod *et al.*, 1990; Hollerman and Grace, 1992; Karmon and Bergman, 1993; Bergman *et al.*, 1994; Wichmann *et al.*, 1994b; Burbaud *et al.*, 1995; Hassani *et al.*, 1996; Murer *et al.*, 1997; Rohlfs *et al.*, 1997; Magill *et al.*, 2000; Tseng *et al.*, 2000, 2001a, 2001b; Vila *et al.*, 2000; Raz *et al.*, 2000; Ni *et al.*, 2001; Belluscio *et al.*, 2003; Tai *et al.*, 2003; Walters *et al.*, 2007; Parr-Brownlie *et al.*, 2007). These results suggest that dopaminergic innervation of the striatum plays a key role in processing cortical oscillatory activity and in preventing these cortical oscillations from invading the basal ganglia.

In the parkinsonian brain, firing in the basal ganglia tends to oscillate in phase or out of phase with firing in the cortex. In the urethane-anesthetized 6-OHDA lesioned rat, activity in the striatum, STN, and SNpr is in phase with cortical oscillations. Oscillations in the GPe, a key nucleus in the indirect pathway, are out of phase with cortical oscillations (Walters *et al.*, 2007) (Fig. 1.3). It is unclear how these phase relationships manifest in motor structures downstream of the basal ganglia (e.g. in the PPN, Fig. 1.3), or how DBS of the STN or PPN could potentially modify these firing patterns.

1.4 Deep brain stimulation of the STN in Parkinson's disease

The STN has become the most common target for DBS in PD (Krack *et al.*, 1997a; Brock *et al.*, 1998; Krause *et al.*, 2001). Several studies have shown that the DBS of the STN at high frequencies (>100 Hz) results in a dramatic

amelioration of parkinsonian bradykinesia and tremor, often resulting in 80-90% improvement of motor Unified Parkinson Disease Rating Scale (UPDRS) scores (Kumar *et al.*, 1998; Rodriguez-Oroz *et al.*, 2005). However, the effect of DBS of the STN on rigidity and akinesia is more limited, resulting in only a 30-60% improvement with stimulation (Kumar *et al.*, 1998; Rodriguez-Oroz *et al.*, 2005). Furthermore, the beneficial effect of STN DBS on axial symptoms (e.g. akinesia, gait abnormalities, and postural instability) significantly lessens with time when comparing on-drug UPDRS scores 1 year and 5 years after the DBS implantation procedure (Krack *et al.*, 2003). The axial symptoms that persist when patients are on dopaminergic medications are also not improved with STN stimulation (Yokoyama *et al.*, 1999; Stolze *et al.*, 2001), further supporting the observation that there is a direct correlation between responsiveness to L-DOPA and the benefit derived from STN DBS (Pahwa *et al.*, 2006). Therefore, though DBS of the STN definitively improves dopamine-responsive tremor and bradykinesia in PD patients, debilitating parkinsonian motor abnormalities can persist even with DBS of the STN and dopamine replacement therapy.

1.5 Deep brain stimulation of the PPN in Parkinson's disease

The role of the PPN in the control of locomotion and posture has been studied extensively. In the intact normal monkey low frequency (10 Hz) stimulation of the PPN increases motor activity significantly, whereas high frequency stimulation reduces it (Nandi *et al.*, 2002b). In the primate model of PD, parkinsonian akinesia can be alleviated by pharmacological disinhibition of the PPN with bicuculline (Nandi *et al.*, 2002a) or by low frequency electrical

stimulation of the PPN (Jenkinson *et al.*, 2004). These results imply that parkinsonian akinesia is at least partly the result of excessive inhibition of the PPN by descending GABAergic projections from the basal ganglia that can be bypassed by stimulating the PPN directly. The increase in movements may occur both by stimulating the ascending projections of the PPN to engage surviving dopaminergic mechanisms in the basal ganglia, but also by stimulating PPN projections descending to brainstem locomotor and postural centers, 'downstream' from the dopaminergic systems. However, it is also known that the beneficial effects of low frequency stimulation of the PPN and those of levodopa treatment are additive (Jenkinson *et al.*, 2006). Thus it has become clear that the PPN plays an important dopamine-independent role in the control of posture and locomotion.

Based on these primate data, the PPN was chosen as a new DBS target for human PD patients with previously medically intractable rigidity and akinesia. Low frequency—20-25 Hz (Plaha and Gill, 2005) or 10 Hz (Mazzone *et al.*, 2005)—stimulation of the PPN significantly improved gait dysfunction and postural instability in patients on or off dopamine medication. High frequency (80 Hz) stimulation had either little or exacerbating effects (Mazzone *et al.*, 2005). Recently, it has also been shown that the effects of high frequency stimulation of the STN, low frequency stimulation of the PPN, and dopaminergic medication are additive, further supporting the theory that the PPN is involved in motor control in PD via dopamine-independent mechanisms (Stefani *et al.*, 2007). Therefore, in contrast to DBS of the STN, DBS of the PPN in PD patients results in improvement of dopamine-resistant gait and postural abnormalities.

1.6 Research question and experiment summaries

DBS of the STN and DBS of the PPN have been shown to effectively ameliorate several parkinsonian symptoms. However, PPN and STN anatomy in humans, the involvement of the PPN in pathological oscillatory synchrony and the electrophysiological interaction between the PPN and the STN, and the different effects of DBS of the PPN and STN on the same parkinsonian symptoms are unknown. Studying differences between PPN and STN connectivity and electrophysiology in the normal and parkinsonian brain may help shed light on these questions and give us a better understanding of the role of these nuclei as DBS targets for PD.

In order to obtain a comprehensive view of the relationship between these two nuclei in the normal and parkinsonian brain, STN and PPN activity was studied in PD patients (at the University of Oxford, Oxford, UK) and in a rat model of PD (at the National Institutes of Health, Bethesda, MD, USA). In humans, the differences between the anatomical connections of the STN and PPN and the differences in STN and PPN LFP activity during voluntary movement were determined. The relationship between LFP and single unit activity in the PPN, motor cortex, and other basal ganglia nuclei was studied in rats.

The roles of the STN and PPN were examined in three general contexts: anatomically (Section 2), electrophysiologically (Sections 3 and 4), and behaviorally (Section 5). Section 2 illustrates how diffusion tensor imaging (DTI) was used to determine the anatomical connections of the healthy human PPN and STN. These DTI results were also validated in a non-human primate brain.

Section 3 examines relationships between neuronal activity in the PPN, motor cortex, and other basal ganglia nuclei in a simplified model of neural network oscillations (the urethane-anesthetized rat). Phase relationships were compared between normal rats and hemi-parkinsonian rats (6-hydroxydopamine lesions of the medial forebrain bundle) to determine the effect of striatal dopamine depletion on PPN electrophysiology. Section 4 examines the relationship between oscillatory activity in the PPN and STN during voluntary movement in patients with PD. PPN and STN LFP modulation was examined in different frequency bands during rapid cued and self-paced voluntary finger flexion to determine the involvement of these nuclei in the execution of simple voluntary movements and in overcoming bradykinesia and tremor in PD. Finally, Section 5 compares the roles of the PPN and STN in parkinsonian motor behavior. The effects of PPN stimulation and STN stimulation on gait and posture in PD patients were compared during walking, turning, and standing to help determine the functional roles of the PPN and STN in large scale motor control.

2. ANATOMICAL COMPARISON OF THE PEDUNCULOPONTINE AND SUBTHALAMIC NUCLEI

The effects of DBS are not limited to the targeted structure, but will affect the distributed anatomical networks to which the target structure belongs. Therefore, understanding the anatomical connections of the PPN and STN will help elucidate treatment effects. In particular, establishing the topography of cortical and sub-cortical connections of STN and PPN in the human brain could aid accurate targeting of critical pathways in DBS. In this section, the connections of the PPN and STN and the distribution of these connections within these nuclei (topography) are determined using diffusion tensor imaging (DTI) in healthy human volunteers. To further validate the human DTI results, the connections and topography of the PPN are also determined in a primate Macaca mulatta *brain and compared to known non-human primate PPN connections and topography determined using conventional anatomical tracing techniques.*

2.1 Anatomy of the human PPN and STN

2.1.1 Introduction and rationale

The need for accurate surgical targeting of the PPN for DBS procedures necessitates better anatomical characterization of the PPN. Currently, PPN connections have been best characterized using tracing and evoked-potential studies in rodents (Garcia-Rill *et al.*, 1987; Rye *et al.*, 1987; Garcia-Rill and

Skinner, 1987a, 1987b; Spann and Grofova, 1989, 1991, 1992), but these connections differ greatly from those shown in non-human primate tracing studies (Lavoie and Parent, 1994a, 1994b, 1994c; Pahapill and Lozano, 2000). Though both the rodent PPN and monkey PPN have strong connections with the STN, substantia nigra (SN), and GP, connections between the PPN and motor cortex have only been shown in non-human primates, and projections from the PPN to the DCN and projections extending down the spinal cord have only been shown in rodents (Section 1). Recently, probabilistic diffusion tractography was used to trace connections of the PPN in humans (Muthusamy *et al.*, 2007). These results show that PPN connections in humans largely match those in non-human primates, but also include descending cerebellar connections. These differing results illustrate the importance of verifying the existence of PPN connections across different species using the same methodological techniques.

In contrast to the PPN, the connections of the STN have been well characterized in both rodents and non-human primates and there is little difference between the species (Hamani *et al.*, 2004). The major connections of the STN are with the GP and SNpr. The STN also receives excitatory input from various parts of the cerebral cortex, including the motor cortex (M1), supplementary motor area (SMA), and the dorsal and ventral PMC (dPMC and vPMC, respectively) (Hamani *et al.*, 2004).

This section investigates the topography of STN and PPN connections. Until now, PPN topography has been explored only in monkeys and has only been demonstrated for cortical connections in one study (Matsumura *et al.*, 2000). Distinct topography has also been demonstrated in the STN, separating

STN regions connected to motor, associative, and limbic brain areas (Hamani *et al.*, 2004). However, PPN or STN topography has not been demonstrated in humans.

DTI was used to test for topographic organization in the cortical and sub-cortical connections of human STN and PPN. DTI can be used to estimate anatomical connections in the human brain *in vivo*. Probabilistic methods for tractography (Behrens *et al.*, 2003b; Parker *et al.*, 2003) allow for tracking of probable fiber pathways between cortical and sub-cortical gray matter structures (Behrens *et al.*, 2003a; Johansen-Berg *et al.*, 2005; Sillery *et al.*, 2005; Muthusamy *et al.*, 2007). For the purposes of this study, connections refer to the estimated anatomical pathways between brain regions (e.g. a fiber path estimated between the STN and a cortical brain region) while topography refers to the size and spatial distribution of the specific parts of a given gray matter structure that connect to other brain regions (e.g. the anterior-medial part of the STN connects with cortical areas). Note that the terms 'connections' and 'topography' are used in a purely anatomical sense. Although tractography cannot determine the direction or sign of functional projections between regions, it does allow for the estimation of the connections and topography of a given brain region *in vivo.* Therefore, in order to further anatomically characterize human PPN and STN, diffusion tractography was used to determine the anatomical connections and topography of cortical and sub-cortical connections of the PPN and STN in healthy human subjects.

2.1.2 Methods

2.1.2.1 Subjects and image acquisition

Magnetic resonance data were acquired from 8 healthy right-handed adult subjects (4 men, 4 women, age range 21-34 years) with no history of psychiatric or neurological disease. All subjects provided written informed consent in accordance with ethical approval from the Central Office for Research Ethics Committees. A 1.5 T Siemens Sonata MR scanner with maximum gradient strength of 40 $mT \cdot m^{-1}$ was used. Diffusion-weighted data were acquired using echo planar imaging (72x2 mm^2 thick axial slices, matrix 128x104, field of view 256x208 mm^2, giving a voxel size of 2x2x2 mm^3). The diffusion weighting was isotropically distributed along 60 directions using a *b* value of 1000 $sec \cdot mm^{-1}$. A T1-weighted anatomical image was also acquired using a 3D flash sequence (repetition time = 12 msec, echo time = 5.65 msec, and flip angle = 19°, with elliptical sampling of *k* space, giving a voxel size of 1x1x1 mm^3 in 5 min and 5 sec).

2.1.2.2 Image pre-processing

Tools from the FMRIB Software library (FSL, www.fmrib.ox.ac.uk/fsl, (Smith *et al.*, 2004)) were used for image processing and analysis. Diffusion-weighted, T1-weighted structural, and Montreal Neurological Institute (MNI) standard brain template images (Evans *et al.*, 2003) were skull-stripped using the FSL Brain Extraction Tool. Affine registration was then performed to derive transformation matrices among the three spaces (diffusion, structural, and standard space). Lastly, probability distributions of fiber direction at each voxel were calculated using previously described methods (Behrens *et al.*, 2003b). A

simple partial volume model of local diffusion was used, with only a single anisotropically diffusing direction in the voxel. A probability distribution function on this principal fibre direction was then estimated using Bayesian techiques. Probability distributions of connectivity between the initial seed voxel and all other points are determined by repeatedly sampling connected pathways through this probability distribution function field. This allows for the visualization of the dominant connection from the seed voxel as a probability distribution gradient (Behrens *et al.*, 2003b). Using this probabilistic diffusion tractography technique, multiple anisotropic diffusion directions within a single voxel manifest as uncertainty in the principal diffusion direction. Newer techniques have optimized modeling of multiple anisotropic diffusion directions within a single voxel using the same Bayesian estimates of probability distribution functions on each diffusion direction. However, multiple diffusion directions are modeled only in voxels which appear to represent regions of fiber crossing. This voxel selection is accomplished using a model selection technique called automatic relevance determination (Hosey *et al.*, 2005; Parker and Alexander, 2005; Behrens *et al.*, 2007). Use of these newer multiple diffusion direction modeling techniques may improve upon the tractography results presented here and could be used to further study the connections demonstrated in this study using the single diffusion direction model.

2.1.2.3 Determining regions strongly inter-connected to the PPN or STN with probabilistic tractography

It is difficult to visualize the boundaries of the PPN and STN on diffusion images and therefore, to initially define the major anatomical connections of

PPN and STN in the human brain, only single seed voxels that could be confidently located within the PPN or STN were identified. These seeds were selected bilaterally for each subject from transverse slices in diffusion space. The voxel used as the PPN seed was located at the level of the superior cerebellar peduncle, in between the medial lemniscus and the decussation of the superior cerebellar peduncle (xscp) (Figs. 2.1, 2.4A). The xscp is clearly visible on the red-green-blue (RGB) representation of the principle diffusion estimate at each voxel (Stieltjes *et al.*, 2001) and so this representation was used to ensure that fibers of the xscp did not overlap with the PPN seed voxel (Fig. 2.1). The STN single voxel seed was located at the level of the superior-most slice showing the red nucleus, medial to the SN, in the middle of the cerebellar peduncle (Fig. 2.7A). These seed voxel locations were independently confirmed to be within the PPN and STN by two licensed neurosurgeons (KA, TZ).

FMRIB's Diffusion Toolbox (FDT, www.fmrib.ox.ac.uk/fsl) allows the user to modify certain tractography parameters to accommodate differences in brain size and diffusion data resolution. For example, the step length (default value is 0.5 mm for diffusion data acquired with 2x2x2 mm^3 voxel resolution in the adult human brain) corresponds to the distance between subsequent sampling points of connected pathways. The curvature threshold (default value is 0.2) corresponds to the angle between the principal diffusion directions in subsequent steps and can be changed to allow for the tracing of more or less tortuous pathways. The streamline samples (default value is 5000 samples) refer to the number of individual pathways that are drawn through the probability distributions on the principal diffusion direction and can be increased

to obtain a better resolution of the overall probability distribution corresponding the dominant connection from the seed voxel. Fiber tracking in this study was initiated from the single voxel seeds (5000 streamline samples, step length of 0.5 mm, curvature threshold of 0.2, excluding connections crossing into the contralateral hemisphere). The paths connected with the seeded PPN or STN voxel were binarized and overlaid onto a standard brain image for population analyses. Areas displaying connections with the single voxel seed in at least half of all subjects were determined to be regions with high probability of connection to the PPN or STN.

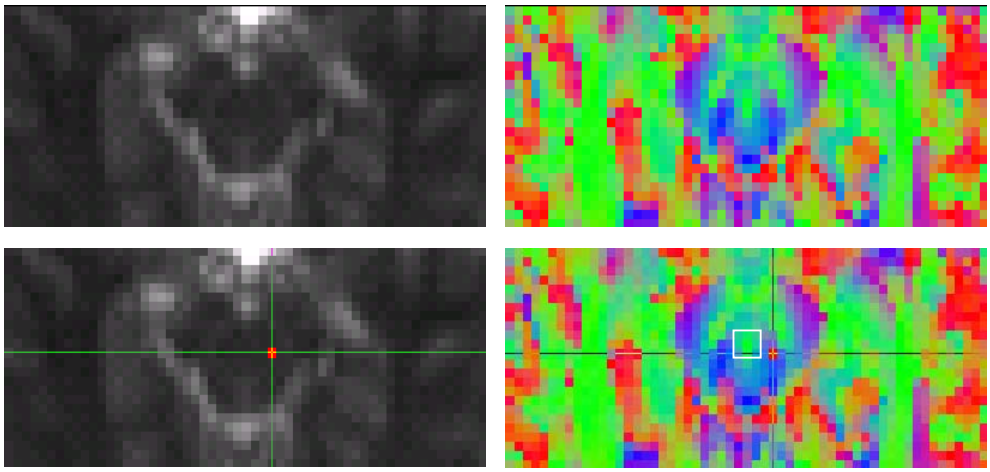

Figure 2.1. Localization of PPN seed voxels in the human brain. A transverse brain slice from one subject is shown as DTI images in diffusion space. In the bottom images, the crosshairs and orange square indicate the location of a PPN seed voxel. The images on the right are the RGB representations of the principle diffusion estimate at each voxel. In the RGB images, the xscp is clearly visible as a green area in the center of the brainstem. In the bottom right RGB image, the xscp is delineated by a white outline (Stieltjes *et al.*, 2001).

2.1.2.4 Creating anatomical masks of inter-connected regions

After determining the cortical and sub-cortical regions strongly inter-connected with STN and PPN, the topography of the STN and PPN was next characterized. Masks were drawn of these cortical and sub-cortical target regions bilaterally on the T1-weighted structural images for each subject based

on visible anatomical landmarks and with reference to the *Atlas of Neuroanatomy and Neurophysiology* (Netter *et al.*, 2002). Somatotopic divisions of the motor cortex were estimated as percentages of the precentral gyrus based on the motor homunculus. These divisions, from medial to lateral are: legs and hips (M1-hind), 7.5%; trunk region (M1-trunk), 17.5%; arm and forearm (M1-fore-U), 15%; wrist and hand (M1-fore-L), 30%; neck and orofacial region, 30% (Fig. 2.2). The SMA and the dPMC were located just anterior to the precentral sulcus on the medial and lateral brain surface, respectively. The border between the SMA and dPMC was set at the same position, mediolaterally, as the border between M1-trunk and M1-fore-U. The lateral/inferior border of the dPMC was at the same position, mediolaterally, as a transverse plane through the midpoint of M1-fore-L (Fig. 2.2). The masks were registered to the diffusion data of the same subject using FMRIB's Linear Image Registration Tool (FLIRT, www.fmrib.ox.ac.uk/fsl). Mask size did not significantly differ between hemispheres or across subjects when normalized to each subject's brain size (paired t-test, $p>0.05$).

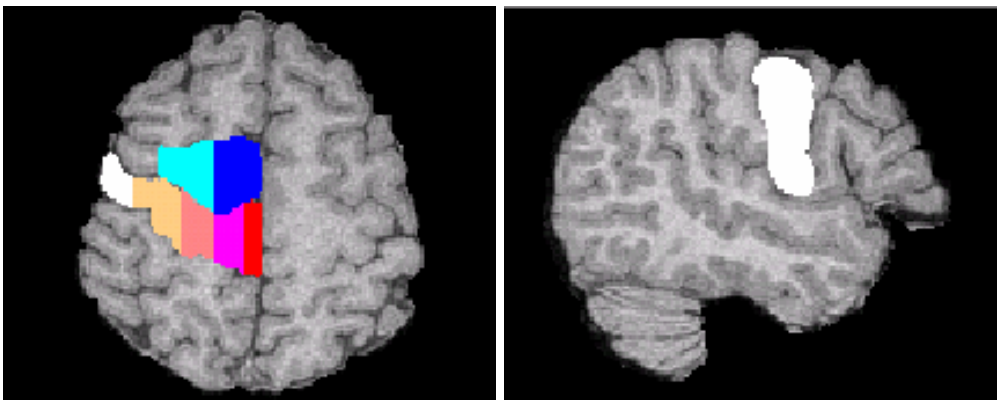

Figure 2.2. Segmentation of cortical regions. Masks of cortical regions are drawn on the T1-weighted structural image from one subject. Left: the M1 (shades of red), SMA (dark blue), and dPMC (light blue) are shown on a transverse slice. From medial to lateral, the motor cortex is subdivided into the hindlimb, trunk, upper forelimb, lower forelimb, and orofacial regions. Right: the motor cortex (white) is also visible on a sagittal slice.

2.1.2.5 Determining the topography of PPN and STN connections

To investigate the topography of anatomical connections from each nucleus, seed masks were created surrounding the PPN and STN single voxel seeds described above, that aimed to include the entire nucleus of interest (Figs. 2.5A, 2.8A). Both the PPN and STN masks were 36 voxels (288 mm^3) in size. *The Human Central Nervous System* atlas (Niewenhuys *et al.*, 1988) shows the PPN to have an approximate volume of 230 mm^3 and the STN to have an approximate volume of 220 mm^3, which is in agreement with other studies calculating human STN volume to be 240 mm^3 (Hardman *et al.*, 2002). The generous size of the seed masks allowed sufficient space for topography to be inferred for the PPN and STN and allowed for clear discernment between areas that preferentially connect with different brain regions. Tractography was run from every voxel inside these seed masks and the co-ordinates of the voxel within each seed mask with the highest probability of connection to a given brain region were determined. The locations of these voxels relative to the mid-point of the seed mask were calculated and these co-ordinates were averaged across all 8 patients (16 voxels). The average voxel location was graphed in the coronal, transverse, and sagittal planes along with error bars indicating the 95% confidence interval of the average location. The areas designated by the error bars indicated the areas of the PPN and STN with highest probability of connection to other brain structures. An example of topography determination is shown in Figure 2.3. In addition to comparing the locations of these PPN and STN regions of connectivity, paired t-tests were performed on the x, y, and z co-ordinates of the PPN and STN voxels to infer existence of topography.

To examine the strength of the connections between the PPN, STN and other brain regions, the number of voxels in each seed mask that had any probability of connection (>0 streamline samples) to a given brain region was also determined. This number was compared, using paired t-tests, across all regions showing high connectivity to the PPN or STN in order to determine whether different volumes of the PPN or STN projected to different brain regions. Furthermore, in order to determine whether the volume of the PPN or STN connecting to a given brain region was proportional to the size of that region, the number of voxels with any probability of connectivity was divided by the number of voxels in the diffusion image mask of the connected brain region. This normalized value was then again compared across all regions using paired t-tests.

2.1.2.6 Determining the paths of connections between the PPN, STN, and other inter-connected brain regions

Connected paths were determined using the two-way symmetrical tracking mode in FDT. This returns only the connection paths that pass through the PPN or STN mask and another brain region mask, regardless of which mask is used as the seed image. The connection paths were binarized and overlaid onto a standard brain image for population analyses. The connection path present in at least half of all subjects was determined to be the most likely path between the PPN or STN and a given brain region. Furthermore, only tracts that showed an uninterrupted path between the two masks in at least half of all subjects were further examined. Key structures via which each tract passed were noted and compared between the PPN and STN.

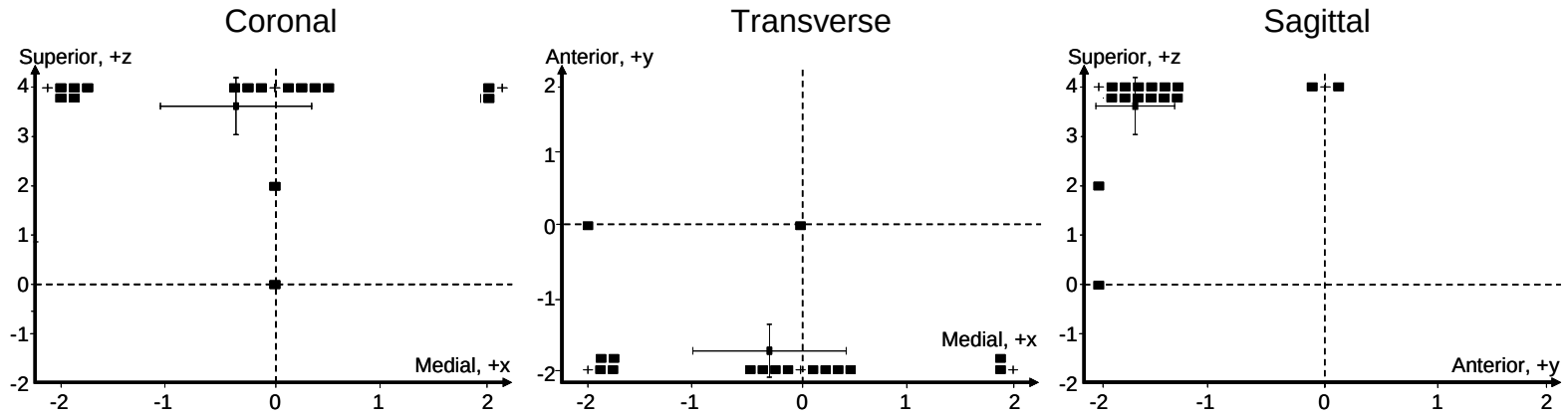

Figure 2.3. Example of topography determination. The PPN voxels with highest probability of connection to the thalamus (Fig. 2.5) are shown in the coronal, transverse, and sagittal planes. The axes show distance in mm relative to the midpoint of the PPN seed mask, located at 0 mm on each axis. The two bold dashed lines in each plot intersect at the midpoint of the seed mask. Voxels that have the same coordinates in a given plane are plotted offset from their actual location (indicated by a '+'). The average voxel location is also shown with error bars indicating the 95% confidence interval for each coordinate. This 95% confidence range is shaded gray and indicates the area of the PPN with highest probability of connection to the thalamus.

2.1.3 Results

2.1.3.1 Connections and topography of the PPN

The PPN exhibited connections with the cerebral cortex, basal ganglia, cerebellum and spinal cord (Table 2.1, Fig. 2.4). The cortical regions with high probability of connection to the PPN were the dPMC, SMA, M1-hind, M1-trunk, M1-fore-U, and M1-fore-L (Fig. 2.4B). Sub-cortical connections of PPN included the thalamus, GP, and STN (Fig. 2.4C). Surprisingly, PPN connections with the SN were found in slightly less than half of all subjects (7 out of 16 PPNs examined, Table 2.1) and, therefore, PPN connections with the SN were not considered sufficiently strong to warrant further analysis using DTI techniques in this study. In addition, PPN connections were also observed throughout the declive and folium regions of the cerebellum (mid-cerebellum) and extending caudally to the spinal cord (Fig. 2.4D).

Significant ($p<0.05$) topography in the PPN was present in the coronal (Fig. 2.5B), transverse (Fig. 2.5C), and sagittal (Fig. 2.5D) planes. The anterior and superior portions of the PPN tended to be connected with more anterior and superior brain regions, respectively. In addition, PPN regions connected to the cortex tended to be located closely together and were generally more laterally located than were PPN regions connected to other brain regions. PPN regions connected to the thalamus, mid-cerebellum, and STN were also located closely together (within the same quadrant of the PPN mask within a given plane). However, the PPN region connected to the GP was distinctly segregated from the regions connecting to other sub-cortical regions (generally located in the opposite quadrant) (Fig. 2.5).

Table 2.1. PPN Connections Across All Subjects.

Brain Regions		*1L*	*1R*	*2L*	*2R*	*3L*	*3R*	*4L*	*4R*	*5L*	*5R*	*6L*	*6R*	*7L*	*7R*	*8L*	*8R*	%
Cortex	PFC					X				X	X						X	25.00
	dPMC	X	X	X						X		X		X	X	X		50.00
	SMA		X	X	X					X		X		X	X		X	50.00
	M1-Hind			X	X	X	X	X		X	X					X		50.00
	M1-Trunk		X	X	X	X	X	X	X	X	X	X	X	X	X	X	X	93.75
	M1-ForeU	X	X		X	X	X		X	X	X	X	X	X	X	X		81.25
	M1-ForeL		X	X	X	X	X	X		X	X	X	X		X	X	X	81.25
	M1-Orof		X				X					X				X		25.00
Basal Ganglia	Thalamus	X	X	X	X	X	X	X	X	X	X	X	X	X	X	X	X	100.00
	GP	X	X	X	X	X		X		X	X	X		X	X	X	X	81.25
	STN	X	X			X	X	X	X	X	X	X	X		X	X	X	81.25
	SN		X	X	X					X	X			X			X	43.75
Cerebellum		X	X	X	X	X	X	X	X	X	X	X	X	X	X	X	X	100.00
Spinal Cord		X	X	X	X	X	X	X	X	X	X	X	X	X	X	X	X	100.00

1L/1R: Subject ID Left/Right PPN; X: Regions connected to the indicated PPN as determined from a single PPN seed voxel; %: Percentage of PPNs, out of the 16 PPNs examined, that are connected to the indicated brain region.

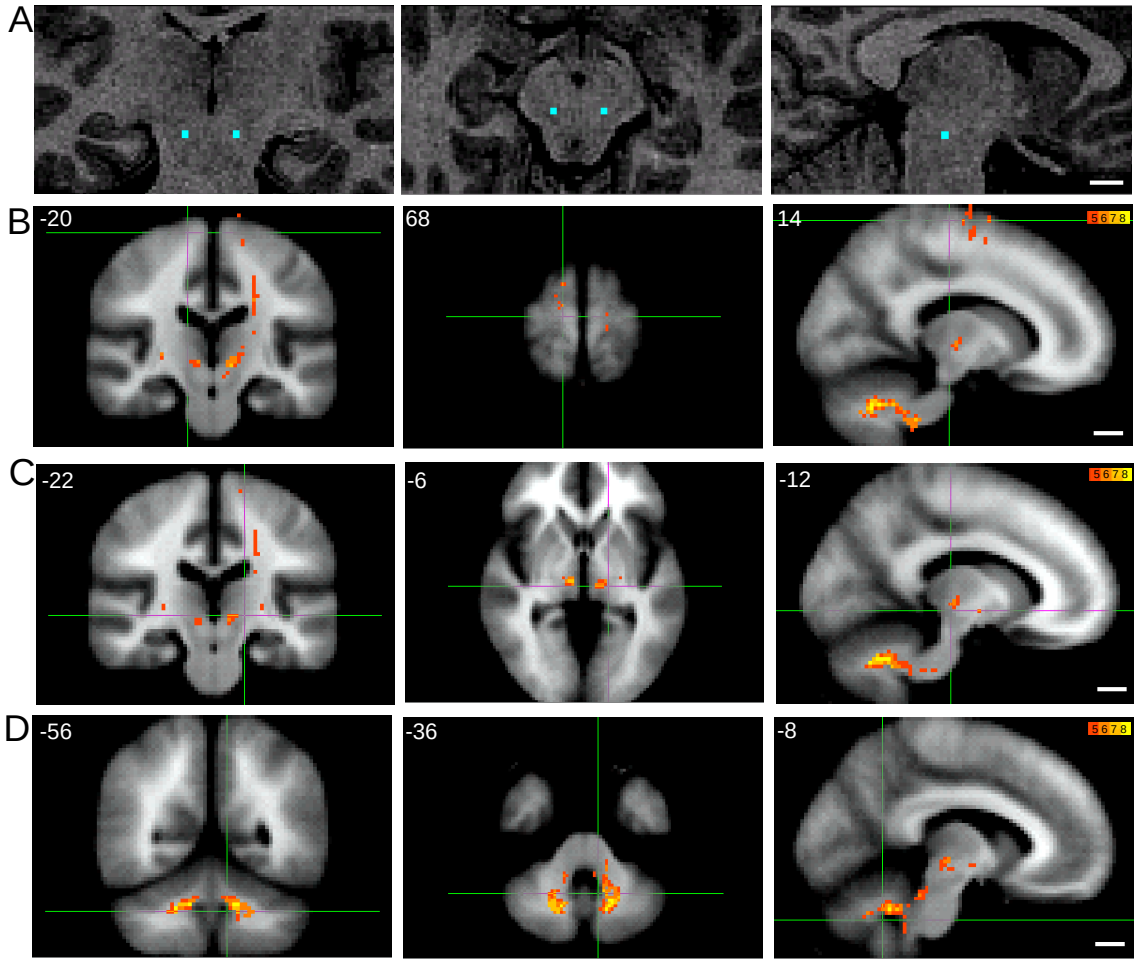

Figure 2.4. Regions with highest connectivity to the PPN as determined from a single seed voxel located within the PPN in each hemisphere. A) Localization of PPN seed voxel (2x2x2 mm^3, selected in diffusion space) is indicated bilaterally by blue squares on a T1-weighted structural image. B-D) Tracts are thresholded to include projections present in only 4 or more of the 8 subjects. The color of the tract indicates the number of subjects with PPN projections running via a given tract (as shown in the color scale in the upper right corner of each row). Each row shows slices that intersect at the voxel location indicated by the green crosshairs. The MNI coordinate of each slice is also shown in the upper left corner of each brain image. White bars at the lower right hand corner of each row show a 1 cm scale for the figures in that row. B) Connectivity between the PPN and the motor cortex, SMA, and dPMC. C) Connectivity between the PPN and the GP, thalamus, and STN. D) Connectivity between PPN and the mid-cerebellum and spinal cord.

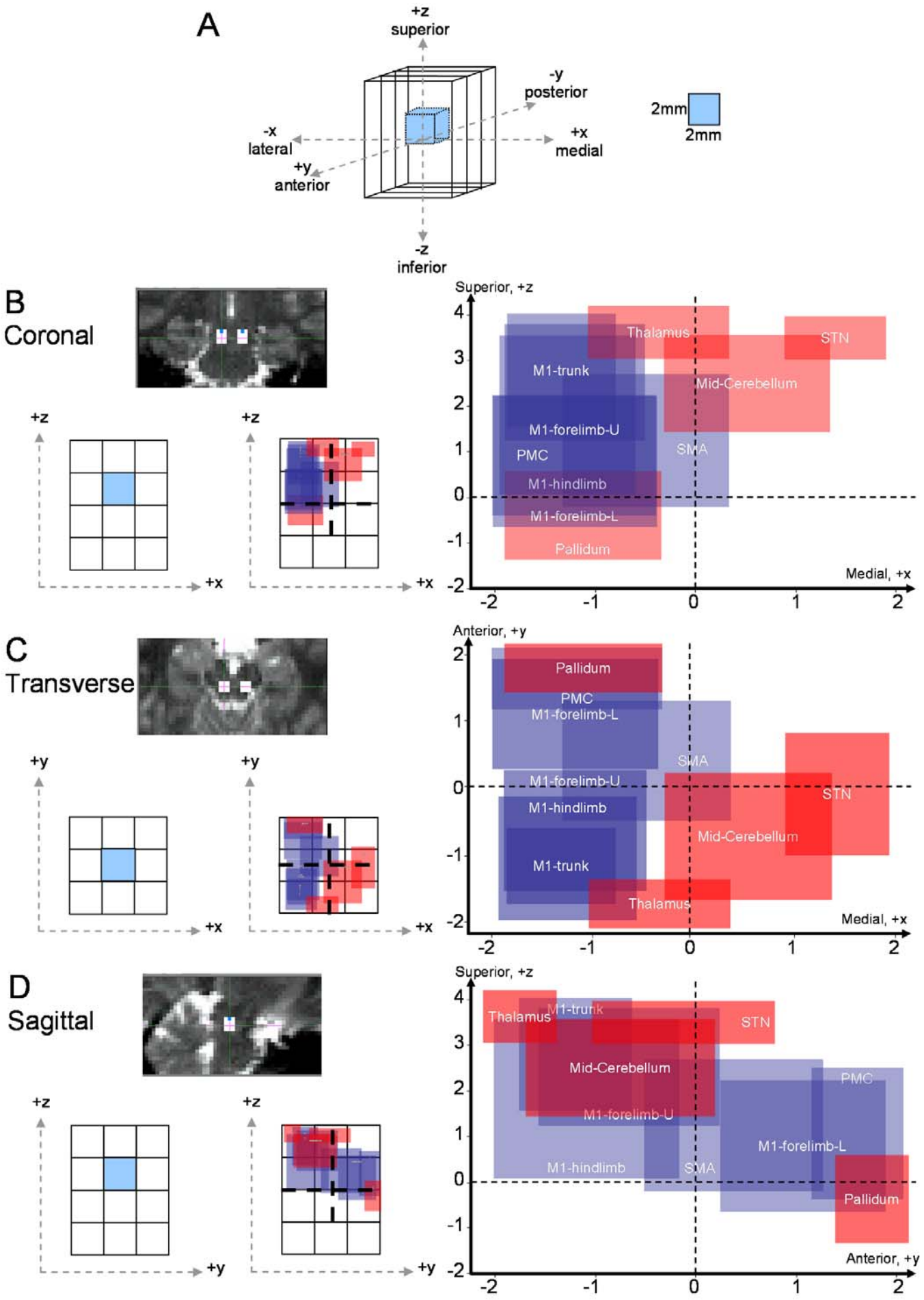
A
+z
superior
-y
posterior
2mm
2mm
-x
lateral
+x
medial
+y
anterior
-z
inferior
B
Coronal
+z
+x
+z
+x
Superior, +z
Thalamus
STN
M1-trunk
Mid-Cerebellum
M1-forelimb-U
SMA
PMC
M1-hindlimb
M1-forelimb-L
Pallidum
Medial, +x
C
Transverse
+y
+x
+y
+x
Anterior, +y
Pallidum
PMC
M1-forelimb-L
SMA
M1-forelimb-U
STN
M1-hindlimb
Mid-Cerebellum
M1-trunk
Thalamus
Medial, +x
D
Sagittal
+z
+y
+z
+y
Superior, +z
Thalamus
M1-trunk
STN
Mid-Cerebellum
PMC
M1-forelimb-U
M1-forelimb-L
M1-hindlimb
SMA
Pallidum
Anterior, +y

Figure 2.5 (on previous page). Topography within the PPN. A) Schematic of the 36-voxel PPN seed mask. The light blue cube shows the location of the single seed voxel used for the determination of the regions of highest connectivity to the PPN (Fig 1). B-D) Seed mask location and topography in the coronal, transverse, and sagittal planes. The left half of each row shows the location of the seed mask in a DTI image in diffusion space (top), a schematic of the seed mask in the given plane (bottom far left), and the topography in that plane (bottom right). Areas of cortical connection are shown in blue and the locations of non-cortical connections are in red. The intersection of the two bold dashed lines in the image showing topography indicates the midpoint of the seed mask. The image on the right of each row zooms in on the areas of highest connectivity as shown in the smaller topography image on the left side of each row. The axes show distance in mm relative to the midpoint of the PPN seed mask, located at 0 mm on each axis. Each red or blue-shaded box is centered at the location of the PPN voxel with the highest probably of connection to the indicated brain region, as determined from the average location across all 8 subjects. The width and height of each box show a 95% confidence interval range, across all 8 subjects, for the location of this PPN voxel (Fig. 2.3).

The volume of the PPN connecting to each of these regions differed as well. The largest portion of the PPN connected to the GP while the smallest portion connected to M1-hind (Fig. 2.6A). Interestingly, this size ordering changed after correcting for the sizes of the targets (by dividing the volumes of the PPN regions by the sizes of the brain regions with which they connect). The largest normalized volume of the PPN connected with the STN, the second largest PPN volume to the GP, and the smallest volume to the mid-cerebellum. However, it is important to note here that the STN was the smallest brain region with which the PPN connected while the mid-cerebellum was the largest (Fig. 2.6B).

Finally, connections between the PPN and cortex differed in the path they took through the brain (Table 2.2). Weaker connections between the PPN and M1-hind and M1-fore-L did not exhibit a continuous path in at least half of all subjects and were therefore excluded from further analysis**.** All connection paths

passed between the PPN and the cortex via the thalamus and internal capsule though the connection between the PPN and the motor cortex avoided the basal ganglia entirely while the connections between the PPN and the dPMC and SMA passed through the STN.

2.1.3.2 Connections and topography of the STN

The STN also showed high probability of connection to several brain regions (Table 2.3). In the cortex, connections were found between the STN and the dPMC, SMA, M1-hind, M1-trunk, and M1-fore-U (Fig. 2.7B). In the basal ganglia, the STN exhibited connections with the thalamus, GP, and SN (Fig. 2.7C). In addition, STN connections were observed with the PPN, throughout the mid-cerebellum, and extending caudally to the spinal cord (Fig. 2.7D).

Table 2.2. Paths of Connections between the PPN and Cortex

Areas of Passage		dPMC	SMA	M1-trunk	M1-fore-U
Motor Cortex	M1-hind				
	M1-trunk			X	
	M1-fore-U			X	X
	M1-fore-L				
Other Cortical Areas	dPMC	X			
	SMA		X		
Basal Ganglia	Thalamus	X	X	X	X
	GP				
	SN				
	STN				

Columns: the path of a connection between the PPN and the indicated cortical area. X: Area of the brain through which the indicated connection passes.

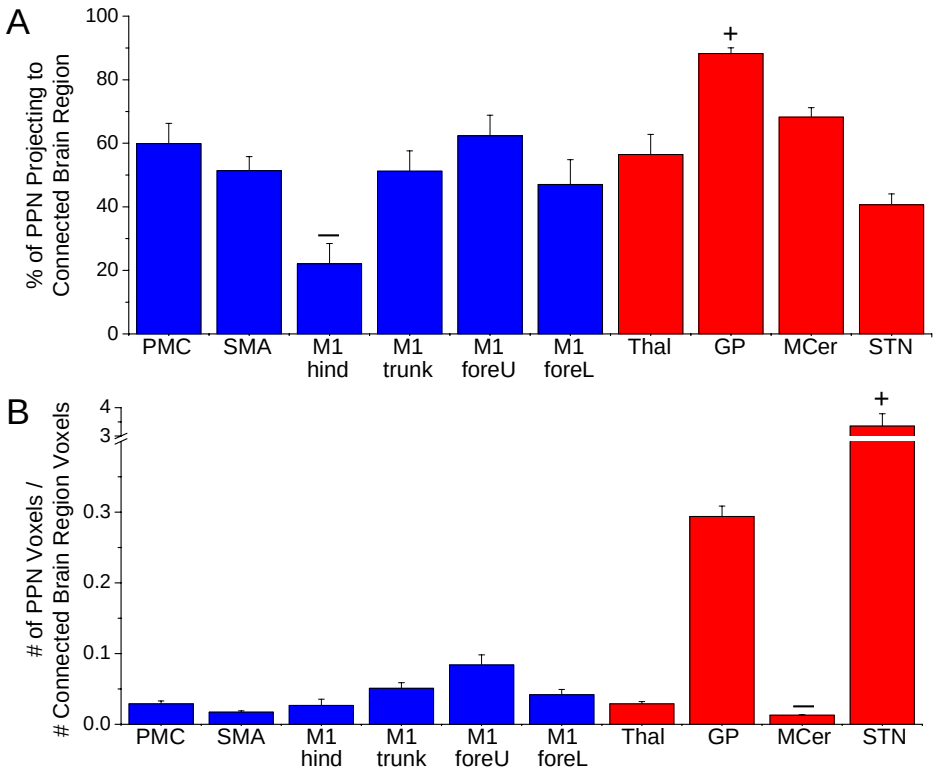

Figure 2.6. Volume of the PPN connected with different brain regions. A) Each bar shows the mean (± SE, across all 8 subjects) percent of the PPN connected to a given brain region (PPN voxels with any probability of connection to a given brain region / total number of PPN voxels). B) The mean percent of the PPN connected to a brain region normalized to the size of that connected region (PPN voxels with any probability of connection to a given brain region / total number of voxels in that brain region). +: largest PPN portion projecting to a given region ($p<0.05$); —: smallest PPN portion projecting to a given region ($p<0.05$).

Significant ($p<0.05$) topography was again shown in the STN in the coronal (Fig. 2.8B), transverse (Fig. 2.8C), and sagittal (Fig. 2.8D) planes. Figure 2.8 shows the location (within a 95% confidence interval across all subjects) of the STN voxel showing the highest probability of connection to the indicated brain area. The general trends in STN topographical organization in the x- and y-directions matched those in the PPN. STN regions connected to the cortex were generally more laterally located than STN regions connected to other brain regions and more anterior portions of the STN tended to be connected with more

anterior brain regions. However, in the superior-inferior (z-axis) direction, unlike the general trend in the PPN, the STN regions connected to the cortex tended to be more superiorly located than regions connecting to other brain areas. When examining topography trends across planes, STN regions connected to the dPMC and SMA tended to be segregated from the STN regions connected to the motor cortex. STN regions connected to the GP, mid-cerebellum, SN, and PPN were located closely together (within the same half of the seed mask in a given plane) in the inferior and medial STN. However, the STN region connected to the thalamus was distinctly segregated, located superior and posterior to the STN regions connecting to other sub-cortical regions (Fig. 2.8).

As in the PPN, there were also differences in the volume of the STN connecting to each of these regions. The portions of the STN connecting to the thalamus and mid-cerebellum were larger than the STN portions connecting to any other brain region. The portion connecting to M1-hind was smallest (Fig. 2.9A). This size ordering altered after correcting for the target structure size. When comparing these corrected STN volumes, the largest portion of the STN was found to connect with the PPN, followed by the SN and GP. The smallest STN portions connected with the mid-cerebellum and SMA (Fig. 2.9B).

The paths of connections between the STN and cortex also differed depending on the cortical region (Table 2.4). The routes between the STN and cortex passed via the internal capsule and almost all of them also passed through the SN and/or the thalamus. The only tract to not pass through the thalamus or the basal ganglia was the one between the STN and the SMA.

Table 2.3. STN Connections Across All Subjects

Brain Regions		*1L*	*1R*	*2L*	*2R*	*3L*	*3R*	*4L*	*4R*	*5L*	*5R*	*6L*	*6R*	*7L*	*7R*	*8L*	*8R*	%
Cortex	PFC	X	X			X										X	X	31.25
	dPMC	X	X		X	X		X	X		X		X			X	X	62.50
	SMA	X			X				X	X	X		X			X	X	50.00
	M1-Hind		X			X		X	X	X			X	X		X	X	56.25
	M1-Trunk	X	X		X	X	X	X		X	X	X		X	X		X	75.00
	M1-ForeU	X	X	X	X		X	X	X	X	X	X	X	X	X	X		87.50
	M1-ForeL		X	X	X			X			X					X		37.50
	M1-Orof		X			X	X						X			X		31.25
Basal Ganglia	Thalamus	X	X	X	X	X	X	X	X	X	X	X	X	X	X	X	X	100.00
	GP	X	X	X	X	X	X	X		X	X	X	X	X	X	X	X	93.75
	SN	X		X	X	X	X	X	X	X	X	X	X	X	X	X	X	93.75
PPN		X	X	X		X	X	X	X	X	X	X	X	X	X	X		87.50
Cerebellum		X		X		X	X		X	X	X		X		X	X	X	68.75
Spinal Cord		X	X		X	X	X			X		X	X			X	X	62.50

1L/1R: Subject ID Left/Right STN; X: Regions connected to the indicated STN as determined from a single STN seed voxel; %: Percentage of STNs, out of the 16 STNs examined, that are connected to the indicated brain region.

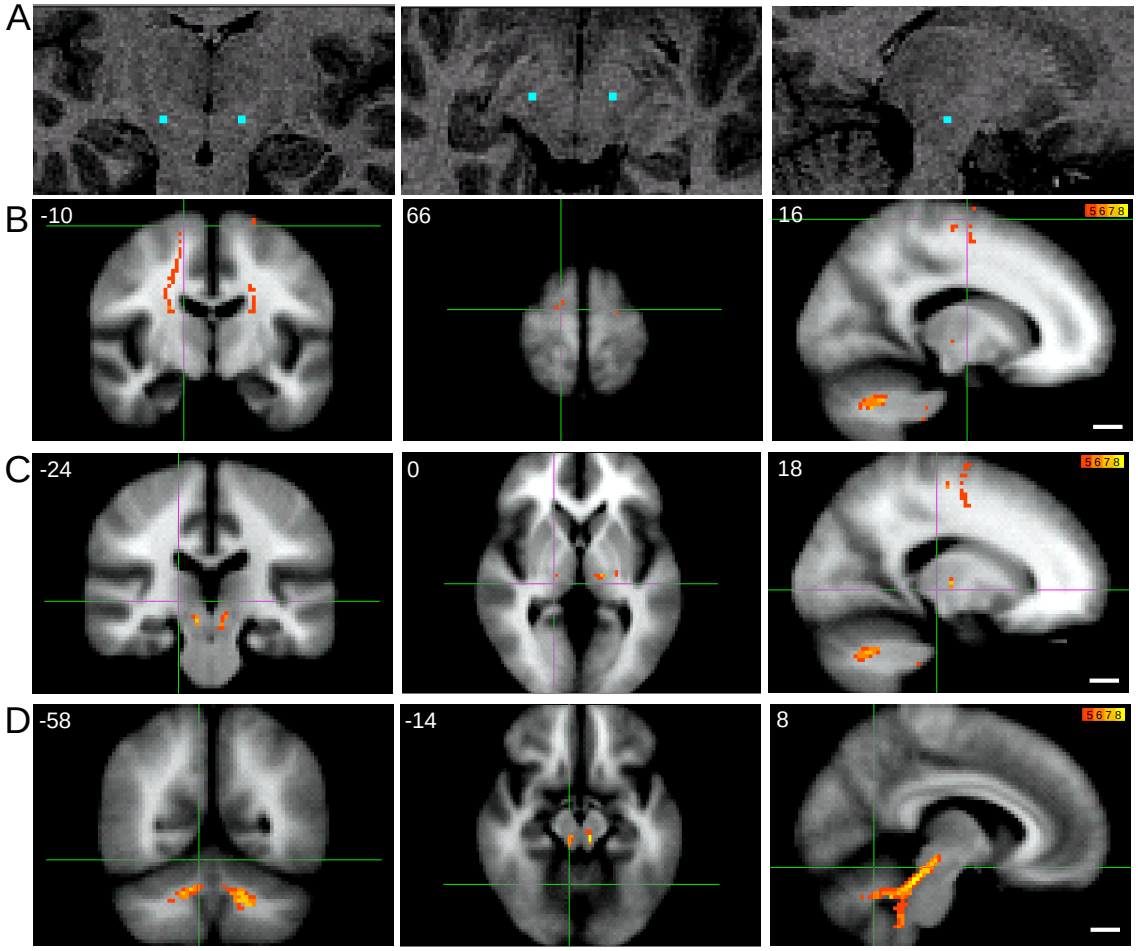

Figure 2.7. Regions with highest connectivity to the STN as determined from a single seed voxel located within the STN in each hemisphere. A) Localization of PPN seed voxel (2x2x2 mm^3, selected in diffusion space) is indicated bilaterally by blue squares on a T1-weighted structural image. B-D) Tracts are thresholded to include projections present in only 4 or more of the 8 subjects. The color of the tract indicates the number of patients with STN projections running via a given voxel (as shown in the color scale in the upper right corner of each row). Each row shows slices that intersect at the voxel location indicated by the green crosshairs. The MNI coordinate of each slice is also shown in the upper left corner of each figure. White bars at the lower right hand corner of each row show a 1 cm scale for the figures in that row. B) Connectivity between the STN and the motor cortex, SMA, and dPMC. C) Connectivity between the STN and the GP, thalamus, and SN. D) Connectivity between STN and the PPN, mid-cerebellum, and spinal cord.

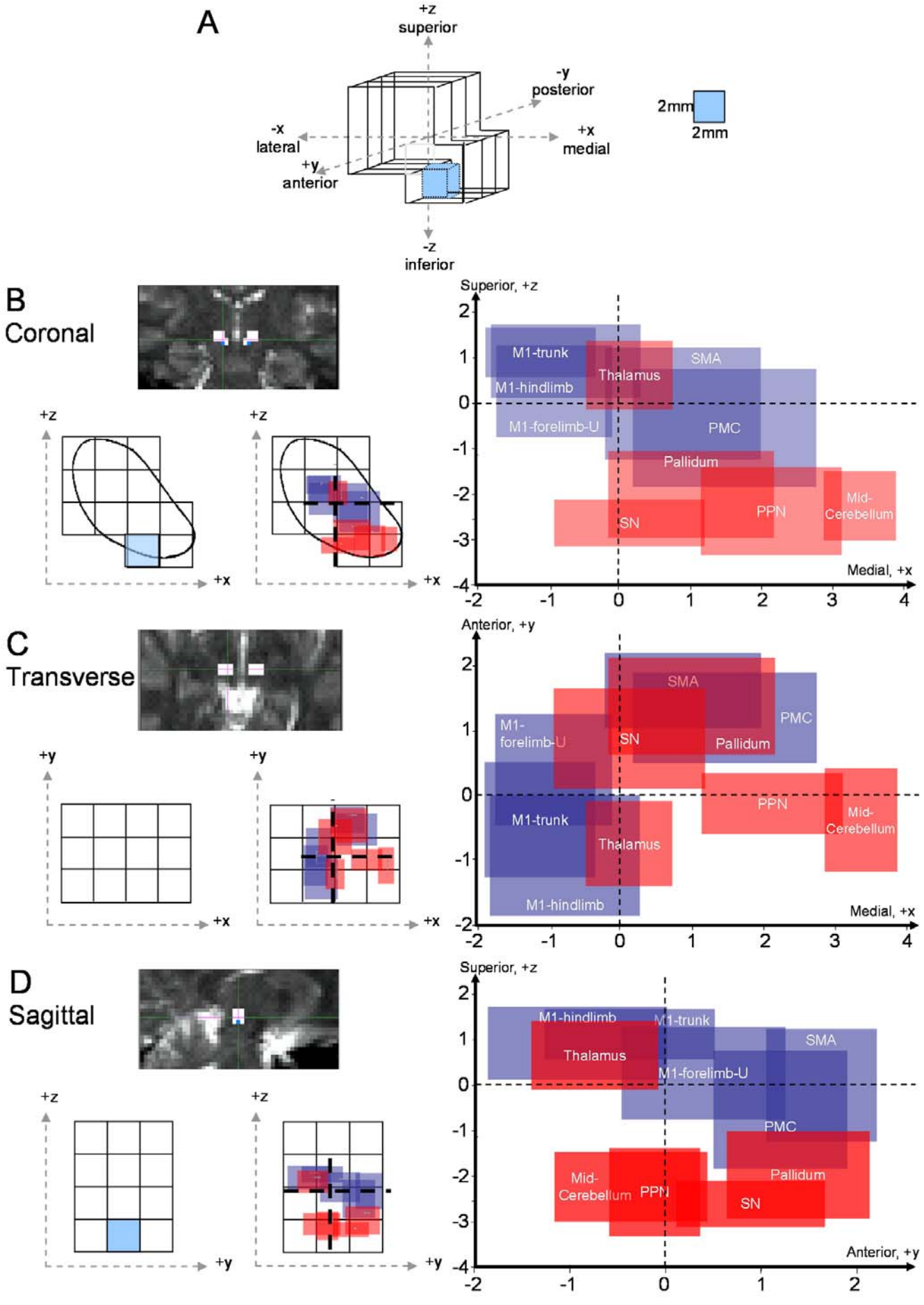
A
+z
superior
-y
posterior
-x
lateral
+x
medial
+y
anterior
-z
inferior
2mm
2mm
B
Coronal
+z
+x
+z
+x
Superior, +z
M1-trunk
SMA
Thalamus
M1-hindlimb
M1-forelimb-U
PMC
Pallidum
Mid-
Cerebellum
PPN
SN
Medial, +x
C
Transverse
+y
+x
+y
+x
Anterior, +y
SMA
PMC
M1-
forelimb-U
SN
Pallidum
PPN
Mid-
Cerebellum
M1-trunk
Thalamus
M1-hindlimb
Medial, +x
D
Sagittal
+z
+y
+z
+y
Superior, +z
M1-hindlimb
M1-trunk
SMA
Thalamus
M1-forelimb-U
PMC
Pallidum
Mid-
Cerebellum
PPN
SN
Anterior, +y

Figure 2.8 (on previous page). Topography within the STN. A) Schematic of the 36-voxel STN seed mask. The light blue cube shows the location of the single seed voxel used for the determination of the regions of highest connectivity to the STN (Fig 2.7). B-D) Seed mask location and topography in the coronal, transverse, and sagittal planes. An outline of the STN is shown overlaid on the seed mask in the coronal view (A). The left half of each row shows the location of the seed mask in a DTI image in diffusion space (top), a schematic of the seed mask in the given plane (bottom far left), and the topography in that plane (bottom right). The image on the right zooms in on the areas of highest connectivity as shown in the smaller topography image on the left side of each row. The axes show distance in mm relative to the midpoint of the STN seed mask, located at 0 mm on each axis. Each red or blue box is centered at the STN voxel location with the highest probably of connection to the indicated brain region, as determined from the average location across all 8 subjects. The width and height of each box show a 95% confidence interval range, across all subjects, for the STN voxel location (Fig. 2.3).

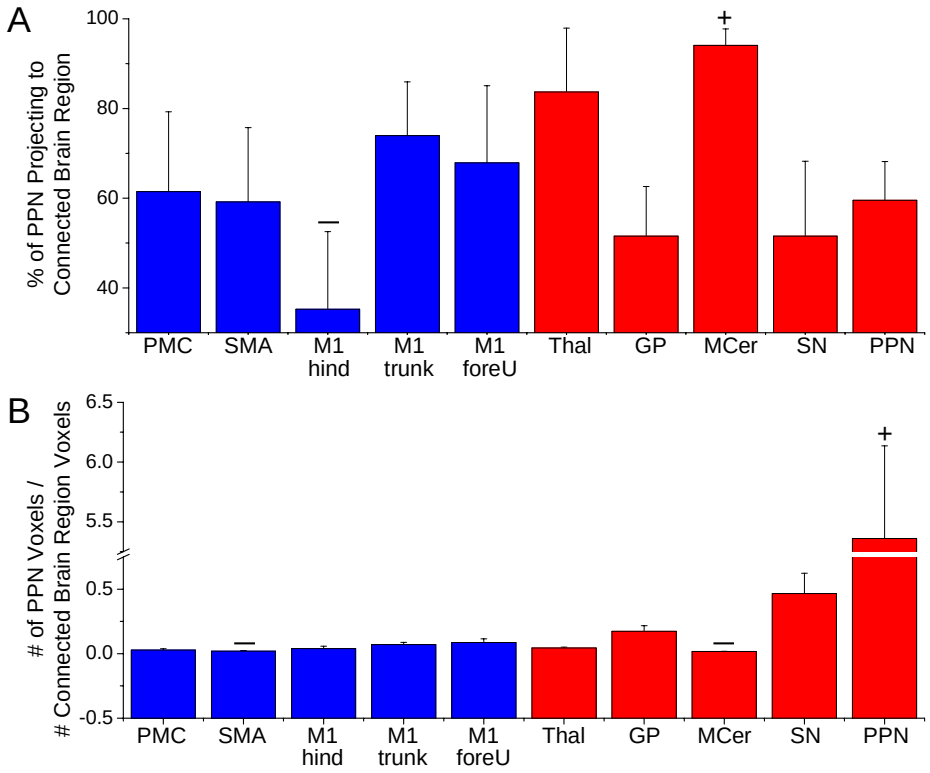

Figure 2.9. Volume of the STN connected with different brain regions. A) Each bar shows the mean (± SE, across all 8 subjects) percent of the STN connected to a given brain region (STN voxels with any probability of connection to a given brain region / total number of STN voxels). B) The mean percent of the STN connected to a brain region normalized to the size of that connected region (STN voxels with any probability of connection to a given brain region / total number of voxels in that brain region). +: largest STN portion projecting to a given region ($p<0.05$); —: smallest STN portion projecting to a given region ($p<0.05$).

Table 2.4. Paths of Connections between the STN and Cortex

Areas of Passage		dPMC	SMA	M1-hind	M1-trunk	M1-fore-U
Motor Cortex	M1-hind			X		
	M1-trunk				X	
	M1-fore-U				X	X
	M1-fore-L					
Other Cortical Areas	dPMC	X				
	SMA	X	X			
Basal Ganglia	Thalamus			X	X	X
	GP					
	SN	X			X	X
PPN				X	X	X

Columns: the path of a connection between the PPN and the indicated cortical area. X: Area of the brain through which the indicated connection passes.

2.1.4 Discussion

2.1.4.1 Methodological considerations

There are several methodological issues that should be considered in interpreting the tractography results presented here. First, diffusion tractography does not allow us to differentiate between anterograde and retrograde pathways, inhibitory and excitatory connections, and direct versus indirect routes. Second, the probabilistic diffusion algorithms used for tractography in this study assume only a single anistropic water diffusion direction, and thus only a single direction of inferred fiber orientation, in each 8 mm^3 voxel. Therefore, tractography is sensitive primarily to large fiber pathways – smaller pathways, or those through regions of fiber crossing or complexity may not be detected with the methods used here. This may have reduced our sensitivity to pathways travelling to lateral parts of the motor strip. Recently developed models that allow for modelling of multi-fiber populations (Hosey *et al.*, 2005; Parker and Alexander, 2005; Behrens *et al.*, 2007) may improve

tracing to these areas and could be used to interrogate these connections in the future. Third, the brainstem can suffer from distortions due to susceptibility gradients; in our data acquired at 1.5 Tesla, however, such distortions were not substantial and it should be noted that previous diffusion studies have successfully traced pathways from nearby brainstem regions (Stieltjes *et al.*, 2001; Sillery *et al.*, 2005; Muthusamy *et al.*, 2007). Finally, the probability of tracing a pathway between two points will be influenced by factors other than the true existence of an anatomical connection – for example, longer or more tortuous paths are less likely to be traced, although the topographic distribution of connections is less likely to be influenced by factors such as distance to the target (Le Bihan *et al.*, 2006).

2.1.4.2 Human PPN and STN connections largely match connections previously shown in non-human primates

Table 2.5 lists the PPN and STN connections determined in this section using diffusion tractography and compares them to the PPN and STN connections determined previously using tracing techniques. In humans, both the STN and PPN exhibit connections with the cortex, basal ganglia, cerebellum, and descending connections via the brainstem to the spinal cord. As expected, the paths between the STN and its major targets passed through more basal ganglia nuclei more frequently than did the paths of PPN connections (Pahapill and Lozano, 2000; Hamani *et al.*, 2004).

Table 2.5. Comparison of Human and Animal PPN and STN Connectivity

Connected Brain Regions		Animal PPN (Trace)		Human PPN (DTI)	Animal STN (Trace)	Human STN (DTI)
		Rat	Primate			
Cortical Areas	Motor Cortex		X	X	X	X
	PMC	X	X	X	X	X
	SMA	X	X	X	X	X
Basal Ganglia	Thalamus	X	X	X	X	X
	GP	X	X	X	X	X
	SN	X	X		X	X
	STN	X	X	X	X	X
PPN		X		X		X
Cerebellum		X	X	X	X	X
Spinal Cord		X		X		X

X: regions showing strong connections to the PPN or STN as determined in humans in this DTI study or as determined previously in animals using tracing techniques. Trace: connections indicated were determined previously using conventional anatomical tracing techniques. DTI: connections indicated were determined using DTI in this Section. Connections in animals characterized as "sparse" or "scant" in the review literature were not included (Lee *et al.*, 2000; Matsumura *et al.*, 2000; Pahapill and Lozano, 2000; Hamani *et al.*, 2004).

The major connections of the human PPN determined using diffusion tractography are similar to those seen in lower primates, except that a strong connection between human PPN and the SN was not found. This may represent a key difference between PPN anatomy in humans and lower primates, or may reflect limitations in our tractography approach. Projections from the SN to the PPN arborize extensively in the PPN (Scarnati *et al.*, 1984; Rye *et al.*, 1987; Spann and Grofova, 1991) and it is possible that, as discussed in Section 2.1.4.1, this arborization limits the ability of DTI to detect the connection between these structures. In addition to demonstrating PPN connections with the basal ganglia, a PPN connection in humans was found to extend caudally to the spinal cord, a connection that has been demonstrated in rodents but only suspected in primates (Lee *et al.*, 2000; Matsumura *et al.*,

2000; Pahapill and Lozano, 2000). In addition to largely matching the PPN connections in monkeys, these results also replicate those of our previous study describing PPN connections in humans using diffusion tractography.

The major connections of the human STN are also very similar to those shown in animal studies except for the presence of mid-cerebellum and spinal cord connections with the human STN (Table 2.5). Furthermore, though animal studies have shown the GP to have the strongest connection with the STN, based on the volume of the human STN projecting to each of its major targets in this study, the human STN seems to have the strongest connection with the mid-cerebellum and thalamus. Nevertheless, once normalized to the size of the connected brain region, the second largest volume of the STN is connected with the GP, while the largest volume of the STN connects with the PPN. Given this strong interconnection between the STN and PPN, it is possible that collaterals from a projection between these two nuclei manifest as the cerebellar and spinal cord connections observed with the human STN in this study.

2.1.4.3 Human STN topography matches topography previously shown in animals

The topography of STN connections with motor and associative brain regions determined in this study exhibits strikingly similar organization to previous reports of STN topography from rodent and non-human primate studies (Parent and Hazrati, 1995b; Shink *et al.*, 1996; Joel and Weiner, 1997; Hamani *et al.*, 2004). In all these species, motor cortical regions (M1, SMA, and

dPMC) all connect to the most superior portion of the STN, while associative regions are connected to the inferior and medial portions of the STN.

It is possible that thalamic fibers running along the superior border of STN may have been included in the tractography seed mask, and this may explain why the STN area connected to the thalamus appears to be segregated from the STN areas connected to other associative regions. Nevertheless, diffusion tractography demonstrates that the connections and topography of the human STN largely matches that shown in animal studies. This further validates the technique and demonstrates its sensitivity.

2.1.4.4 Demonstration of the existence of PPN topography in humans

Human PPN connections displayed a clear topographical organization within the nucleus with respect to cortical and sub-cortical areas. Previously, one study in non-human primates reported that PPN connections with M1-orof, M1-fore-U and M1-fore-L, and M1-hind extend, in that order, from the medial to lateral areas of the nucleus, while projections to the dPMC and SMA are restricted to the middle of the nucleus (Matsumura *et al.*, 2000). In contrast to the monkey anatomy, the PPN topography in human subjects displayed little medial to lateral distinction between the different areas of the human PPN projecting to the cortex. However, motor and associative areas of the human PPN were separated, with connections to motor cortical areas located in the most lateral portion of the superior PPN.

In addition to the cortical PPN topography, these results are the first to demonstrate that PPN connections with sub-cortical brain regions are topographically organized. The PPN connections with the thalamus, mid-

cerebellum, and STN were primarily located in the medial, posterior, and superior eighth of the PPN. Interestingly, the GP connections were located in the opposite corner of the PPN, in the lateral, anterior, and inferior eighth. This is a part of the PPN seed mask relatively far away from the GP itself, suggesting that this segregation of GP connections is probably not due to the inclusion of GP fibers in the PPN seed mask but is an accurate depiction of PPN topography.

2.1.4.5 Functional implications in humans

Cortical stimulation has been tried as an experimental therapy for PD and has been shown to ameliorate bradykinesia, tremor, and akinesia, although not to the extent observed with DBS of the PPN or STN (Fregni *et al.*, 2005; Helmich *et al.*, 2006). Cortical stimulation does, however, have effects on a wider range of PD symptoms than does DBS of the PPN or STN alone (Fregni *et al.*, 2005; Helmich *et al.*, 2006). The strong cortical connections observed with both the PPN and STN in this section may help explain the therapeutic effects of cortical stimulation. Interestingly, the distinct differences between the paths of tracts connecting the PPN and STN with the cortex, as shown by DTI, suggest that direct cortical connections with these nuclei may exist in humans. The tracts between the PPN and M1-trunk and M1-fore-U largely bypass the basal ganglia, indicating the possibility of a hyperdirect pathway between the PPN and cortex. The tract between the STN and the SMA also bypasses the basal ganglia, suggesting that the hyperdirect pathway between the cortex and STN shown in non-human primates is also present in humans (Hamani *et al.*, 2004).

Perhaps our most striking finding, however, is that the strongest connections of the PPN and STN appear to be between each other, when normalized to the size of the connected region. Noting that neither the directionality nor sign of this connection can be inferred from DTI analysis and that the proximity of the PPN and STN to each other may play a large role in the strong connection between the two nuclei, it is still very likely that there is a robust interconnection between the human PPN and STN. This suggests that electrical stimulation of one of these nuclei during DBS should greatly affect activity in the other nucleus. Furthermore, since their interconnection is so strong, the differences in symptom alleviation seen with DBS of the PPN and DBS of the STN cannot be primarily attributed to differences in PPN and STN connections, though this may play some role.

2.1.4.6 Concluding remarks

These results are the first to demonstrate topographic organization of cortical and sub-cortical connections of STN and PPN in the human brain. Our data confirm that the STN topography found in animals is also present in humans. This provides validation of the accuracy of diffusion tractography in determining the topography of small gray matter structures, such as the STN and PPN. These results also demonstrate that topography exists in the human PPN and that there is a distinction between PPN areas connected to cortical and sub-cortical structures.

As aforementioned, it is important to confirm that diffusion tractography results in humans can be reproduced in other species. This is especially true in the case of the PPN, a structure whose connections differ greatly across

species (Lee *et al.*, 2000; Pahapill and Lozano, 2000). Studies examining the connections and topography of the STN and PPN in non-human primates can be compared directly to the results of anatomical tracing studies. This could further validate the use of diffusion tractography to non-invasively determine the connections and topography of small gray matter structures as has been done here for the human PPN and STN.

2.2 Anatomy of the PPN in a normal primate (*Macaca mulatta*) brain

2.2.1 Introduction and rationale

The techniques used to determine PPN connections in previous studies—anterograde and retrograde tracers, evoked-potential studies, and immunohistochemistry—have several advantages for the study of neuroanatomy, especially when used in combination. They allow for differentiation between chemically heterogenous neuronal populations, accurate confirmation of tracing origin via sectioning of tissue and examination of injection site location, and the determination of projection directionality. However, although these tracing methods provide valuable information about the functionality of connections between different brain structures, they also have several disadvantages. First, it is difficult to do tract tracing while still obtaining the cellular details of the traced neurons as tract tracing generally requires large tracer injection volumes to ensure that the tracer signal does not fade over long fiber distances (Vercelli *et al.*, 2000). Newer methods of tract tracing using neurotropic viruses (e.g. rabies) circumvent this problem as the virus signal is amplified in each infected neuron, but these tracing methods are

highly dependent on the injected virus concentration and come with a host of safety issues (Kelly and Strick, 2000). Second, it is difficult to detect the connections of several different structures within the same brain when each injection site induces some neuronal damage or when using tracers like biotinylated dextran amine that are known for their labelling permanence (Reiner *et al.*, 2000). Third, few tracers work well in fixed tissue, and those that do (e.g. lipophillic carbocyanine dyes) diffuse very slowly through fixed tissue and thus require several weeks to complete a tracing experiment (Vercelli *et al.*, 2000). Finally, as these procedures are invasive and require post-mortem histological analysis, they clearly cannot be carried out *in vivo* in humans.

Probabilistic diffusion tractography enables tracking of probable fiber pathways between cortical and sub-cortical gray matter structures *in vivo* (Behrens *et al.*, 2003a; Johansen-Berg *et al.*, 2005; Sillery *et al.*, 2005; Aravamuthan *et al.*, 2007; Muthusamy *et al.*, 2007). However, unlike histological tracing techniques, probabilistic methods for diffusion tractography (Parker *et al.*, 2003; Behrens *et al.*, 2003b) cannot determine the direction of projections between brain regions, nor whether they are interrupted by synapses.

Section 2.1 demonstrates the use of diffusion tractography to trace connections of the PPN in healthy human subjects. These results show that PPN connections in humans are similar to those traced in lower primates, including descending connections with the spinal cord. However, the organization of PPN connections differed from what has previously been described in monkeys. For example, Matsumura *et al.* (2000) reported that the medial PPN connected with the ventral M1 whereas the lateral PPN was

connected with the dorsal M1; but this did not seem to be the case in humans. Instead, human PPN connections with the motor cortex overlapped greatly in the lateral and dorsal PPN. In addition, though no segregation of PPN connections with sub-cortical regions has been observed in animals, human PPN regions connected with sub-cortical brain structures were shown to be significantly segregated from each other. These differing results illustrate the importance of verifying the existence of PPN connections across different species using the same methodological techniques.

In this study, the connections of the PPN and the organization of these connections within the PPN are examined in a post-mortem *Macaca mulatta* brain using diffusion tractography. To demonstrate the use of diffusion tractography as a non-invasive anatomical tracing technique, PPN connections determined using diffusion tractography are compared to the connections determined previously in anatomical tracer and evoked-potential studies. We also compare the organization of monkey PPN connections with those obtained using diffusion tractography in humans to determine differences in the role of the PPN across species.

2.2.2 Methods

2.2.2.1 Brain extraction and fixation

One male macaque (*Macaca mulatta*, 9 years old) was used in this experiment. The studies were conducted under project and personal licences issued by the British Home Office and in accordance with the British Animal Scientific Procedures Act (1986). The animal was deeply anesthetized with a lethal dose of sodium pentobarbitone (80 mg/kg, i.v.). Immediately after cardiac arrest, the

animal was perfused transcardially with 90% normal saline and 10% formalin. The brain was removed whole and kept in 10% sucrose formalin until imaging. For imaging purposes, the brain was immersed in Fomblin LC/8 (Solvay Solexis Inc., Brussels, Belgium) and tightly secured in a close-fitting plastic container.

2.2.2.2 Image acquisition

Images were acquired using a 3T clinical MR scanner with 4 channel-carotid coils for signal reception. Post-mortem diffusion imaging is extremely difficult (particularly with the limited gradient strengths of a clinical scanner) because *ex vivo* tissue exhibits more rapid signal decay and lower diffusion rates compared to *in vivo* tissues (Sun *et al.*, 2003; Pfefferbaum *et al.*, 2004; Yong-Hing *et al.*, 2005; D'Arceuil *et al.*, 2007). The size differential between human and macaque brains also places high demands on the resolution required to visualize homologous structures between the two species. For these reasons, a custom pulse sequence was implemented and optimized for the purposes of high resolution, post-mortem diffusion imaging (D'Arceuil *et al.*, 2007). The pulse sequence was a 3D diffusion-weighted twice-refocused spin-echo with a segmented echo planar imaging read-out (TE/TR = 111/690 ms, 70° excitation pulse, b=3000 s/mm^2, 60 directions x 5 averages, b=0 x 40 averages, BW = 806 Hz/pixel, maximum gradient strength = 40mT/m, matrix size = 104 x 132 x 96, 720 μm isotropic voxels (without interpolation), 21 lines per readout, 5/8 partial Fourier, 34 hours total scan time). Averaging was carried out offline to ensure that there were not any artifactual differences between image acquisitions.

2.2.2.3 Image pre-processing and determining regions strongly inter-connected to the PPN

The PPN seed location was determined relative to the superior cerebellar decussation on the RGB representation of the principle diffusion estimate at each voxel (Stieltjes *et al.*, 2001) (Fig. 2.10B). These seed voxel locations were confirmed to be within the PPN by a licensed neurosurgeon (TZ).

Using FMRIB's Diffusion Toolbox (FDT, www.fmrib.ox.ac.uk/fsl), fiber tracking was initiated from the PPN single voxel seed in each hemisphere (200,000 streamline samples, step length of 0.2 mm, curvature threshold of 0.0, excluding connections crossing into the contralateral hemisphere). The curvature threshold was reduced from the adult human brain default value of 0.2 and the step length was reduced from the adult human brain default value of 0.5 mm (Section 2.1) to allow for the tracking of long-distance fiber connections between the brainstem and cortex in the lower resolution diffusion data (when comparing voxel size to brain size) acquired from the smaller (relative to the adult human) *Macaca mulatta* brain. Areas displaying connections with the single voxel seed (black voxel, Fig. 2.10B) were determined from the diffusion scan after thresholding tracts to 99% of the total number of samples in the path distribution estimate. For a more detailed account of these methods, please see Sections 2.1.2.3 and 2.1.2.4.

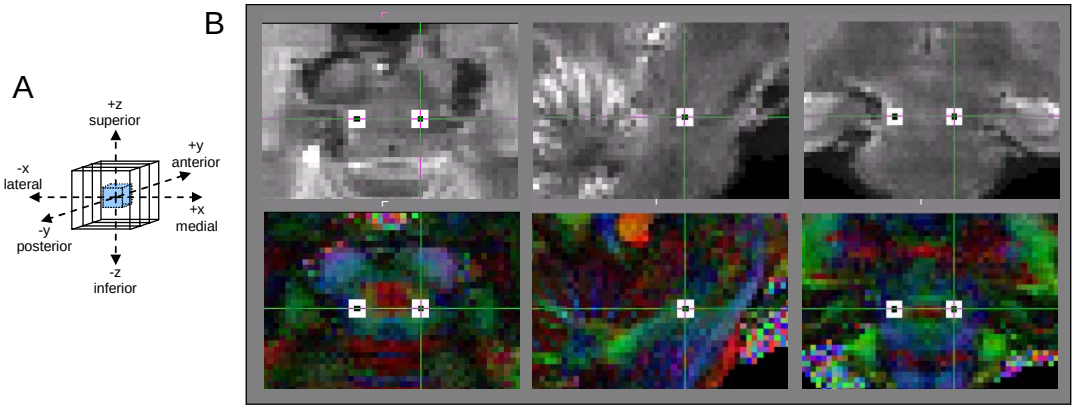

Figure 2.10. Localization of the PPN in the *Macaca mulatta* brain. A) Schematic of the 27-voxel PPN seed mask. The light blue cube shows the location of the single seed voxel (0.72x0.72x0.72 mm^3) used for the determination of the regions of highest connectivity to the PPN (Fig. 4A). B) From left to right, the PPN seed mask is shown in the transverse, sagittal, and coronal planes. The single seed voxel is shown in black. The green crosshairs intersect at the same voxel in all images. The top row shows the mask on a non-diffusion weighted image (i.e. *b*=0) while the bottom row shows the masks over the red-green-blue (RGB) representations of the principal diffusion estimate with the image intensity modulated by fractional anisotropy (which quantifies the strength of local tract structure directionality). In the RGB images, the superior cerebellar decussation is clearly visible as a bright red area in the center of the brainstem.

2.2.2.4 Creating anatomical masks of inter-connected regions

Masks were drawn bilaterally of the cortical and sub-cortical regions with the highest probability of connection with the monkey PPN on the non-diffusion weighted image (i.e. *b*=0) based on visible anatomical landmarks and with reference to a *Macaca mulatta* brain atlas (Martin and Bowden, 2000). The STN was located at the level of the dorsal-most transverse slice showing the red nucleus (which appeared lighter in color than did the surrounding tissue), medial to the SN, in the middle of the cerebellar peduncle (Fig. 2.11). The

thalamus, GP, and SN were clearly visible on the diffusion image as regions colored darker than the surrounding tissue (Fig. 2.11). Somatotopic divisions of the M1 were estimated as percentages of the precentral gyrus based on the motor homunculus. These divisions, from medial to lateral are: hindlimb and hips, 7.5%; trunk region, 17.5%; forelimb, 15%; wrist and hand, 30%; neck and orofacial region, 30% (Fig. 2.12A). The SMA and the dPMC were located just rostral to the precentral sulcus on the medial and lateral brain surface, respectively. The M1 orofacial region was further subdivided into 5 masks that separated dorsal from ventral portions (Fig. 2.12B). The border between the SMA and the dPMC was set at the same position, mediolaterally, as the border between the M1 trunk and M1 forelimb regions. The lateral/ventral border of the dPMC was at the same position, mediolaterally, as a transverse plane through the midpoint of the M1 wrist and hand region (Fig. 2.12).

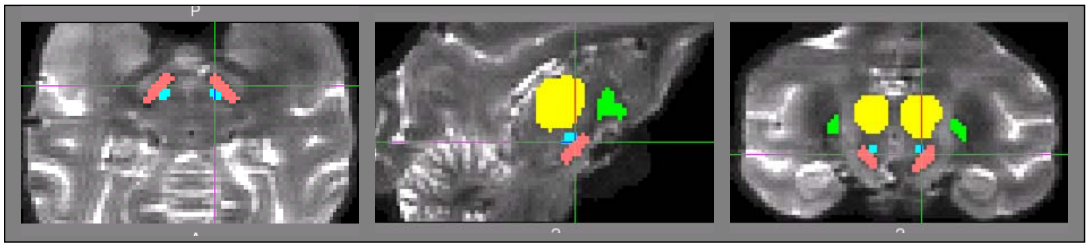

Figure 2.11. Masks of the basal ganglia. Masks of the basal ganglia are drawn on the non-diffusion weighted image (i.e. *b*=0). The green crosshairs intersect at the same voxel. From left to right, transverse, sagittal, and coronal slices are shown. Thalamus (yellow); GP (green); SN (pink); STN (blue).

2.2.2.5 Determining the organization of PPN connections

To investigate the organization of anatomical connections from each nucleus, we created seed masks, surrounding the PPN single voxel seeds described above (Fig. 2.10A). The PPN mask was drawn as a region 3x3x3 voxels (~10 mm^3) in size. As estimated from a *Macaca mulatta* brain atlas (Martin and Bowden, 2000), the size of the *Macaca mulatta* PPN is approximately 9 mm^3. Effort was made to make the seed mask size large enough to allow sufficient space for inferring the organization of PPN connections and to allow for clear discernment between areas that preferentially connect with different brain regions. However, in order to avoid including fibers from the xscp in the seed mask, the relative size of the PPN seed mask drawn for the *Macaca mulatta* brain (comparable to the size of the *Macaca mulatta* PPN) was smaller than the relative size of the seed mask drawn for the human subjects (about 30% larger than the size of the human PPN) (Section 2.1). Tractography was run from every voxel inside these seed masks and the co-ordinates of the voxel within each seed mask with the highest probability of connection to a given brain region was determined. As only one *Macaca mulatta* brain was available for this study, no statistical analyses were conducted.

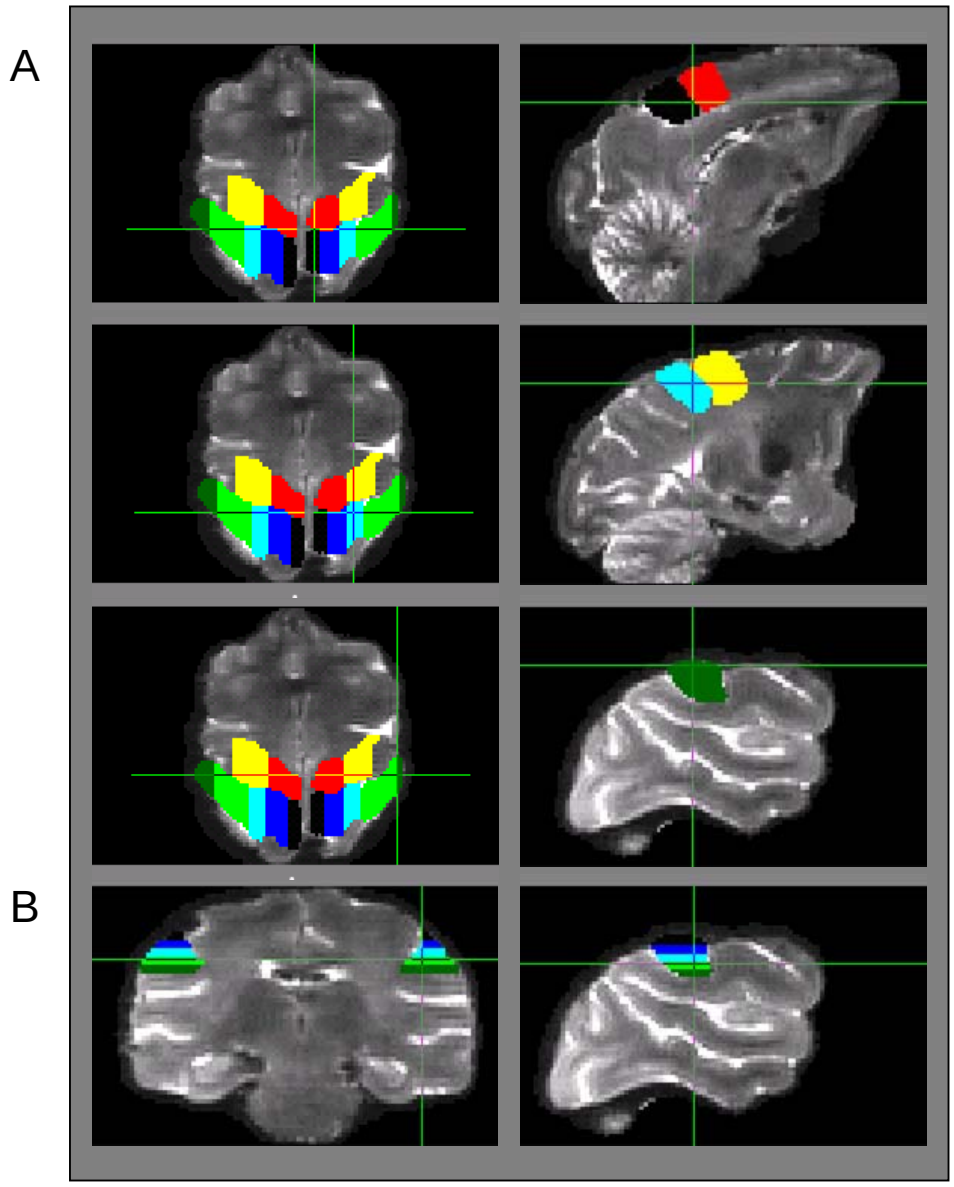

Figure 2.12. Masks of cortical regions. Masks of cortical regions are drawn on the non-diffusion weighted image (i.e. *b*=0). The green crosshairs intersect at the same voxel in each row. The left column shows a transverse slice through all cortical regions and the right column shows sagittal slices. A) Primary motor cortex regions: hindlimb (black), trunk (dark blue), forelimb (light blue), wrist and hand (light green), orofacial (dark green); supplementary motor area (red); dorsal premotor cortex (yellow). B) The M1 orofacial region is segmented further in the dorsal-ventral direction into five masks (ranging in color from most dorsal to most ventral: black, dark blue, light blue, light green, and dark green). The left image shows a coronal slice and the right image shows a sagittal slice through the monkey brain.

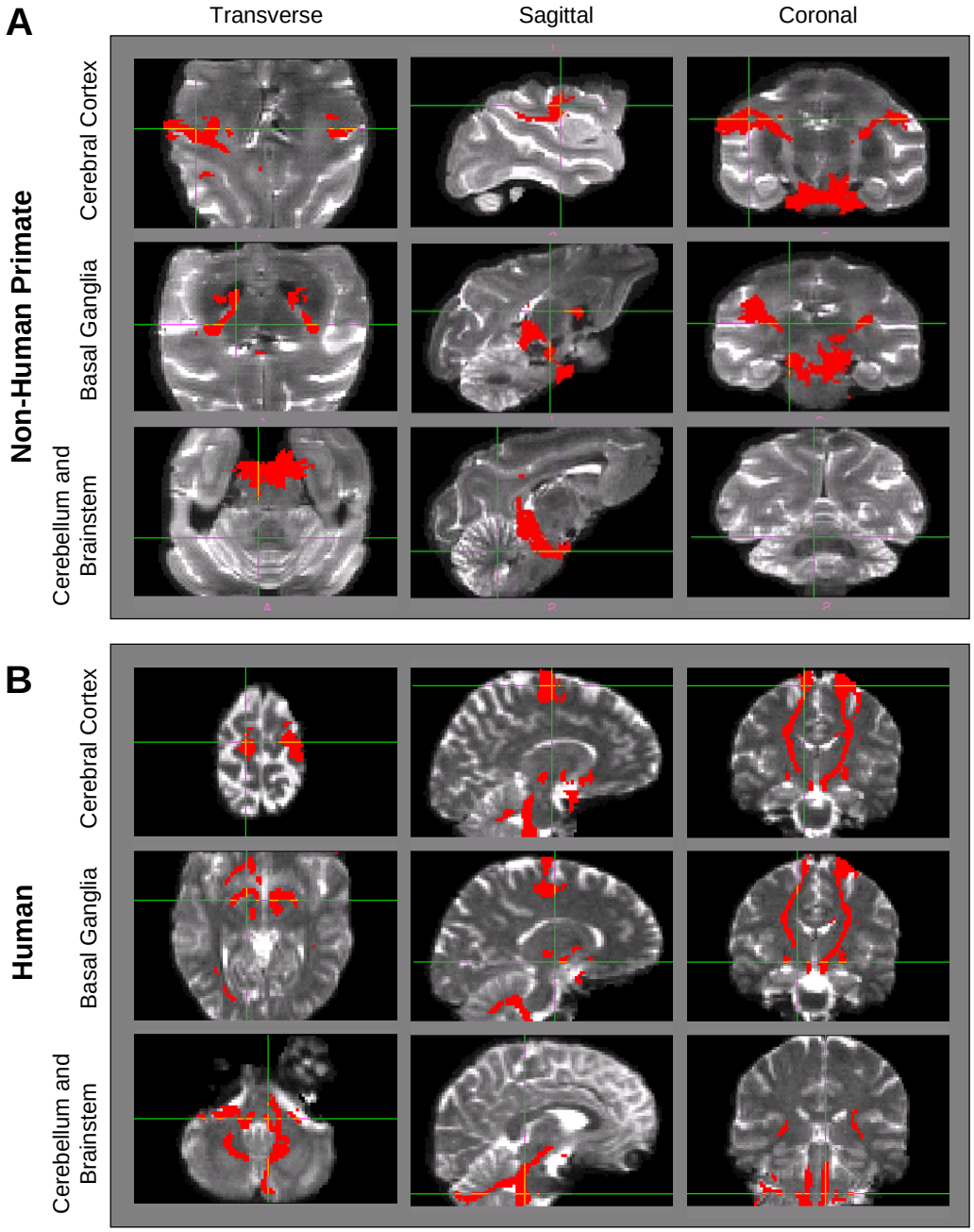

Figure 2.13. Regions with highest connectivity to the monkey and human PPN. Human data are shown for one subject and were acquired as previously described (Section 2.1; Aravamuthan *et al.*, 2007; Muthusamy *et al.*, 2007). Both monkey and human data show the results of tractography run from single voxel PPN seeds in each brain hemisphere with exclusion of tracts crossing to the contralateral hemisphere. Tracts are shown in red, thresholded to 99% of the total number of samples in the path distribution estimate and overlaid on the non-diffusion weighted image (i.e. *b*=0). Each row shows slices that intersect at the voxel location indicated by the green crosshairs.

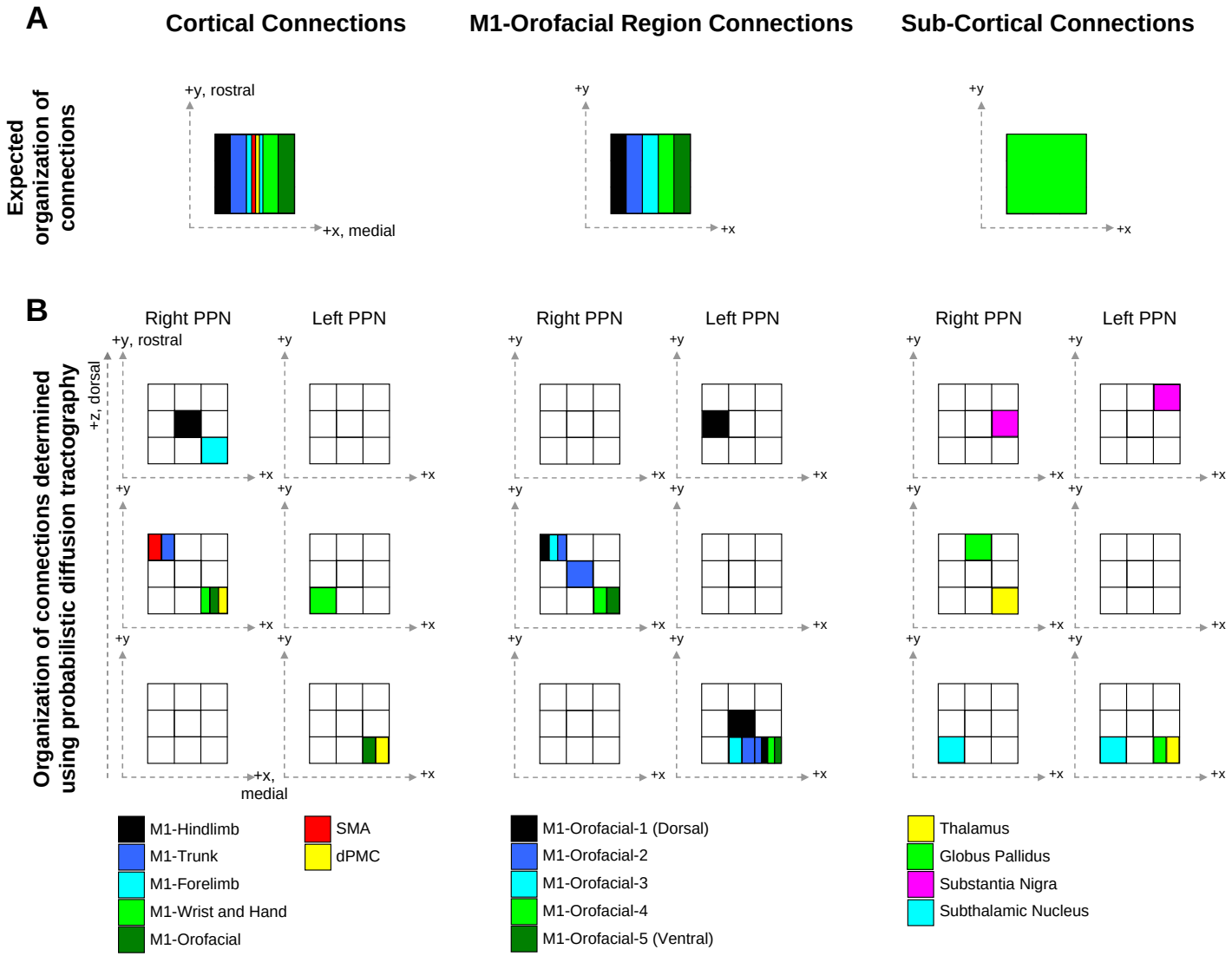
A
Cortical Connections
M1-Orofacial Region Connections
Sub-Cortical Connections
Expected organization of connections
+y, rostral
+x, medial
+y
+x
+y
+x
B
Organization of connections determined using probabilistic diffusion tractography
Right PPN
Left PPN
+z, dorsal
+y, rostral
+x, medial
M1-Hindlimb
M1-Trunk
M1-Forelimb
M1-Wrist and Hand
M1-Orofacial
SMA
dPMC
M1-Orofacial-1 (Dorsal)
M1-Orofacial-2
M1-Orofacial-3
M1-Orofacial-4
M1-Orofacial-5 (Ventral)
Thalamus
Globus Pallidus
Substantia Nigra
Subthalamic Nucleus

Figure 2.14 (on previous page). Organization of monkey PPN connections. In columns from left to right, the organization of PPN connections is shown separately for motor cortical regions, for specifically the orofacial region of the primary motor cortex, and for sub-cortical regions. A) The expected organization of monkey PPN connections is shown based on the results of previous anatomical tracing studies (Shink *et al.*, 1997; Matsumura *et al.*, 2000). B) Transverse slices through the PPN seed mask are shown, drawn as 3 voxel x 3 voxel squares. Within each slice in both (A) and (B), the voxel with the highest probability of connection to a given brain region is colored according to the keys at the bottom of each column. From top to bottom, slices are arranged from dorsal to ventral. Abbreviations: M1-primary motor cortex, SMA-supplementary motor area; dPMC-dorsal premotor cortex.

2.2.3 Results

2.2.3.1 Connections of the PPN

The PPN exhibited connections with the cerebral cortex and basal ganglia but not with the cerebellum or spinal cord (Table 2.6, Figs. 2.13A, 2.14). The cortical regions that showed connections with the right PPN were the dPMC, SMA, and with all M1 regions (Figs. 2.13A, 2.14), though only the dPMC, M1 wrist and hand, and M1 orofacial regions showed connections with the left PPN as well (Fig. 2.14). Sub-cortical connections of both the left and right PPN included the thalamus, GP, SN, and STN (Figs. 2.13A, 2.14).

2.2.3.2 Organization of PPN connections

Organization of PPN connections with both cortical and subcortical structures was evident in this brain. More dorsal portions of the M1 connected with the lateral aspect of the PPN while more ventral portions of the M1 connected with the medial PPN. This distribution was observed for the SMA, dPMC, across different M1 regions, and also within M1 regions as is shown for the M1 orofacial region (Fig. 2.14). Furthermore, organization of sub-cortical PPN connections was also observed. Though the locations of PPN regions with highest probability of connection to the GP were different between the left and

right PPN, connections with other sub-cortical structures did appear to have consistent topographical organization. The SN connects with the medial and dorsal PPN, the thalamus appears to connect preferentially with the medial and caudal portion of the PPN, while the STN has the highest probability of connection with the lateral, caudal, and ventral part of the PPN (Fig. 2.14).

Table 2.6. Comparison of Human and Monkey PPN Connectivity Determined Using Probabilistic Diffusion Tractography and Histological Tracing Techniques

Connected Brain Regions		Monkey PPN		Human PPN
		Conventional Tracing	PDT	
Cortical Areas	M1	X	X	X
	dPMC	X	X	X
	SMA	X	X	X
Basal Ganglia	Thalamus	X	X	X
	GP	X	X	X
	SN	X	X	
	STN	X	X	X
Cerebellum		X		X
Spinal Cord				X

X: regions showing strong connections to the PPN as determined in non-human primates using probabilistic diffusion tractography (PDT) in this study or as determined previously using histological tracing methods. Connections in animals characterized as “sparse” or “scant” in the review literature were not included. (Lee *et al.*, 2000; Matsumura *et al.*, 2000; Pahapill and Lozano, 2000; Aravamuthan *et al.*, 2007; Muthusamy *et al.*, 2007).

2.2.4 Discussion

These results have demonstrated that diffusion tractography can be used to probe the anatomical connections of the primate in a fixed post mortem *Macaca mulatta* brain. The PPN exhibited connections with the SMA, dPMC, and M1 all regions, though connections with the dPMC and the M1 wrist, hand,

and orofacial regions were most robust. The PPN was also connected with the thalamus, GP, SN, and STN. No connections between the PPN and the cerebellum or spinal cord were observed.

2.2.4.1 Monkey PPN anatomy determined using diffusion tractography compared to monkey PPN anatomy described previously

The connections of the monkey PPN determined in this study using diffusion tractography are nearly the same as those previously determined by histological techniques. However, though no connections between the PPN and cerebellum were observed using diffusion tractography, efferents from the DCN to the PPN have been described in one tracer study in the squirrel monkey (Hazrati and Parent, 1992b) (Table 2.6). It is possible that the cerebellar connections with the PPN are too extensively arborized to be effectively traced using a single voxel PPN seed. Also, as the spinal cord and brainstem were not completely intact in this brain, it is possible that the PPN connections with the brainstem, spinal cord, and cerebellum could not be traced due to tissue damage. The descending connections of the PPN are especially important to document as the PPN is thought play a role in locomotion independent of the dopaminergic pathways of the basal ganglia (Jenkinson *et al.*, 2006; Stefani *et al.*, 2007). Future study could involve running diffusion tractography from single seed voxels located in the DCN and determining whether connections with the PPN seed mask become evident. It is also possible that probing the connections of other single seed voxels within the PPN will yield evidence of connections between the PPN, cerebellum, and spinal cord.

Organization of cortical connections with the PPN appeared similar to that previously demonstrated in monkeys (Matsumura *et al.*, 2000) (Fig. 2.14A). In both the left and right PPN, connections with dorsal cortical regions are found more laterally in the PPN than are PPN connections with more ventral cortical regions (Fig. 2.14B). Matsumura *et al.* (2000) showed this explicitly for M1 as we have done (Fig. 2.14), but did not show this for PPN connections with the dPMC and SMA, which appeared to overlap in the mediolateral middle of the nucleus (Fig. 2.14A). Our results suggest that the more dorsal SMA projects laterally while the more ventral dPMC projects medially (Fig. 2.14B), though this requires confirmation in a larger number of brains. Furthermore, as Matsumura *et al.* (2000) showed for sub-regions of M1 (Fig. 2.14A), we have shown that dorsal portions of the M1 orofacial region connect with the lateral PPN while ventral portions connect with the medial PPN (Fig. 2.14B).

Finally, as discussed previously, organization of sub-cortical PPN connections has not been demonstrated though efferents from the internal segment of the GP to the PPN have been shown to project throughout the nucleus (Shink *et al.*, 1997) (Fig. 2.14A). Our results show less consistency in the location of PPN connections with the GP, relative to the location of PPN connections with other sub-cortical structures, and thus appear to confirm the work of Shink *et al.* (1997) showing that connections with the GPi are not necessarily restricted to one part of the PPN (Fig. 2.14B).

2.2.4.2 Monkey PPN anatomy compared to human PPN anatomy using diffusion tractography

Broad comparisons between human PPN anatomy and monkey PPN anatomy must be made tentatively as only one monkey brain was examined in this study. However, noting that the diffusion tractography algorithms previously used to examine human PPN anatomy (Aravamuthan *et al.*, 2007; Muthusamy *et al.*, 2007) are similar to those used to examine monkey PPN anatomy in this study, it is interesting to postulate possible differences between human and monkey PPN anatomy that may be elucidated via the use of diffusion tractography.

There are four main anatomical differences between the human PPN and the monkey PPN, as determined using diffusion tractography. First, the connections between the human PPN and M1 are primarily with the trunk and forelimb regions (Aravamuthan *et al.*, 2007; Muthusamy *et al.*, 2007) (Fig. 2.13B) while the connections between the monkey PPN and M1 are primarily with the wrist, hand, and orofacial regions (Fig. 2.13A). As the PPN plays a large role in locomotion in both humans and lower primates, the different demands of maintaining bipedal as opposed to quadrupedal gait may help explain these anatomical findings. Perhaps, the human PPN plays more of a role in maintenance of standing posture via control of the trunk and upper arm swinging during walking while the monkey PPN is more involved with modulation of stepping itself during quadrupedal gait via wrist and hand control. It is also possible that the monkey PPN connection with the M1 orofacial region signifies a greater role for the monkey PPN in maintaining balance via the control of head-trunk angles.

Second, confirmation of the connection between the PPN and SN in monkeys using diffusion tractography (Table 2.6, Fig. 2.13A) supports the accuracy of diffusion tractography and lends credence to the surprising finding that the human PPN does not have a strong connection with the SN (Aravamuthan *et al.*, 2007; Muthusamy *et al.*, 2007) (Table 2.6, Fig. 2.13B). This is also in accordance with the hypothesis that the main inhibitory drive to the PPN is likely from the GP and not from SN (Lee *et al.*, 2000).

Third, the human PPN exhibits descending connections while the monkey PPN does not (Table 2.6, Fig. 2.13). As aforementioned, the lack of monkey PPN connections with the DCN may be due to extensive arborization of cerebellar efferents throughout the PPN or due to brainstem tissue damage in the brain used. On the other hand, few studies have described descending PPN connections in monkeys at all (Hazrati and Parent, 1992b). Perhaps connections with the cerebellum and spinal cord are, in fact, stronger in the human PPN than they are in the monkey PPN. Repeating this study with a larger number of brains and with tracking initiated from the deep cerebellar nuclei is necessary to explore these hypotheses.

Finally, the organization of cortical connections is completely different between the human and monkey PPN. There is no mediolateral distribution of PPN connections with cortical regions in humans, though there is topographical distinction between cortical PPN connections (generally found in the lateral PPN) and sub-cortical PPN connections (found more medially in the PPN). This is in direct contrast to the cortical organization demonstrated in the monkey PPN, both in this study and previously (Matsumura *et al.*, 2000). However, since the organization of monkey PPN connections determined using diffusion

tractography in this study matches the organization previously documented using conventional anatomical tracing techniques, it is possible that the organization of human PPN connections determined using diffusion tractography could also be accurate. Perhaps the differences between the organization of human and monkey PPN connections can be attributed to a changing role for the PPN in maintaining bipedal as opposed to quadrupedal gait. However, since very few studies have described the organizaton of PPN connections at all, it is important to verify the results of this study with additional brains before drawing any further conclusions about the functional and anatomical differences between the human and monkey PPN.

2.2.4.3 Usefulness for the study of animal neuroanatomy

We have accurately determined the neuroanatomy of a relatively small gray matter structure from a fixed post-mortem *Macaca mulatta* brain. In addition to helping confirm the accuracy of diffusion tractography results obtained in humans *in vivo*, this finding also creates possibilities for the study of neuroanatomy in monkeys. As we have demonstrated here, the anatomy of several brain structures can be examined in a fixed post-mortem brain without destroying tissue integrity using diffusion tractography. In addition to increasing the number of animals available for neuroanatomical research, the use of diffusion tractography and post-mortem brains from a variety of animal species allows for greater study of comparative neuroanatomy and for a direct comparison with neuroanatomical data obtained from humans.

2.2.4.4 Concluding remarks

The post-mortem macaque diffusion tractography results presented in this section offer a bridge between the *in vivo* human diffusion tractography and animal tracer studies that have been carried out previously. Since the post-mortem macaque diffusion tractography agrees with both of the aforementioned data, it inspires confidence in the diffusion tractography methodology itself. Few studies have attempted to compare diffusion tractography results with other forms of tract tracing and it is critically important that diffusion tractography is validated before being adopted clinically. The post-mortem diffusion imaging results presented here, also demonstrate the potential for further study of animal neuroanatomy via the use of diffusion tractography in fixed post-mortem brains.

Main Findings

- *The connections of and topography of the human STN, the connections of the human PPN, and the connections and topography of the* Macaca mulatta *PPN, determined using DTI, largely match connections previously demonstrated in non-human primates using conventional anatomical tracing techniques.*
- *Topography in the human PPN determined using DTI differs from monkey PPN topography determined using either DTI or conventional tracing techniques. This difference in PPN topography may be due to differences in gait between humans and monkeys.*
- *These results could help optimize surgical targeting of the PPN for DBS electrode implantation procedures.*

3. DIFFERENCES IN THE ELECTROPHYSIOLOGICAL RELATIONSHIP BETWEEN THE PPN AND THE BASAL GANGLIA IN THE NORMAL AND PARKINSONIAN BRAIN

Dopamine loss in PD is thought to result in increased transmission of oscillatory activity from the cortex to the basal ganglia. The PPN is robustly connected with the basal ganglia (Section 2) and has emerged as a therapeutically effective DBS target for PD (Section 1). However, little is known about PPN firing pattern alterations in PD. To investigate the impact of dopamine cell lesion-induced changes in basal ganglia output on activity in the PPN, this section examines PPN spike timing with reference to M1 LFP activity in urethane- and ketamine-anesthetized rats.

3.1 Introduction and rationale

The PPN has robust connections with the basal ganglia (Spann and Grofova, 1989, 1991; Lavoie and Parent, 1994a, 1994c; Shink *et al.*, 1996, 1997), thalamus (Lavoie and Parent, 1994b), cerebellum (Hazrati and Parent, 1992b), and spinal cord (Spann and Grofova, 1989) and has been suggested to play a key role in the control of posture and locomotion (Masdeu *et al.*, 1994; Lee *et al.*, 2000; Pahapill and Lozano, 2000). The PPN has also recently emerged as a target for DBS in PD and early DBS results show amelioration of medically intractable akinesia and gait abnormalities (Mazzone *et al.*, 2005; Plaha and Gill, 2005; Stefani *et al.*, 2007).

However, there is conflicting information about the effects of dopamine depletion on PPN neuronal activity in PD. Non-human primate and patient data suggest that the PPN is over-inhibited in PD. While excitotoxic lesions of the PPN in normal non-human primates cause akinesia (Kojima *et al.*, 1997; Munro-Davies *et al.*, 1999; Matsumura and Kojima, 2001), low-frequency (2.5-10 Hz) stimulation (Jenkinson *et al.*, 2004) or pharmacological disinhibition (Nandi *et al.*, 2002a) of the PPN can dramatically improve motor behavior in parkinsonian MPTP-lesioned primates. Stimulation in the 10-25 Hz range, generally thought to drive local neuronal activity, is also effectively used in the PPN to ameliorate motor symptoms in PD patients (Mazzone *et al.*, 2005; Plaha and Gill, 2005; Stefani *et al.*, 2007). However, in contrast to the non-human primate and patient results, rodent studies suggest either excitation of the PPN (Breit *et al.*, 2001, 2005; Jeon *et al.*, 2003), inhibition of the PPN (Florio *et al.*, 2007; Gomez-Gallego *et al.*, 2007), or no change in PPN neuronal activity following dopamine cell lesion (Mena-Segovia *et al.*, 2005; Heise and Mitrofanis, 2006).

The urethane-anesthetized rat has been shown to be a useful model for investigating the effects of dopamine loss on the transmission of oscillatory cortical activity through basal ganglia structures. Cortical activity in the urethane-anesthetized rat is highly synchronized, characteristically oscillates at ~1 Hz, and is relatively stable over time (Steriade *et al.*, 1993; Contreras and Steriade, 1995, 1997; Amzica and Steriade, 1998). Many studies have shown changes in firing pattern and increased oscillatory activity in the basal ganglia following dopamine cell lesion in the anesthetized rat (Sanderson *et al.*, 1986; MacLeod *et al.*, 1990; Hollerman and Grace, 1992; Burbaud *et al.*, 1995;

Hassani *et al.*, 1996; Murer *et al.*, 1997; Rohlfs *et al.*, 1997; Perier *et al.*, 2000; Tseng *et al.*, 2000, 2001a, 2001b; Vila *et al.*, 2000; Magill *et al.*, 2001; Ni *et al.*, 2001; Belluscio *et al.*, 2003; Tai *et al.*, 2003; Walters *et al.*, 2005, 2007; Parr-Brownlie *et al.*, 2007; Zold *et al.*, 2007). Recently, this cortical oscillatory activity has been used as a probe signal in the urethane-anesthetised rat to investigate the effects of dopamine loss on the phase relationships between oscillatory activity in the GPe, SNpr, STN, and the striatum (Walters *et al.*, 2007). Increases in slow oscillations (0.3–2.5 Hz) in firing rate emerged in all structures following dopamine cell lesion (Walters *et al.*, 2007). Phase relationships of oscillatory activity in the GPe, STN, and SNpr suggest that the increased incidence of oscillatory activity in the SNpr is supported by the convergence of antiphase inhibitory oscillatory input from the GPe and excitatory oscillatory input from the STN (Walters *et al.*, 2007).

It is unknown whether the oscillatory cortical activity that is transmitted through basal ganglia structures following dopamine loss is also transmitted to the PPN. Evidence of a connection between the PPN and the M1 in non-human primates (Matsumura *et al.*, 2000) and the recent evidence of this connection in humans (Section 2) suggest that this direct transmission of cortical oscillations is possible. Cortical oscillatory activity could also be transmitted to the PPN indirectly via the basal ganglia. Most input to the PPN comes from three basal ganglia regions. The GPi and SNpr send inhibitory efferents to the PPN (Shink *et al.*, 1996, 1997) while excitatory input comes predominantly from the STN (Spann and Grofova, 1991). Therefore, convergent excitatory oscillatory input from the STN and inhibitory oscillatory input from the GPi/SNpr (Walters *et al.*, 2007) may shape oscillatory activity in the PPN in PD.

The aim of the present study was to investigate whether loss of dopamine affects the relationship between neuronal activity in the PPN and M1 in rats under urethane or ketamine-xylazine anesthesia. Effects of dopamine cell lesion on spike timing relationships between PPN and M1 were assessed by simultaneously recording spike trains in the PPN and LFP activity in the M1 and PPN in anesthetized intact rats and in the lesioned hemisphere of hemi-parkinsonian rats 7 – 10 days after a unilateral injection of 6-OHDA into the medial forebrain bundle.

3.2 Methods

All experiments were conducted in accordance with the NIH Guide for Care and Use of Laboratory Animals and approved by the NINDS Animal Care and Use Committee. Every effort was made to minimize the number of animals used and their discomfort.

3.2.1 Nigrostriatal lesions and behavioral testing

Male Sprague–Dawley rats (Taconic Farms, Rockville, MD, USA) weighing 275–325 g at the time of surgery were anesthetized with ketamine (100 mg/kg, i.p.) and xylazine (10 mg/kg, i.p.) and placed in a stereotaxic apparatus with the incisor bar at −3.5 mm. Ocular lubricant Lacrilube was applied to prevent corneal drying. A hole was drilled in the skull above the appropriate coordinates and a 27-gauge injection cannula lowered to the left medial forebrain bundle: 4.4 mm anterior to the lambdoid suture, 1.2 mm lateral to the sagittal suture and 8.3 mm ventral to the surface of the skull. Six μg of 6-

OHDA HBr in 3 µl of 0.9% saline containing 0.01% ascorbic acid were infused via the cannula over 3 min. The cannula was left in place for 3 min after the infusion. Rats were injected with desmethylimipramine (15 mg/kg, i.p.) 30 min prior to the intracerebral infusion to protect noradrenergic neurons. The post-operative diet of lesioned rats was supplemented with fruit and enriched gelatin to maintain weight. Five to seven days after surgery, rats were screened for lesion efficacy by step testing (Olsson *et al.*, 1995). Only rats that demonstrated a strong lesion effect in behavior (number of steps by contralateral limb/number of steps by ipsilateral limb<5%, previously shown to correlate with 99% loss of dopamine in the striatum ipsilateral to the lesioned hemisphere (Parr-Brownlie *et al.*, 2007)) were used for electrophysiology.

3.2.2 Surgical and recording procedures

Recordings were made in intact rats and in rats with unilateral 6-OHDA-induced dopamine cell lesions 7 to 10 days after the lesioning surgery. Extracellular unit activity and LFPs of PPN neurons were recorded through the same electrode in intact rats or in lesioned rats ipsilateral to the dopamine cell lesion. PPN activity was also simultaneously recorded with LFP activity in the ipsilateral M1. Recordings were conducted in rats under either urethane anesthesia (1.6 g/kg i.p. administered over 1.5 hours initially, with additional supplements as needed) or ketamine-xylazine anesthesia (100 mg/kg ketamine and 10 mg/kg xylazine i.p., with supplemental doses of ketamine as needed). LFP activity also provided an indication of depth of anesthesia, and effort was made to achieve levels of anesthesia that were sufficient to limit reflexive responses and whisking movements but not induce burst suppression

patterning (where LFP activity would be mainly oscillating at frequencies <0.3 Hz).

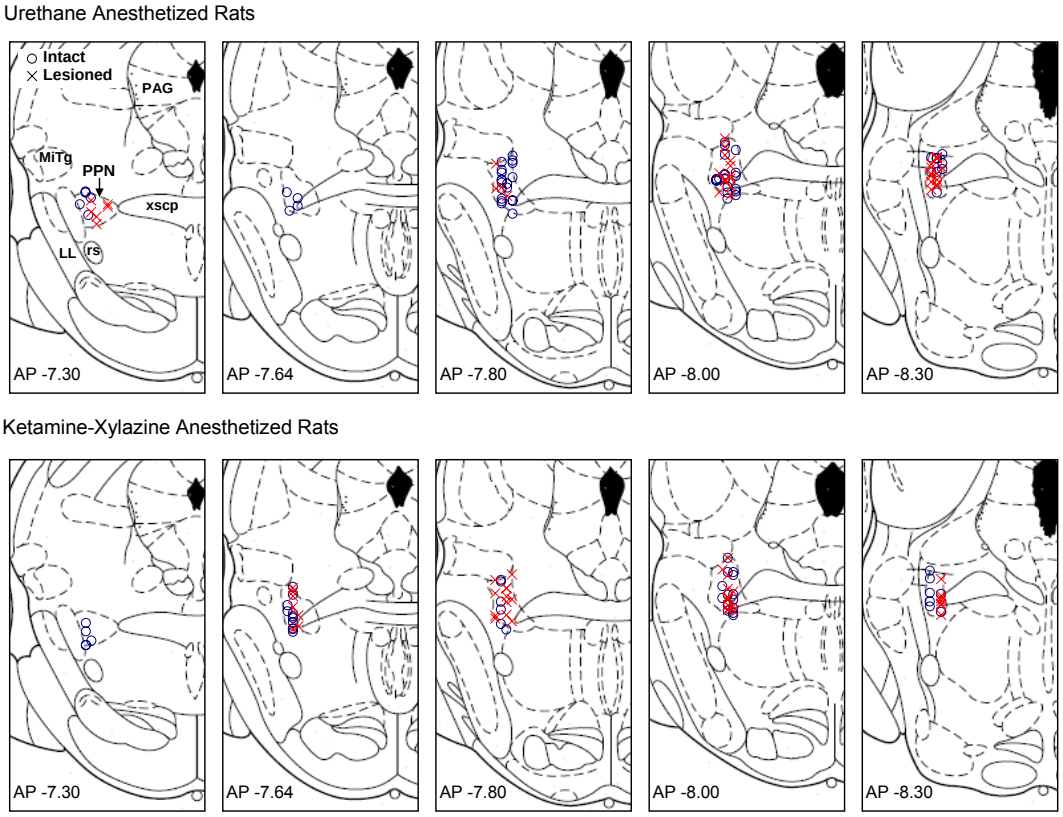

Figure 3.1. Location of recorded PPN cells in intact and 6-OHDA lesioned urethane- and ketamine-anesthetized rats. Distance from bregma is indicated in each coronal slice in mm. Recordings in intact rats are shown as circles and recordings in lesioned rats are shown as crosses. Abbreviations: PPN: pedunculopontine nucleus, PAG: periaqueductal gray, xscp: decussation of the superior cerebellar peduncle, MiTg: microcellular tegmental nucleus, LL: lateral lemniscus, rs: rubrospinal tract. Schematics of coronal slices are adapted from *The Rat Brain in Stereotaxic Coordinates, 2nd Ed.* (Paxinos and Watson, 1986).

Rats were placed into a stereotaxic apparatus, the scalp reflected, and holes drilled in the skull over the target areas. Body temperature was maintained at 36–38 °C using a heating pad. With micromanipulators (MO-8, Narishige, East Meadow, NY, USA), single barrel glass recording electrodes filled with 2% Pontamine Sky Blue dye in 2 M NaCl were lowered through craniotomies to the PPN or M1. Spike trains and LFPs were recorded with

microelectrodes with 3-4 MΩ resistances (measured at 135 Hz) with tip diameter of 1–2 μm. Electrode location varied in the PPN without consistent placement in a specific subregion. M1 LFP recording sites were targeted to layer V (1.6 mm anterior and 2.2 mm lateral from bregma and 2.0 mm below the surface of the cortex). Recording sites were similarly distributed in lesioned and intact rats (Fig. 3.1).

Extracellularly recorded action potentials were amplified (World Precision Instruments Duo 773, World Precision Instruments, Sarasota, FL, USA) and monitored on digital oscilloscopes (Hewlett-Packard, Palo Alto, CA, USA) and audio monitors (Grass, West Warwick, RI, USA). Spikes and LFPs were sampled at 25 kHz and 1000 Hz and band pass filtered at 250–5000 Hz and 0.1–100 Hz, respectively. Discriminated signals were collected on a PC with a CED interface and Spike2 data acquisition and analysis software (Cambridge Electronic Design, Cambridge, UK). All waveforms were biphasic. Final recording sites were marked by iontophoresis of dye with 40 min of constant current injection (-20 μA). Anesthetized animals were sacrificed by decapitation. Brains were removed and frozen and 20 μm brain sections were mounted on subbed slides for histological examination. Only units confirmed as being within the target nucleus with reference to the location of dye deposit and/or electrolytic lesion were analyzed. The location of recording sites within the PPN was confirmed by staining the slices for acetylcholinesterase (Paxinos and Watson, 1986). Slides were incubated overnight in a 4 mM $CuSO_4$, 16 mM glycine, and 0.4 mM acetylthiocholine-iodide solution in 50 mM $Na^+CH_3COO^-$ buffer (pH 5.0). The solution was also supersaturated with ethopropazine, an anticholinergic compound. Slides were rinsed in water and the tissue fixed in

formaldehyde overnight. The tissue was dehydrated in ethanol, rinsed in Histo-Clear, and coverslipped with Permount.

3.2.3 Data analysis

For data analyses, 300 sec of spike train and LFP data were isolated from baseline recordings. These epochs were selected from the 5–10 min of baseline activity, were representative of neuronal activity, and free from artifacts. In addition to determining firing rate, spiking and LFP activity were analyzed for significant oscillatory activity maintained over time within the frequency range of 0.3–2.5 Hz. LFPs were smoothed to 20 Hz and high pass filtered at 0.2 Hz. Spike channels were converted from event channels to waveform channels with a 20 Hz sampling rate using a Spike2 script. Fast Fourier transform (FFT) analyses were used to determine the dominant frequency in the spike train and LFP for each 300 sec data segment using a block size of 256 (yielding a frequency resolution of 0.078 Hz). Coherence between spiking and LFP activity and coherence between LFP activity in the two recording locations were examined as well using a script in Spike2. Each 300 sec data segment was binned at 50 msec, using a block size of 256 yielding 23 non-overlapping 12.8 sec windows. For these parameters, coherence >0.127 was considered significant ($p<0.05$), as determined by the equation $1-(1-\alpha)^{1/(L-1)}$, where α is 0.95 and L is the number of windows used (Rosenberg *et al.*, 1989). In order to determine whether there were differences in amplitude between LFPs, the root mean square (RMS) of the amplitude of the LFP for each 300 sec epoch was calculated. As all signals are corrected for any DC offset, the mean of the LFP signal is ~0 mV. Therefore, the RMS about the mean LFP amplitude (equal to the standard deviation of LFP amplitude)

serves as a good measure of neuronal activity (Goldberg *et al.*, 2004; Moran *et al.*, 2006; Zaidel *et al.*, 2008).

LFP power spectra, LFP total power between 0.3-2.5 Hz, the main peak frequencies in LFP power spectra, the RMS of LFP amplitude, and LFP-LFP coherence spectra were averaged by rat while spike power spectra, spike total power, and spike-to-LFP coherence spectra were averaged across all cells. In order to ensure that LFP power spectra and LFP total power comparisons were evaluated between rats at similar levels of anesthesia, recordings with total power values outside of a 2 standard deviation (SD) range from the mean total power (between 0.3-2.5 Hz, 0.3-1.2 Hz, or 1.2-2.5 Hz, averaged across rats) were excluded from analysis. All LFP recordings excluded using the above criteria were also excluded from LFP-LFP coherence analyses.

Phase relationships between spikes and LFPs were assessed using spike-triggered waveform averages (STWAs) and plotted as polar histograms. LFP channels were smoothed to 20 Hz and band pass filtered at 0.3–2.5 Hz. Spike-triggered waveform averages were calculated for 4 sec before and after the spike trigger over a 300 sec epoch. Spiking at the peaks and troughs of LFP oscillations was considered to be at 0° and 180° phase, respectively. STWAs were determined to be significant if the peak-to-trough amplitude of the STWA around the time of spiking was greater than 4 SDs of the amplitude of a STWA generated from the same data using randomly distributed spikes.

Data are presented as the mean ± standard error of the mean (SE). Data were statistically evaluated with grouped *t*-test. Criterion of significance was $p<0.05$. Statistics were generated with Microsoft Excel (Microsoft Corporation, Redmond, WA, USA, 2002). Polar data are presented as the

mean phase angle of the distribution±the angular deviation (analogous to SD) and as polar histograms. Distribution of phase angles was tested against the null hypothesis of a random distribution with the Rayleigh test (Batschelet, 1981). The p-value for the Rayleigh test indicates the degree of grouping of the polar data and depends on the strength of the phase concentration and the number of data points.

3.3 Results

3.3.1 PPN and M1 spike and LFP relationships in the urethane-anesthetized rat

Slow ~1 Hz oscillations are dominant in cortical output in the urethane-anesthetized state (Steriade *et al.*, 1993) and loss of dopamine is thought to facilitate the transmission of these oscillations through the basal ganglia network (Murer *et al.*, 2002). This cortical oscillatory activity could also be transmitted to the PPN directly via a connection between the M1 and PPN (demonstrated in non-human primates and humans (Section 2) but not verified in rodents) or indirectly via the basal ganglia (Inglis and Winn, 1995; Lee *et al.*, 2000; Pahapill and Lozano, 2000). To examine relationships between oscillatory activity in the PPN and M1 after dopamine cell lesion, PPN spike and PPN LFP activity were recorded simultaneously with M1 LFP activity in intact rats and in lesioned rats 7-10 days after injection of 6-OHDA into the medial forebrain bundle.

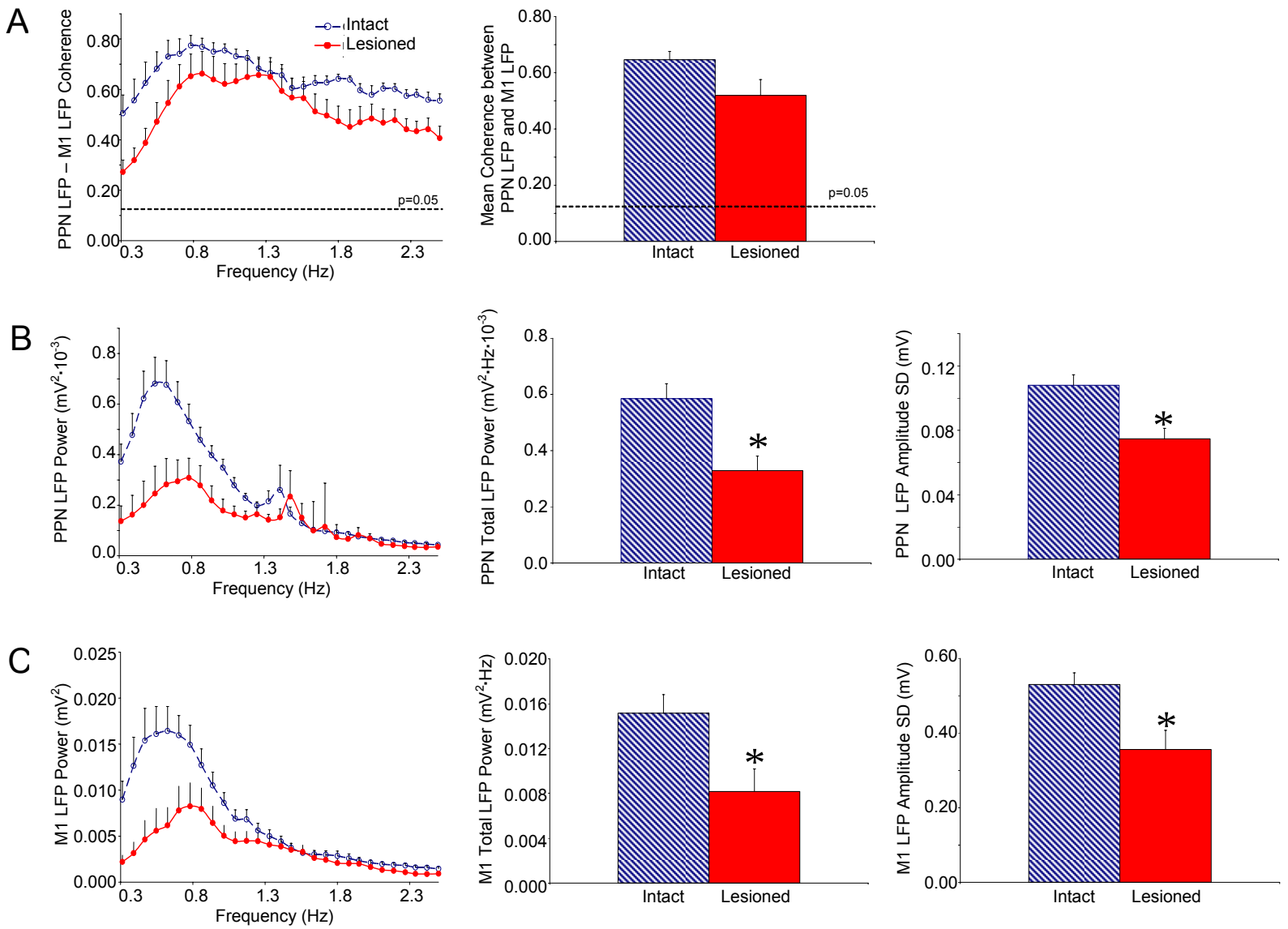
A
PPN LFP – M1 LFP Coherence
Intact
Lesioned
p=0.05
Frequency (Hz)
Mean Coherence between PPN LFP and M1 LFP
B
PPN LFP Power (mV²·10⁻³)
PPN Total LFP Power (mV²·Hz·10⁻³)
PPN LFP Amplitude SD (mV)
C
M1 LFP Power (mV²)
M1 Total LFP Power (mV²·Hz)
M1 LFP Amplitude SD (mV)

Figure 3.2 (on previous page). Characteristics of PPN LFP and M1 LFP activity in the urethane-anesthetized preparation. Coherence between PPN and M1 LFP activity (A, n=10 intact rats, 11 lesioned rats) does not change significantly in the ~1 Hz range (left) following dopamine cell lesion nor does mean coherence in the 0.3-2.5 Hz range (right). Dashed horizontal lines indicate the p=0.05 level of significance for coherence. LFP activity recorded in the PPN (B, n=15 intact rats, 11 lesioned rats) and M1 (C, n=11 intact rats, 11 lesioned rats) is described by comparing LFP power spectra in the 0.3-2.5 Hz range (left), total LFP power in the 0.3-2.5 Hz range (middle), and the RMS of LFP amplitude (right) between intact and lesioned rats. Both PPN and M1 LFP activity exhibit decreases in power in the ~1 Hz range (left), decreases in total power between 0.3-2.5 Hz (middle), and decreases in LFP amplitude (right) following dopamine cell lesion. *p<0.05 compared with intact.

3.3.1.1 Effect of dopamine cell lesion on PPN and M1 LFP activity

Slow ~1 Hz oscillations that emerge in LFP and spike trains in the basal ganglia of urethane-anesthetized rats after dopamine cell lesion have been shown to be highly coherent with slow oscillations in cortical activity (Magill *et al.*, 2001; Tseng *et al.*, 2001b; Belluscio *et al.*, 2003; Walters *et al.*, 2007; Parr-Brownlie *et al.*, 2007; Zold *et al.*, 2007). In the present study, PPN LFPs were significantly coherent with M1 LFPs in the ~1 Hz range (0.3-2.5 Hz) in intact rats (0.65 ± 0.03, n=10 rats) and lesioned rats (0.52 ± 0.06, n=11 rats) (Fig. 3.2A). Dopamine cell lesion had no effect on the coherence between PPN and M1 LFPs.

However, dopamine cell lesion did result in significant decreases in LFP power in both the M1 and PPN. PPN LFP power in the lesioned rat (n=11 rats) was significantly less than PPN LFP power in the intact rat (n=15 rats) in the ~1 Hz range. Total PPN LFP power between 0.3-2.5 Hz showed a 44% decrease with dopamine cell lesion (0.59 ± 0.05 $mV^2 \cdot Hz \cdot 10^{-3}$ in the intact rat vs. 0.33 ± 0.05 $mV^2 \cdot Hz \cdot 10^{-3}$ in the lesioned rat). In addition, PPN LFP amplitude was significantly decreased following dopamine cell lesion. The RMS of PPN LFP

amplitude in the lesioned rat (0.08 ± 0.01 mV) was 31% less than that in the intact rat (0.11 ± 0.01 mV) (Fig. 3.2B).

Similarly, M1 LFP power in the lesioned rat (n=11 rats) was significantly less than M1 LFP power in the intact rat (n=11 rats) in the ~1 Hz range, though the peak spectral frequency was not significantly different between lesioned (0.77 ± 0.03 Hz) and intact (0.67 ± 0.05 Hz) animals. Total M1 LFP power was decreased by 46% (15.2 ± 1.7 $mV^2 \cdot Hz \cdot 10^{-3}$ in the intact rat vs. 8.2 ± 2.0 $mV^2 \cdot Hz \cdot 10^{-3}$ in the lesioned rat) and the RMS of M1 LFP amplitude was decreased by 33% with dopamine cell lesion as well (0.36 ± 0.05 mV in the lesioned rat vs. 0.53 ± 0.03 mV in the intact rat) (Fig. 3.2C).

3.3.1.2 Effect of dopamine cell lesion on PPN neuronal activity

To gain further insight into processes underlying decreases in PPN LFP amplitude and examine the potential impact of oscillatory output from the basal ganglia on the PPN, rate and temporal dynamics of PPN spiking were examined. Oscillatory activity in PPN spiking was examined by converting PPN spike trains to Gaussian waveforms with a 20 Hz sampling rate and then determining the power of this waveform signal using FFT analysis. In contrast to the decreased power and amplitude observed in PPN LFP following dopamine cell lesion, increased oscillatory activity was observed in PPN spike trains. A comparison of the power in PPN spike trains revealed that spike train power in the lesioned rat was significantly greater than spike train power in the intact rat in the ~1 Hz range (Fig. 3.3A). Total spike power between 0.3-2.5 Hz in the lesioned rat (0.52 ± 0.12 Hz^3, n=38 cells) was double the total spike power in the intact rat (0.26 ± 0.03 Hz^3, n=59 cells).

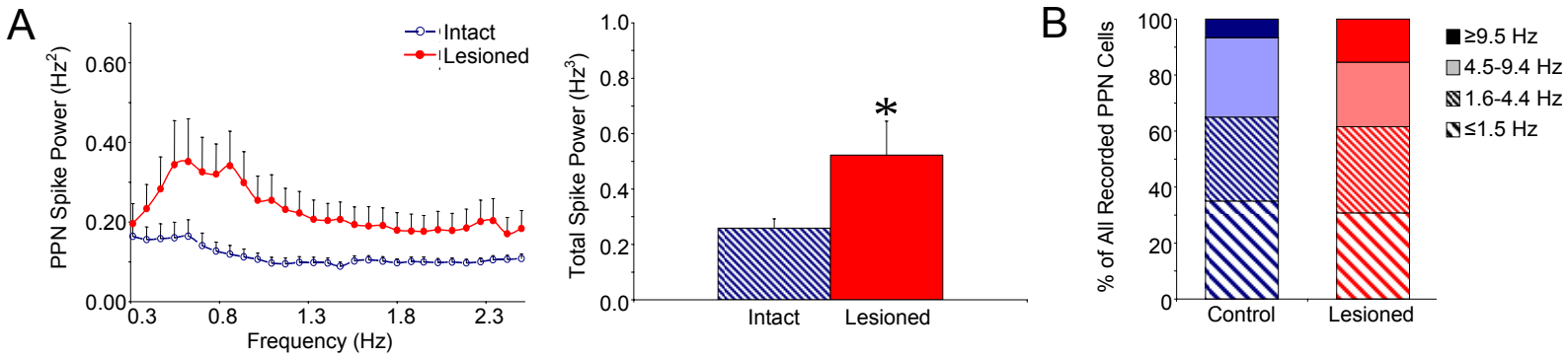

Figure 3.3. Characteristics of PPN spike trains in the urethane-anesthetized preparation. Oscillatory activity in PPN spike trains (A, n=59 PPN cells in intact rats, 38 cells in lesioned rats) was determined by converting PPN spike trains to Gaussian waveforms with a 20 Hz sampling rate and then using FFT to determine power in the 0.3-2.5 Hz range. There is an increase in power in the ~1 Hz range in PPN spike trains following dopamine cell lesion (left) with a significant increase in total power between 0.3-2.5 Hz following dopamine cell lesion (right). *$p<0.05$ compared with intact. Firing rate distributions (B, n=59 cells in intact rats, 38 cells in lesioned rats) are indicated for the intact and 6-OHDA lesioned animals. There was no significant difference in firing rate between intact and lesioned rats.

This increase in PPN spike train oscillatory activity was not associated with significant changes in PPN firing rate. Dopamine cell lesion had no significant effect on PPN firing rate and the percentages of PPN neurons categorized as very slow (≤1.5 Hz), slow (1.6-4.4 Hz), medium (4.5-9.4 Hz), or fast (≥9.5 Hz) firing were comparable between the intact and lesioned preparations. In the intact animal, the mean firing rate in the PPN (n=59 cells, 17 rats) was 3.8 ± 0.5 Hz and ranged from 0.01 – 13.8 Hz with 93% of all cells firing at rates less than 9.5 Hz. The mean PPN firing rate in the lesioned rat (n=38 cells, 11 rats) was 5.8 ± 1.3 Hz and ranged from 0.1 – 39.8 Hz with 85% of all cells firing at rates less than 9.5 Hz (Fig. 3.3B).

3.3.1.3 Relationship between PPN spiking and LFP activity in the PPN and M1

Consistent with increased oscillatory activity in PPN spike trains, coherence between PPN spiking and LFP oscillatory activity in the PPN and M1 increased in the ~1 Hz range following dopamine cell lesion; PPN spiking and LFP oscillatory activity, which were not significantly coherent in the intact rat, became significantly coherent following dopamine cell lesion. Mean coherence between PPN spiking and PPN LFP increased by 50% with dopamine cell lesion from 0.10 ± 0.01 in the intact animals (n=59 cells) to 0.15 ± 0.02 in the lesioned animals (n=38 cells) (Fig. 3.4A). In addition, coherence between PPN spiking and M1 LFP activity was significantly greater in the lesioned rat in the ~1 Hz range and mean coherence between PPN spiking and M1 LFP activity increased by 73% from 0.11 ± 0.09 in the intact rat (n=42 cells) to 0.19 ± 0.02 in the lesioned

rat (n=38 cells). This increased coherence between spiking and LFP activity, in addition to the increased oscillatory activity in PPN spike trains in the ~1 Hz range, predict increased phase locking between PPN spiking and LFP activity following dopamine cell lesion (Fig. 3.4B).

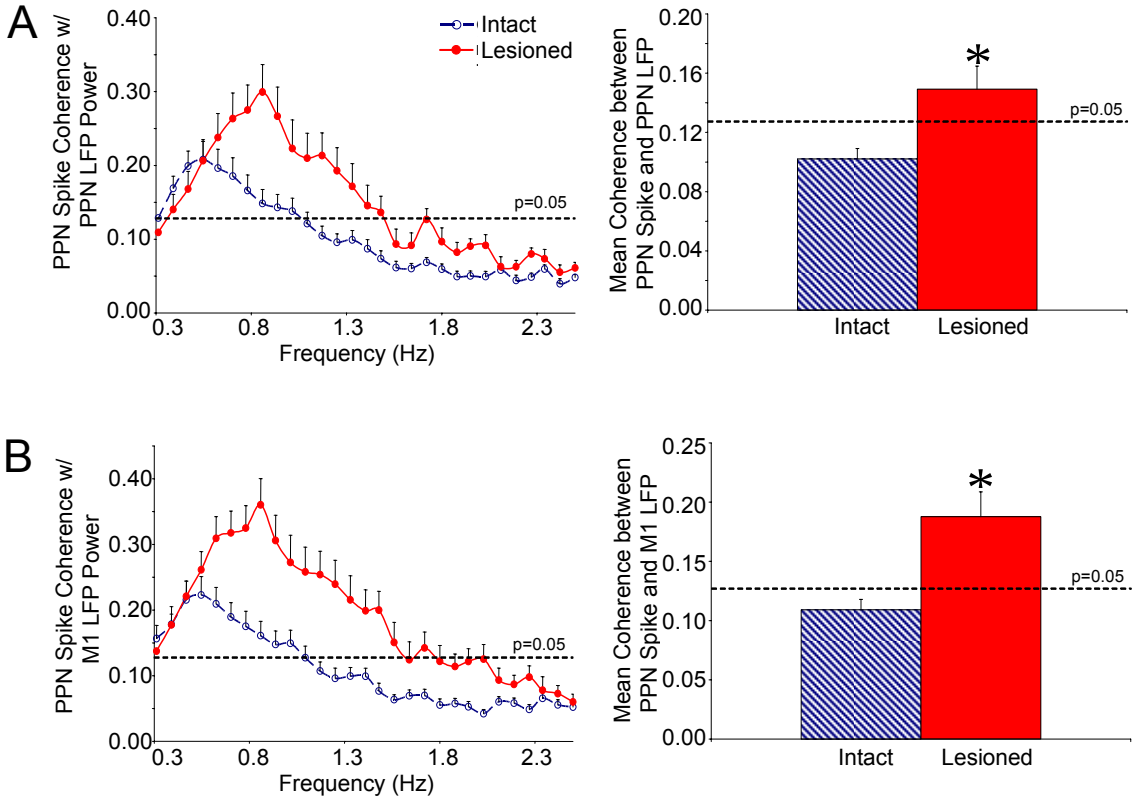

Figure 3.4. Relationships between oscillatory activity in PPN spiking and LFP activity in the urethane-anesthetized preparation. Coherence between PPN spike trains and PPN LFP (A, n=59 cells in intact rats, 38 cells in lesioned rats) and coherence between PPN spike trains and M1 LFP (B, n=42 cells in intact rats, 38 cells in lesioned rats) activity increase following dopamine cell lesion in the ~1 Hz range (left). Mean coherence between PPN spiking and PPN LFP activity and mean coherence between PPN spiking and M1 LFP activity also increase across the 0.3-2.5 Hz range (right). *p<0.05 compared with intact.

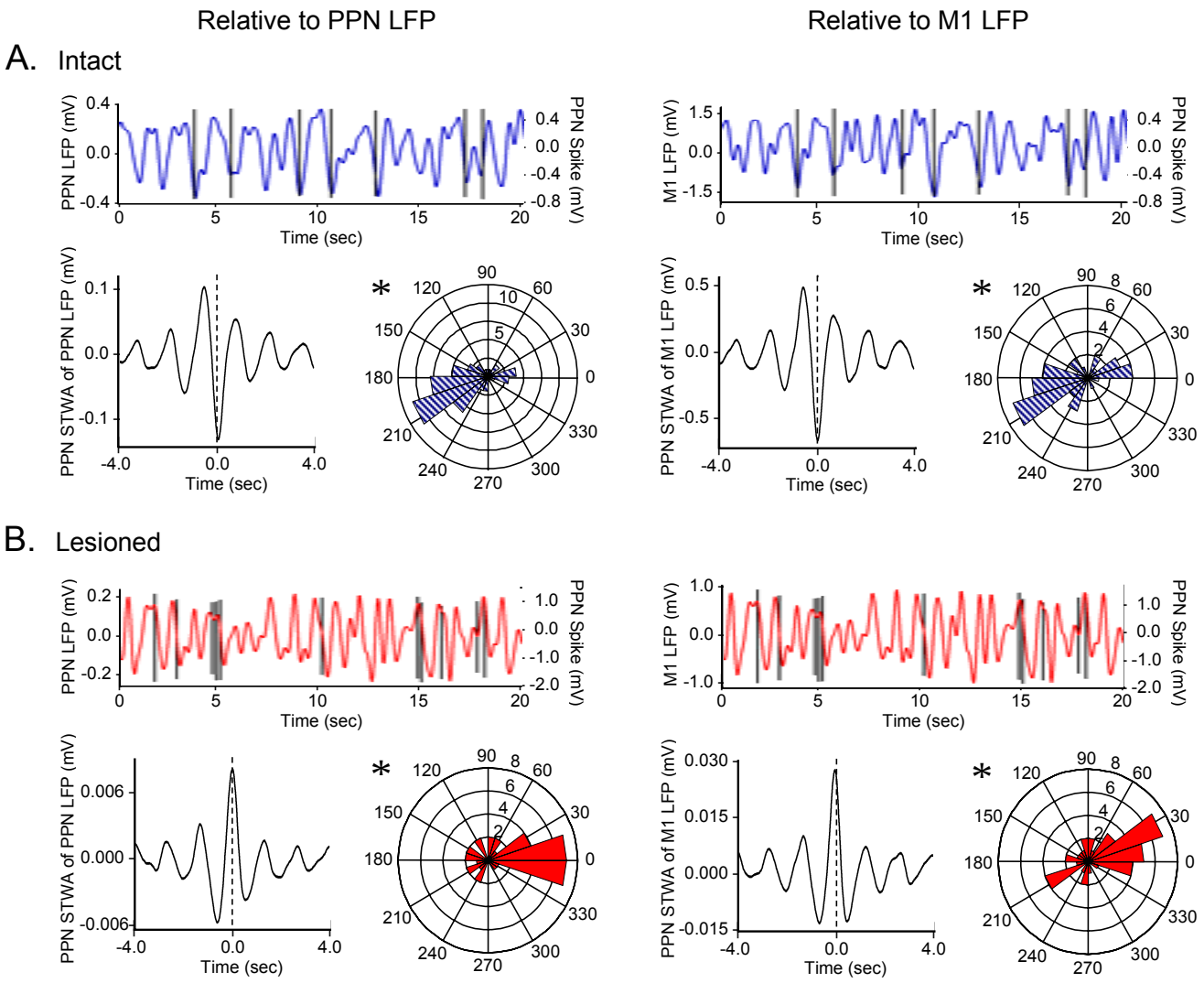
Relative to PPN LFP
Relative to M1 LFP
A. Intact
B. Lesioned
PPN LFP (mV)
PPN Spike (mV)
M1 LFP (mV)
Time (sec)
PPN STWA of PPN LFP (mV)
PPN STWA of M1 LFP (mV)
*

Figure 3.5 (on previous page). PPN spike timing relative to LFP oscillatory activity in the urethane-anesthetized preparation. Typical PPN spike trains in intact (A) and lesioned (B, n=37 significantly oscillatory cells in lesioned rats) rats are shown at the top of each panel overlaid on simultaneously recorded PPN LFP (left, n=37 cells with significant peaks in their STWAs in intact rats, 39 cells in lesioned rats) or M1 LFP (right, n=54 cells in intact rats, 37 cells in lesioned rats) activity. PPN spike-triggered LFP waveform averages (lower left of each panel) illustrate the time of PPN spiking relative to the phase of LFP oscillatory activity in the example spike train. Polar histogram plots (lower right of each panel) summarize the distribution of phases of PPN spikes with respect to PPN LFP (left) and M1 LFP (right) oscillations. In the intact rat, spiking occurs at or near the trough (~180°) of PPN and M1 LFP activity. Dopamine cell lesion significantly changes this phase relationship as PPN spiking occurs primarily at the peaks (~0°) of LFP oscillations in lesioned rats. * Significantly ($p<0.05$) unimodal distributions of phase relationships between PPN spiking and LFP activity.

Consistent with this prediction, significant phase locking between PPN spiking and LFP oscillations was evident in both the intact and lesioned rats. In the intact rat, PPN spiking occurred predominantly at the troughs (periods of peak negativity or greatest depolarization) of PPN and M1 LFP oscillations. The phase angles between PPN spiking and PPN LFP oscillations were significantly unimodally clustered around 180 ± 62° (n=54 cells) with 76% of PPN cells firing in the troughs of PPN LFP oscillations (exhibiting phase angles between 90 and 270°). Similarly, the phase angles between PPN spiking and M1 LFP activity were significantly unimodally clustered around 180 ± 69° (n=37 cells) with 71% of all cells firing in the troughs of M1 LFP oscillations. This suggests that PPN firing occurs in phase with firing in the M1 in the intact rat (Fig. 3.5A) since cortical firing also tends to occur at the troughs of cortical LFPs (Murthy and Fetz, 1996a, 1996b; Donoghue *et al.*, 1998; Destexhe *et al.*, 1999; Parr-Brownlie *et al.*, 2007; Rasch *et al.*, 2008).

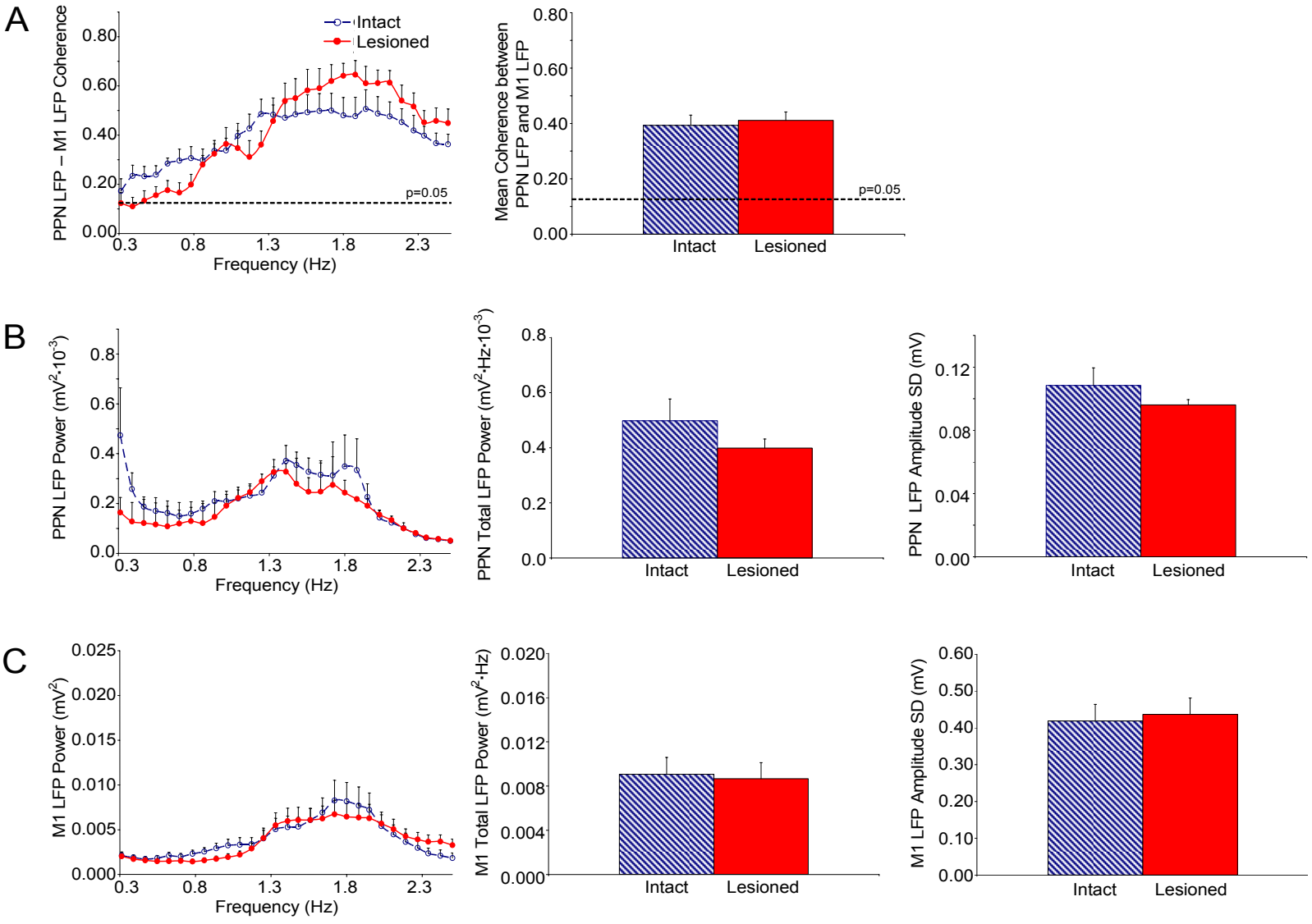
A
PPN LFP – M1 LFP Coherence
Intact
Lesioned
p=0.05
Frequency (Hz)
Mean Coherence between PPN LFP and M1 LFP
B
PPN LFP Power (mV²·10⁻³)
PPN Total LFP Power (mV²·Hz·10⁻³)
PPN LFP Amplitude SD (mV)
C
M1 LFP Power (mV²)
M1 Total LFP Power (mV²·Hz)
M1 LFP Amplitude SD (mV)

Figure 3.6 (on previous page). Characteristics of PPN LFP and M1 LFP activity in the ketamine-anesthetized preparation. Coherence between PPN LFP and M1 LFP activity (A, n=9 intact rats, 10 lesioned rats) does not change significantly in the ~1 Hz range (left) following dopamine cell lesion nor does mean coherence in the 0.3-2.5 Hz range (right). LFP activity recorded in the PPN (B, n=9 intact rats, 10 lesioned rats) and M1 (C, n=9 intact rats, 12 lesioned rats) is described by comparing LFP power spectra in the 0.3-2.5 Hz range (left), total LFP power in the 0.3-2.5 Hz range (middle), and the RMS of LFP amplitude (right) between intact and lesioned rats.

Dopamine cell lesion resulted in significantly different spike-timing relationships between PPN spiking and LFP oscillatory activity. In contrast to the trough-locked firing observed in intact animals, PPN firing tended to occur at the peaks (periods of least depolarization) of LFP oscillations in the lesioned rats. The phase angles between PPN spiking and PPN LFP oscillations were significantly unimodally clustered around 0 ± 65° (n=37 cells) with 68% of all cells firing in the peaks of PPN LFP oscillations (exhibiting phase angles that are less than 90° and greater than 270°). The phase angles between PPN spiking and M1 LFP were also significantly unimodally clustered around 1 ± 68° (n=39 cells) with 62% of all cells firing in the peaks of M1 LFP oscillations. This demonstrates a predominantly antiphase relationship between spiking in the PPN and M1 following dopamine cell lesion (Fig. 3.5B).

3.3.2 PPN and M1 spike and LFP relationships in the ketamine-anesthetized rat

Ketamine, a common anesthetic and non-competitive NMDA antagonist, is often used in conjunction with xylazine as an anesthetic or as an anesthetic supplement to urethane during rat electrophysiological recordings (Rudolph and

Antkowiak, 2004; Wolff and Winstock, 2006). Ketamine differs from urethane in its mechanism of action and has also been shown to induce slow oscillations in the cortex but at somewhat faster frequencies (Magill *et al.*, 2000; Fontanini *et al.*, 2003; Musizza *et al.*, 2007). To study the effects of dopamine cell lesion in this different commonly-used anesthetic preparation, PPN spiking, PPN LFP, and M1 LFP were examined in intact and hemi-parkinsonian ketamine-xylazine anesthetized rats.

Similar to results observed with urethane anesthesia, coherence between PPN and M1 LFPs in the 0.3-2.5 Hz range was significant in both intact and lesioned ketamine-anesthetized rats with mean coherence at 0.41 ± 0.03 in the intact animals (n=9 rats) and at 0.44 ± 0.02 in the lesioned animals (n=10 rats) (Fig. 3.6A). However, in contrast to the urethane-anesthetized preparation, PPN LFP power (0.50 ± 0.08 $mV^2 \cdot Hz \cdot 10^{-3}$ in the intact rat and 0.40 ± 0.03 $mV^2 \cdot Hz \cdot 10^{-3}$ in the lesioned rat) and the RMS of LFP amplitude (0.11 ± 0.01 mV in the intact rat and 0.10 ± 0.01 mV in the lesioned rat) did not differ significantly between the intact (n=9 rats) and lesioned ketamine-anesthetized animals (n=10 rats) (Fig. 3.6B). M1 LFP power (9.1 ± 1.5 $mV^2 \cdot Hz \cdot 10^{-3}$ in the intact rat and 8.7 ± 1.5 $mV^2 \cdot Hz \cdot 10^{-3}$ in the lesioned rat) and the RMS of LFP amplitude (0.42 ± 0.05 mV in the intact rat and 0.44 ± 0.04 mV in the lesioned rat) also did not differ significantly between the intact (n=9 rats) and lesioned ketamine-anesthetized animals (n=12 rats) (Fig. 3.6C). As expected, ketamine anesthesia induced higher frequency cortical oscillations than did urethane, though there was no

significant difference in peak spectral frequency between intact (1.66 ± 0.07 Hz) and lesioned (1.64 ± 0.07 Hz) animals.

Also in contrast to the results obtained in the urethane-anesthetized preparation, dopamine cell lesion had no effect on oscillatory activity in PPN spike trains in the ketamine-anesthetized rat. Mean total PPN spike power between 0.3-2.5 Hz was 0.77 ± 0.16 Hz^3 in the intact rat (n=37 cells) and 0.65 ± 0.14 Hz^3 in the lesioned rat (n=38 cells) (Fig. 3.7A). PPN firing rates were also comparable between the dopamine cell-lesioned and intact ketamine-anesthetized animals. In the intact rat, the mean firing rate in the PPN (n=37 cells, 9 rats) was 5.2 ± 0.9 Hz and ranged from 0.1 – 18.3 Hz with 93% of all cells firing at rates less than 9.5 Hz. The mean PPN firing rate in the lesioned rat (n=38 cells, 12 rats) was 5.1 ± 1.0 Hz and ranged from 0.1 – 31 Hz with 95% of all cells firing at rates less than 9.5 Hz (Fig. 3.7B).

Finally, the spike-LFP relationships observed in the urethane-anesthetized preparation were also not observed in the ketamine-anesthetized preparation. There was no change in the coherence between PPN spiking and PPN LFP or M1 LFP oscillations following dopamine cell lesion in the ketamine-anesthetized animals. Mean coherence between PPN spiking and PPN LFP activity was 0.15 ± 0.02 in the intact rat (n=37 cells) and 0.17 ± 0.02 in the lesioned rat (n=38 cells) (Fig. 3.8A). Mean coherence between PPN spiking and M1 LFP activity was 0.18 ± 0.02 in the intact rat (n=37 cells) and 0.19 ± 0.02 in the lesioned rat (n=38 cells) (Fig. 3.8B). PPN spike timing relationships with PPN LFP or M1 LFP oscillations were also not evident in either the intact or lesioned animals; the distribution of

phase relationships between PPN spiking and PPN LFP (n=38 significantly oscillatory cells in the intact rat, 32 cells in the lesioned rat) or M1 LFP (n=36 cells in the intact rat, 35 cells in the lesioned rat) was not significantly unimodally or bimodally clustered (Fig. 3.8C).

3.4 Discussion

The robust connections between the PPN and basal ganglia (Spann and Grofova, 1989, 1991; Lavoie and Parent, 1994a, 1994c; Shink *et al.*, 1996, 1997) indicate that the PPN will be affected by changes in basal ganglia output after dopamine loss. The aim of this study was to explore this issue by determining how loss of dopamine affects PPN activity and its relationship to slow oscillatory M1 activity in a rodent model of PD. Both urethane and ketamine-xylazine anesthetized preparations were used to examine this relationship 7-10 days after unilateral 6-OHDA-induced dopamine cell lesion. Changes in PPN spike timing with respect to M1 LFP slow oscillations were observed in the urethane-anesthetized preparation. Viewed in the context of the oscillatory activity that emerges in basal ganglia nuclei following dopamine cell lesion, these results suggest that the increased oscillatory activity in basal ganglia output is transmitted to the PPN most directly via inhibitory oscillatory output from the SNpr or GPi. These changes in spike timing and oscillatory activity were not observed in rats anesthetized with ketamine-xylazine, suggesting that the NMDA

antagonist properties of ketamine may attenuate some of the effects of dopamine cell lesion.

3.4.1 Increased oscillatory PPN activity after dopamine cell lesion in the urethane-anesthetized rat

Dopamine depletion increases transmission of oscillatory activity from the cortex to the basal ganglia via the striatum (Murer *et al.*, 2002). Consistent with this phenomenon, increases in burstiness and oscillatory activity have been shown in spike trains of several basal ganglia nuclei following dopamine cell lesion in the anesthetized rat model of PD (Sanderson *et al.*, 1986; MacLeod *et al.*, 1990; Hollerman and Grace, 1992; Burbaud *et al.*, 1995; Hassani *et al.*, 1996; Murer *et al.*, 1997; Rohlfs *et al.*, 1997; Magill *et al.*, 2000; Perier *et al.*, 2000; Tseng *et al.*, 2000, 2001a; Vila *et al.*, 2000; Ni *et al.*, 2001; Belluscio *et al.*, 2003; Tai *et al.*, 2003; Walters *et al.*, 2005, 2007; Parr-Brownlie *et al.*, 2007; Zold *et al.*, 2007). These firing pattern changes are especially notable in the STN where the percentage of cells firing in a significantly oscillatory manner (as determined from Lomb periodogram analysis) increases from ~20% to ~90% in the urethane-anesthetized rat following dopamine cell lesion (Walters *et al.*, 2005, 2007; Parr-Brownlie *et al.*, 2007). Dopamine cell lesion also resulted in an increase in oscillatory firing in the SNpr. Relative to the STN, few SNpr cells have oscillatory firing patterns in the intact rat, but 35-44% of SNpr cells are oscillatory in the 6-OHDA lesioned rat (Tseng *et al.*, 2001a; Walters *et al.*, 2007).

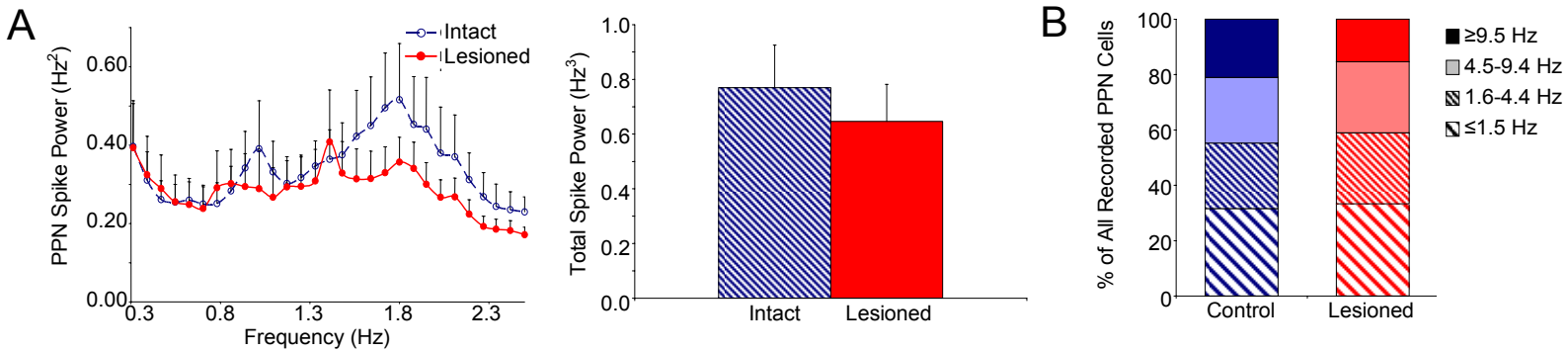

Figure 3.7. Characteristics of PPN spike trains in the ketamine-anesthetized preparation. Oscillatory activity in PPN spike trains (A, n=37 cells in intact rats, 38 cells in lesioned rats) was not significantly different between intact and lesioned rats in the ~1 Hz range (left). Dopamine cell lesion had no significant effect on total power in PPN spike trains between 0.3-2.5 Hz (right). Firing rate distributions (B, n=37 cells in intact rats, 38 cells in lesioned rats) are indicated for the intact and dopamine cell lesioned animals. There was also no significant difference in firing rate between the intact and lesioned rat.

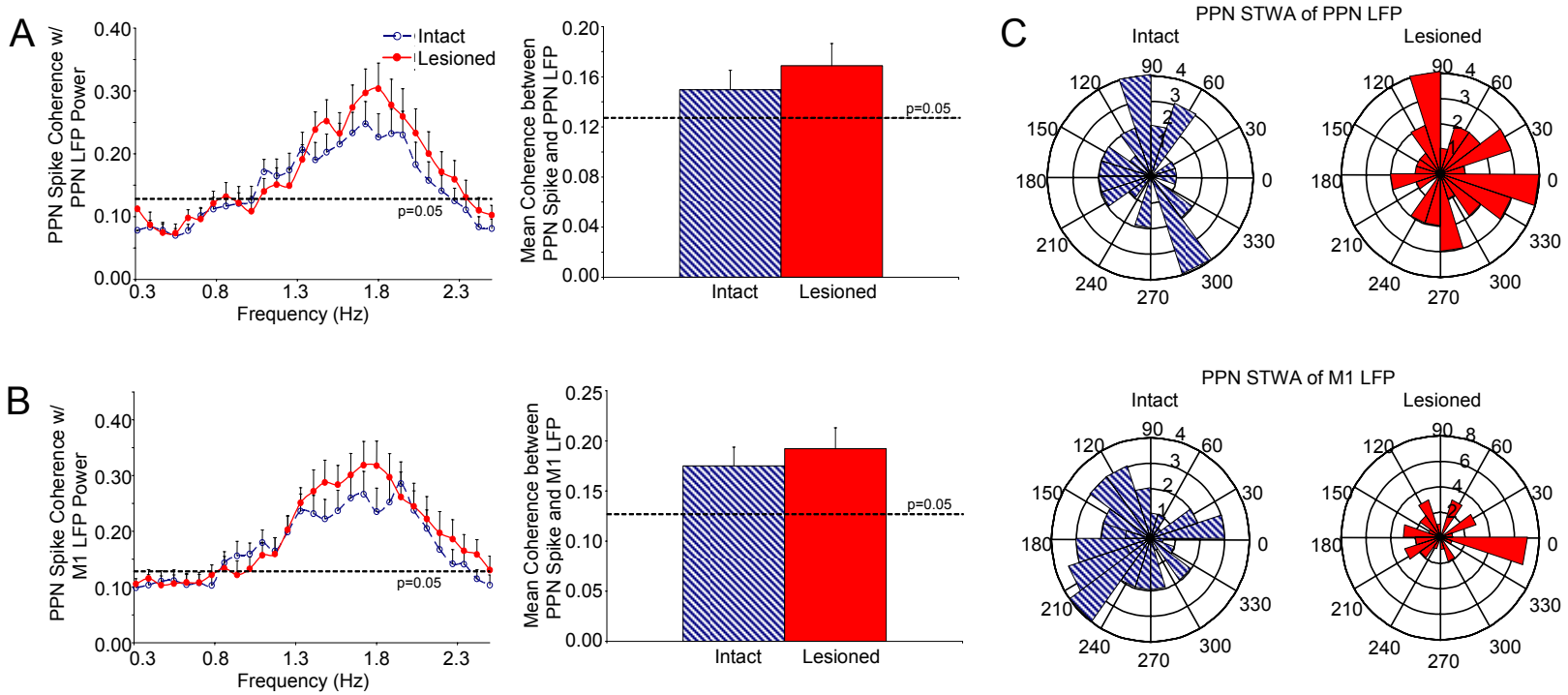

Figure 3.8. Relationships between PPN spiking and LFP activity in the ketamine-anesthetized preparation. Coherence between PPN spike trains and PPN LFP (A, n=37 cells in intact rats, 38 cells in lesioned rats) and coherence between PPN spike trains and M1 LFP (B, n=37 cells in intact rats, 38 cells in lesioned rats) do not change following dopamine cell lesion. There is also no change in mean coherence between PPN spiking and PPN LFP or M1 LFP activity in the 0.3-2.5 Hz range (right). Polar histogram plots (C) summarize the distribution of phases of PPN spikes with respect to PPN LFP (top, n=38 significantly oscillatory cells in the intact rat, 32 cells in the lesioned rat) and M1 LFP (bottom, n=36 cells in the intact rat, 35 cells in the lesioned rat) oscillations. There is no consistent phase-locking between PPN spiking and LFP activity in the intact (left) or lesioned (right) rats.

The effect of oscillatory output from the basal ganglia on spike timing in the PPN is an interesting issue with respect to mechanisms underlying motor dysfunction in PD as the PPN has been suggested to play a role in the control of gait (Garcia-Rill *et al.*, 1985, 1987; Reese *et al.*, 1995) and is in a position to be affected by DBS of the STN (Florio *et al.*, 2007; Stefani *et al.*, 2007). Since the PPN is strongly interconnected with both the STN (Spann and Grofova, 1991) and SNpr (Shink *et al.*, 1996, 1997), the oscillatory outputs of these nuclei are likely to affect PPN spike timing. However, as increased oscillatory input to the PPN from the STN is excitatory and in phase with increased inhibitory oscillatory input from the SNpr (Walters *et al.*, 2007), these temporally coincident oscillatory inputs might effectively cancel each other in the PPN at the level of individual neurons or at the level of the overall PPN neuronal population.

The present results show that PPN spiking activity becomes more oscillatory in the urethane-anesthetized rat. Mean power in PPN spike trains in the ~1 Hz range significantly increased following dopamine cell lesion and total power in PPN spike trains in the 0.3-2.5 Hz range doubled. Furthermore, coherence between PPN spiking and PPN LFP and coherence between PPN spiking and M1 LFP activity also increased significantly following dopamine cell lesion indicating that PPN spiking becomes more entrained to the slow oscillations observed in the M1 following dopamine loss in the urethane-anesthetized rat. These results are consistent with the view that phase cancellation in PPN spiking activity is not the dominant result of the coincident excitatory and inhibitory oscillatory input from the STN and SNpr/GPi.

3.4.2 Effect of basal ganglia output on PPN spike timing following dopamine cell lesion in the urethane-anesthetized rat

To further explore the relationship between oscillatory activity in the PPN and oscillatory activity in the basal ganglia and motor cortex, PPN spike-triggered M1 LFP averages were analyzed. The troughs of LFP oscillations represent the periods of greatest negative potential in the extracellular space and thus correspond to the periods of greatest membrane depolarization of recorded cells. Consistently, cortical spiking activity has been shown to predominantly occur at the troughs of cortical LFP oscillations in awake animals (Murthy and Fetz, 1996a, 1996b; Donoghue *et al.*, 1998), in anesthetized animals (Parr-Brownlie *et al.*, 2007; Rasch *et al.*, 2008), and at the troughs of slow cortical LFP oscillations (<1 Hz) observed during sleep (Destexhe *et al.*, 1999). Firing in the STN and SNpr is also locked to the troughs of M1 LFP oscillations after dopamine loss suggesting that firing in these structures is in phase with firing in the M1 (Magill *et al.*, 2001; Tseng *et al.*, 2001b; Murer *et al.*, 2002; Belluscio *et al.*, 2003; Sharott *et al.*, 2005a; Walters *et al.*, 2007).

Changes in phase relationships observed between PPN spiking and M1 LFP activity in the urethane anesthetized preparation support the view that inhibitory oscillatory output from the basal ganglia, i.e. from the SNpr and GPi, dominates PPN spike timing following dopamine loss. In the intact urethane-anesthetized rat, PPN spiking most frequently coincided with the troughs of M1 LFP oscillations. These results suggest that input from the STN may influence PPN spike timing relationships resulting in the more frequent occurrence of trough-locked PPN firing in phase with firing in the M1. Excitatory input to the PPN directly from the M1 could also result in PPN firing in phase with M1 firing

in the intact rat. However, it is unknown whether a direct connection in the rat exists. In contrast, in the parkinsonian 6-OHDA lesioned rat, PPN spiking most frequently coincided with the peaks of M1 LFP oscillations. Since increases in bursty and oscillatory activity in the STN are associated with in phase increases in oscillatory activity in the SNpr in the lesioned rat (Walters *et al.*, 2007), the results from this study suggest that PPN neurons are more influenced by trough-locked inhibitory input from the SNpr resulting in predominantly peak-locked PPN firing out of phase with firing in the M1. These results also corroborate observations in PD patients and evidence from parkinsonian non-human primates that suggest that the PPN is over-inhibited in PD (Nandi *et al.*, 2002a; Jenkinson *et al.*, 2004; Mazzone *et al.*, 2005; Plaha and Gill, 2005; Stefani *et al.*, 2007).

It should be pointed out that while the majority (62-76%) of PPN cells exhibited the phase locking described above (firing in phase with M1 firing in the intact rat, but antiphase to M1 firing in the lesioned rat), 24-38% of all PPN cells exhibited the opposite phase relationship (firing antiphase to M1 firing in the intact rat but in phase with M1 firing in the lesioned rat). This diversity in spike timing within the PPN, despite the transmission of a stable ~1 Hz cortical rhythm, is not surprising noting the numerous inputs (Inglis and Winn, 1995; Lee *et al.*, 2000; Pahapill and Lozano, 2000) and the multiple neurochemically-defined PPN neuronal subtypes including cholinergic (Spann and Grofova, 1992), glutamatergic (Rye *et al.*, 1987), dopaminergic (Rye *et al.*, 1987), and GABAergic (Ford *et al.*, 1995) neuronal populations.

3.4.3 Causes of coherent decreases in M1 and PPN LFP power in the urethane-anesthetized rat

Studies have shown that LFPs in the basal ganglia are highly correlated with cortical EEG/cortical LFP in anesthetized rats in the slow oscillation frequency range (Magill *et al.*, 2000, 2001; Tseng *et al.*, 2001b; Murer *et al.*, 2002; Sharott *et al.*, 2005a; Walters *et al.*, 2007; Parr-Brownlie *et al.*, 2007). In the present study, PPN LFP activity was also significantly and highly coherent with M1 LFP activity in both the intact and lesioned urethane-anesthetized rat. However, the present results raise interesting questions regarding: 1) discrepant relationships between PPN spike timing and PPN LFP and 2) effects of dopamine cell lesion on LFP power and amplitude in both the PPN and M1.

Intriguingly, PPN spike timing relationships with PPN LFP oscillations were similar to PPN spike timing relationships with M1 LFP oscillations. Since the troughs of LFPs should correspond to the periods when cells closest to the recording site are most likely to fire, one might expect PPN spiking to be predominantly trough-locked to PPN LFP oscillations in both the intact and lesioned rat. However, the results show that PPN spiking is predominantly peak-locked to PPN LFP oscillations in the lesioned rat. This dissociation between PPN spike timing and PPN LFP phase after dopamine cell lesion raises questions about the extent to which PPN LFP reflects local net depolarization related solely to the observed PPN spiking activity.

The present study also demonstrated dopamine cell lesion induced changes in LFP power in the ~1 Hz range in both the M1 and PPN. Specifically, significant decreases in M1 and PPN LFP total power between 0.3-2.5 Hz were observed in conjunction with mean decreases in LFP amplitude. Decreases in

PPN LFP power are incongruent with the observed increases in synchronization in PPN firing and the increased coherence between PPN spiking and PPN LFP activity discussed above, both of which suggest that PPN LFP power should increase with dopamine cell lesion. In addition, decreases in cortical LFP in the ~1 Hz frequency range after dopamine cell lesion is inconsistent with the idea that basal ganglia-thalamo-cortical circuits may become more entrained to the slow oscillatory rhythm after loss of dopamine (Goldberg *et al.*, 2002, 2004; Leblois *et al.*, 2006).

A number of factors may contribute to the decrease in power and amplitude in the PPN and M1 LFPs. Inhibitory oscillatory input from the SNpr could compete with excitatory oscillatory input from the STN resulting in the decreased PPN LFP amplitude and power observed in this study. In addition, since the generation of cortical LFPs is thought to be due to the regular columnar and laminar organization of cortical cells (Elul, 1971; Klee and Rall, 1977; Mitzdorf, 1985; Goldberg *et al.*, 2004), it is unclear whether LFPs are similarly generated in a structure with sparse and irregular cytoarchitecture like the PPN (Rye *et al.*, 1987; Inglis and Winn, 1995; Pahapill and Lozano, 2000). In this context, it is interesting to note that the M1 LFP amplitude observed in this study is almost 5 times larger than PPN LFP amplitude which is indicative of the more regular organization of M1 neuronal elements contributing to the generation of M1 LFP. Therefore, it is likely that PPN LFP may not be as robust a measure of neuronal activity as M1 LFP.

A factor that could contribute to decreases in M1 LFP amplitude and LFP power following dopamine cell lesion is a reduction in the number of regularly firing M1 cells. As basal ganglia output from the SNpr is inhibitory and

in phase with cortical activity (Murer *et al.*, 1997; Tseng *et al.*, 2000, 2001a; Walters *et al.*, 2007), this inhibitory basal ganglia output might modulate excitatory thalamocortical activity and thus reduce the number of M1 cells firing synchronously in the urethane-anesthetized rat following dopamine lesion. This is supported by studies in animal models of PD demonstrating hypoactivity of glutamatergic thalamic projection neurons to the cortex (Palombo *et al.*, 1988; Schwartzman *et al.*, 1988; Mitchell *et al.*, 1989; Gnanalingham *et al.*, 1995; Brownell *et al.*, 2003; Rolland *et al.*, 2007). Evidence for attenuation of cortical output following dopamine cell lesion also supports this hypothesis. Decreased striatal dendritic length and a decrease in the number of striatal dendritic spines have been observed in 6-OHDA lesioned rats and transgenic mouse models of PD (Ingham *et al.*, 1989, 1993, 1998; Day *et al.*, 2006; Solis *et al.*, 2007) and could be related to decreased connectivity and glutamatergic cortical input to the striatum (McAllister, 2000; Day *et al.*, 2006).

3.4.4 Comparison of the neurological effects of urethane and ketamine

Ketamine anesthesia is associated with a faster slow oscillation in M1 LFP (Magill *et al.*, 2000; Fontanini *et al.*, 2003; Musizza *et al.*, 2007) and a different mechanism of action from urethane. In the present study, a second series of animals were studied under ketamine anesthesia. Results showed that PPN spike timing with respect to M1 was not significantly modulated in ketamine-xylazine anesthetized rats. Unlike in the urethane-anesthetized preparation, 6-OHDA lesion in the ketamine-anesthetized rat had no significant effect on PPN spike power, PPN or M1 LFP power, coherence between PPN

spike and LFP activity, coherence between PPN LFP and M1 LFP activity, or on the phase relationships between PPN spiking and LFP oscillations.

Urethane has been shown to have a modest effect on several neurotransmitter-gated ion channels at concentrations close to those used for maintaining anesthesia (Hara and Harris, 2002) but may preferentially affect Ba^{2+}-sensitive K^+ leak conductance (Sceniak and Maciver, 2006). These effects on ion channel physiology may confer urethane with its anesthetic properties. Ketamine's anesthetic effect, on the other hand, is thought to result from its action as a non-competitive NMDA-receptor antagonist (Rudolph and Antkowiak, 2004; Wolff and Winstock, 2006), which ultimately results in depression of neuronal responses by interfering with the excitatory effects of glutamate (Anis *et al.*, 1983; Wolff and Winstock, 2006).

Ketamine may have effects similar to NMDA antagonists such as amantadine which are effective adjuvant parkinsonian therapies (Papa *et al.*, 1995; Papa and Chase, 1996; Blanchet *et al.*, 1997, 2003; Verhagen *et al.*, 1998; Luginger *et al.*, 2000). Furthermore, NMDA antagonists acting at the level of the STN could reduce glutamatergic STN output (Greenamyre and O'Brien, 1991; Allers *et al.*, 2005). In the intact rat, reduction of excitatory oscillatory output from the STN to the PPN would decrease the incidence of PPN firing phase-locked to firing in the cortex. In the 6-OHDA lesioned rat, the reduction of excitatory oscillatory output from the STN to the basal ganglia output nuclei would result in decreased inhibitory oscillatory output from the SNpr/GPi to the PPN which would also decrease oscillatory firing in the PPN.

Therefore, ketamine could compensate for the effects of dopamine cell lesion via its NMDA antagonist properties and consequent effects on basal

ganglia-thalamocortical networks. In contrast, though urethane is not a neurologically inert compound, its limited and non-specific effects on inhibitory and excitatory neurotransmission (Hara and Harris, 2002) make it a good anesthetic candidate for studying the effects of striatal dopamine depletion.

3.4.5 Relevance to faster oscillations in Parkinson's disease patients

Anesthetized preparations were used in the present investigation to probe the effect of dopamine cell lesion on the transmission of slow ~1 Hz oscillatory activity from the M1 to the basal ganglia and PPN. However, oscillations in the θ (3-8 Hz), α (8-12 Hz), and β (12-30 Hz) frequencies tend to dominate LFP recordings in the cortex and basal ganglia of awake PD patients (Salinas and Sejnowski, 2001; Brown, 2003). Our results in the anesthetized animal should be interpreted conservatively with regard to phase relationships during the transmission of faster frequency oscillations through basal-ganglia/PPN/thalamocortical networks as lags due to axonal conduction and synaptic transmission may become more relevant. However, the network dynamics observed in this study may be relevant to transmission of lower physiological frequencies such as the <30 Hz frequencies that have been associated with parkinsonian motor symptoms (Brown, 2003).

Main Findings

- *PPN spike timing in PD is dominated by increased inhibitory oscillatory output from the basal ganglia output nuclei (GPi/SNpr).*
- *The effect of this inhibitory oscillatory basal ganglia output on PPN spike timing may be attenuated by NMDA antagonists.*

4. MODULATION OF STN AND PPN LFP ACTIVITY DURING SIMPLE VOLUNTARY MOVEMENT

Although the PPN and STN are strongly interconnected (Section 2), inhibitory oscillatory output from the GPi/SNpr appears to have a greater effect on PPN spike timing in PD (Section 3) suggesting that oscillatory activity could be differently modulated in the STN and PPN in the parkinsonian brain. Modulation of β and γ oscillations in the STN has been correlated with voluntary movements and motor imagery in PD patients. The PPN has not been studied as extensively in the context of LFP activity modulation during voluntary movement, but the PPN has been shown to be responsive to sensory input and has been implicated in sensory gating and integration. To further examine and compare the roles of the STN and PPN in voluntary movement, we compared STN and PPN LFP activity recorded from PD patients performing internally-generated (IG) and externally-cued (EC) voluntary movements.

4.1 Modulation of STN LFP activity during cued and self-paced voluntary movements

4.1.1 Introduction and rationale

The role of STN oscillatory activity can be probed by recording LFPs from DBS macroelectrodes implanted in the STNs of PD patients. As discussed earlier (Section 1.2), it is thought that low frequency basal ganglia oscillations

(8-30 Hz, α and β bands) are generally “antikinetic” while γ oscillations (>60 Hz) are “prokinetic” (Brown, 2003).

Further studies have correlated STN LFP activity in either the full β band (11-30 Hz, though this definition varies across studies) or in the grouped α and β bands (8-30 Hz) with various motor tasks. Event-related desynchronization (ERD) in the full β range and the grouped α and β range has been observed in STN LFPs during self-paced (Paradiso *et al.*, 2003; Alegre *et al.*, 2005; Doyle *et al.*, 2005; Kempf *et al.*, 2007) and visually-cued voluntary movements (Cassidy *et al.*, 2002; Kuhn *et al.*, 2004, 2006; Williams *et al.*, 2005; Klostermann *et al.*, 2007).

However, there is a functional distinction between the α (8-12 Hz), low β (12-20 Hz), and high β (20-30 Hz) frequency bands. For example, suppression of the low β band is more accentuated in PD patients by the administration of L-DOPA than is suppression of the high β band (Priori *et al.*, 2002, 2004). Also, while the task-related modulation of the full β band is similar between the thalamus, cortex, and the STN, modulation of α band activity appears to differ greatly between these structures (Klostermann *et al.*, 2007).

Therefore, several issues regarding the motor function of STN oscillations need to be addressed: (1) The modulation of oscillatory activity in narrow frequency bands in the STN has not been compared directly between IG and EC movements in the same subject group; (2) A direct comparison of STN LFP activity between IG and EC tasks may allow for further functional decomposition of STN LFP signals; and (3) While the modulation of STN activity has been examined only during slow voluntary movement in PD patients, with a median inter-movement interval of 8 sec (ranging from 5-30

sec) (Priori *et al.*, 2002; Cassidy *et al.*, 2002; Williams *et al.*, 2003, 2005; Paradiso *et al.*, 2003; Kuhn *et al.*, 2004, 2006; Loukas and Brown, 2004; Alegre *et al.*, 2005; Doyle *et al.*, 2005), parkinsonian bradykinesia may be more exposed during rapid movements (Sheridan *et al.*, 1987; Agostino *et al.*, 1998; Taylor Tavares *et al.*, 2005).

In this study, we hypothesize that modulation of STN LFP oscillations may be coded in narrower frequency bands than those previously studied, and may be attributable to the different sensorimotor events of voluntary movements in PD. To test this hypothesis, modulation of STN LFP signals was compared between IG and EC movements with short inter-movement intervals ranging from 1 to 5 sec. Furthermore, event-related desynchronization (ERD) and synchronization (ERS) were investigated in the STN LFP signals decomposed into the θ (3-8 Hz), α (8-12 Hz), low (12-20 Hz) and high β (20-30 Hz), and low (30-60 Hz) and high γ frequency bands (60-90 Hz), and compared between tasks in their magnitudes, timings, and laterality.

4.1.2 Methods

4.1.2.1 Patients, electrode implantation, and electrode placement confirmation

Six patients (age 58 ± 2 years) with PD participated in this study. Their clinical details are summarized in Table 4.1. All subjects provided informed consent and approval of the study was obtained from the local research ethics committee.

Detailed surgical procedures have been described previously (Liu *et al.*, 2001, 2002) and are summarized here. The DBS electrodes (Model 3387, Medtronic Neurological Division, Minneapolis, MN, USA) were bilaterally

implanted in STN for the treatment of severe PD. LFPs were recorded via the externalized leads from the STN during the week immediately post-implantation before the pulse generator was implanted. The electrode has 4 platinum-iridium cylindrical contacts (1.27 mm in diameter and 1.5 mm in length) that are separated by a 1.5 mm gap. Patients underwent bilateral implantation of DBS electrodes in the STN using Radionics Image Fusion and Stereoplan (Integra Radionics, Burlington, MA, USA). The T2-weighted MRI images are fused and spatially corrected to the stereotactic CT scan to minimize the inherent errors secondary to field inhomogeneities in MRI scanning. The STN is localized as a hyperintense area 2–4 mm anterolateral to the red nucleus and 2–4 mm above the SN in the Stereoplan programme. The electrode position was confirmed by noting a decrease in parkinsonian symptoms during intra-operative electrical stimulation of the target STN site and by examining the post-operative MRI scan or the fused images of pre-implantation MRI with post-implantation CT. Figure 4.1 shows representative post-operative fused images, 2 mm in thickness, of bilateral DBS electrode positions in one patient. In all patients, the contact positions were estimated by their proximity to the electrode tip upwards based on the geometry of the electrode. The positions of the electrode contacts could be directly identified as hollow rings of high intensity in transverse sections (Fig. 4.1A) which could be visually differentiated from the electrode wires which appeared as smaller solid dots in the transverse and coronal sections (Fig. 4.1B).

The center of the STN was identified on the transverse slice in which the red nuclei appeared largest in diameter (Fig. 4.1A). The relative positions of electrode contacts to the STN center were then estimated on the images

around this slice. The contacts visually confirmed to be within the STN are indicated in Table 4.1 for each patient. The contact pair (composed of contacts 0-1, 1-2, or 2-3) within the STN chosen for analysis demonstrated the greatest percentage β (12-30 Hz) modulation surrounding the movement (Williams *et al.*, 2003; Chen *et al.*, 2006) relative to the amplitude of β modulation during the baseline activity period occurring 1-2 sec before the registration of the motor response (see *Signal Processing and Analysis* in Methods). In one patient exhibiting tremor during the recording session, all contacts demonstrated similar amounts of β modulation with movement, so the contact pair that appeared to show maximum oscillations at the tremor (θ) frequency was chosen for analysis (Liu *et al.*, 2001).

A methodological issue here is correlation of the STN LFPs with detailed anatomical localization so that the generator of the modulated activity may be identified. This has been attempted using a combination of single unit and LFP recordings in a recent study (Trottenberg *et al.*, 2006), in which activity during rest was best described as being recorded in the upper STN and bordering the zona incerta. In this study, we relied on post-operative fused CT/MRI images and LFP recordings to localize the electrode contact relative to the STN and were thus unable to determine whether a pair of electrode contacts or only one contact was actually inside of the STN as β modulation could be detected in both situations with a bipolar setting. The spatial resolution of the electrode localization in this study was defined by two sets of parameters: (1) the 2 mm thickness of post-operative CT scans; and (2) the distance between neighboring pairs of electrode contacts in the DBS electrode (1.5 mm for each contact + 1.5 mm separation between contacts). These two factors allowed us

to achieve a spatial resolution of 2.0 to 3.0 mm. Therefore, the STN LFPs described in this study may have been recorded from a region including, but not completely limited to, the STN. It is important to note, however, that the field potential generated by the STN can radially conduct outwards to the surrounding brain area (Liu, 2003; Kuhn *et al.*, 2005; Chen *et al.*, 2006). The amplitude of the LFPs correlates with the proximity of the recording electrode to the 'source nucleus' (Liu, 2003; Kuhn *et al.*, 2005) and slight differences in electrode localizations between recordings do not affect the time-frequency profile of LFPs (Chen *et al.*, 2006).

4.1.2.2 Visuomotor paradigms

STN LFPs and surface EMGs were recorded together during two finger-pressing tasks which were carried out in a random order with short resting periods between tasks.

Patients were seated approximately 60 cm from a computer screen. Prior to each motor task, patients were instructed to place their left and right index fingers on distinct keys on the left or right hand side of a standard keyboard, respectively, and to look at a 10 mm cross that was continuously displayed in the center of the screen. In the IG motor task, the subjects were asked to press a key with either their left or right index finger at random self-paced intervals. Movements that were executed <1 sec before or >5 sec after the previous movement were excluded to ensure a finite range of inter-movement intervals and to specifically examine rapid repetitive movements.

Table 4.1. Summary of Subjects' Clinical Details

Subject No./ DBS Target	Age	Sex	Disease Duration (years)	Motor UPDRS Score (on / off med)	Electrode Contacts used for Stimulation (+/-)	Electrode Contacts Located w/in Target	Electrode Pair Used for Analysis	Medication (daily dose)
1 / STN	64	M	13	15 / 36	System removed due to infection	L2 R1	L12 R01	Sinemet 625 mg Entacapone 800 mg Ropinirole 96 mg Amitryptiline 25 mg
2 / STN	60	M	13	10 / 35	L1, - R1, -	L1 R2	L12 R23	Sinemet 625-750 mg Selegiline (Eldepryl) 5 mg Ropinirole 10 mg
3 / STN	58	M	7	- / 43	L0, L1 R2, R1	L2 R2	L23 R23	Trihexyphenidyl 8-10 mg
4 / STN	57	F	10	21 / 44	L0, - R2, R1	L0 R1	L01 R12	Sinemet 500 mg Mirapexin 2.8 mg Thyroxine 150 mcg
5 / STN	55	M	10	33 / 60	L1, - R1, -	L1 R1	L12 R12	Apomorphine 200 mg + 6 mg bolus (pen)
6 / STN	53	F	3	19 / 30	L1, - R2, -	L2 R2	L23 R12	Madopar 375 mg Fluoxetine 40 mg Domperidone 20 mg
STN Mean± SE	***58±4***	**----**	***9±4***	***20±9 / 41±11***	**----**	**----**	**----**	**----**
7 / PPN	55	M	12	29 / 57	L1, L2	L2	L12	Madopar 500 mg Pramipexole 0.7mg Amantadine 100 mg Apomorphine 50 mg Domperidone 40 mg

L/R: Side of DBS electrode implantation (left/right), 0/1/2/3: DBS electrode contact.

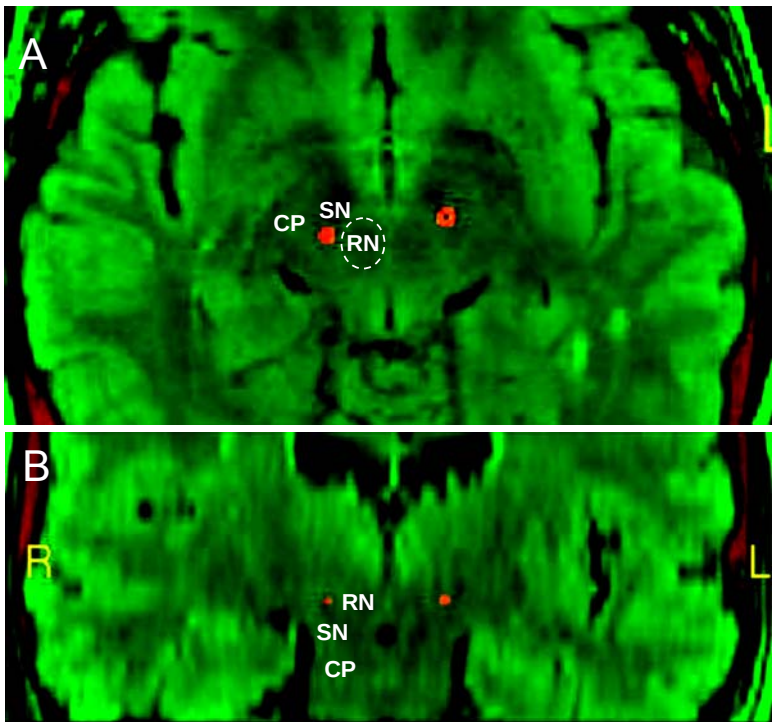

Figure 4.1. Localization of DBS Contacts within the STN. A) DBS contacts within the STN are shown in a transverse slice (2 mm thick slices parallel to the anterior commissure-posterior commissure line) obtained by fusion of pre-operative MRI scan with post-operative CT scan (Liu *et al.*, 2001). Key structures used for localization are labeled. B) The DBS electrode wires are visible in a coronal slice. CP-cerebellar peduncle; RN- red nucleus; SN-substantia nigra.

In the EC task, a visual cue (the letter A, 8 mm in height and 7 mm in width) appeared on the screen for a period of 400 msec to the immediate left or right of the central cross as a signal cueing the onset and laterality of the subsequent finger movement response. The prediction of the timing or laterality of the visual cue was limited as the cues were presented at random intervals between 1 and 5 sec, comparable to those of the IG task, and cue laterality to the fixation cross was pseudo-randomized as well. Subjects were instructed to press the key ipsilateral to the cue with the corresponding index finger as quickly as possible. Movements associated with reaction times >1 sec were excluded from

further analysis. The size of the visual cue ensured a small visual angle (<0.7°) from the central cross thus preventing significant ocular movements from occurring (Young and Sheena, 1975; Oster and Stern, 1980).

4.1.2.3 LFP and EMG recordings

STN LFP recordings were made from the externalized electrodes 4-6 days post-operatively after the patients had been off medication over night. The LFPs were recorded with a bipolar configuration from the three adjacent pairs of 4 contacts of each macroelectrode (contacts 0-1, 1-2, and 2-3). Signal segments containing premature, absent, or erroneous responses to visual cues were excluded. In addition to noting the time of the key press as registration of the motor response, the onset of the motor response and the onset of other voluntary or involuntary movements were monitored using surface EMGs recorded from the index finger extensor (*Extensor digitorum*) and flexor (*Flexor digitorum*). The full finger movement, as indicated by EMG activity, involved flexion from resting state on top of the key (finger downswing) to the point of motor response registration (the key press, recorded as a TTL signal from the keyboard) and then recovery to resting state on top of the key (finger upswing). In studies examining the average duration of muscle activation during finger tapping, the time from the beginning of finger downswing to the end of finger upswing is well within ± 100 msec from the time of motor response registration (Dennerlein *et al.*, 1998; Kuo *et al.*, 2006). That is, the actual period of motor execution began <100 msec before the time of motor response registration and lasted for <100 msec after the

time of motor response registration. This was corroborated by EMG recordings in this experiment as well (data not shown) and, consequently, reactive finger movements could be identified as sharp EMG bursts within 200 msec in duration. Signals were amplified using isolated CED 1902 amplifiers (×10,000 for LFPs and x1000 for EMGs), filtered at 0.5-500 Hz and digitized using CED 1401mark II at a rate of 4000 Hz, displayed on line and saved onto a hard disk using a custom written program in Spike 2 (Cambridge Electronic Design, CED, Cambridge, UK).

4.1.2.4 Signal processing and analysis

STN LFP and EMG recordings were processed in a custom written program Neural Signal Processing Lab (NSPL) in MATLAB (Version 7.0, The MathWorks Inc., Natick, MA, USA). LFP recordings were selected by excluding the segments contaminated with unintended movements based on surface EMGs. LFPs, originally recorded with a sampling rate of 4000 Hz, were re-sampled at 500 Hz in order to design the filters with varied bandwidth for extracting LFP activity in the selected frequency ranges. The LFPs were then digitally bandpass-filtered between 3-8 Hz (θ), 8-12 Hz (α), 12-20 Hz (low β), 20-30 Hz (high β), 30-60 Hz (low γ), and 60-90 Hz (high γ) frequencies using a Chebyshev Type I filter with zero-phase shifting. As the bandwidth varies from 5 to 30 Hz in a given frequency band, the Hilbert transform was used to extract the instantaneous amplitude of the filtered signal to achieve optimal temporal resolution in each band. The Hilbert Transform is preferable to other methods

such as ‘squaring’ the signal which tends to maintain or amplify signal noise and also poorly handles small inter-trial phase offsets when multiple trials are averaged (Hahn, 1996; Oppenheim and Schafer, 1998; Marple, 1999). The Hilbert transform algorithm is summarized as: Let x(n) be the filtered signal and X(k) be the Fourier transform of x(n), where n, k=1, 2, …., N. Then, Y(k) are obtained from X(k) by multiplying X(k) with 2 for k=2, 3, …., N/2 and setting X(k) as zeros for k=N/2+2, N/2+3, …., N. The analytic signal x_a(n) of x(n) is computed by performing the inverse Fourier transform of Y(k). x_a(n) is a complex signal and can be expressed as $x_a(n)=A(n)*\exp(i*\phi(n))$, where A(n) and ϕ(n) are the instantaneous amplitude and phase of x(n), respectively. Figure 4.2 shows the compound STN LFP signal (left, Fig. 4.2), the signal bandpass-filtered to the low β band (middle, Fig. 4.2), and the instantaneous amplitude-modulation of the bandpass-filtered signal processed using the Hilbert transformation (right, Fig. 4.2). Data are shown over three consecutive EC movement trials each composed of visual cue presentation (the downward bars in the top trace, Fig. 4.2) and the registration of the subsequent motor response (the upward bars in the top trace, Fig. 4.2).

The amplitude of the bandpass-filtered transformed signals was observed in each trial between 2 sec before and 3 sec after each external cue and/or motor response registration in each subject. An example is shown for one patient in Figure 4.3, which presents amplitude modulation of each frequency band, coded in color, during the EC task over 80 trials. Signals were analyzed time-locked to the presentation of the visual cue (left, Fig. 4.3) or to the time of motor response

registration (right, Fig. 4.3) and were ordered by motor reaction time (top figure of each row, Fig. 4.3) or averaged across trials (bottom graph of each row, Fig. 4.3) in each frequency band confirming that activity in the low and high β bands is primarily locked to the time of motor response (Williams *et al.*, 2005). In addition, activity in the θ, α, and γ bands appeared to show activity time-locked to the time of motor response. Therefore, all further statistical analyses were conducted on signals time-locked to the registration of the motor response.

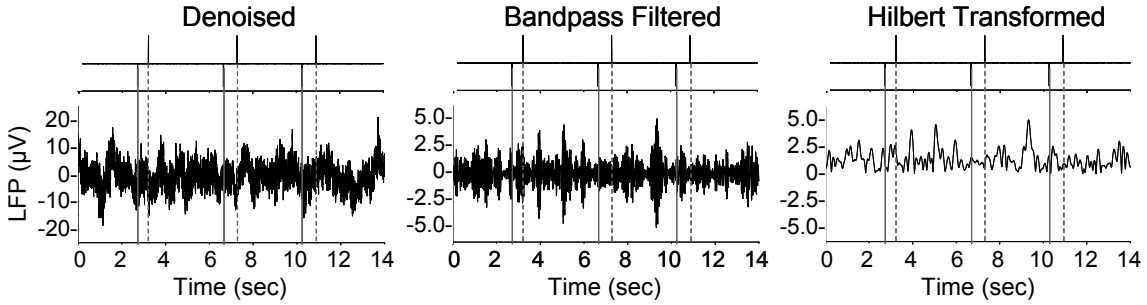

Figure 4.2. Processing of STN LFPs. An example of a signal recorded during an externally-cued movement task in one patient is shown bandpass-filtered between 12 and 20 Hz (low β band). STN LFPs recorded during the movement task are denoised (left) and decomposed in the time-frequency domain using bandpass-filtering (middle). The power envelope signals in each frequency band were extracted using the Hilbert transform (right). The time of stimulus presentation and the registration of the subsequent motor response are shown using solid and dashed vertical lines, respectively, and, in the top traces, as downward and upward bars, respectively.

Given that the minimum inter-movement interval in the EC and IG tasks is 1 sec, when averaging event-related potentials (ERP) across all trials, LFP modulation related to the previous and subsequent movements relative to each trial may have also been averaged in the time period ranging from 2 sec before to 3 sec following the motor response. However, since there is inherent variability in the inter-movement intervals between 1 and 5 sec for each patient in the IG

task, and since the inter-cue intervals in the EC task are comparably randomized within a 1 to 5 sec range, a baseline-amplitude of ERP modulation is still clearly discernable from the modulation surrounding the motor response itself (bottom graphs in each row, Fig. 4.3). It is important to note that this baseline period does not necessarily represent a state of motor rest, but it does represent a consistent background level of LFP activity in a given frequency band relative to which changes in LFP activity modulation can be examined. This method allows for the examination of LFP modulation related to the brisk and rapidly-executed movements in this study. The bandpass-filtered LFPs in a given task for each patient were expressed as a percentage of this baseline amplitude value, calculated as the mean amplitude over the period between 1 and 2 sec prior to the registration of the motor response.

The cross-patient average of these normalized traces was then calculated. The time and amplitude of ERD or ERS induced by the motor response for each patient were determined from the local minimum or maximum between 0.5 sec before and 0.5 sec after motor response registration in the normalized trace. Visual examination of the normalized traces confirmed that the peak amplitude was not outside of this 1 sec window centered at the time of motor response registration. The onset of frequency band modulation was not directly calculated as the cut-off between baseline activity and task-related amplitude modulation because it could not be accurately determined given the short inter-movement intervals in the EC and IG tasks. Instead, the time of greatest modulation (ERD or ERS) of each frequency band was determined relative to the time of motor

response registration. While onset represents the time of event occurrence, the time of greatest amplitude modulation represents the length of process of the event from occurrence to its peak. Any delay of this process will delay the peak latency. The normalized values in amplitude and time of peak ERD or ERS were averaged across the all subjects to represent the population.

4.1.2.5 *Statistical analyses*

Five subjects completed both tasks and one additional subject completed the IG task only. In the EC movement task, 9 electrodes were analyzed for each STN hemisphere (in one subject, only information on EC movement executed by the right index finger was available). After excluding trials with incorrect EC responses or artifacts, 96±25 trials (ranging from 43 to 171 trials) were analyzed for each electrode for the EC movement task. During the IG movement task, 7 electrodes were analyzed for each STN hemisphere (in one subject, only information on EC movement executed by the right index finger was available and another subject performed the vast majority of movements within 1s of the previous movement). After excluding movement artifacts or movements that were performed within 1 sec or greater than 5 sec after the previous movement, 94±28 trials (ranging from 40 to 150 trials) were analyzed for each electrode in the IG movement task.

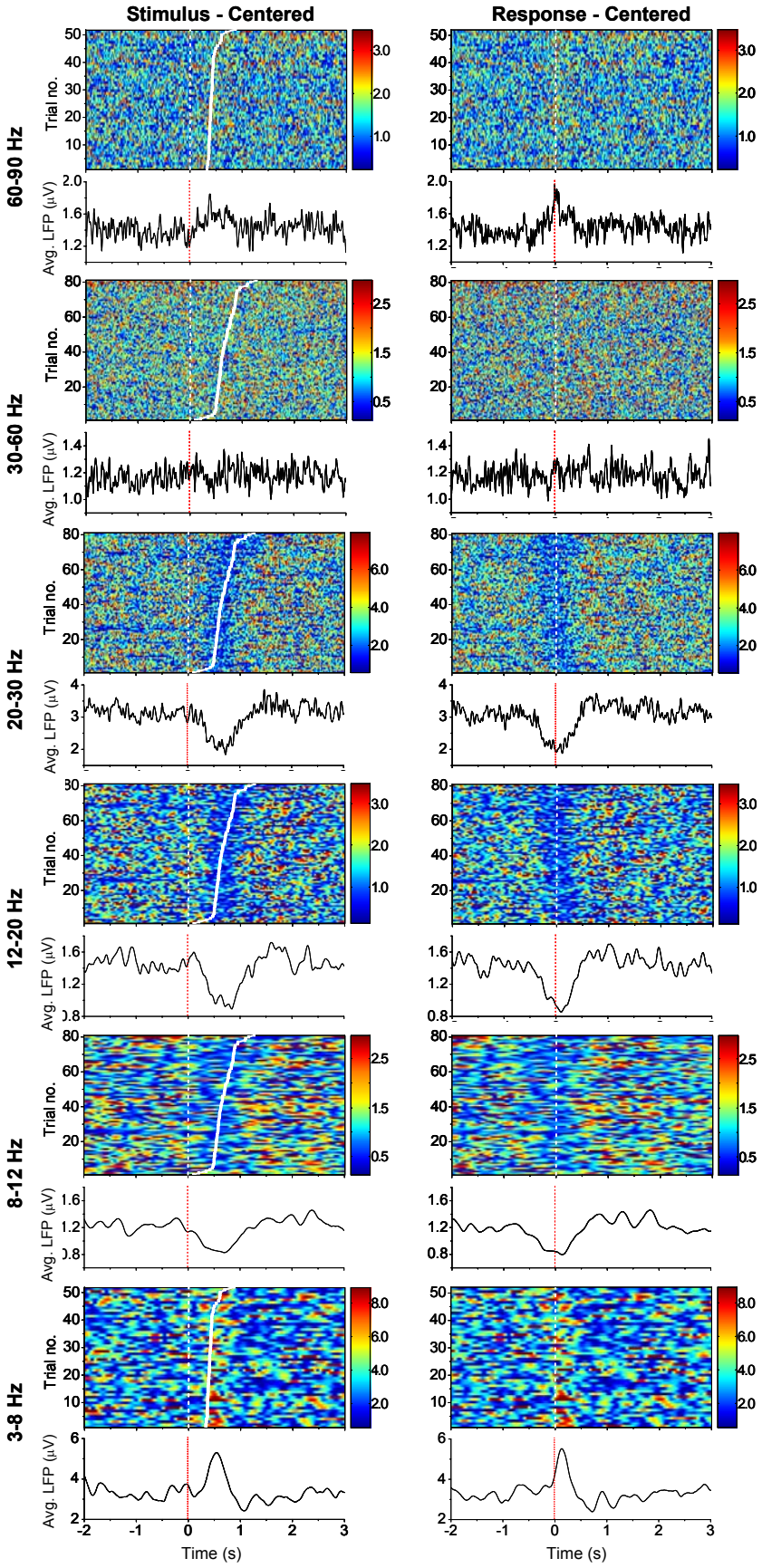
Stimulus - Centered
Response - Centered
60-90 Hz
30-60 Hz
20-30 Hz
12-20 Hz
8-12 Hz
3-8 Hz
Trial no.
Avg. LFP (μV)
Time (s)

Figure 4.3 (on previous page). STN LFPs recorded during an externally-cued movement task in one subject are shown in a 5 sec window across frequency bands (rows) centered at either the time of stimulus presentation (left column) or the time of the response registration (right column). The top figure in each row shows the power in a given frequency band over time for each trial (visual cue followed by a response) with trials ordered by increasing reaction time. Time zero is marked by a vertical thin dotted line indicating the time of stimulus presentation (left column) or response registration (right column). In the stimulus-centered figures, the time of response registration is indicated by a thick dotted line. LFP power is coded in color with a unit of μV. The bottom figure in each row shows the power in the frequency band over time averaged across all trials. Modulation of the θ, α, low and high β, and high γ bands appears locked to the time of response and there is no modulation of the low γ frequency band.

All statistical analyses were processed using SPSS (SPSS Inc., Chicago, IL, USA). Normal distributions of the ERD/ERS values in amplitude and timing across all STNs were tested using the Shapiro-Wilk and Kolmogorov-Smirnov tests. Amplitude data were normally distributed. Three-way ANOVA analysis using a univariate general linear model was used to test the interaction between and the influence of task type (IG vs. EC), STN LFP frequency, and laterality of the STN on the amplitude of peak ERD/ERS and, separately, on the timing of peak ERD/ERS. One-way ANOVA was used to test changes in STN activity across frequency bands in each task, followed by t-tests to compare activity in two frequency bands directly. T-tests were also used to test changes between EC and IG tasks and between contralateral and ipsilateral STNs. Criterion of significance was $p<0.05$. The values in the figures and in the text are all presented as mean ± SEM.

Table 4.2. Mean Amplitudes and Times of Peak Modulation of STN LFP Activity in Each Frequency Band

	Amplitude of Peak Modulation				Time of Peak Modulation			
	Contralateral		Ipsilateral		Contralateral		Ipsilateral	
	EC	IG	EC	IG	EC	IG	EC	IG
3-8 Hz	119.7±8.6 (*)	100.3±6.2	108.2±10.6	101.1±5.7	-0.07±0.07	0.09±0.09	-0.07±0.07	0.08±0.08
8-12 Hz	74.9±3.1 (*)ξ	88.5±3.9 (*)ξ	76.6±4.8 (*)	103.8±6.7	0.15±0.05 (*)ξ	-0.03±0.06 ξ	0.13±0.05 (*)	-0.02±0.06
12-20 Hz	63.7±2.9 (*)ξ	78.8±2.2 (*)ξ	65.0±3.5 (*)	85.5±4.8 (*)	-0.01±0.03	0.06±0.05	-0.04±0.04	0.09±0.04
20-30 Hz	74.8±2.8 (*)	81.3±5.0 (*)	79.4±5.0 (*)	91.1±5.3	0.12±0.08	0.03±0.04	0.05±0.07	0.04±0.07
60-90 Hz	110.1±6.9 (*)	111.8±8.2	109.8±5.3	111.0±8.0	0.10±0.06	0.00±0.07	-0.02±0.10	-0.04±0.10

All values show the mean ± SEM, averaged across all subjects. The amplitude values indicate the percent of the baseline level of STN LFP activity in a given frequency band at the time of peak modulation (baseline = 100%). The times (sec) are shown relative to the time of motor response registration (0 sec). Values that are significantly different from the baseline level of activity or from the time of motor response registration are indicated with an asterisk ((*)). Values that are significantly different between tasks are indicated with a lower-case sigma (ξ).

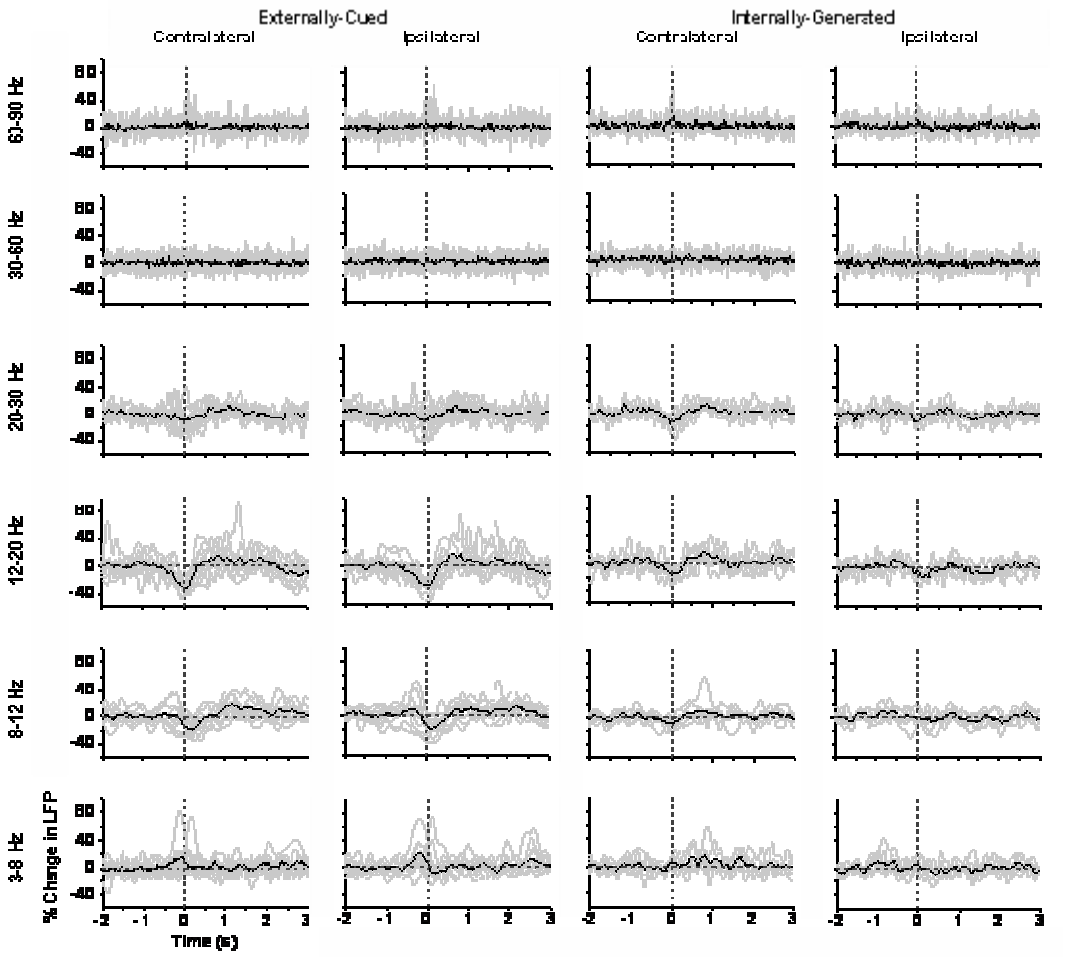

Figure 4.4. STN LFP traces, averaged across all trials, and normalized to average baseline LFP amplitude, are shown overlaid for all patients (gray) along with a mean trace averaged across patients (bold black) for each frequency band in the contralateral and ipsilateral STN. The registration of the motor response (vertical dashed line) and the mean base line at 0% (horizontal dashed line) are indicated in each plot. Only the α, low β, and high β bands are modulated in both the EC (left) and IG (right) tasks (Fig. 4.6).

4.1.3 Results

The mean reaction time in the EC task, across all patients, was 0.55±0.01 sec. The averaged minimum and averaged maximum times between subsequent movements were 1.0 and 4.1 sec for the EC task and 1.0 and 3.6 sec in the IG task. The normalized STN LFP traces in the θ, α, low and high β,

and low and high γ frequency bands were averaged across all patients and grouped by laterality to the movement (Figs. 4.4, 4.5).

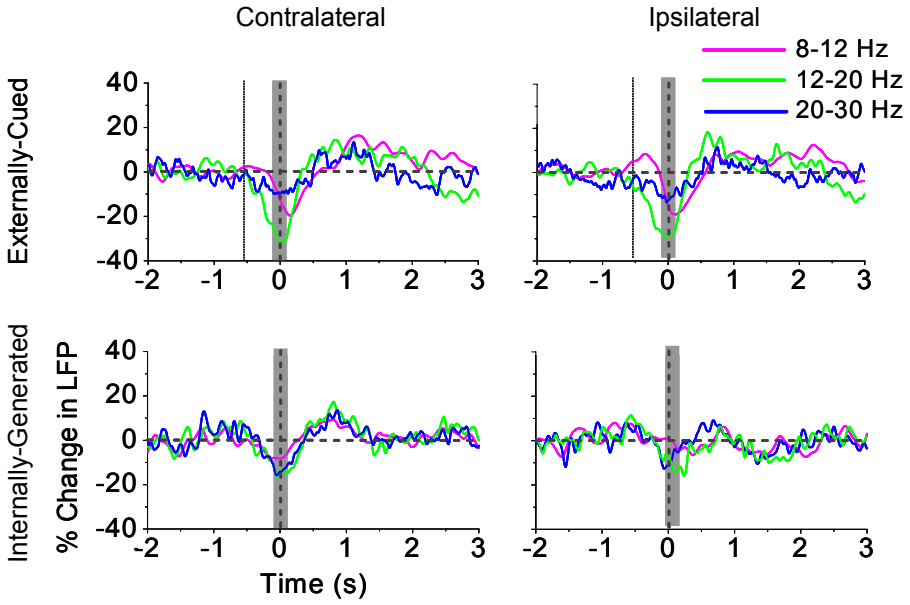

Figure 4.5. As only the α, low β, and high β bands are modulated in both the EC (top row) and IG (bottom row) tasks (Figs. 4.4, 4.7), comparison of the average normalized traces of STN LFP activity in the α (pink), low β (green), and high β (blue) frequency bands is shown. LFP modulation in the contralateral STN is shown in the left column and modulation in the ipsilateral STN is shown in the right column. In each plot, the vertical dashed line at time '0' shows the time of motor response registration. The horizontal dashed line shows the mean base line power value at 0%. The gray boxes indicate the average duration of EMG activation (Dennerlein *et al.*, 1998; Kuo *et al.*, 2006). For the EC task (top row), the first vertical dashed line shows the average time of the cue presentation relative to the time of motor response registration (average reaction time was 0.55±0.01 sec from the time of cue). There is greater bilateral modulation of these frequency bands with EC movement than there is with the IG movement.

Across all data, there was a significant difference in the peak amplitude of ERD/ERS across frequency bands (*three-factor ANOVA; n = 32;* $p<0.001$) and between the contralateral and ipsilateral STN ($n = 80$; $p<0.05$). There was also a significant interaction between task and frequency band in both the time ($p<0.05$) and peak amplitude of ERD/ERS ($p<0.005$). Table 4.2 shows the mean (±SEM) values for the amplitude and time of peak modulation in each

frequency band in the contralateral STN and ipsilateral STN during the EC and IG motor tasks.

4.1.3.1 Similarities in STN LFP modulation between EC and IG tasks

The most clear similarity between tasks was that significant ERD of the low β band was observed in the STN bilaterally during both EC and IG movements (t-test; $p<0.05$) (Table 4.2, Figs. 4.4, 4.5, 4.6), with the peak modulation of the low β band occurring close to the time of motor response registration (Table 4.2, Figs. 4.4, 4.5, 4.7). ERD of the low β band began before and lasted after the time of EMG activation in both tasks as well (Fig. 4.5). This suggests that the ERD of the low β band specifically represents the motor execution element of the 'button pressing' movement, which was identical in both tasks. Modulation of the α and high β bands was also observed during both EC and IG movements but modulation of the low γ band was not observed in either task (Fig. 4.4).

4.1.3.2 Differences in STN LFP modulation between EC and IG tasks

There were four main differences between STN activity modulation during EC and IG movements. First, EC movement was associated with greater bilateral modulation of STN activity than IG movement. Significant ERD was observed bilaterally in the α ($p<0.001$), low β ($p<0.001$), and high β bands ($p<0.01$) during the EC task, while bilateral modulation only occurred in the low β band with IG movement ($p<0.05$) (Table 4.2, Fig. 4.6). This may represent the difference between tasks in motor preparation as bilateral preparation was

needed preceding the directional cue in the EC task while the laterality of the movement was self-defined by the subjects in the IG task.

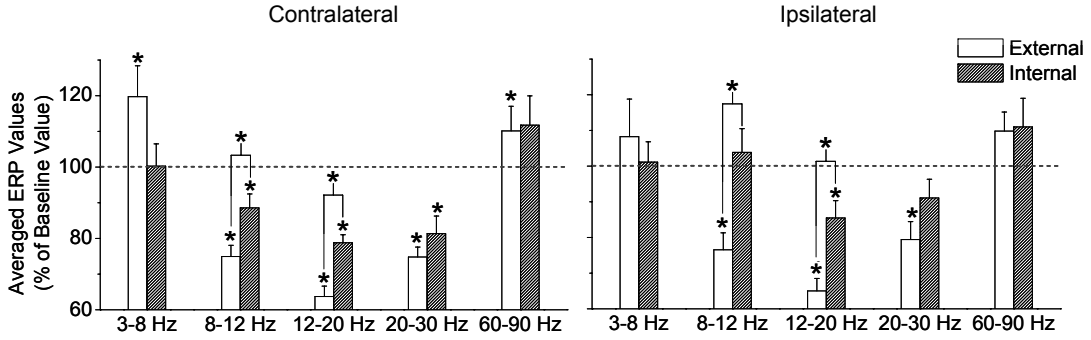

Figure 4.6. Mean levels of ERD and ERS (±SEM) in the θ, α, low and high β, and γ frequency bands in the contralateral (left) and ipsilateral (right) STN. ERD and ERS are shown as a percentage of the baseline value ± SEM (100%, horizontal dashed line). (*): significant modulation of STN LFP activity in a given frequency band relative to baseline or a significant difference in modulation amplitude between tasks in a given frequency band ($p<0.05$). Only the low β band is significantly modulated bilaterally during both types of movement. Greatest ERD occurs in the low β band bilaterally in the EC task and ERD in the α and low β bands is greater with EC movement than with IG movement bilaterally in the STN.

Second, STN activity modulation was observed in a wider frequency range during EC movement than during IG movement. In addition to bilateral suppression of the α, low β, and high β bands, significant ERS was observed contralaterally in the θ ($p<0.05$) and high γ bands ($p<0.05$) during EC movement (Table 4.2, Fig. 4.6). In contrast, IG movement modulation was limited to just the low β band bilaterally and to the α ($p<0.05$) and high β bands ($p<0.05$) contralaterally (Table 4.2, Fig. 4.6).

Third, EC and IG movement also differed in the amplitude of STN activity modulation. The magnitude of ERD in the α and low β bands was greater during the EC task than during the IG task, bilaterally ($p<0.05$) (Table 4.2, Fig. 4.6). Furthermore, during EC movement, the ERD in low β band was greater than ERD in the other frequency bands ($p<0.05$) though no such

differentiation in the amplitude of frequency band modulation occurred during the IG task (Table 4.2, Figs. 4.5, 4.6).

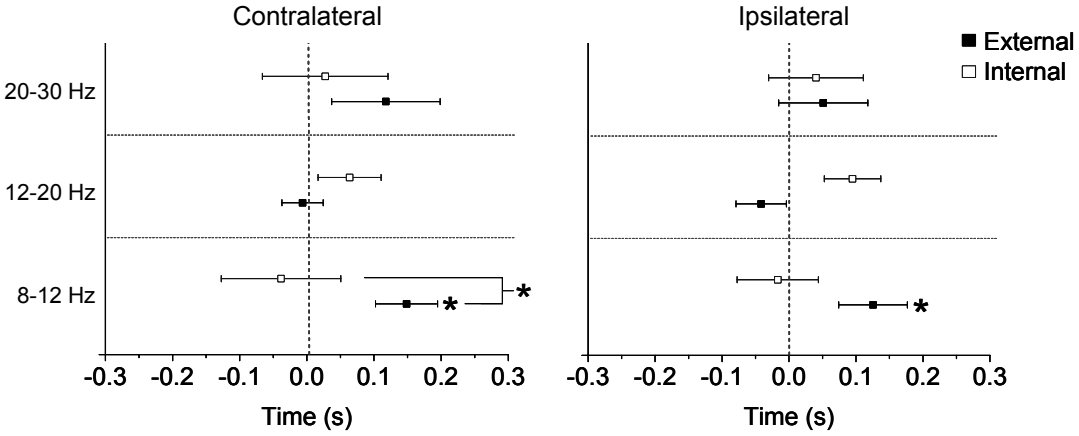

Figure 4.7. Mean time of peak STN modulation relative to the motor response (vertical dashed line) in the α, low β, and high β frequency bands in the contralateral (left) and ipsilateral (right) STN during IG (□) and EC movement (■). Error bars indicate SEM of the mean. (*): significant difference in the time of peak modulation and the time of motor response registration or a significant difference in the time of peak modulation between tasks in a given frequency band ($p<0.05$). Peak modulation of the α band occurs significantly after the motor response bilaterally with EC movement and significantly after it does during IG movement in the contralateral STN.

Finally, EC and IG movement also differed in the temporal profile of STN modulation. In the IG task, the times of peak ERD also did not differ between the α, low β, and high β bands and were all close to the time of motor response registration in the IG task (Table 4.2, Figs. 4.5, 4.7). On the other hand, in the EC task, peak desynchronization of the α band occurred significantly after peak ERD in the low β band ($p<0.05$) and after motor response registration ($p<0.05$) (Table 4.2, Figs. 4.5, 4.7). The onset and termination of α ERD also appeared to be later than ERD onset and termination, respectively, of the low and high β bands. Perhaps most interesting, however, is the delay in the onset and peak of α ERD in the EC task. This delay appeared to begin around the time of the visual cue and was absent in the IG task where there was no visual cue. Furthermore, the delay was consistently maintained relative to low β or high β

ERD (Figs. 4.5, 4.7). It is possible that this delay in α ERD is related to a period of processing the randomized directional cue.

4.1.4 Discussion

4.1.4.1 Modulation of STN activity related to motor preparation, selection, and execution

The EC and IG tasks can be compared in terms of the steps involved in a motor task: motor preparation, cue processing and/or movement selection, and motor execution (Goodale, 1998). The EC task required bilateral motor preparation to respond to a directional cue while motor preparation in the IG task was required only unilaterally. Also unlike the IG task, the EC task involved a period of movement selection following a visual cue. However, the finger movement itself was identical in both tasks. Therefore, by directly comparing EC and IG movements in this study, we can associate modulation of LFP activity in different frequency bands with these three motor task steps.

The high β band is most likely associated with motor preparation. High β ERD was observed bilaterally during EC and contralaterally during IG movement. This is in accordance with the different movement preparation demands of the two tasks and with several studies linking maximal high β cortical activity to motor preparation (Sanes and Donoghue, 1993; MacKay and Mendonca, 1995; Hamada *et al.*, 1999; Neuper and Pfurtscheller, 2001; Wheaton *et al.*, 2005). The peri-movement high β ERD observed here may be a more indirect reflection of motor preparation. Noting that even small movements can block high β activity related to motor preparation in the cortex (Sanes and Donoghue, 1993; Neuper and Pfurtscheller, 2001), perhaps the

existence of bilateral preparation during the EC task results in a bilateral decrease of high β oscillations with movement.

The most striking difference in α band modulation between the IG and EC tasks in this study is the delay in α ERD onset with cued movement. Following the cue in the EC movement task, the rates of desynchronization in the α and low β bands are similar but are consistently offset from each other by a delay that appears to occur at the time of cue presentation (Fig. 4.5). Therefore, an increase in or maintenance of α activity (Fig. 4.5) may be associated with a period of cue-processing and movement selection. Indeed, modulation of α activity has been associated with discriminating the meaning of visual cues in the sensory domain (Schmiedt *et al.*, 2005) and higher levels of basal α power in cortical EEGs are associated with better motor performance following a go cue (Klimesch *et al.*, 1996). However, given that α ERD in the EC task begins after movement onset and given the absence of this delay in the IG task, one may argue for an alternative explanation for α activity. It is possible that α ERD reflects processing of motor-related and non-motor-related visual information as the processing of the non-motor related visual information may last well after the time of movement itself. It has also been suggested that α ERD represents idle motor state cessation (Pfurtscheller and Neuper, 1994; Pfurtscheller *et al.*, 1997, 2000) necessary for voluntary motor execution. The delay and accentuation of α ERD in the EC task may, therefore, represent anticipatory motor facilitation of subsequent movements during a rapid motor task. This may help explain why a delay in α ERD onset has not been observed previously during more slow-paced voluntary motor tasks (Alegre *et al.*, 2005; Klostermann *et al.*, 2007).

Finally, the modulation of STN activity related to motor execution appears to mainly involve suppression of low β activity. Low β ERD occurs bilaterally in both tasks and its temporal profile is similar between tasks as well, consistently spanning the average duration of EMG activation (Fig. 4.5). Therefore, it is likely that low β ERD is primarily related to motor execution since it is similarly modulated between the EC and IG tasks. Previous conclusions that bilateral suppression across the entire β band occurs with movement (Williams *et al.*, 2003, 2005; Alegre *et al.*, 2005; Doyle *et al.*, 2005; Kuhn *et al.*, 2006; Kempf *et al.*, 2007; Klostermann *et al.*, 2007) may now be modified according to the results presented in this section to show that low β and high β activity in the STN may preferentially encode different pathophysiological information (motor execution and motor preparation, respectively).

4.1.4.2 Greater bilateral STN involvement during externally-cued movement

It is interesting to see bilateral STN involvement across a wider frequency range during EC movement than during IG movement. This may further reflect bilateral motor preparation or may reflect bilateral whole field visual input in the EC task. It is unlikely that bilateral involvement is only due to visual processing since the magnitude of β band modulation during cued movement can differ depending on the type of cue (Williams *et al.*, 2003) and the amount of motor involvement (Kuhn *et al.*, 2006). Furthermore, as shown in the present study, bilateral low β modulation occurs during IG movement, although to a lesser extent than it does during EC movement. Thus, the greater bilateral STN involvement during cued movement may be induced by the

demands of both bilateral acquisition of visual stimulation and the greater processing required for the visuomotor integration towards movement selection and preparation.

4.1.4.3 Role of the STN in facilitation of movement by an external cue in Parkinson's disease

It is known that the presence of a spatial or temporal external cue facilitates voluntary movement for PD patients (Glickstein and Stein, 1991; Georgiou *et al.*, 1993; Morris *et al.*, 1994; Thaut *et al.*, 1996; Burleigh-Jacobs *et al.*, 1997; Curra *et al.*, 1997; Majsak *et al.*, 1998; Kelly *et al.*, 2002). However, the mechanism underlying this facilitation is unclear.

There are two STN activity modulation phenomena observed in this study that may help shed light on this mechanism. First, there is a greater magnitude of α band ERD during cued movement than there is during self-paced movement. As aforementioned, α oscillations have been associated with cortical inactivity (Pfurtscheller and Neuper, 1994; Pfurtscheller *et al.*, 1997, 2000; Pfurtscheller and Lopes da Silva, 1999) and administration of L-DOPA has been shown to reduce α oscillations in the STN and GPi of PD patients (Brown *et al.*, 2001). Similarly, the results presented in this section show that the presence of an external cue further reduces α activity during movement in PD patients. Second, low β ERD during cued movement is greater than that during self-paced movement and is also greater than α and high β ERD during cued movement. Therefore, similar to what happens with administration of L-DOPA in PD patients (Priori *et al.*, 2004; Foffani *et al.*, 2005), an external cue preferentially accentuates low β band suppression.

Taken together, these results suggest that the presentation of an external-cue and the administration of dopaminergic medication may facilitate movement via a similar mechanism. This is especially plausible when considering that the improvement in voluntary movement conferred with cue-presentation and the improvement in movement following dopamine replacement therapy are not additive (Burleigh-Jacobs *et al.*, 1997; Kelly *et al.*, 2002).

4.1.4.4 STN LFP modulation specific to Parkinson's disease patients

As all recordings were done in PD patients off anti-parkinsonian medication, it is possible that certain modulation phenomena observed here were unique to PD. For example, antikinetic θ ERS was observed contralaterally during cued movement in this study. However, tremor-related oscillations also fell in this frequency band. Therefore, it is possible that the θ activity observed with cue presentation is related to attentional tremor and not necessarily to voluntary movement.

In addition, the lack of γ ERS during self-paced movement and the relatively small ERS observed during cued movement may be unique to PD patients. It has been shown that administration of L-DOPA to PD patients results in a shift from antikinetic β oscillation to prokinetic γ oscillation in the STN (Brown, 2003). Furthermore, bilateral γ band oscillation has been observed during self-paced movement performed by PD patients while on-medication. This suggests that, in parkinsonian patients off-medication, the role of synchronous γ frequency oscillations in the STN during motor execution may be diminished relative to healthy individuals or relative to patients on-

medication. The presence of an external cue, similar to L-DOPA, may help partially recover these prokinetic γ oscillations.

4.1.4.5 Concluding remarks

We have correlated STN LFP activity in different frequency bands with specific events related to voluntary movement. The results presented in this seciton suggest that: (1) Modulation of the high β band is related to motor preparation; (2) The delay in α ERD onset with cued movement may underlie a period of visual cue processing and movement selection or may be related to the facilitation of rapid movement execution; and (3) Bilateral ERD in the low β band is specifically related to motor execution.

4.2 Modulation of PPN LFP activity during cued and self-paced rapid voluntary movements

4.2.1 Introduction and rationale

The link between PPN activity and simple voluntary movement is a tenuous one. Primate studies have correlated akinesia with PPN lesions (Kojima *et al.*, 1997) and motor hyperactivity with PPN excitation (Nandi *et al.*, 2002a, 2002b). On the other hand, in rodents, it is argued that there may be a more nuanced relationship between the PPN and reward-directed motor behavior (Inglis and Winn, 1995; Winn, 2006). However, studies in decerebrate rodents and cats have shown that pharmacological or electrical stimulation of the PPN results in graded increases in locomotion during treadmill walking (higher current electrical stimulation corresponds to faster walking cadence)

(Garcia-Rill *et al.*, 1985, 1987; Reese *et al.*, 1995). This has also been corroborated by studies showing that unrestricted movement in an open field increases in intact rats following pharmacological or electrical PPN stimulation (Brudzynski *et al.*, 1986; Milner and Mogenson, 1988).

The PPN has also been implicated in attentional processes. PPN lesions in rats result in selective deficits in the execution of the classic five-choice serial reaction time task and also impair performance in a simpler attention task where an increase in the brightness of a light stimulus cues a given motor behavior (Inglis *et al.*, 2001; Kozak *et al.*, 2005). In addition, visual and auditory stimuli also modulate PPN activity (Reese *et al.*, 1995; Dormont *et al.*, 1998; Kobayashi *et al.*, 2002; Pan and Hyland, 2005) as PPN firing tends to increase in as little as 9 msec after the presentation of a sensory stimulus (Dormont *et al.*, 1998). These results suggest that the PPN plays a role in relaying the timing of sensory cues to other motor areas (Pan and Hyland, 2005) and possibly serves as a centre for sensory gating and integration (Winn, 2006).

Therefore, it is possible that PPN LFP modulation may occur during the preparation and execution of simple voluntary movements. Furthermore, this modulation may differ between IG and EC movement as these tasks require different levels of attention and sensory processing.

However, information on PPN LFP oscillatory activity in PD is limited. Although it is known that β oscillatory activity is prominent in the STN in PD, it is unclear whether this “antikinetic” oscillatory activity can also be found in the parkinsonian PPN. Furthermore, if β frequency oscillations are present in the PPN, it is difficult to predict how these oscillations would be modified by voluntary movement, if at all. Recently, α (7-11 Hz) oscillatory activity has been

reported in the PPN area of PD patients on dopaminergic medication. Furthermore, this activity appears to increase 3 sec before an IG movement (Androulidakis *et al.*, 2008). However, the location of the recording sites in this study (as described by Stefani *et al.*, 2007) have been questioned (Yelnik, 2007; Zrinzo *et al.*, 2007a, 2007b). Even if the recorded LFPs accurately reflect PPN activity, the modulation of oscillatory activity in the PPN during rapid IG and EC movement in PD patients off medication is still unknown.

In order to determine the range of oscillatory activity present in the PPN in the PD and whether this activity is modulated by different types of rapid voluntary movement, we repeated the experiments used to examine STN LFP modulation during IG and EC motor tasks (Section 4.1) in one patient who had received bilateral DBS electrode implants in the PPN (Patient 7, see Table 4.1).

4.2.2 Methods

The clinical details of Patient 7 are summarized in Table 4.1. Patient 7 provided informed consent and approval of the study was obtained from the local research ethics committee. The DBS electrodes (Model 3387, Medtronic Neurological Division, Minneapolis, MN, USA) were bilaterally implanted in the PPN as described earlier (Section 4.1.2, Fig. 4.2). Contact locations were determined on transverse and coronal sections of fused images of pre-implantation MRI with post-implantation CT. The PPN was identified on the transverse slice on which the superior cerebellar decussation was most prominent. The relative position of the contacts to the PPN center were then estimated on the images around this slice (Fig. 4.8). The contacts visually confirmed to be within the PPN in Patient 7 are indicated in Table 4.1 and the

contact pair closest to the center of the PPN, L12, was the contact pair chosen for analysis.

We first examined power spectra of PPN LFP activity when Patient 7 was at rest (seated with hands placed on lap) and during the IG and EC motor tasks. LFP recordings 100 sec in length were selected by excluding the segments contaminated with unintended movements based on surface EMGs. Windowed FFT was used to determine the dominant frequencies (the frequencies with the greatest spectral power) in the LFP for each 100 sec data segment binning at 2 msec, using a block size of 2048 yielding a frequency resolution of 0.24 Hz. This frequency resolution was sufficient for examining the presence of β (12-30 Hz) oscillations in the LFP signal. Figure 4.9 shows the PPN LFP power spectra when the patient was at rest, performing a series of IG movements, or performing a series of EC movements. As has been previously demonstrated in STN LFPs in PD patients, β oscillatory activity is also present in the PPN in the PD patient in this study. Therefore, after confirming that β oscillations were present in the PPN, we next examined whether these oscillations could be modified with an individual IG or EC movement event.

The EC and IG visuomotor paradigms, LFP and EMG recording procedures, and signal analysis techniques were the same as those used for examination of STN LFP activity modulation (Sections 4.1.2.2, 4.1.2.3, and 4.1.2.4). The amplitude of the bandpass-filtered transformed signals was observed in each trial between 2 sec before and 3 sec after each external cue and/or motor response registration. Figure 4.10 presents amplitude modulation of each frequency band, coded in color, during the IG task over 47 left index finger clicking events (the side ipsilateral to the PPN recording pair) and 37

right index finger clicking events (the side contralateral to the PPN recording pair). Figures 4.11 and 4.12 similarly present amplitude modulation during the EC task over 41 right index finger clicking events (the side contralateral to the PPN recording contact pair, Fig. 4.11) and 36 left index finger clicking events (the side ipsilateral to the PPN recording contact pair, Fig. 4.12). For the EC task (Figs. 4.11, 4.12), signals were analyzed time-locked to the presentation of the visual cue (left column, Figs. 4.11, 4.12) or to the time of motor response registration (right column, Figs. 4.11, 4.12) and were ordered by motor reaction time (top figure of each row, Figs. 4.11, 4.12) or averaged across trials (bottom graph of each row, Figs. 4.11, 4.12) in each frequency band. Figure 4.10 similarly presents amplitude modulation of each frequency band, coded in color, during the IG task. No comparative statistics or signal normalizations were performed as data were only collected from one patient.

4.2.3 Results

The mean reaction time in the EC task was 0.49±0.01 sec. The minimum and maximum times between subsequent movements were 1.5 and 5.0 sec for the EC task (77 EC events) and 1.1 and 5.0 sec in the IG task (84 IG events). The normalized PPN LFP traces in the θ, α, low and high β, and low and high γ frequency bands were grouped by laterality to the movement (Figs. 4.10, 4.11, 4.12).

The power spectra obtained from PPN LFP recordings revealed a clear delineation between the θ, α, low β, high β, and γ frequency bands. Power was highest in the θ band, followed by the β bands, the α band, the low γ band, and the high γ band. There was little discernable difference between the power

spectra obtained during periods of rest, performance of the IG task, and performance of the EC task (Fig 4.9).

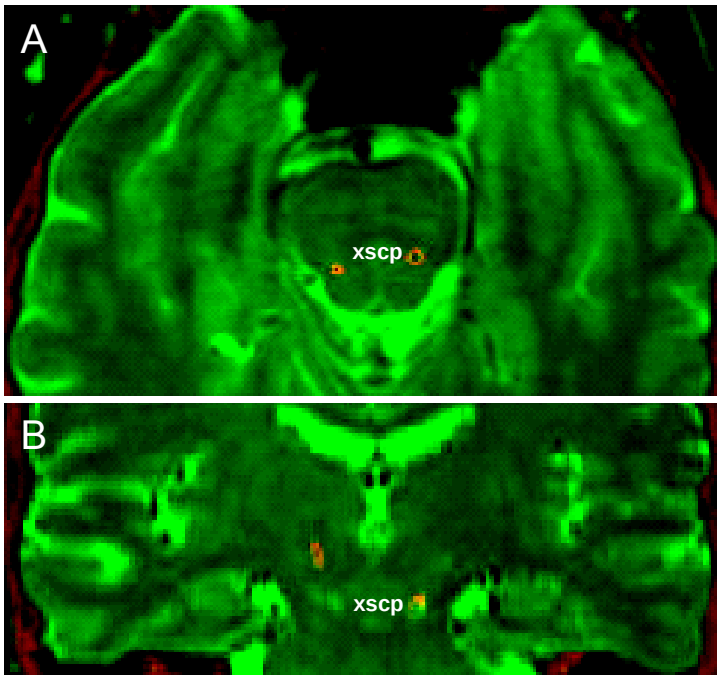

Figure 4.8. Localization of DBS contacts within the PPN. A) DBS contacts within the left PPN are shown in a transverse slice (2 mm thick slices parallel to the AC-PC line) obtained by fusion of pre-operative MRI scan with post-operative CT scan (Liu *et al.*, 2001). Key structures used for localization are labeled. B) The DBS electrode wires are visible in a coronal slice. xscp-decussation of the superior cerebellar peduncle.

4.2.3.1 Similarities in PPN LFP modulation between EC and IG tasks

The main similarity between the EC and IG tasks was that both tasks involved high β band desynchronization in the contralateral PPN (Figs. 4.10A, 4.11A). Low γ band desynchronization was also apparent in both the IG and EC tasks, but since the β band has been previously defined to include frequencies as high as 35 Hz (Neuper and Pfurtscheller, 2001; Foffani *et al.*, 2005), the low γ band was further sub-divided to 30-35 Hz and 35-60 Hz frequency bands. As expected, ERD in the low γ band was predominantly localized to the 30-35 Hz frequency range (Figs. 4.10B, 4.11B) suggesting that

any low γ modulation was likely a residual effect of high β band modulation. This is further supported by the relatively large amplitude high β band ERD in both the EC and IG tasks (Figs. 4.10, 4.11). This high β ERD began before and lasted after motor response-related EMG activation in both tasks (Figs. 4.10, 4.11) (EMG activations lasts, on average ±100 msec around the time of motor response registration (Dennerlein *et al.*, 1998; Kuo *et al.*, 2006).

Finally, in both the EC and IG tasks, there was no significant modulation of either the θ, α, or high γ bands in either the ipsilateral or contralateral PPN. Therefore, the high β band (including the 30-35 Hz range) is the only frequency band that is modulated during both EC and IG movements.

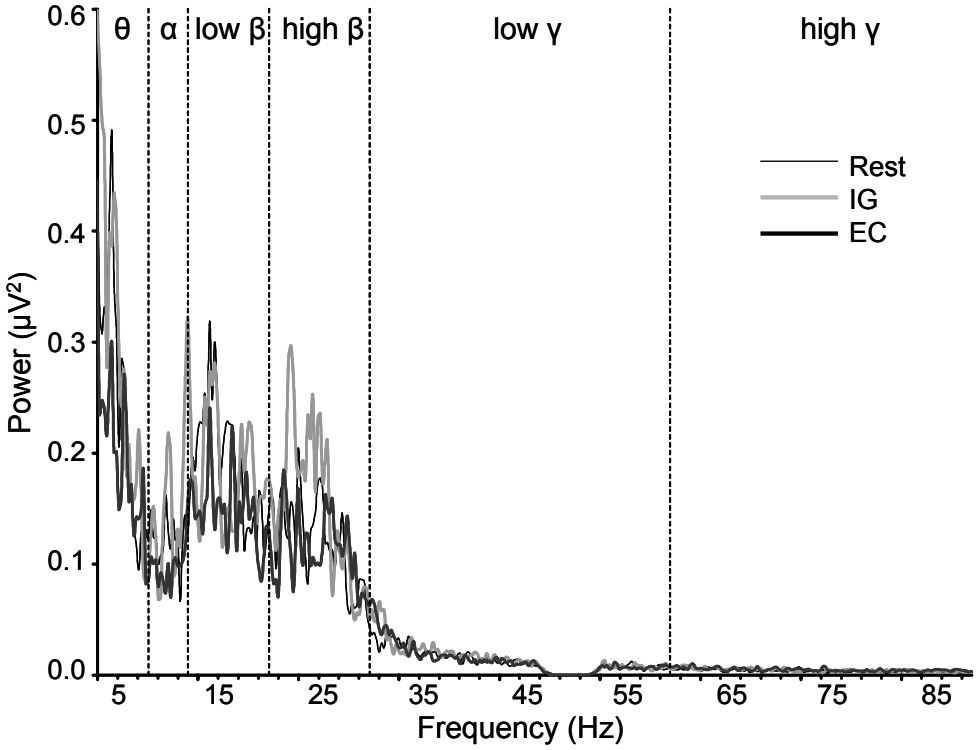

Figure 4.9. PPN LFP power spectra during rest, IG movement, and EC movement. The power spectra in the 0-90 Hz range in a 100 sec PPN LFP recording taken while the patient was at rest (thick back line), performing the IG movement task (thick gray line), or performing the EC movement task (thick black line). Line noise was flitered out in the ~50 Hz range. High spectral power can be observed in the θ, α, low β, and high β bands.

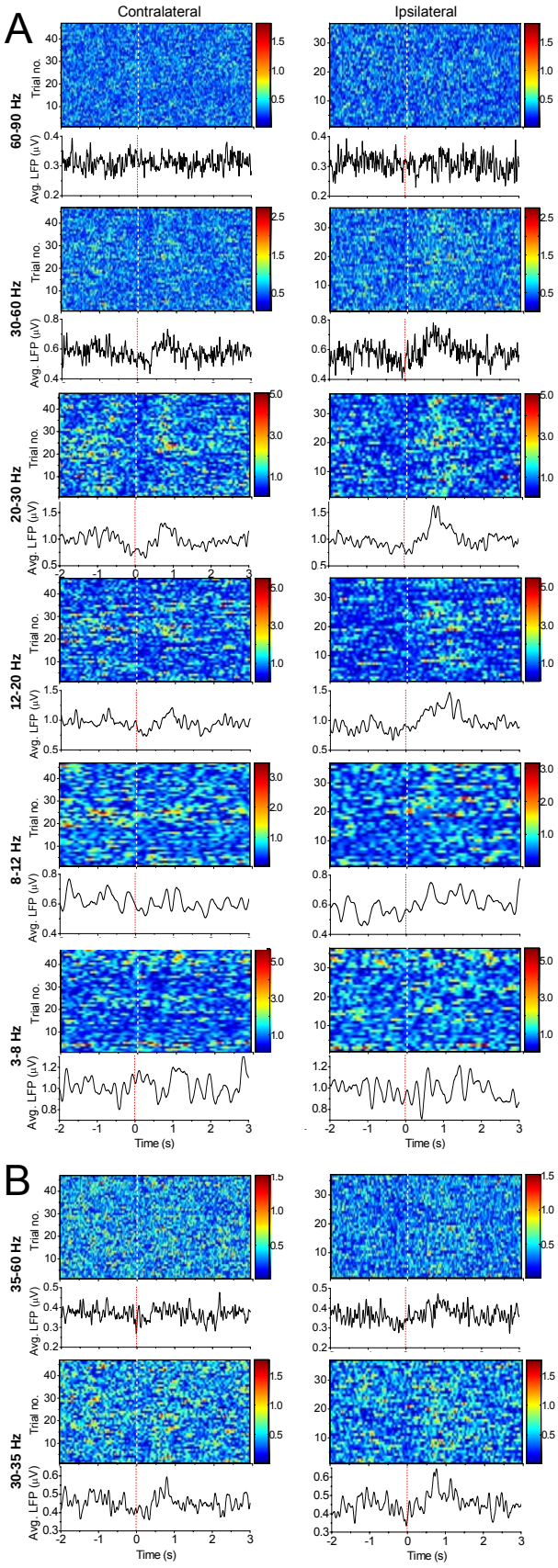

Figure 4.10. PPN LFPs recorded during the IG movement task are shown in a 5 sec window across frequency bands (rows) in the contralateral PPN (left column) or the ipsilateral PPN (right column). The top figure in each row shows the power in a given frequency band over time for each trial. Time '0' is marked by a vertical thin dotted line indicating the time of motor response registration. LFP power is coded in color with a unit of μV. The bottom figure in each row shows the power in the frequency band over time averaged across all trials. A) Peri-movement ERD is apparent in the low β, high β, and low γ bands in the contralateral PPN, while post-movement ERS occurs in these bands in the ipsilateral PPN. B) A separation of the low γ band into 30-35 Hz and 35-60 Hz frequency ranges reveals that modulation of the low γ band is localized to the 30-35 Hz frequency band.

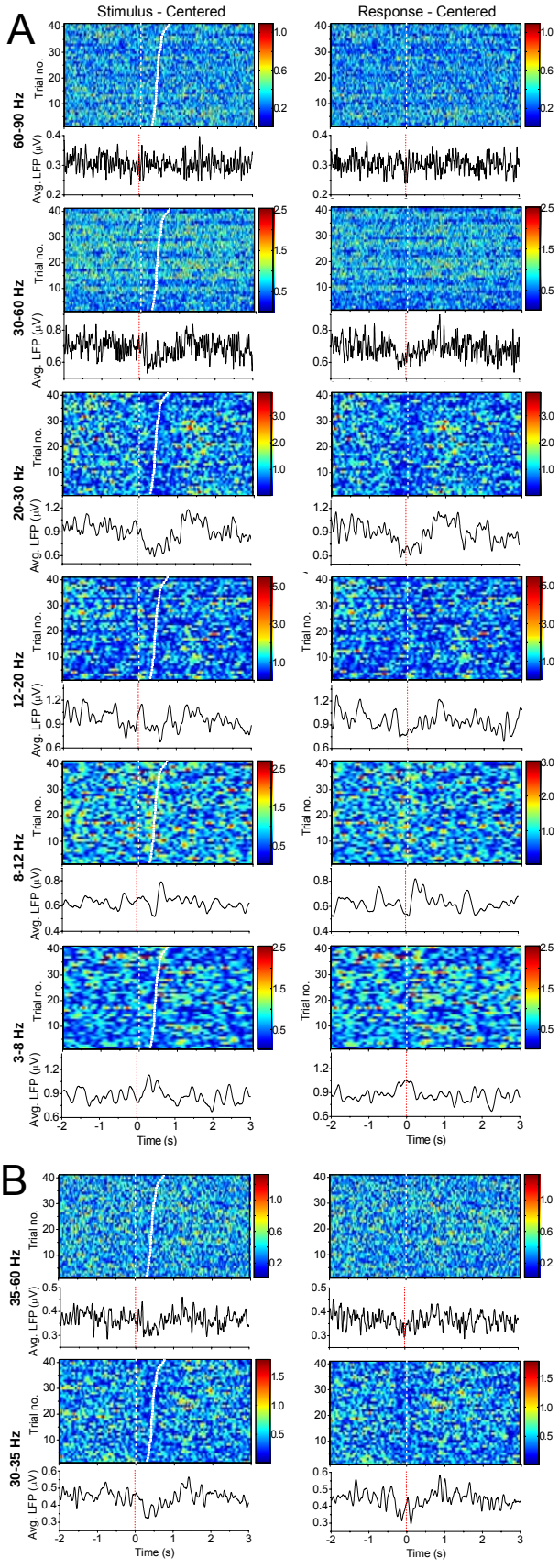

Figure 4.11. LFPs recorded in the contralateral PPN during the EC movement task are shown in a 5 sec window across frequency bands (rows) centered at either the time of stimulus presentation (left column) or the time of the response registration (right column). The top figure in each row shows the power in a given frequency band over time for each trial (visual cue followed by a response) with trials ordered by increasing reaction time. Time zero is marked by a vertical thin dotted line indicating the time of stimulus presentation (left column) or response registration (right column). In the stimulus-centered figures, the time of response registration is indicated by a thick dotted line. LFP power is coded in color with a unit of μV. The bottom figure in each row shows the power in the frequency band over time averaged across all trials. A) ERD of the high β and low γ appears to begin at the time of stimulus presentation and continue after the time of motor response. B) ERD in the low γ band appears limited to the 30-35 Hz frequency range.

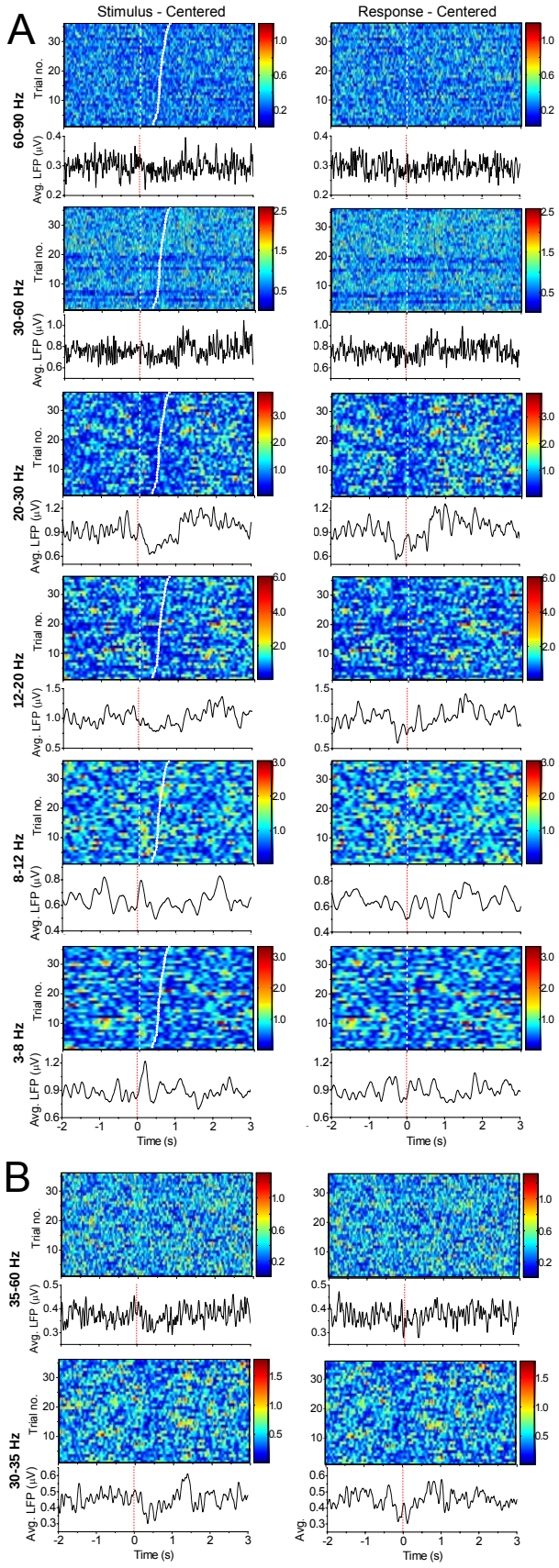

Figure 4.12. LFPs recorded in the ipsilateral PPN during the EC movement task are shown in a 5 sec window across frequency bands (rows) centered at either the time of stimulus presentation (left column) or the time of the response registration (right column). A) ERD of the high β and low γ appears to begin at the time of stimulus presentation and continue after the time of motor response. B) ERD in the low γ band appears limited to the 30-35 Hz frequency range.

4.2.3.2 Differences in PPN LFP modulation between EC and IG tasks

There were three main differences in PPN LFP modulation between the EC and IG tasks. First, the IG task involved modulation of both the low and high β bands, while the EC task involved only high β band modulation. In the ipsilateral PPN during the IG task, there was low β synchronization following the motor response beginning after the period of EMG activation (Fig. 4.10A). EC movements, on the other hand, did not appear to correlate with any modulation of the low β band in either the ipsilateral PPN (Fig. 4.12A) or contralateral PPN (Fig. 4.11A).

Second, although high β ERD in the contralateral PPN was observed in both tasks, high β modulation in the ipsilateral PPN differs between the IG and EC tasks. In the IG task, there is high β synchronization beginning after the period of EMG activation in the ipsilateral PPN. In the EC task, on the other hand, there is high β desynchronization beginning before and lasting after the period of EMG activation in the ipsilateral PPN. The low γ band exhibits modulation similar to that of the high β band in the ipsilateral PPN (post-movement ERS in the IG task and peri-movement ERD in the EC task) (Figs. 4.10A, 4.12A), but, as in the contralateral PPN (Fig. 4.11B), this low γ modulation in the ipsilateral PPN appears to be limited to the 30-35 Hz frequency band suggesting that it is a residual effect of high β band modulation (Figs. 4.10B, 4.12B).

Third, the main difference between the EC and IG tasks may be that high β band modulation in the EC task appears locked to the time of stimulus (Figs. 4.11, 4.12) and not to the onset of movement (as in the IG task, by

default). Therefore, high β modulation in the PPN can be correlated with both cue-processing and motor-processing.

4.2.4 Discussion

4.2.4.1 High β band modulation in the PPN is related to motor preparation and cue processing

High β modulation has been correlated with motor preparation in the STN (Section 4.1) and in the cortex (Sanes and Donoghue, 1993; MacKay and Mendonca, 1995; Hamada *et al.*, 1999; Neuper and Pfurtscheller, 2001; Wheaton *et al.*, 2005). In the PPN, peri-movement high β desynchronization occurs contralateral to both IG and EC movements. Furthermore, since high β modulation is locked to the time of the stimulus in the EC task, the results of this study demonstrate the presentation of a preparatory visual cue can initiate high β ERD. Therefore, it is most likely that high β desynchronization is correlated with motor preparation in the contralateral PPN.

Bilateral high β desynchronization may also be correlated with cue-processing and sensorimotor integration in the PPN since high β ERD is initiated by cue-presentation in the EC task bilaterally in the PPN. This is further supported by a lack of bilateral high β ERD when a cue is not present (high β ERD occurs only contralaterally in the IG task).

High β ERD is probably not associated with motor execution. Even though both the IG and EC tasks involved high β band desynchronization in the contralateral PPN, high β ERD was locked to the time of stimulus during the EC task suggesting that high β modulation is most likely correlated with motor preparation in the IG task as well. Furthermore, though the PPN has been

implicated in cue processing and sensory gating (Reese *et al.*, 1995; Dormont *et al.*, 1998; Kobayashi *et al.*, 2002; Pan and Hyland, 2005; Winn, 2006), PPN activity is thought to be more related to gait and large scale movements and not necessarily to fine voluntary movements (Garcia-Rill *et al.*, 1985, 1987; Inglis and Winn, 1995; Reese *et al.*, 1995; Lee *et al.*, 2000; Pahapill and Lozano, 2000).

4.2.4.2 Role of the PPN in facilitation of movement by an external cue in Parkinson's disease

Post-movement synchronization is present in both the low and high β band in the ipsilateral PPN during self-paced movement, but is greatly reduced by the present of a visual cue. Synchronization in the β bands has been shown to be antikinetic and post-movement synchronization in these bands would likely make it difficult to execute rapid movements. Therefore, noting that the presentation of an external cue greatly facilitates voluntary movement execution (Glickstein and Stein, 1991; Georgiou *et al.*, 1993; Morris *et al.*, 1994; Thaut *et al.*, 1996; Burleigh-Jacobs *et al.*, 1997; Curra *et al.*, 1997; Majsak *et al.*, 1998; Kelly *et al.*, 2002), it is possible that one of the ways this movement facilitation occurs is via attenuation of β ERS in the ipsilateral PPN.

4.2.4.3 PPN LFP modulation specific to Parkinson's disease patients

PPN LFP modulation in the low β band may be unique to PD patients. Low β modulation of PPN LFP was present only in the IG task and the presence of an external cue attenuates all low β modulation in the PPN LFP during the EC task. L-DOPA has also been shown to reduce power in

specifically the low β band in the basal ganglia (Priori *et al.*, 2002) further supporting the hypothesis that the presentation of external cue facilitates motor execution via a similar mechanism (Section 4.1.4.3).

The synchronization in the high β band observed in the ipsilateral PPN during the IG task may also be unique to PD patients. Although, rebound synchronization in the full β band has been reported previously in the STN and M1 following discrete voluntary movements (Pfurtscheller and Neuper, 1994; Neuper and Pfurtscheller, 2001; Kuhn *et al.*, 2006), this synchronization is usually preceded by peri-movement β ERD (Neuper and Pfurtscheller, 2001; Kuhn *et al.*, 2006). The presence of high β synchronization independent of peri-movement ERD is likely to be an antikinetic and pathological phenomenon. This is further supported by the results of this study that show that the presentation of an external cue (which has been previously shown to facilitate movement) eliminates high β synchronization in the ipsilateral PPN.

Finally, high γ band ERS was not observed in the PPN in the PD patient in this study who was off medication. As it has been established that high γ oscillatory activity serves a prokinetic function in the basal ganglia, it is possible that the lack of high γ modulation in the PPN with voluntary movement is demonstrative of parkinsonian pathology and not necessarily representative of what happens in the normal PPN. However, since high γ activity is associated directly with motor execution (Brown, 2003; Alegre *et al.*, 2005) while PPN LFP modulation is not, it is also possible that high γ ERS would not be present in the normal PPN.

4.2.4.4 Differences between LFP modulation in the PPN and STN

There are two differences between LFP modulation in the PPN and STN. First, LFP modulation in both the PPN and STN appears to be associated with motor preparation and cue processing, but only STN LFP modulation appears to be associated with motor execution. The STN has long been associated with the control of fine voluntary movement (Williams *et al.*, 2003, 2005; Kuhn *et al.*, 2004, 2006; Alegre *et al.*, 2005; Foffani *et al.*, 2005) while the PPN is generally associated with whole-body movements such as gait and postural control (Garcia-Rill *et al.*, 1985, 1987; Lee *et al.*, 2000; Pahapill and Lozano, 2000) and also, to some extent, with sensorimotor integration (Reese *et al.*, 1995; Dormont *et al.*, 1998; Kobayashi *et al.*, 2002; Pan and Hyland, 2005). The findings of this study further corroborate the distinction between these two nuclei with regards to their roles in motor control.

Second, the main difference between PPN and STN LFP modulation during IG and EC movement observed in this study is that the greatest magnitude LFP modulation in the PPN occurred in the high β band while the greatest magnitude LFP modulation in the STN occurred in the α and low β bands. It is possible that this is a distinction between oscillatory activity within the basal ganglia and oscillatory activity downstream from the basal ganglia. L-DOPA administration preferentially decreases oscillatory activity in θ, α, and low β bands, and has relatively little effect on high β band oscillatory activity (Priori *et al.*, 2002). Perhaps movement-related modulation of oscillatory activity occurs in lower frequency bands in networks that respond to dopamine in the parkinsonian brain and occurs in the higher β ranges in parkinsonian networks relatively independent from dopaminergic input. In this context, it is interesting

to note that the clinical effects of STN DBS and dopaminergic medication are not additive in PD patients (Krack *et al.*, 1997a, 2003; Rodriguez-Oroz *et al.*, 2005), while the effects of PPN DBS and dopaminergic medication are additive (Jenkinson *et al.*, 2006; Stefani *et al.*, 2007) which suggests that the STN is part of a dopamine-responsive network (i.e. the basal ganglia) while the PPN is not. This supports the hypothesis that the modulation of oscillatory activity related to motor execution occurs in lower frequency ranges in the STN and in higher frequency ranges downstream from the basal ganglia in the PPN.

4.2.4.5 Concluding remarks

PPN LFPs were recorded from one patient from one contact pair that could be confidently located in the PPN. Further study with a greater number of patients is required to corroborate the results describing movement-related LFP modulation in the PPN. Oscillatory activity in the θ, α, low β, and high β bands was present in PPN LFP power spectra, but only the low β and high β bands were modulated during IG or EC movement. The results presented here associate high β desynchronization in the PPN with motor preparation and cue processing, but suggest that low β modulation in the PPN is a pathological parkinsonian phenomenon. Intriguingly, though lower frequency movement-related modulation is not present in the PPN, the greatest STN LFP modulation occurs in the α and low β bands. This suggests that modulation of low frequency oscillatory activity related to motor execution is present in the STN while modulation of higher frequency oscillatory activity related to motor preparation is found downstream of the basal ganglia in the PPN.

Main Findings

- *In the STN, bilateral low β band desynchronization is related to motor execution, the laterality of high β band desynchronization is related to motor preparation, and a delay in α band synchronization may be associated with cue processing.*
- *In the PPN, high β desynchronization appears to be related to motor preparation and the processing of a visual cue. There does not appear to be any PPN LFP modulation related solely to motor execution.*
- *The greatest magnitude LFP modulation occurred in the α and low β bands in the STN but in the high β band in the PPN. This suggests that oscillatory activity is not directly transmitted from the STN to the PPN, despite the strong anatomical connection between these nuclei (Section 2).*

5. EFFECTS OF STN AND PPN STIMULATION ON GAIT

Gait abnormalities are a common motor symptom of PD and often persist even with dopamine replacement therapy. Though DBS of the STN does reduce some gait problems, this effect is limited as STN stimulation tends to best alleviate dopamine-responsive parkinsonian symptoms. DBS of the PPN has recently been demonstrated to ameliorate these previously medically intractable and dopamine-resistant gait abnormalities (Section 1). In this section, the differences in gait improvement following DBS of the STN and DBS of the PPN are compared using modern gait analysis motion capture techniques to better understand the roles of these nuclei in large-scale motor control.

5.1 Introduction and rationale

Locomotion is primarily controlled by the autonomic system (Dietz, 1997) via central pattern generators in the spinal cord (Grillner, 1981; Dietz, 1997; Grillner *et al.*, 2008). These central pattern generators are also affected by input from the brainstem mesencephalic locomotor region which, in turn, responds to higher "executive" areas of motor control (such as the basal ganglia and motor cortex) (Grillner, 1981; Grillner *et al.*, 2008). These executive control regions are thought to be responsible for goal-directed movement and specific gait program selection (Grillner, 1981; Grillner *et al.*, 2008) while the mesencephalic locomotor region (including the PPN (Lee *et al.*, 2000; Pahapill

and Lozano, 2000)) is thought to be responsible for activating the central pattern generators (Grillner, 1981; Dietz, 1997; Grillner *et al.*, 2008). These central pattern generators then sequentially activate a specific set of motor units and muscle groups to execute a gait cycle (Grillner, 1981; Perry, 1992; Dietz, 1997; Kaufman and Sutherland, 2006; Grillner *et al.*, 2008).

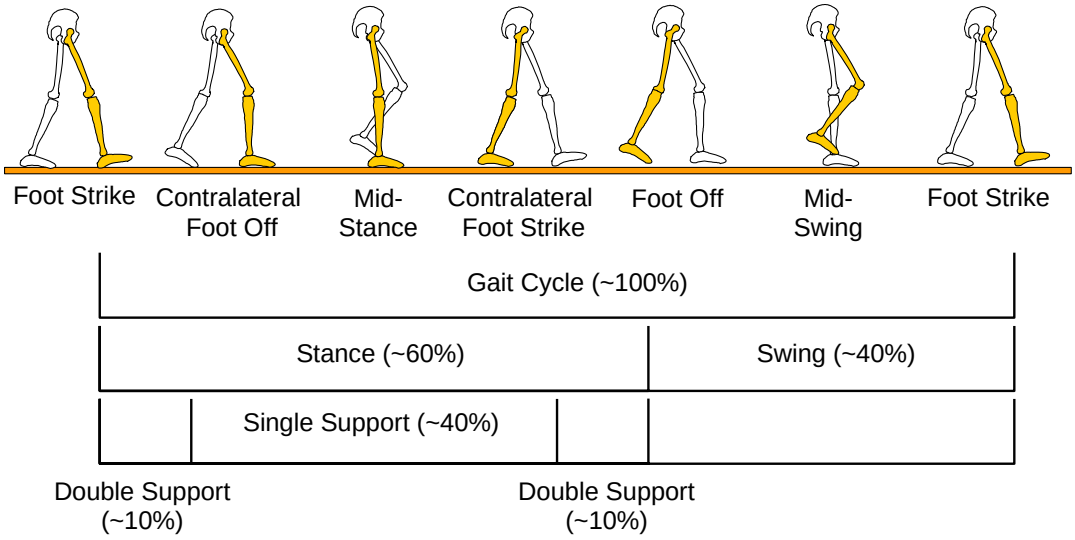

Figure 5.1. The normal gait cycle is shown subdivided into phases demarcated by gait events. A diagram of lower body motion is shown for each gait event. The duration of gait cycle phases is indicated relative to the duration of the entire gait cycle.

The gait cycle is the time period during which one set of regularly recurring gait events is completed. During normal walking, these gait events are foot-strike, contralateral foot-off, contralateral foot-strike, foot-off, and then the foot-strike beginning the next gait cycle. Different periods of the gait cycle can be described with reference to these basic gait events. The stance phase occurs between foot-strike and foot-off and comprises 60% of the cycle while the swing phase occurs between foot-off and the subsequent foot-strike and comprises 40% of the cycle. The stance phase can be further subdivided into periods of double support (when both feet are in contact with the ground) and single support (when only one foot is in contact with the ground). The initial

double support phase (10% of the gait cycle) occurs between foot-strike and contralateral foot-off. It is followed by the single support phase (40% of the gait cycle) that occurs between contralateral foot-off and contralateral foot-strike, and then, finally, by the terminal double support phase (10% of the gait cycle) that occurs between the contralateral foot-strike and foot-off (Fig. 5.1) (Perry, 1992; Kaufman and Sutherland, 2006). Therefore, the total time spent in double support should be approximately half of the total time spent in single support. An increase in this ratio indicates poor balance and/or shuffling gait.

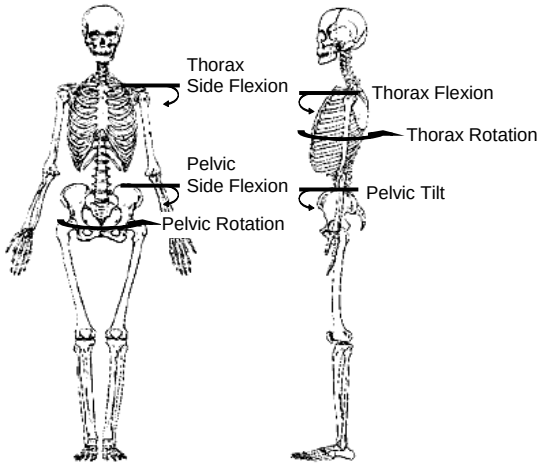

Figure 5.2. Diagram of thoracic and pelvic motion in the transverse (rotation), coronal (side flexion), and sagittal (thoracic flexion and pelvic tilt) planes.

In addition to examining the duration of gait cycle phases, gait can also be studied by conducting kinematics analysis which allows for the determination of body angles during various phases of the gait cycle (Fig. 5.2). Lower-body kinematics have been examined extensively during straight walking in healthy individuals (Perry, 1992; Kaufman and Sutherland, 2006). For example, it is known that the pelvis tilts forward during walking but tilts the least at the end of the double support phase, that the contralateral pelvis drops during stance, and that maximal internal pelvic rotation occurs at foot strike while maximal external pelvic rotation occurs at contralateral foot strike (Perry, 1992; Kaufman and Sutherland, 2006). Considerably less research has been

done on upper-body kinematics during walking, though it is expected that thoracic angles should mirror pelvic angles as forward foot swing occurs concurrently with ipsilateral backward arm swing (Perry, 1992).

Gait, postural abnormalities, and other axial symptoms are major motor problems in PD. Several studies have shown that walking speed and stride length (the distance between two consecutive ipsilateral foot strikes during straight line walking) are decreased in PD (Murray *et al.*, 1978; Defebvre *et al.*, 1996, 1999; Morris *et al.*, 1996, 1998, 2001). Some studies have suggested increased double support duration during walking as well (Murray *et al.*, 1978a; Morris *et al.*, 2001). The incidence of falls is also much greater in PD patients (Morris *et al.*, 2001; Bloem *et al.*, 2004b) and PD patients are more likely to fall or experience akinetic episodes when turning or walking around a corner (Hausdorff *et al.*, 1997; Morris *et al.*, 2001; Bloem *et al.*, 2004a). DBS of the STN results in some improvement in gait abnormalities (Kumar *et al.*, 1998; Krystkowiak *et al.*, 2003; Ferrarin *et al.*, 2004, 2005, 2007; Rodriguez-Oroz *et al.*, 2005; Carpinella *et al.*, 2007), but STN stimulation has a limited effect on dopamine-resistant parkinsonian gait and postural abnormalities (Yokoyama *et al.*, 1999; Stolze *et al.*, 2001; Pahwa *et al.*, 2006). DBS of the PPN, on the other hand, has been shown to improve the akinesia and gait abnormalities that remained intractable with dopaminergic medication (Mazzone *et al.*, 2005; Plaha and Gill, 2005). Furthermore, when patients are on dopaminergic medication, the beneficial effects of PPN DBS and STN DBS are additive (Stefani *et al.*, 2007). This suggests that DBS of the PPN and DBS of the STN both beneficially affect gait in PD patients via at least partially distinct mechanisms. However, the effects of DBS of the PPN and STN on gait,

turning, and balance have not been compared using modern gait analysis motion capture techniques that allow for accurate determination of temporal and kinematic gait parameters.

This section will compare the effects of DBS of the STN and DBS of the PPN on gait and posture in PD patients. Data will be collected from PD patients on and off STN or PPN stimulation and from age and weight-matched controls during straight walking, turning, and standing. Gait deficiencies in patients off stimulation and improvement in gait on stimulation will be examined to compare the effects of PPN and STN DBS on large-scale motor control.

5.2 Methods

5.2.1 Subjects

Five PD patients who have had bilateral STN DBS electrode implants (Section 4.1.2.1) and 1 PD patient with bilateral PPN implants (patient GF, Section 4.2.2) participated in this study. Data from 6 age- and weight-matched controls were also collected. Patient clinical details and control subject demographic details are summarized in Table 5.1. Control subjects had no previous history of gait or neurological abnormalities. PD patients were not co-morbid for any other gait or neurological abnormalities and were asked to be off medication for at least six hours before the gait recording session.

5.2.2 Gait task design

Three conditions were recorded: standing, walking in a straight line, and turning. During standing, the subject stood for 100 sec with feet shoulder-width

apart. During walking, the subject walked in a straight line across the room. During turning, the subject walked around a chair that was consistently placed at the same distance from all subjects and at the same angle from the point of gait initiation. The subject turned left or right around the chair and then continued to walk in a straight line (Fig. 5.3). Turns were defined as contralateral (turning in the direction opposite to the foot initiating the first gait cycle of the turn) or ipsilateral (turning in the direction of the foot initiating the first gait cycle of the turn). For example, a right turn was defined as contralateral if the first gait cycle was initiated with a left foot-strike, but it was defined as ipsilateral if the first gait cycle was initiated with a right foot-strike. Each subject completed at least 2 walking trials, one contralateral left turn, one ipsilateral left turn, one contralateral right turn, one ipsilateral right turn, and two periods of standing. In the turning trials, the first, second, and third gait cycles of the turn were analyzed separately. Each task (walking, left turn, right turn, and standing) was physically demonstrated by the experimenter at the beginning of the gait recording session and cued verbally by stating “walking”, “left turn”, “right turn”, or “standing”. The order of each task was randomized for each subject. PD patients always performed the tasks on DBS stimulation first and, if the patient felt physically capable, DBS stimulation was turned off for 20 min before they were asked to repeat the gait tasks off stimulation. The stimulation settings had already been optimized in all patients studied. The PPN patient was stimulated at 20 Hz and the STN patients were all stimulated at frequencies >100 Hz. All PD patients completed all gait tasks on and off stimulation.

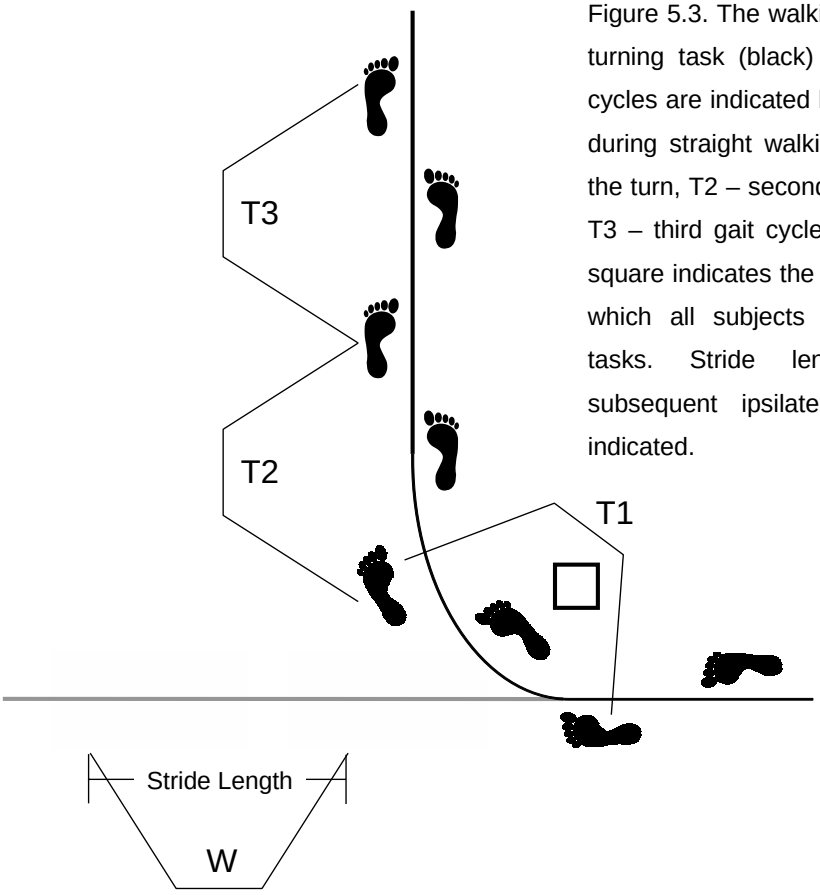

Figure 5.3. The walking task (gray) and the right turning task (black) are shown. Analyzed gait cycles are indicated by a letter (W – a gait cycle during straight walking, T1 – first gait cycle of the turn, T2 – second gait cycle of the right turn, T3 – third gait cycle of the right turn). A white square indicates the position of the chair around which all subjects turned during the turning tasks. Stride length (distance between subsequent ipsilateral foot strikes) is also indicated.

5.2.3 Data capture and processing

A 12 camera VICON 612 system (Oxford Metrics Group Ltd., Oxford, UK) was used to collect kinematic data in three dimensions, sampling at 100 Hz. Twenty 14 mm retro-reflective markers were attached to the patient at the shoulder (left and right acromial processes), upper back (C7 and T10), sternum (xiphoid process), clavicular notch, pelvis (left and right anterior superior iliac spines), sacral notch, thigh (along the femur), knee (at the lateral aspect of the joint), shank (along the tibia), ankle (lateral malleolus), and foot (between the first and second metatarsals). Figure 5.4 shows the location of the 12 cameras relative to the subject (top) and the resultant marker rendering (bottom). Gait kinematic and temporal data were recorded using VICON Nexus software,

version 1.1 (Oxford Metrics Group Ltd., Oxford, UK) and gait data processing was performed using VICON Polygon Authoring Tool software (Oxford Metrics Group Ltd., Oxford, UK).

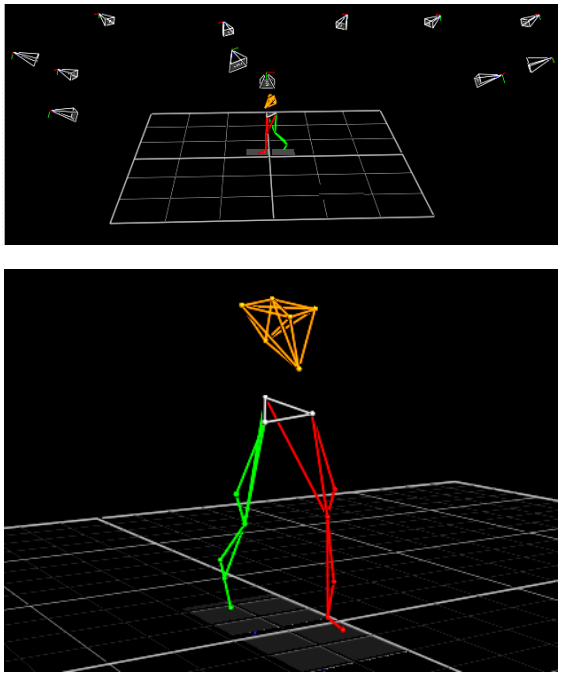

Figure 5.4. Sample images obtained using the VICON 612 motion capture system are shown. The top image shows the location of all 12 cameras relative to the subject (colored figure walking on floor grid). The bottom image shows how the VICON system renders markers (small spheres) and body segments (yellow – thorax, gray – pelvis, red – left leg, green – right leg).

Walking speed (m/sec), stride length (m), the ratio of double support duration to single support duration (DS/SS), thoracic angles, and pelvic angles were determined for all subjects during all walking trials. In the standing trials, the standard deviation of thoracic and pelvic movement in each plane (transverse, coronal, sagittal) over 100 sec was determined as a measure of balance since balance-impaired adults have been shown to have much greater trunk movement while standing than do adults without a history of falls (Shumway-Cook *et al.*, 1997; Woollacott and Shumway-Cook, 2002). Two representative gait cycles were selected for walking and for the first, second, and third gait cycles of each turn. Data from corresponding representative gait cycles were averaged for each subject as were data from two 100 sec standing trials.

Table 5.1. Summary of Subjects' Clinical Details

Subject No./ DBS Target or Control	Age	Sex	Height (m)	Weight (kg)	Disease Duration (years)	Motor UPDRS Score (on / off med)	Electrode Contacts used for Stimulation (+/-)	Years with DBS Implant	Medication (daily dose)
1 / Control	60	M	1.77	84.2	----	----	----	----	----
2 / Control	63	M	1.68	68.9	----	----	----	----	----
3 / Control	55	F	1.60	74.0	----	----	----	----	----
4 / Control	53	F	1.69	64.3	----	----	----	----	----
5 / Control	60	F	1.62	67.1	----	----	----	----	----
6 / Control	58	M	1.81	92.8	----	----	----	----	----
Control Mean± SE	***58±2***	***----***	***1.70±0.03***	***75±4.5***	***----***	***----***	***----***	***----***	***----***
7 / STN	63	F	1.70	81.2	15	25 / 40	L0, L1 R1, R2	6	Sinemet 100 mg Amantadine 100 mg Benzhexol 16 mg
8 / STN	54	M	1.74	87.5	9	20 / 36	L1, - R2, -	5	Madopar 62.5 mg Selegiline 10 mg Cabergoline 6 mg Amantadine 200 mg
9 / STN	50	M	1.81	89.0	6	24 / 40	L0, L1 R0, R1	1	Sinemet 250 mg
10 / STN	53	M	1.62	63.2	8	21 / 42	L2, L3 R1, R2	8	Sinemet 200 mg Entacapone 200 mg Ropinerole 5 mg Selegiline 5 mg
11 / STN	60	F	1.69	67.2	14	23 / 39	L2,- R3,-	6	Sinemet 437.5 mg Ropinerole 25 mg Amantadine 100 mg
STN Mean± SE	***56±2***	***----***	***1.71±0.03***	***78±5***	***10.4±1.7***	***22±1 / 39±1***	***----***	***5.2±1.1***	***----***
12 / PPN	55	M	1.59	65.7	12	29 / 57	L1, L2	1 week	Madopar 500 mg Pramipexole 0.7 mg Amantadine 100 mg Apomorphine 50 mg Domperidone 40 mg

Only one patient with PPN DBS implants was available for this study so no statistical analyses were performed using data derived from that patient. Walking speed, stride length, DS/SS, and thoracic and pelvic angles during standing were compared between patients on STN stimulation, patients off STN stimulation, and control subjects using grouped t-tests. Data in bar graphs (Figs. 5.5, 5.7) are presented as mean ± SEM. Criterion for significance was $p<0.05$. Gait angles during walking and turning (Figs. 5.6, 5.8) are presented as the mean value over the duration of the gait cycle. Gait angles during walking are shown ± SEM, but gait angles during turning are presented as just the mean trace for purposes of visual clarity. PD patients off stimulation will be referred to as "STN DBS OFF" or "PPN DBS OFF". Data from STN DBS OFF and PPN DBS OFF patients are analyzed separately since selection criteria for STN DBS and PPN DBS greatly differ (Section 6.2).

5.3 Results

5.3.1 Effect of turning on gait performance of healthy control subjects

The average walking speed (1.42 ± 0.06 m/sec), stride length (1.40 ± 0.04 m), and DS/SS (0.47 ± 0.03) of control subjects (58 ± 2 years old, Table 5.1) during straight walking matched expected values for healthy individuals between 50 and 65 years old (walking speed: 1.50 m/sec, stride length: 1.45 m, DS/SS: 0.5 (Perry, 1992; Kaufman and Sutherland, 2006)). Walking speed decreased during the first gait cycle of the turn (though this effect was not significant) and progressively increased to straight walking speed during the second and third gait cycles of the turn. Stride length did not consistently vary

with turning in this manner suggesting that the observed differences in walking speed during turning may be because control subjects are taking longer to complete the initial gait cycles of a turn (as opposed to taking smaller steps). Finally, DS/SS also appeared to be greater during the turning gait cycles than during a straight walking gait cycle, but this effect was also not significant (Figs. 5.5A, 5.7A).

The pelvic angles of the control subjects during normal straight walking matched the angles previously determined in other studies examining normal gait (Perry, 1992; Kaufman and Sutherland, 2006). As expected, thoracic angles mirrored pelvic angles during normal walking in the coronal and transverse planes of movement, and matched pelvic angles in the sagittal plane of movement (Perry, 1992; Kaufman and Sutherland, 2006). It is interesting to note that both the pelvis and thorax were tilted/flexed forward throughout the walking trial indicating the stooped posture that is common in older walkers (Perry, 1992; Kaufman and Sutherland, 2006) (Figs. 5.6, 5.8).

Turning had little effect on thoracic movement in the sagittal plane (thoracic flexion) or on movement in the coronal plane (thoracic and pelvic side flexion). However, pelvic tilt and thoracic and pelvic movement in the transverse plane (rotation) were markedly different between the turning and walking trials. The pelvis was tilted forward (relative to pelvic tilt during straight walking) in the second gait cycles of both ipsilateral and contralateral turns and pelvic tilt varied less across these gait cycles as well. Increased pelvic tilt, but not increased thoracic flexion, indicates a forward jutting of the hips that may be helpful in maintaining balance (Morris *et al.*, 2001; Crenna *et al.*, 2007) following the sudden center-of-mass displacement necessitated by an abrupt

90° turn. Internal rotation of the thorax and pelvis was also much greater during the stance phases of the first and second gait cycles of an ipsilateral turn, while external rotation in the stance phases of these gait cycles was greater during contralateral turns. Thoracic and pelvic rotation returned to straight walking values during the swing phases of the first and second turning gait cycles and during the entire third turning gait cycle (Figs. 5.6, 5.8). Increased rotation values during the first gait cycle of a turn are expected as the direction of movement is also rotating in this transverse plane. As soon as the direction of movement becomes straight, thoracic and pelvic rotation values should rapidly return to values that would be observed during straight walking. In control subjects, this return is almost complete during the second gait cycle of a turn and is totally complete during the third gait cycle (Figs. 5.6, 5.8).

5.3.2 Effects of STN stimulation on gait

5.3.2.1 Effects of STN stimulation on gait performance and standing balance

Gait impairment was clearly visible in all STN DBS OFF patients. Relative to gait performance of the control subjects, speed and stride length during straight walking and turning were significantly decreased for STN DBS OFF patients ($p<0.05$). In addition, DS/SS during straight walking and turning was also significantly greater in STN DBS OFF patients ($p<0.05$) (Fig. 5.5).

STN stimulation tended to improve walking speed, stride length, and DS/SS, but this effect was variably significant. Walking speed was significantly improved with STN stimulation during the all gait cycles of a contralateral turn but only during the first gait cycle of an ipsilateral turn ($p<0.05$). STN stimulation had no significant effect on stride length during any gait task, and only resulted

in a significant improvement in DS/SS during straight walking ($p<0.05$) (Fig. 5.5A). Despite some improvement in gait performance following STN stimulation, walking speed, stride length, and DS/SS were still significantly worse for STN DBS ON patients relative to these gait performance parameters for the control subjects ($p<0.05$).

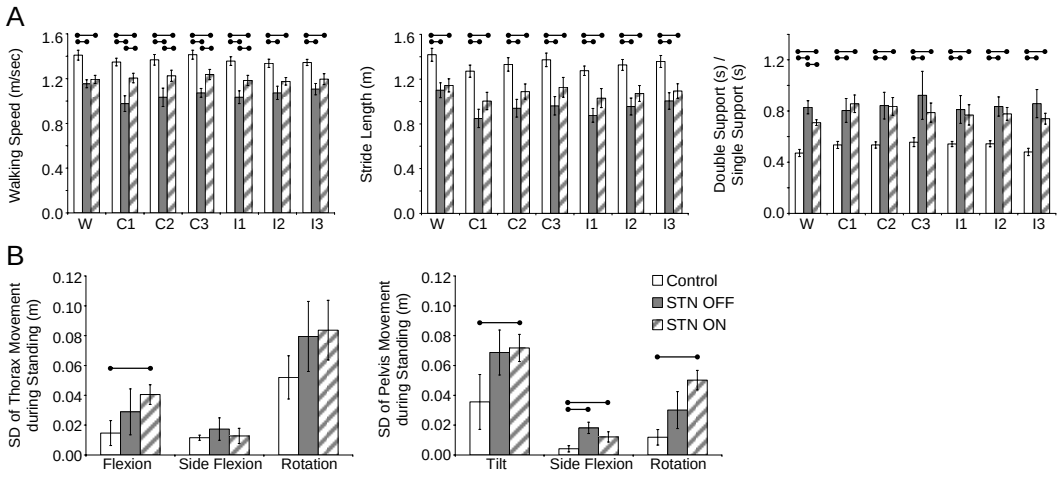

Figure 5.5. Effects of STN stimulation on temporal gait parameters and standing balance. A) Walking speed, stride length, and double-support / single-support duration are shown during walking and turning for control subjects and PD patients on (STN ON) and off (STN OFF) STN stimulation (W – gait cycle during straight walking, C1/2/3 –first, second, and third gait cycles of a contralateral turn, I1/2/3 – first, second, and third gait cycles of an ipsilateral turn). B) The standard deviations (SD) of thoracic and pelvic motion in the transverse (rotation), coronal (side flexion), and sagittal (thoracic flexion and pelvic tilt) planes are shown during 100 sec of standing for control subjects and PD patients on and off STN stimulation. Horizontal lines (●—●) indicate significant differences between groups ($p<0.05$).

Furthermore, STN stimulation did not appear to have a significantly beneficial effect on balance during turning since STN stimulation did not result in a significant decrease in DS/SS during any of the turning gait cycles (Fig. 5.5A). STN DBS OFF patients tended to move more during the standing task than did the control subjects, but only pelvic side flexion movements were significantly greater in PD patients off stimulation ($p<0.05$). However, STN DBS ON patients exhibited significantly greater thoracic flexion, pelvic tilt, pelvic side

flexion, and pelvic rotation movements during standing than did the control subjects. Surprisingly, STN stimulation also appeared to increase thoracic and pelvic movement during standing in the sagittal and transverse planes (relative to thoracic and pelvic movement in these planes in the same patients off STN stimulation), although this effect was not significant (Fig. 5.5B).

5.3.2.2 Effects of STN stimulation on thoracic and pelvic angles during walking

There were two main abnormalities in thoracic and pelvic gait angles of STN DBS OFF patients during straight walking. First, STN DBS OFF patients exhibited slightly more forward thoracic flexion and more forward pelvic tilt during straight walking than did the control subjects. This is indicative of greater stooped posture in these patients relative to healthy controls (Perry, 1992; Morris *et al.*, 2000; Woollacott and Shumway-Cook, 2002). Second, STN DBS OFF patients did not increase thoracic side flexion during the swing phase of a straight walking gait cycle as would be expected from changes in thoracic side flexion during straight walking in healthy control subjects. Since decreased forward arm swing would selectively result in a dampening of thoracic side flexion (but not dampening of pelvic side flexion), these results support the observation that arm swinging is reduced during walking in PD patients (Perry, 1992; Carpinella *et al.*, 2007). STN stimulation did not appear to improve either of these gait angle abnormalities during straight walking (Fig. 5.6).

5.3.2.3 Effects of STN stimulation on thoracic and pelvic angles during turning

Thoracic and pelvic angles during turning were abnormal in STN DBS OFF patients in all planes of movement. In the sagittal plane, both the thorax

and pelvis were flexed/tilted more forward during the second gait cycle of the turn (relative to angles during straight walking in these patients). In control subjects, only pelvic tilt increased in the second gait cycle of a turn while thoracic flexion remained unchanged (Fig. 5.6). The similarity between thoracic and pelvic angles in STN DBS OFF patients during turning may be due to increased trunk rigidity which would reduce independent movement of the thorax and pelvis.

In the coronal plane of movement, thoracic and pelvic side flexion were more variable across each turning gait cycle in STN DBS OFF patients than they were during turning in the control subjects, and this increased variability did not seem to follow any pattern across the different turning gait cycles (Fig. 5.6). Increased, and apparently random, gait variability has been previously reported in PD patients and has been thought to reflect increased demands on attention and decreased autonomic control of gait in PD (Sheridan and Flowers, 1990; Hausdorff *et al.*, 1998, 2003a, 2003b; Springer *et al.*, 2006). It is possible that increased gait variability during turning in thoracic and pelvic side flexion corresponds to this phenomenon.

Finally, in the transverse plane of movement, internal rotation was much greater in the first and second gait cycles of ipsilateral turns and external rotation was much greater during the first and second gait cycles of contralateral turns in STN DBS OFF patients relative to these rotation values in control subjects. This increased rotation is apparent in both the stance and swing phases of the first and second gait cycle, but was only apparent during the stance phase in control subjects (Fig. 5.6). Therefore, it appears that changes in direction of motion have a greater effect on trunk rotation in STN

DBS OFF patients. It also may take longer STN DBS OFF patients longer (more gait cycles) to restore thoracic and pelvic rotation values to those observed in straight walking.

STN stimulation had the same effect on thoracic and pelvic angles in all planes of movement: it appeared to reduce differences in thoracic and pelvic movement between walking and turning. This effect was most dramatic in the transverse plane of movement where the extent and duration of abnormally high thoracic and pelvic rotation was reduced with STN stimulation and brought much closer to rotation values observed in control subjects during turning. However, it is possible that STN stimulation may have detrimentally affected pelvic tilt during turning. In control subjects, the pelvis is tilted more forward during the second gait cycle of a turn (relative to pelvic tilt during straight walking). STN stimulation reduced forward pelvic tilt during the second gait cycle of a turn to more closely resemble pelvic angles during straight walking, which may have resulted in poorer balance during this gait cycle (Fig. 5.6).

5.3.3 Effects of PPN stimulation on gait

5.3.3.1 Effects of PPN stimulation on gait performance and standing balance

Abnormalities in walking speed, stride length, and DS/SS were more pronounced in the PPN DBS OFF patient than they were in the STN DBS OFF patients. PPN stimulation appeared to increase walking speed and stride length during straight walking, but this effect was inconsistent during turning.

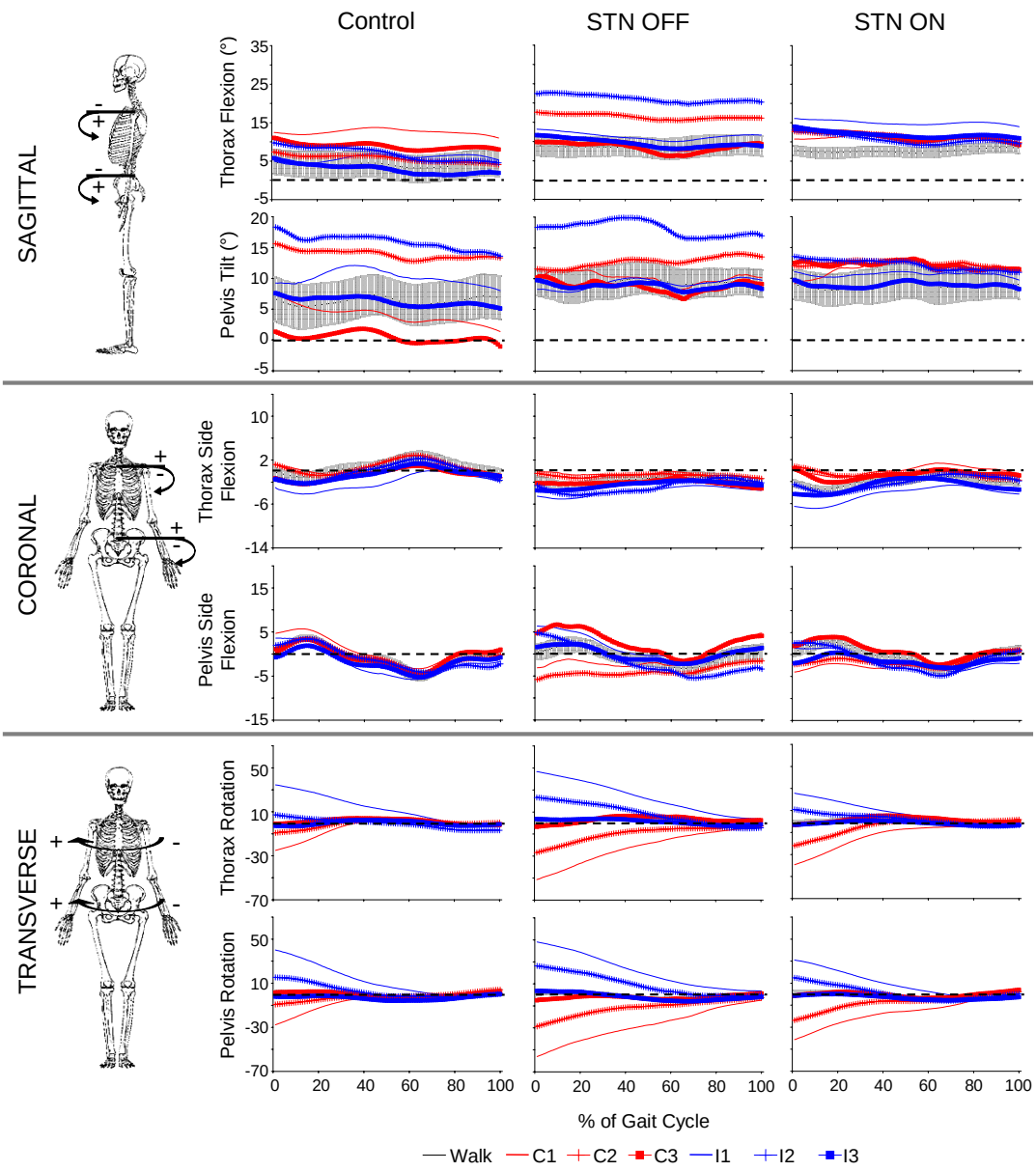

Figure 5.6. Effects of STN stimulation on thoracic and pelvic angles during walking and turning. Thoracic and pelvic angles are shown in each plane of motion (indicated on the left) normalized across a gait cycle during walking (W, black with gray error bars indicating SEM), and the first, second, and third gait cycles of an ipsilateral (I1/2/3, red) and contralateral (C1/2/3, blue) turn for control subjects and PD patients on (STN ON) and off (STN OFF) STN stimulation. The direction of motion corresponding to a positive (+) or (–) angle value is indicated on diagrams of thoracic and pelvic angles to the left of the corresponding graphs.

PPN stimulation did, however, result in dramatic improvements in balance measures. During both straight walking and turning, PPN stimulation resulted in large decreases in DS/SS. This effect was most prominent during walking (a reduction in DS/SS from 1.20 off PPN stimulation to 0.76 on PPN stimulation) and ipsilateral turning. PPN stimulation also resulted in far less movement during standing causing marked decreases in thoracic flexion (by 30%), thoracic rotation (by 53%), and pelvic rotation (by 17%) (Fig. 5.7B).

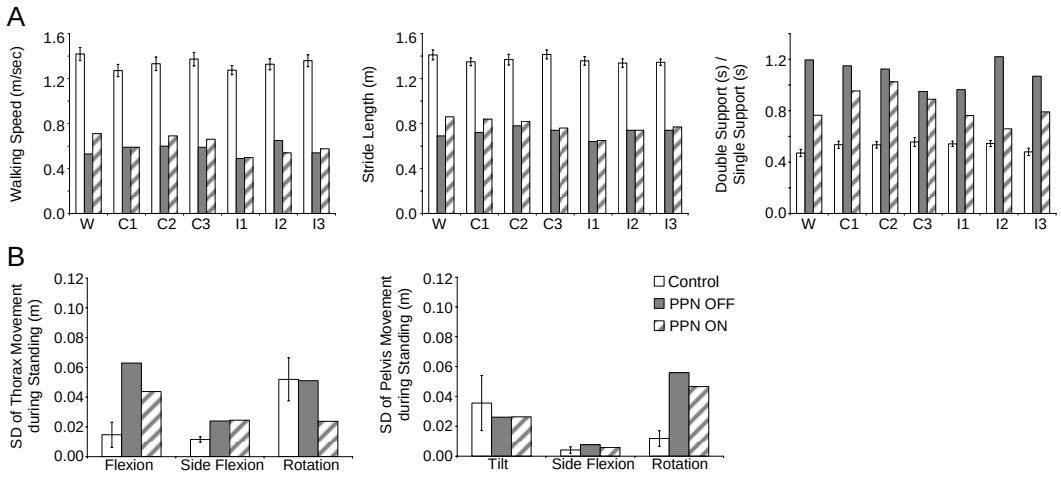

Figure 5.7. Effects of PPN stimulation on temporal gait parameters and standing balance. A) Walking speed, stride length, and double-support / single-support duration are shown during walking and turning for control subjects and for one PD patient on (PPN ON) and off (PPN OFF) PPN stimulation (W – gait cycle during straight walking, I1/2/3 –first, second, and third gait cycles of an ipsilateral turn, C1/2/3 – first, second, and third gait cycles of a contralateral turn). B) The standard deviations (SD) of thoracic and pelvic motion in the transverse (rotation), coronal (side flexion), and sagittal (thoracic flexion and pelvic tilt) planes are shown during 100 sec of standing for control subjects and for one PD patient on and off PPN stimulation.

5.3.3.2 Effects of PPN stimulation on thoracic and pelvic angles during walking

The three abnormalities in trunk angles in the PPN DBS OFF patient were more pronounced than they were in the STN DBS OFF patients. First, the PPN DBS OFF patient had much greater forward thoracic flexion during straight walking than did the STN DBS OFF patients or the control subjects, indicating a more stooped posture. Second, thoracic side flexion was more

negative for the PPN DBS OFF patient than it was for the STN DBS OFF patients or for the control subjects, but pelvic side flexion during straight walking was comparable to control values. This suggests that the PPN patient exhibited far less arm swinging than did the STN DBS OFF patients. Finally, the PPN DBS OFF patient's thorax and pelvis were more externally rotated during walking. In contrast, trunk rotation in the STN DBS OFF patients was not different from trunk rotation in the control subjects. The increased trunk rotation in the PPN DBS OFF patient may be due to decreased arm swinging (suggested by the negative thoracic side flexion) since restriction of arm movement during walking has been shown to greatly increase trunk torque and rotation (Kubo *et al.*, 2006). PPN stimulation did not appear to have an effect on these trunk angle abnormalities during straight walking.

5.3.3.3 Effects of PPN stimulation on thoracic and pelvic angles during turning

Abnormalities in trunk angles during turning permeated all planes of movement in the PPN DBS OFF patient just as they did in the STN DBS OFF patients. In the sagittal and coronal planes, thoracic and pelvic angles deviated from walking trunk angles during each of the turning gait cycles in PPN DBS OFF patients. However, this deviation did not appear to follow any pattern across the gait cycles. This may again be related to the attention-related gait variability in PD patients (Sheridan and Flowers, 1990; Hausdorff *et al.*, 1998, 2003a; 2003b; Springer *et al.*, 2006). PPN stimulation reduced this variability and resulted in turning trunk angles that were similar to walking trunk angles in both the sagittal and coronal planes of movement.

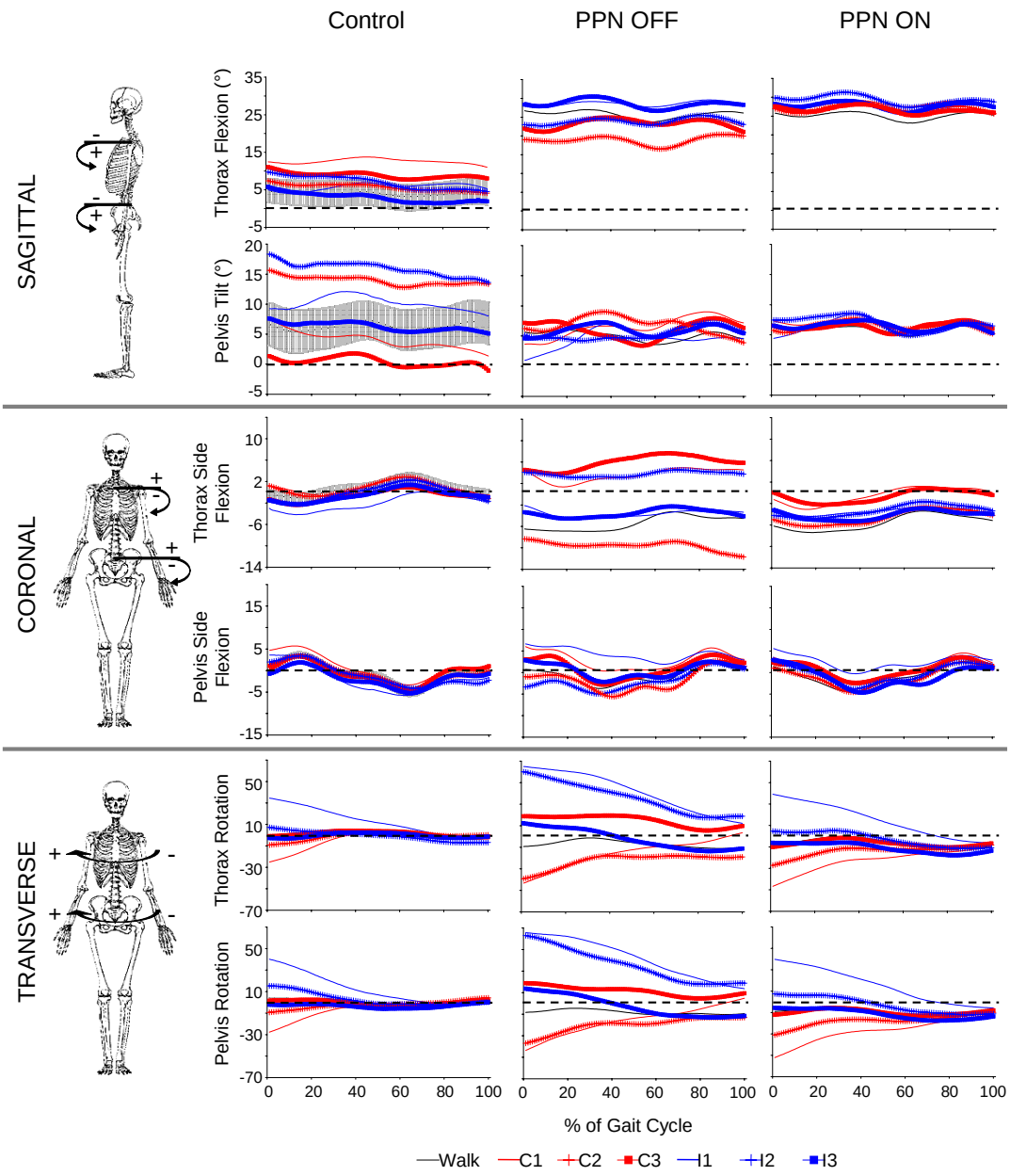

Figure 5.8. Effects of PPN stimulation on thoracic and pelvic angles during walking and turning. Thoracic and pelvic angles are shown in each plane of motion (indicated on the left) normalized across a gait cycle during walking (W, black with gray error bars indicating SEM), and the first, second, and third gait cycles of an ipsilateral (I1/2/3, red) and contralateral (C1/2/3, blue) turn for control subjects and for one PD patient on (PPN ON) and off (PPN OFF) PPN stimulation. The direction of motion corresponding to a positive (+) or (–) angle value is indicated on diagrams of thoracic and pelvic angles to the left of the corresponding graphs.

The most obvious abnormality in the PPN DBS OFF patient during turning was in the transverse plane of movement. Similar to the STN DBS OFF patients, the PPN DBS OFF patient over-rotated the trunk during the first gait cycle of each turn (relative to trunk rotation during this cycle in control subjects). However, though both the STN DBS OFF patients and the control subjects began re-orienting the trunk to straight walking rotation values in the second gait cycle of the turn and had completed this re-orientation by the third gait cycle, the PPN DBS OFF patient did not correct trunk rotation at all in the second gait cycle and had not achieved trunk re-orientation by the third gait cycle. Instead, the PPN DBS OFF patient appeared to over-compensate for poor trunk rotation in the first and second turning gait cycles by rotating the trunk excessively in the opposite direction during the third gait cycle (excessive external rotation during the third gait cycle of ipsilateral turns and excessive internal rotation during the third gait cycle of contralateral turns). This abnormal trunk rotation in the PPN DBS OFF patient during turning may be due to decreased autonomic control of balance (Grillner, 1981; Sheridan and Flowers, 1990; Dietz, 1997; Hausdorff *et al.*, 1998, 2003a, 2003b; Springer *et al.*, 2006; Grillner *et al.*, 2008). Executive control of balance maintenance may explain the forced compensatory trunk rotation in the third gait cycle following the autonomic inability to re-orient trunk rotation in the second gait cycle of the turn. PPN stimulation greatly ameliorated the abnormal trunk rotation in the PD patient studied. In addition to reducing trunk rotation during the first gait cycle of the turn, PPN stimulation also helped the patient begin re-orientation of the trunk during the second gait cycle and complete this re-orientation by the third gait cycle.

5.4 Discussion

The effects of STN DBS and PPN DBS on gait performance, balance, and trunk kinematics during walking and turning were studied. Control subjects exhibited the walking speed, stride length, DS/SS, and slightly stooped posture during straight walking that are representative of older walkers. Relative to the control subjects, PD patients had decreased walking speeds, decreased stride length, increased DS/SS, more trunk movement during standing, greater stooped posture, and impaired arm swinging. These gait abnormalities were more severe in the PPN DBS OFF patient than they were in the STN DBS OFF patients. Perhaps due to greater restriction of arm movement, the PPN DBS OFF patient also displayed increased trunk rotation during straight walking. Both STN DBS and PPN DBS helped improve walking speeds, stride length, and DS/SS, but PPN DBS resulted in much greater improvement of DS/SS and in a greater reduction of trunk movement during standing than did STN DBS.

During turning, trunk angles in the sagittal and coronal planes of movement were highly variable for PD patients, but more so in the PPN DBS OFF patient than in the STN DBS OFF patients. PD patients also tended to over-rotate the trunk during the first gait cycle of each turn and took longer to re-orient the trunk to straight-walking rotation values. Again this effect was most pronounced in the PPN DBS OFF patient who was unable to re-orient the trunk at all in the second gait cycle of the turn and appeared to over-compensate for this by rotating the trunk in the opposite direction during the third gait cycle. STN DBS and PPN DBS reduced trunk angle variability and trunk over-rotation during turning.

5.4.1 Differences between PPN and STN DBS

There are two main differences between the effects of PPN DBS and the effects of STN DBS on gait performance in PD patients. First, based on results from the 1 PD patient studied, PPN DBS may be more effective at restoring balance. During walking and turning PPN DBS resulted in greater improvement of DS/SS than did STN DBS. Also, PPN DBS decreased thoracic flexion, thoracic rotation, and pelvic rotation during standing which is indicative of improvements in balance (Shumway-Cook *et al.*, 1997; Woollacott and Shumway-Cook, 2002). In contrast, STN DBS did not have a significant effect on trunk movement relative to PD patients off stimulation and may have even increased trunk movement during standing. Since the STN DBS OFF patients participating in this study had been on STN DBS stimulation for several years (5.2 ± 1.1 years, Table 5.1), it is possible that the beneficial effects of STN DBS on balance have waned over time in these patients (Krack *et al.*, 2003). Therefore, at least initially, PPN DBS may result in greater improvements in balance than does STN DBS after several years of stimulation.

Second, in the patient receiving PPN DBS that participated in this study, PPN stimulation appears to improve turning by reducing dependence on executive control of gait. In contrast, in the patients receiving STN DBS that participated in this study, STN stimulation appears to optimize executive control of gait. The PPN DBS OFF patient had increased trunk angle variability during turning (a task that places greater demands on attention than does straight walking) and was unable to re-orient the trunk after turning without over-rotating the trunk in the third gait cycle of the turn. Increased gait variability (Sheridan and Flowers, 1990; Hausdorff *et al.*, 1998, 2003a, 2003b; Springer *et al.*, 2006)

and the apparent forced compensatory trunk rotation during turning are both indicative of decreased autonomic control and a greater dependence on executive control of gait and balance. In contrast, the STN DBS OFF patients exhibited less trunk angle variability during turning (relative to the PPN DBS OFF patient) and were able to progressively re-orient the trunk during turning. Therefore, when examining PD patients off stimulation, the patients with STN DBS implants appeared to have retained more autonomic gait control than did the patient with PPN DBS implants.

Both PPN and STN stimulation improved trunk angles in PD patients during turning. In the 1 PD patient studied, PPN DBS decreased trunk angle variability during turning and also restored a more normal progression of trunk re-orientation following a turn, both of which suggest an increase in autonomic control of gait. In contrast, STN stimulation reduced excessive trunk rotation during all gait cycles of turning. This effect may be more indicative of the optimization of executive gait control and motor program selection.

5.4.2 Concluding remarks

Gait analysis was performed on 6 healthy older walkers and on 6 PD patients (5 with STN DBS implants, 1 with PPN DBS implants) who were off medication. Since PPN DBS was only recently introduced clinically, future research could compare the long term effects of PPN DBS to the long term effects of STN DBS. It is also necessary to determine trunk kinematics during turning for a larger number of STN and PPN DBS patients to verify the results presented here. Finally, the possible synergistic effects of dopaminergic medication with STN and PPN stimulation (Stefani *et al.*, 2007) should also be

determined with regards to trunk kinematics during turning. The results of this study suggest that the patient selected to receive PPN DBS, relative to those selected for STN DBS, had greater trunk angle variability, poorer balance, increased stooping, decreased autonomic gait control, and increased dependence on executive gait control. A comparison of the effects of STN and PPN DBS suggests that PPN DBS may result in a greater improvement in balance and that it may increase autonomic gait control. STN DBS may have a more limited effect on balance and may optimize executive gait control and motor program selection.

Main Findings

- *PPN DBS may be more effective than STN DBS at improving balance measures in PD patients (as evidenced by greater relative decreases in DS/SS and in trunk movement during standing).*
- *PD patients all displayed difficulty re-orienting the trunk promptly and accurately following a 90° turn.*
- *Both STN and PPN DBS decreased excessive trunk rotation during turning, but PPN DBS also appeared to restore some autonomic control of gait during turning while STN DBS appeared to optimize executive gait control during turning.*

6. IMPLICATIONS FOR DBS IN PARKINSON'S DISEASE

This thesis has compared the anatomy, electrophysiology, and motor control relationships of the STN and PPN in order to better understand their roles as DBS targets for PD. Probabilistic diffusion tractography was used to study the connections of the human STN and PPN in Section 2. Transmission of oscillatory activity from the basal ganglia to the PPN was examined using electrophysiological recordings in anesthetized rats in Section 3. Modulation of oscillatory activity was examined in the PPN and STN during simple voluntary movement in PD patients in Section 4. Finally, Section 5 compared the effects of PPN and STN stimulation on gait in PD patients. This section summarizes the results from these experiments and discusses their implications for DBS in PD.

6.1 Summary of results

6.1.1 Comparison of PPN and STN anatomy

Since rodent and primate studies differ in their description of the relative strengths of the connections between the PPN and the basal ganglia (reviewed in Lee *et al.*, 2000), the anatomical connections of the PPN and STN and the topography of these connections were determined using probabilistic diffusion tractography in healthy human subjects (Section 2.1) and in the non-human primate (Section 2.2).

Both the human PPN and human STN showed connections with the cortex, basal ganglia, cerebellum, and down the spinal cord, largely matching connections previously demonstrated in monkeys (Fig. 6.1). The topography of motor and associative brain areas in the human STN was strikingly similar to that shown in animals. PPN topography has not been extensively demonstrated in rodents or monkeys, but significant topography of cortical and sub-cortical connections was demonstrated in the human PPN in Section 2.1. In addition to demonstrating the usefulness of diffusion tractography in determining the connections and topography of small gray matter structures *in vivo*, these results allow for inference of optimal DBS target locations (Section 6.3) and add to our understanding of the role of these nuclei in PD (Section 6.4).

In order to further compare the anatomical connections of the PPN in healthy humans to the histologically demonstrated connections of the PPN in monkeys, and thus to support the use of diffusion tractography in humans, diffusion tractography was also carried out in a fixed *Macaca mulatta* brain.

PPN connections with the basal ganglia and motor cortical areas observed in the monkey brain using diffusion tractography matched those previously demonstrated using conventional anatomical tracing techniques. Furthermore, the results presented in Section 2.2 demonstrate clearly distinct regions of the PPN that connect with the thalamus, SN, and STN in the monkey brain.

Thus in addition to increasing confidence in the accuracy of diffusion tractography for tracing PPN connections and determining the organization of these connections within the PPN *in vivo*, these observations suggest that

diffusion tractography will be a useful new technique for rapidly identifying connections in animal brains pre and post mortem.

6.1.2 Electrophysiological relationship between the PPN and basal ganglia

After observing that the PPN was strongly connected with the STN and the other basal ganglia nuclei in humans in Section 2, the electrophysiological relationship between the PPN and STN was examined in Section 3. The anesthetized rat has been a useful model for investigating the effects of dopamine loss on the transmission of oscillatory cortical activity through basal ganglia structures. Previous studies have shown that, after dopamine cell lesion, synchronous oscillatory activity emerges in the STN and SNpr in phase with M1 oscillations (Magill *et al.*, 2001; Tseng *et al.*, 2001b; Belluscio *et al.*, 2003; Walters *et al.*, 2005, 2007; Parr-Brownlie *et al.*, 2007). However, the impact of these changes in basal ganglia output on the timing of PPN spiking remained unknown. Section 3 investigated the effect of dopamine loss on spike timing in the PPN using M1 LFP activity as a reference in urethane-anesthetized and ketamine-anesthetized rats.

Simultaneous recordings of PPN spike trains and LFP activity in the PPN and M1 were conducted in anesthetized intact and hemi-parkinsonian rats 7-10 days after a unilateral injection of 6-hydroxydopamine into the medial forebrain bundle. Increased spectral power in PPN spike trains and increased coherence between PPN spiking and PPN LFP activity were observed following dopamine cell lesion in urethane-anesthetized rats. PPN spike timing also changed from the PPN firing predominantly in phase with M1 slow oscillatory

activity in the intact urethane-anesthetized rat to firing predominantly antiphase to M1 oscillations in the hemi-parkinsonian rat (Fig. 6.1). These changes were not observed in the ketamine-anesthetized preparation suggesting that the NMDA antagonist properties of ketamine may attenuate some of the effects of dopamine cell lesion.

The results from Section 3 suggest that PPN spike timing after dopamine cell lesion is altered by increased inhibitory oscillatory input to the PPN from basal ganglia output nuclei. These findings highlight processes that may be involved in motor dysfunction and PPN DBS efficacy in PD patients (Section 6.4).

6.1.3 Modulation of STN and PPN oscillatory activity during simple voluntary movement

The results from Section 3 demonstrated that, following dopamine loss, there is increased transmission of oscillatory cortical activity to the PPN via the basal ganglia in the anesthetized rat model of PD. However, in that preparation, output from the GPi/SNpr, not output from the STN, dominated PPN spike timing in the parkinsonian brain. Therefore, these results suggest that oscillatory activity present in the STN in PD patients may not necessarily be present in the PPN. As a result, modulation of oscillatory activity related to movement may differ between the STN and PPN and may speak to the different roles of these nuclei in motor control. To explore these questions, Section 4 examined PPN and STN activity in PD patients performing simple voluntary movements. LFPs were recorded during IG and EC finger movement tasks. Recordings were made from 12 DBS electrodes implanted in the STNs

of 6 PD patients and from 1 DBS electrode implanted in the PPN of 1 PD patient. As has been previously demonstrated in STN LFPs recorded from PD patients (Brown, 2003; Brown and Williams, 2005), β (12-30 Hz) frequency oscillations were also present in PPN LFPs.

To determine how oscillations present in both PPN and STN LFPs were modulated with voluntary movement, STN and PPN LFP signals were decomposed into θ (3-8 Hz), α (8-12 Hz), low (12-20 Hz) and high (20-30 Hz) β, and low (30-60 Hz) and high (60-90 Hz) γ frequency bands. The instantaneous amplitude of the decomposed signal in each frequency band was extracted using the Hilbert transform over time and expressed as percentage changes relative to baseline activity levels. Changes in synchronization were compared between EC and IG tasks and frequency bands.

In STN LFPs, bilateral low β band desynchronization was observed during both IG and EC tasks. Our results associate this modulation with motor execution, as finger movements were similar between tasks. Furthermore, unlike the IG task, the EC task also involved bilateral α and high β band desynchronization and a delay in the onset and peak of α band desynchronization. Since the EC task involved bilateral motor preparation and cue processing while the IG task did not, our results suggest that laterality of high β band desynchronization is related to motor preparation and that a delay in α band desynchronization is associated with cue processing or motor facilitation of subsequent movements in a repetitive motor task.

In PPN LFPs, high β band ERD during the EC task occurred bilaterally and was locked to the time of stimulus presentation. However, in the IG task, peri-movement high β ERD occurred only in the contralateral PPN while post-movement low β ERS and high β ERS occurred in the ipsilateral PPN. Therefore, our results associate bilateral high β ERD with the processing of a visual cue and contralateral high β ERD with motor preparation and execution. On the other hand, low β ERS and high β ERS in the ipsilateral PPN during the IG task are most likely a pathological antikinetic phenomenon as this ERS is eliminated following the presentation of a prokinetic visual cue.

The main difference between LFP modulation in the STN and in the PPN is that the greatest magnitude LFP modulation in the PPN occurred in the high β band while the greatest magnitude LFP modulation in the STN occurred in the α and low β bands. These results in PD patients (Section 4), taken together with the results from rodent studies (Section 3), suggest that oscillatory activity from the STN may not be directly transmitted to the PPN in the parkinsonian brain (Fig. 6.1). The results from PD patients (Section 4) also suggest that movement-related modulation of oscillatory activity occurs at the α and low β frequencies in the basal ganglia and may be more related to motor execution. In contrast, downstream of the basal ganglia in the PPN, movement-related modulation of oscillatory activity may preferentially occur at the high β frequencies and may be more closely associated with motor preparation and sensory cue processing.

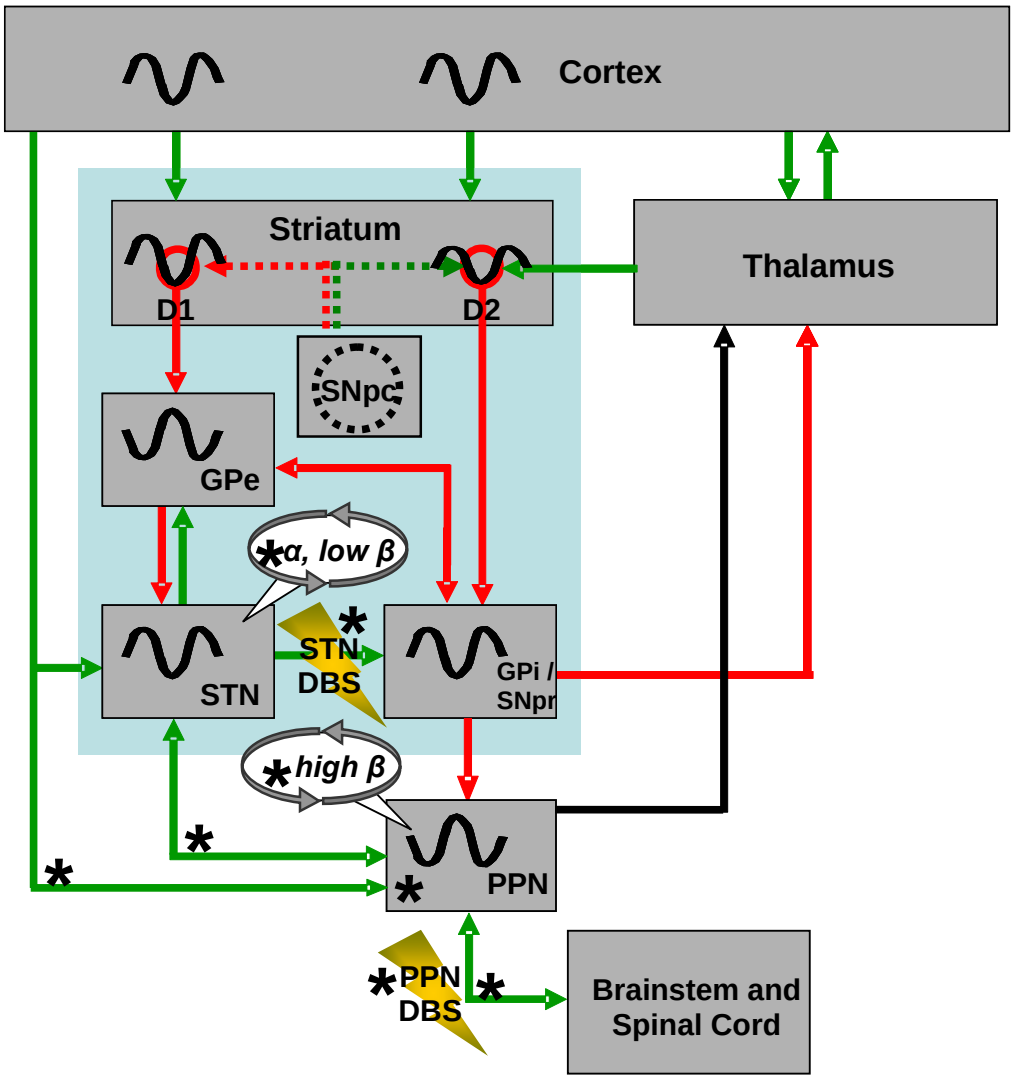

Figure 6.1. Summary of results from Sections 1-4. Novel findings and hypotheses presented in this thesis are indicated with asterisks (*) on a schematic of basal ganglia network connections. Dashed lines around and emerging from the SNpc indicate degeneration of dopamine neurons in the SNpc in the parkinsonian brain. Example local field potential traces are indicated in each structure as they would appear if recorded simultaneously (Walters *et al.*, 2007). Troughs indicate periods of greatest depolarization in the structure while peaks indicate periods of least depolarization. Arrows encircling frequency ranges indicate the frequency of oscillatory activity that is predominantly modulated during simple voluntary movement in the designated oscillatory network loop. “STN DBS” and “PPN DBS” labels are placed near the connections that may be the most important for improving gait when affected by STN and PPN stimulation. Arrows between structures indicate direct connections (green: excitatory, red: inhibitory, black: either inhibitory or excitatory).

6.1.4 Effects of STN and PPN DBS on gait

The results presented in Section 4 demonstrate that oscillatory activity is differently modulated in the STN and PPN during simple voluntary movement. To determine how the STN and PPN differ in the control of large-scale coordinated voluntary movement, the effects of STN and PPN DBS on gait were examined in Section 5.

Five PD patients with bilateral STN DBS implants, 1 PD patient with bilateral PPN DBS implants, and 6 age- and weight-matched controls were recruited to participate in this study. Walking speed, stride length, the ratio of double support duration to single support duration (DS/SS), and trunk angles during standing, walking, and turning were evaluated for all PD patients on and off stimulation and compared to values obtained from healthy control subjects.

PD patients exhibited decreased walking speed, decreased stride length, increased DS/SS, and increased trunk movement during standing. Both PPN DBS and STN DBS improved these gait performance parameters, but results from 1 PD patient with PPN DBS implants suggested that PPN DBS may be more effective than STN DBS at improving balance (decreasing DS/SS and reducing trunk movement during standing).

PD patients also displayed abnormal trunk angles during turning. STN DBS OFF patients took longer to straighten the trunk following a turn, but still progressively decreased trunk rotation after the turn was completed similar to the progressive decrease in trunk rotation exhibited by control subjects following a turn. In contrast, the PPN DBS OFF patient was unable to progressively straighten the thorax following a turn and ultimately compensated for this by over-rotating the thorax in the direction opposite to the turn. In

addition, the PPN DBS patient also exhibited greater trunk angle variability during turning, indicative of decreased autonomic gait control (via spinal central pattern generators and brainstem locomotor centers) and an increased dependence on executive gait control (via motor cortex and basal ganglia-mediated selection of motor programs). That is, assuming that the patients participating in this gait study were representative of the criteria used to differentiate between PD patient candidates for STN DBS and PPN DBS, these results suggest that PD patients selected for STN DBS appear to retain greater autonomic control of gait than do PD patients selected for PPN DBS.

Both STN stimulation and PPN stimulation decreased the excessive trunk rotation during turning that was present in PD patients. PPN DBS also appeared to restore the ability to progressively decrease thoracic rotation following turn and eliminated compensatory thoracic over-rotation in the 1 patient studied. Therefore, these preliminary results suggest that PPN DBS may improve turning in PD patients by restoring autonomic control of gait while STN DBS may improve turning by optimizing the executive control of gait (Section 6.4, Fig. 6.1).

6.2 Choosing Parkinson's disease patient candidates for STN and PPN DBS

PD patients usually selected to receive STN DBS exhibit dopamine-responsive motor symptoms (usually limited to tremor and bradykinesia) (Kumar *et al.*, 1998; Yokoyama *et al.*, 1999; Stolze *et al.*, 2001; Krack *et al.*, 2003; Rodriguez-Oroz *et al.*, 2005). In contrast, candidates for PPN DBS

exhibit axial rigidity and gait abnormalities that are medically intractable, even with dopaminergic medication (Mazzone *et al.*, 2005; Plaha and Gill, 2005; Jenkinson *et al.*, 2006; Stefani *et al.*, 2007).

The gait analysis described in Section 5 also reveals several differences between PD patients chosen to receive STN DBS and the PD patient chosen to receive PPN DBS implants. The PPN DBS OFF patient, relative to the STN DBS OFF patients, exhibited much lower walking speed, decreased stride length, increased DS/SS, greater stooped posture, greater external trunk rotation during walking, inability to re-orient trunk rotation following a turn, and a tendency to over-rotate the trunk following a turn to compensate for this inability. These gait analysis measures may be useful for quantifying parkinsonian gait abnormalities and for possibly helping to determine PD patient candidates for PPN DBS. Trunk rotation during turning appears to reveal the greatest difference between STN DBS OFF patients and the PPN DBS OFF patient. This difference, if it proves to be a valid predictor of clinical outcome, could be further exposed by giving patients dual-attention tasks during turning and thus creating greater demands on executive function (Woollacott and Shumway-Cook, 2002; Hausdorff *et al.*, 2003a; Yogev *et al.*, 2005; Springer *et al.*, 2006; Rochester *et al.*, 2007). The results of this study suggest that the PPN DBS OFF patient relied much more on executive control of gait than did the STN DBS OFF patients. Therefore, PD patient candidates for PPN DBS may be the patients who show the most dramatic decline in the ability to control thoracic rotation during turning given increased demands on attention.

6.3 Optimally targeting the STN and PPN for DBS

The topography of the human STN and PPN, as revealed by tractography studies (Section 2), has distinct implications for targeting in functional neurosurgery. For example, it has been previously suggested that the optimal site for targeting in the STN should be the area most connected to sensorimotor brain regions (Romanelli *et al.*, 2004). Our work shows that this target site should be in the superior portion of the STN, which has, in fact, been shown to be the optimal target site (Lanotte *et al.*, 2002; Voges *et al.*, 2002; Hamel *et al.*, 2003; Caire *et al.*, 2006; Godinho *et al.*, 2006). In addition, as several studies still dispute that DBS of the STN is more effective than DBS of GPi for PD (Burchiel *et al.*, 1999; Volkmann, 2004; Anderson *et al.*, 2005; Rodriguez-Oroz *et al.*, 2005), stimulation of the portion of the PPN connected with the GP, in addition to STN stimulation, may be beneficial for PD patients. Though the directionality of the connection between the GP and PPN cannot be determined using diffusion tractography, it is known that the GPi sends an inhibitory projection to the PPN in monkeys. Low frequency stimulation of the portion of the PPN connected with the GP may help counter the excessive inhibitory drive from the GPi observed in PD (Albin *et al.*, 1989; Bergman *et al.*, 1998a).

The topography results from Section 2 demonstrate that sensorimotor brain regions connect with the lateral half of the PPN and that the GP also connects in the lateral portion of the PPN. Therefore, our PPN topography results suggest that DBS of the PPN will achieve maximum therapeutic benefit by aiming for the lateral portion of the PPN for stimulation. This targeting

suggestion is especially interesting when considering preliminary evidence that the beneficial effects of DBS of the STN and DBS of the PPN in PD patients are additive (Stefani *et al.*, 2007). Perhaps by targeting a portion of the PPN that does not already connect with the STN, this additive benefit will be maximized.

6.4 Insights into the mechanisms underlying STN and PPN DBS efficacy

DBS is thought to ameliorate parkinsonian symptoms by disrupting pathological oscillations that emerge in the basal ganglia in the parkinsonian brain (Benazzouz and Hallett, 2000; Obeso *et al.*, 2000; Brown, 2003; Brown and Williams, 2005; Wichmann and DeLong, 2006). The PPN exhibits robust connections with the basal ganglia and dopamine cell lesion has been suggested to result in increased transmission of oscillatory activity from the cortex to the basal ganglia (Murer *et al.*, 2002; Walters *et al.*, 2007). The results from Section 3 suggest that this increased oscillatory activity in the basal ganglia is also transmitted downstream to the PPN as evidenced by increased power in PPN spike trains following dopamine cell lesion. Therefore, similar to DBS of the STN, it is possible that DBS of the PPN works by optimally disrupting pathological oscillations in the PPN.

DBS of the PPN could also drive PPN activity in the parkinsonian brain. Low frequency stimulation, generally thought to drive neuronal activity, is found to be most therapeutically effective when stimulating the PPN in PD patients (Mazzone *et al.*, 2005; Plaha and Gill, 2005; Stefani *et al.*, 2007) and studies in

non-human primates suggest that the PPN is over-inhibited in PD (Kojima *et al.*, 1997; Munro-Davies *et al.*, 1999; Matsumura and Kojima, 2001; Nandi *et al.*, 2002a; Jenkinson *et al.*, 2004). Our results also suggest that the PPN is dominated by inhibitory oscillatory input from the SNpr in the parkinsonian brain. Therefore, driving PPN neuronal activity via low frequency stimulation could attenuate the effects of excessive inhibitory input to the PPN in PD.

Alternatively, DBS of the PPN could also affect PPN spike timing relationships. The significant changes in PPN spike timing following dopamine cell lesion observed in this study suggest that PPN spike timing in the parkinsonian brain is potentially dysfunctional. Low frequency stimulation of the PPN, in addition to driving PPN neuronal activity, may disrupt this pathological spike timing relationship or properly synchronize PPN firing with excitatory input from the STN.

Low frequency stimulation of the PPN could also result in PD symptom amelioration by introducing functionally beneficial oscillatory activity into the PPN. As demonstrated in Section 4, simple voluntary movement results in modulation of α and low β frequency oscillations (8-20 Hz) in the STN. However, movement-related modulation occurs primarily in the high β band (20-30 Hz) in the PPN. Since high β movement-related modulation in the PPN appears to extend slightly into the low γ range (up to 35 Hz), it is also possible that the functional high β range in the PPN may be limited to higher frequencies. In the context of these results, it is possible that the 10-25 Hz PPN stimulation used in PD patients (Mazzone *et al.*, 2005; Plaha and Gill, 2005; Stefani *et al.*, 2007) could ameliorate parkinsonian symptoms by synchronizing

PPN oscillatory activity with the lower frequency oscillatory activity found in the STN.

The effectiveness of high frequency (>100 Hz) STN stimulation may also be partially attributable to its downstream effects on PPN oscillatory activity. In the PD patients selected to receive STN DBS (patients with dopamine-responsive motor symptoms), STN stimulation appears to improve turning by optimizing executive control of gait. In contrast, in the PD patients selected to receive PPN DBS (patients with medically intractable axial symptoms), PPN DBS appears to improve turning by restoring autonomic control of gait. It has been suggested that executive motor control centers facilitate motor program selection by disinhibiting the mesencephalic locomotor region and thus allowing it to activate the central pattern generators in the spinal cord that are responsible for basic gait execution (Grillner, 1981; Grillner *et al.*, 2008). Disinhibition of the mesencephalic locomotor region (which includes the PPN) could involve decreasing inhibitory oscillatory output from the GPi/SNpr to the PPN. In this context, it is interesting to note that oscillatory activity in the PPN appears to be dominated by inhibitory oscillatory output from the GPi/SNpr in the anesthetized rat model of PD (Section 3). STN DBS could decrease this inhibitory oscillatory output from the GPi/SNpr to the PPN, and ultimately facilitate the executive control of gait, by decreasing excitatory oscillatory output from the STN to the GPi/SNpr. PPN DBS could restore the autonomic control of gait by directly activating the central pattern generators in the spinal cord (Fig. 6.1).

6.5 The efficacy of dual STN and PPN DBS for Parkinson's disease: Insights and future research

DBS of the PPN appears to alleviate the parkinsonian gait and postural abnormalities that persist even with dopaminergic medication or, ostensibly, STN stimulation. As a result, it appears that DBS of the STN and DBS of the PPN could have additive beneficial effects. Information regarding the effects of dual stimulation of the STN and PPN in PD patients has been limited. There has only been one clinical study describing the effects of dual STN and PPN DBS (Stefani *et al.*, 2007), and it suggests that combined stimulation may only provide added benefit when PD patients are also on dopaminergic medication. Furthermore, as DBS of the STN is done at high frequencies (>100 Hz), while DBS of the PPN is done at lower frequencies (<25 Hz), it is unclear how dual stimulation of two connected and relatively proximal nuclei can be optimally maintained given such different stimulation parameters.

However, the results presented in this thesis suggest that the PPN and STN are more segregated than is belied by their anatomical connections alone. The results from Section 2 demonstrate a robust connection between the PPN and STN which suggests that it is anatomically possible for oscillatory activity or stimulation in one nucleus to directly affect activity of the other. However, the results from Section 3 show that PPN spike timing in the anesthetized parkinsonian rat brain is actually dominated by increased inhibitory oscillatory output from the GPi/SNpr, and not by the increased excitatory oscillatory output from the STN, suggesting that oscillatory activity may not be directly transmitted between the STN and PPN. This is corroborated by results from

Section 4 showing that voluntary movement predominantly involves modulation of different frequency ranges of oscillatory activity in the STN and PPN, further highlighting the electrophysiological schism between the two nuclei. The effects of STN and PPN DBS on gait presented in Section 5 also illustrate differences in the behavioral effects of stimulation of these two nuclei. DBS of the PPN appears to restore autonomic control of gait, perhaps via its connections with spinal cord motor centers and central pattern generators. DBS of the STN appears to optimize executive control of gait, possibly via its connections to other basal ganglia nuclei involved in the fine-scale modulation of motor control.

These differences in STN and PPN electrophysiology and behavioral roles suggest that dual STN and PPN stimulation at different frequencies may still be additively beneficial. PPN topography (Section 2) shows that the portion of the PPN connected to the STN is more medial than the portions of the PPN connected to any other motor structure (M1, cerebellar nuclei, GP). Perhaps to maximize the additive benefit of dual stimulation and prevent a virtual stalemate of clashing oscillatory activity, dual STN and PPN stimulation could involve targeting the lateral portion of the PPN to avoid directly co-stimulating portions of the PPN that may be receiving at least some input from the STN. In addition, it may also be worthwhile to synchronize stimulation pulses in the PPN and STN (for example, stimulating the PPN coincident with every 10^{th} stimulation pulse in the STN). This technique may also foster increased synchrony in oscillatory activity between the STN and PPN and thus reduce the dominant effects of excessive inhibitory oscillatory input to the PPN from the basal ganglia output nuclei (Section 3).

Alternatively, though much of the neurosurgical focus has been on dual stimulation of the STN and PPN for PD, perhaps dual stimulation of the GPi and PPN would be equally or more effective. The GPi and PPN are robustly connected to each other anatomically (Section 2) and electrophysiologically in the parkinsonian brain (Section 3). Perhaps the best stimulation paradigm for dual GPi and PPN stimulation would involve stimulating the lateral portion of the PPN (which exhibits connections with the GP) with pulses that are out of synchrony with the stimulation pulses in the GPi in order to optimally disrupt the pathologically dominant effect of GPi oscillatory output on PPN activity in the parkinsonian brain (Section 3).

Future clinical studies could address these hypotheses regarding the optimization of dual target stimulation. Repeating the gait analyses (Section 5) for PD patients with DBS electrode implants in the GPi and recording LFP activity from the GPi in awake PD patients during simple voluntary movement (Section 4) may also shed light on the hypotheses presented above. In addition, the upstream and downstream electrophysiological effects of co-stimulation of the PPN and STN or GPi could be examined in the anesthetized rat model to determine the more global effects of dual stimulation paradigms and to even further understand the role of these nuclei as DBS targets for PD.

7. REFERENCES

Agostino R, Berardelli A, Curra A, Accornero N, Manfredi M (1998) Clinical impairment of sequential finger movements in Parkinson's disease. Mov Disord 13:418-421.

Albin RL, Young AB, Penney JB (1989) The functional anatomy of basal ganglia disorders. Trends Neurosci 12:366-375.

Alegre M, Alonso-Frech F, Rodriguez-Oroz MC, Guridi J, Zamarbide I, Valencia M, Manrique M, Obeso JA, Artieda J (2005) Movement-related changes in oscillatory activity in the human subthalamic nucleus: ipsilateral vs. contralateral movements. Eur J Neurosci 22:2315-2324.

Alexander GE, Crutcher MD (1990) Functional architecture of basal ganglia circuits: neural substrates of parallel processing. Trends Neurosci 13:266-271.

Alexander GE, DeLong MR, Strick PL (1986) Parallel organization of functionally segregated circuits linking basal ganglia and cortex. Annu Rev Neurosci 9:357-381.

Allers KA, Bergstrom DA, Ghazi LJ, Kreiss DS, Walters JR (2005) MK801 and amantadine exert different effects on subthalamic neuronal activity in a rodent model of Parkinson's disease. Exp Neurol 191:104-118.

Amalric M, Koob GF (1993) Functionally selective neurochemical afferents and efferents of the mesocorticolimbic and nigrostriatal dopamine system. Prog Brain Res 99:209-226.

Amzica F, Steriade M (1998) Cellular substrates and laminar profile of sleep K-complex. Neuroscience 82:671-686.

Anderson VC, Burchiel KJ, Hogarth P, Favre J, Hammerstad JP (2005) Pallidal vs subthalamic nucleus deep brain stimulation in Parkinson disease. Arch Neurol 62:554-560.

Androulidakis AG, Mazzone P, Litvak V, Penny W, Dileone M, Doyle Gaynor LM, Tisch S, Di Lazarro, V, Brown P (2008) Oscillatory activity in the pedunculopontine area of patients with Parkinson's disease. Exp Neurol doi:10.1016/j.expneurol.2008.01.002.

Andy OJ, Jurko MF, Sias FR (1963) Subthalamotomy in treatment of parkinsonian tremor. J Neurosurg 20:860-870.

Anis NA, Berry SC, Burton NR, Lodge D (1983) The dissociative anaesthetics, ketamine and phencyclidine, selectively reduce excitation of central mammalian neurones by N-methyl-aspartate. Br J Pharmacol 79:565-575.

Aosaki T, Kimura M, Graybiel AM (1995) Temporal and spatial characteristics of tonically active neurons of the primate's striatum. J Neurophysiol 73:1234-1252.

Apicella P, Legallet E, Trouche E (1997) Responses of tonically discharging neurons in the monkey striatum to primary rewards delivered during different behavioral states. Exp Brain Res 116:456-466.

Apicella P, Legallet E, Trouche E (1996) Responses of tonically discharging neurons in monkey striatum to visual stimuli presented under passive conditions and during task performance. Neurosci Lett 203:147-150.

Apicella P, Scarnati E, Schultz W (1991) Tonically discharging neurons of monkey striatum respond to preparatory and rewarding stimuli. Exp Brain Res 84:672-675.

Aravamuthan BR, Muthusamy KA, Stein JF, Aziz TZ, Johansen-Berg H (2007) Topography of cortical and subcortical connections of the human pedunculopontine and subthalamic nuclei. NeuroImage 37:694-705.

Aziz TZ, Peggs D, Agarwal E, Sambrook MA, Crossman AR (1992) Subthalamic nucleotomy alleviates parkinsonism in the 1-methyl-4-phenyl-1,2,3,6-tetrahydropyridine (MPTP)-exposed primate. Br J Neurosurg 6:575-582.

Aziz TZ, Peggs D, Sambrook MA, Crossman AR (1991) Lesion of the subthalamic nucleus for the alleviation of 1-methyl-4-phenyl-1,2,3,6-tetrahydropyridine (MPTP)-induced parkinsonism in the primate. Mov Disord 6:288-292.

Batschelet E (1981) Circular Statistics in Biology. New York: Academic Press.

Behrens TEJ, Johansen-Berg H, Jbabdi S, Rushworth MF, Woolrich MW (2007) Probabilistic diffusion tractography with multiple fibre orientations: What can we gain? NeuroImage 34:144-155.

Behrens TEJ, Johansen-Berg H, Woolrich MW, Smith SM, Wheeler-Kingshott CA, Boulby PA, Barker GJ, Sillery EL, Sheehan K, Ciccarelli O, Thompson AJ, Brady JM, Matthews PM (2003a) Non-invasive mapping of connections between human thalamus and cortex using diffusion imaging. Nat Neurosci 6:750-757.

Behrens TEJ, Woolrich MW, Jenkinson M, Johansen-Berg H, Nunes RG, Clare S, Matthews PM, Brady JM, Smith SM (2003b) Characterization and propagation of uncertainty in diffusion-weighted MR imaging. Magn Reson Med 50:1077-1088.

Belluscio MA, Kasanetz F, Riquelme LA, Murer MG (2003) Spreading of slow cortical rhythms to the basal ganglia output nuclei in rats with nigrostriatal lesions. Eur J Neurosci 17:1046-1052.

Benazzouz A, Hallett M (2000) Mechanism of action of deep brain stimulation. Neurology 55:S13-S16.

Berney A, Panisset M, Sadikot AF, Ptito A, Dagher A, Fraraccio M, Savard G, Pell M, Benkelfat C (2007) Mood stability during acute stimulator challenge in Parkinson's disease patients under long-term treatment with subthalamic deep brain stimulation. Mov Disord 22:1093-1096.

Bennett BD, Bolam JP (1994) Synaptic input and output of parvalbumin-immunoreactive neurons in the neostriatum of the rat. Neuroscience 62:707-719.

Bergman H, Feingold A, Nini A, Raz A, Slovin H, Abeles M, Vaadia E (1998a) Physiological aspects of information processing in the basal ganglia of normal and parkinsonian primates. Trends Neurosci 21:32-38.

Bergman H, Raz A, Feingold A, Nini A, Nelken I, Hansel D, Ben Pazi H, Reches A (1998b) Physiology of MPTP tremor. Mov Disord 13 Suppl 3:29-34.

Bergman H, Wichmann T, DeLong MR (1990) Reversal of experimental parkinsonism by lesions of the subthalamic nucleus. Science 249:1436-1438.

Bergman H, Wichmann T, Karmon B, DeLong MR (1994) The primate subthalamic nucleus. II. Neuronal activity in the MPTP model of parkinsonism. J Neurophysiol 72:507-520.

Beurrier C, Bezard E, Bioulac B, Gross C (1997) Subthalamic stimulation elicits hemiballismus in normal monkey. NeuroReport 8:1625-1629.

Blanchet PJ, Metman LV, Chase TN (2003) Renaissance of amantadine in the treatment of Parkinson's disease. Adv Neurol 91:251-257.

Blanchet PJ, Papa SM, Metman LV, Mouradian MM, Chase TN (1997) Modulation of levodopa-induced motor response complications by NMDA antagonists in Parkinson's disease. Neurosci Biobehav Rev 21:447-453.

Bloem BR, Hausdorff JM, Visser JE, Giladi N (2004) Falls and freezing of gait in Parkinson's disease: a review of two interconnected, episodic phenomena. Mov Disord 19:871-884.

Bolam JP (1984) Synapses of identified neurons in the neostriatum. Ciba Found Symp 107:30-47.

Bouyer JJ, Park DH, Joh TH, Pickel VM (1984) Chemical and structural analysis of the relation between cortical inputs and tyrosine hydroxylase-containing terminals in rat neostriatum. Brain Res 302:267-275.

Breit S, Bouali-Benazzouz R, Benabid AL, Benazzouz A (2001) Unilateral lesion of the nigrostriatal pathway induces an increase of neuronal activity of the pedunculopontine nucleus, which is reversed by the lesion of the subthalamic nucleus in the rat. Eur J Neurosci 14:1833-1842.

Breit S, Lessmann L, Benazzouz A, Schulz JB (2005) Unilateral lesion of the pedunculopontine nucleus induces hyperactivity in the subthalamic nucleus and substantia nigra in the rat. Eur J Neurosci 22:2283-2294.

Brock M, Kern BC, Funk T, Afshar HF (1998) Pallidal or subthalamic stimulation. J Neurosurg 89:345-346.

Brown P (2003) Oscillatory nature of human basal ganglia activity: relationship to the pathophysiology of Parkinson's disease. Mov Disord 18:357-363.

Brown P, Kupsch A, Magill PJ, Sharott A, Harnack D, Meissner W (2002) Oscillatory local field potentials recorded from the subthalamic nucleus of the alert rat. Exp Neurol 177:581-585.

Brown P, Mazzone P, Oliviero A, Altibrandi MG, Pilato F, Tonali PA, Di Lazarro V (2004) Effects of stimulation of the subthalamic area on oscillatory pallidal activity in Parkinson's disease. Exp Neurol 188:480-490.

Brown P, Oliviero A, Mazzone P, Insola A, Tonali P, Di Lazarro V (2001) Dopamine dependency of oscillations between subthalamic nucleus and pallidum in Parkinson's disease. J Neurosci 21:1033-1038.

Brown P, Williams D (2005) Basal ganglia local field potential activity: character and functional significance in the human. Clin Neurophysiol 116:2510-2519.

Brownell AL, Canales K, Chen YI, Jenkins BG, Owen C, Livni E, Yu M, Cicchetti F, Sanchez-Pernaute R, Isacson O (2003) Mapping of brain function after MPTP-induced neurotoxicity in a primate Parkinson's disease model. NeuroImage 20:1064-1075.

Brudzynski SM, Houghton PE, Brownlee RD, Mogenson GJ (1986) Involvement of neuronal cell bodies of the mesencephalic locomotor region in the initiation of locomotor activity of freely behaving rats. Brain Res Bull 16:377-381.

Burbaud P, Gross C, Benazzouz A, Coussemacq M, Bioulac B (1995) Reduction of apomorphine-induced rotational behaviour by subthalamic lesion in 6-OHDA lesioned rats is associated with a normalization of firing rate and discharge pattern of pars reticulata neurons. Exp Brain Res 105:48-58.

Burchiel KJ, Anderson VC, Favre J, Hammerstad JP (1999) Comparison of pallidal and subthalamic nucleus deep brain stimulation for advanced Parkinson's disease: results of a randomized, blinded pilot study. Neurosurgery 45:1375-1382.

Burleigh-Jacobs A, Horak FB, Nutt JG, Obeso JA (1997) Step initiation in Parkinson's disease: influence of levodopa and external sensory triggers. Mov Disord 12:206-215.

Caire F, Derost P, Coste J, Bonny JM, Durif F, Frenoux E, Villeger A, Lemaire JJ (2006) [Subthalamic deep brain stimulation for severe idiopathic Parkinson's disease. Location study of the effective contacts.]. Neurochirurgie 52:15-25.

Calabresi P, Centonze D, Marfia GA, Pisani A, Bernardi G (1999) An *in vitro* electrophysiological study on the effects of phenytoin, lamotrigine and gabapentin on striatal neurons. Br J Pharmacol 126:689-696.

Carpenter MB, Carleton SC, Keller JT, Conte P (1981) Connections of the subthalamic nucleus in the monkey. Brain Res 224:1-29.

Carpinella I, Crenna P, Marzegan A, Rabuffetti M, Rizzone M, Lopiano L, Ferrarin M (2007) Effect of L-dopa and subthalamic nucleus stimulation on arm and leg swing during gait in Parkinson's Disease. Conf Proc IEEE Eng Med Biol Soc 2007:6665-6668.

Cassidy M, Mazzone P, Oliviero A, Insola A, Tonali P, Di Lazarro V, Brown P (2002) Movement-related changes in synchronization in the human basal ganglia. Brain 125:1235-1246.

Castelli L, Perozzo P, Zibetti M, Crivelli B, Morabito U, Lanotte M, Cossa F, Bergamasco B, Lopiano L (2006) Chronic deep brain stimulation of the subthalamic nucleus for Parkinson's disease: effects on cognition, mood, anxiety and personality traits. Eur Neurol 55:136-144.

Chang HT, Wilson CJ, Kitai ST (1981) Single neostriatal efferent axons in the globus pallidus: a light and electron microscopic study. Science 213:915-918.

Chen CC, Pogosyan A, Zrinzo LU, Tisch S, Limousin P, Ashkan K, Yousry T, Hariz MI, Brown P (2006) Intra-operative recordings of local field potentials can help localize the subthalamic nucleus in Parkinson's disease surgery. Exp Neurol. 198:214-221.

Cheramy A, Leviel V, Glowinski J (1981) Dendritic release of dopamine in the substantia nigra. Nature 289:537-542.

Contreras D, Steriade M (1995) Cellular basis of EEG slow rhythms: a study of dynamic corticothalamic relationships. J Neurosci 15:604-622.

Contreras D, Steriade M (1997) Synchronization of low-frequency rhythms in corticothalamic networks. Neuroscience 76:11-24.

Crenna P, Carpinella I, Rabuffetti M, Calabrese E, Mazzoleni P, Nemni R, Ferrarin M (2007) The association between impaired turning and normal straight walking in Parkinson's disease. Gait Posture 26:172-178.

Crossman AR, Sambrook MA, Jackson A (1980) Experimental hemiballismus in the baboon produced by injection of a gamma-aminobutyric acid antagonist into the basal ganglia. Neurosci Lett 20:369-372.

Crossman AR, Sambrook MA, Jackson A (1984) Experimental hemichorea/hemiballismus in the monkey. Studies on the intracerebral site of action in a drug-induced dyskinesia. Brain 107 (Pt 2):579-596.

Csillag A (1999) Striato-telencephalic and striato-tegmental circuits: relevance to learning in domestic chicks. Behav Brain Res 98:227-236.

Curra A, Berardelli A, Agostino R, Modugno N, Puorger CC, Accornero N, Manfredi M (1997) Performance of sequential arm movements with and without advance knowledge of motor pathways in Parkinson's disease. Mov Disord 12:646-654.

D'Arceuil HE, Westmoreland S, de Crespigny AJ (2007) An approach to high resolution diffusion tensor imaging in fixed primate brain. NeuroImage 35:553-565.

Day M, Wang Z, Ding J, An X, Ingham CA, Shering AF, Wokosin D, Ilijic E, Sun Z, Sampson AR, Mugnaini E, Deutch AY, Sesack SR, Arbuthnott GW, Surmeier DJ (2006) Selective elimination of glutamatergic synapses on striatopallidal neurons in Parkinson disease models. Nat Neurosci 9:251-259.

Defebvre L, Blatt JL, Blond S, Bourriez JL, Guieu JD, Destee A (1996) Effect of thalamic stimulation on gait in Parkinson disease. Arch Neurol 53:898-903.

Defebvre LJ, Blatt JL, Blond SC, Bourriez JL, Guieu JD, Destee A (1999) Effect of long-term stimulation of the ventral intermediate thalamic nucleus on gait in Parkinson's disease. Adv Neurol 80:627-630.

DeLong MR (1990) Primate models of movement disorders of basal ganglia origin. Trends Neurosci 13:281-285.

DeLong MR, Alexander GE, Georgopoulos AP, Crutcher MD, Mitchell SJ, Richardson RT (1984) Role of basal ganglia in limb movements. Hum Neurobiol 2:235-244.

DeLong MR, Crutcher MD, Georgopoulos AP (1985) Primate globus pallidus and subthalamic nucleus: functional organization. J Neurophysiol 53:530-543.

DeLong MR, Wichmann T (2007) Circuits and circuit disorders of the basal ganglia. Arch Neurol 64:20-24.

Deniau JM, Menetrey A, Charpier S (1996) The lamellar organization of the rat substantia nigra pars reticulata: segregated patterns of striatal afferents and relationship to the topography of corticostriatal projections. Neuroscience 73:761-781.

Dennerlein JT, Mote CD, Jr., Rempel DM (1998) Control strategies for finger movement during touch-typing. The role of the extrinsic muscles during a keystroke. Exp Brain Res 121:1-6.

Destexhe A, Contreras D, Steriade M (1999) Spatiotemporal analysis of local field potentials and unit discharges in cat cerebral cortex during natural wake and sleep states. J Neurosci 19:4595-4608.

Dietz V (1997) Neurophysiology of gait disorders: present and future applications. Electroencephalogr Clin Neurophysiol 103:333-355.

Donoghue JP, Sanes JN, Hatsopoulos NG, Gaal G (1998) Neural discharge and local field potential oscillations in primate motor cortex during voluntary movements. J Neurophysiol 79:159-173.

Dormont JF, Conde H, Farin D (1998) The role of the pedunculopontine tegmental nucleus in relation to conditioned motor performance in the cat. I. Context-dependent and reinforcement-related single unit activity. Exp Brain Res 121:401-410.

Doyle LM, Kuhn AA, Hariz M, Kupsch A, Schneider GH, Brown P (2005) Levodopa-induced modulation of subthalamic beta oscillations during self-paced movements in patients with Parkinson's disease. Eur J Neurosci 21:1403-1412.

Dube L, Smith AD, Bolam JP (1988) Identification of synaptic terminals of thalamic or cortical origin in contact with distinct medium-size spiny neurons in the rat neostriatum. J Comp Neurol 267:455-471.

Dybdal D, Gale K (2000) Postural and anticonvulsant effects of inhibition of the rat subthalamic nucleus. J Neurosci 20:6728-6733.

Edley SM, Graybiel AM (1983) The afferent and efferent connections of the feline nucleus tegmenti pedunculopontinus, pars compacta. J Comp Neurol 217:187-215.

Elul R (1971) The genesis of the EEG. Int Rev Neurobiol 15:227-272.

Evans AC, Collins DL, Mills SR, Brown ED, Kelly RL (2003) 3-D Statistical Neuroanatomical Models from 305 MRI Volumes. pp 1813-1817.

Ferrarin M, Carpinella I, Rabuffetti M, Rizzone M, Lopiano L, Crenna P (2007) Unilateral and bilateral subthalamic nucleus stimulation in Parkinson's disease: effects on EMG signals of lower limb muscles during walking. IEEE Trans Neural Syst Rehabil Eng 15:182-189.

Ferrarin M, Rizzone M, Bergamasco B, Lanotte M, Recalcati M, Pedotti A, Lopiano L (2005) Effects of bilateral subthalamic stimulation on gait kinematics and kinetics in Parkinson's disease. Exp Brain Res 160:517-527.

Ferrarin M, Rizzone M, Lopiano L, Recalcati M, Pedotti A (2004) Effects of subthalamic nucleus stimulation and L-dopa in trunk kinematics of patients with Parkinson's disease. Gait Posture 19:164-171.

Flaherty AW, Graybiel AM (1991) Corticostriatal transformations in the primate somatosensory system. Projections from physiologically mapped body-part representations. J Neurophysiol 66:1249-1263.

Flaherty AW, Graybiel AM (1993) Output architecture of the primate putamen. J Neurosci 13:3222-3237.

Flores-Hernandez J, Galarraga E, Bargas J (1997) Dopamine selects glutamatergic inputs to neostriatal neurons. Synapse 25:185-195.

Florio T, Scarnati E, Confalone G, Minchella D, Galati S, Stanzione P, Stefani A, Mazzone P (2007) High-frequency stimulation of the subthalamic nucleus modulates the activity of pedunculopontine neurons through direct activation of excitatory fibres as well as through indirect activation of inhibitory pallidal fibres in the rat. Eur J Neurosci 25:1174-1186.

Foffani G, Bianchi AM, Baselli G, Priori A (2005) Movement-related frequency modulation of beta oscillatory activity in the human subthalamic nucleus. J Physiol 568:699-711.

Fontanini A, Spano P, Bower JM (2003) Ketamine-xylazine-induced slow (< 1.5 Hz) oscillations in the rat piriform (olfactory) cortex are functionally correlated with respiration. J Neurosci 23:7993-8001.

Ford B, Holmes CJ, Mainville L, Jones BE (1995) GABAergic neurons in the rat pontomesencephalic tegmentum: codistribution with cholinergic and other tegmental neurons projecting to the posterior lateral hypothalamus. J Comp Neurol 363:177-196.

Fox CA, Rafols JA (1976) The striatal efferents in the globus pallidus and in the substantia nigra. Res Publ Assoc Res Nerv Ment Dis 55:37-55.

Fox CA, Rafols JA (1975) The radial fibers in the globus pallidus. J Comp Neurol 159:177-199.

Fregni F, Simon DK, Wu A, Pascual-Leone A (2005) Non-invasive brain stimulation for Parkinson's disease: a systematic review and meta-analysis of the literature. J Neurol Neurosurg Psychiatry 76:1614-1623.

Fujimoto K, Kita H (1993) Response characteristics of subthalamic neurons to the stimulation of the sensorimotor cortex in the rat. Brain Res 609:185-192.

Gale K, Casu M (1981) Dynamic utilization of GABA in substantia nigra: regulation by dopamine and GABA in the striatum, and its clinical and behavioral implications. Mol Cell Biochem 39:369-405.

Garcia-Munoz M, Young SJ, Groves PM (1991) Terminal excitability of the corticostriatal pathway. II. Regulation by glutamate receptor stimulation. Brain Res 551:207-215.

Garcia-Rill E, Houser CR, Skinner RD, Smith W, Woodward DJ (1987) Locomotion-inducing sites in the vicinity of the pedunculopontine nucleus. Brain Res Bull 18:731-738.

Garcia-Rill E, Skinner RD (1987a) The mesencephalic locomotor region. I. Activation of a medullary projection site. Brain Res 411:1-12.

Garcia-Rill E, Skinner RD (1987b) The mesencephalic locomotor region. II. Projections to reticulospinal neurons. Brain Res 411:13-20.

Garcia-Rill E, Skinner RD, Fitzgerald JA (1985) Chemical activation of the mesencephalic locomotor region. Brain Res 330:43-54.

Georgiou N, Iansek R, Bradshaw JL, Phillips JG, Mattingley JB, Bradshaw JA (1993) An evaluation of the role of internal cues in the pathogenesis of parkinsonian hypokinesia. Brain 116 (Pt 6):1575-1587.

Gerfen CR (1984) The neostriatal mosaic: compartmentalization of corticostriatal input and striatonigral output systems. Nature 311:461-464.

Gerfen CR (1989) The neostriatal mosaic: striatal patch-matrix organization is related to cortical lamination. Science 246:385-388.

Gerfen CR (1985) The neostriatal mosaic. I. Compartmental organization of projections from the striatum to the substantia nigra in the rat. J Comp Neurol 236:454-476.

Gerfen CR (1988) Synaptic organization of the striatum. J Electron Microsc Tech 10:265-281.

Gerfen CR, Staines WA, Arbuthnott GW, Fibiger HC (1982) Crossed connections of the substantia nigra in the rat. J Comp Neurol 207:283-303.

Gimenez-Amaya JM, Graybiel AM (1991) Modular organization of projection neurons in the matrix compartment of the primate striatum. J Neurosci 11:779-791.

Glickstein M, Stein J (1991) Paradoxical movement in Parkinson's disease. Trends Neurosci 14:480-482.

Gnanalingham KK, Milkowski NA, Smith LA, Hunter AJ, Jenner P, Marsden CD (1995) Short and long-term changes in cerebral [14C]-2-deoxyglucose uptake in the MPTP-treated marmoset: relationship to locomotor activity. J Neural Transm Gen Sect 101:65-82.

Godinho F, Thobois S, Magnin M, Guenot M, Polo G, Benatru I, Xie J, Salvetti A, Garcia-Larrea L, Broussolle E, Mertens P (2006) Subthalamic nucleus stimulation in Parkinson's disease : Anatomical and electrophysiological localization of active contacts. J Neurol. 253:1347-1355.

Goldberg JA, Boraud T, Maraton S, Haber SN, Vaadia E, Bergman H (2002) Enhanced synchrony among primary motor cortex neurons in the 1-methyl-4-phenyl-1,2,3,6-tetrahydropyridine primate model of Parkinson's disease. J Neurosci 22:4639-4653.

Goldberg JA, Rokni U, Boraud T, Vaadia E, Bergman H (2004) Spike synchronization in the cortex/basal-ganglia networks of Parkinsonian primates reflects global dynamics of the local field potentials. J Neurosci 24:6003-6010.

Gomez-Gallego M, Fernandez-Villalba E, Fernandez-Barreiro A, Herrero MT (2007) Changes in the neuronal activity in the pedunculopontine nucleus in chronic MPTP-treated primates: an *in situ* hybridization study of cytochrome oxidase subunit I, choline acetyl transferase and substance P mRNA expression. J Neural Transm 114:319-326.

Goodale MA (1998) Visuomotor control: where does vision end and action begin? Curr Biol 8:R489-R491.

Gould E, Woolf NJ, Butcher LL (1989) Cholinergic projections to the substantia nigra from the pedunculopontine and laterodorsal tegmental nuclei. Neuroscience 28:611-623.

Greenamyre JT, O'Brien CF (1991) N-methyl-D-aspartate antagonists in the treatment of Parkinson's disease. Arch Neurol 48:977-981.

Grillner S (1981) Control of locomotion in biped, tetrapods, and fish. In: Handbook of Physiology pp 1179-1236. Washington, D.C., USA: American Physiological Society.

Grillner S, Wallen P, Saitoh K, Kozlov A, Robertson B (2008) Neural bases of goal-directed locomotion in vertebrates--an overview. Brain Res Rev 57:2-12.

Guridi J, Luquin MR, Herrero MT, Obeso JA (1993) The subthalamic nucleus: a possible target for stereotaxic surgery in Parkinson's disease. Mov Disord 8:421-429.

Hahn SL (1996) Hilbert transforms in signal processing. London: Artech House.

Hamada Y, Miyashita E, Tanaka H (1999) Gamma-band oscillations in the "barrel cortex" precede rat's exploratory whisking. Neuroscience 88:667-671.

Hamani C, Saint-Cyr JA, Fraser J, Kaplitt M, Lozano AM (2004) The subthalamic nucleus in the context of movement disorders. Brain 127:4-20.

Hamel W, Fietzek U, Morsnowski A, Schrader B, Herzog J, Weinert D, Pfister G, Muller D, Volkmann J, Deuschl G, Mehdorn HM (2003) Deep brain stimulation of the subthalamic nucleus in Parkinson's disease: evaluation of active electrode contacts. J Neurol Neurosurg Psychiatry 74:1036-1046.

Hammond C, Feger J, Bioulac B, Souteyrand JP (1979) Experimental hemiballism in the monkey produced by unilateral kainic acid lesion in corpus Luysii. Brain Res 171:577-580.

Hammond C, Rouzaire-Dubois B, Feger J, Jackson A, Crossman AR (1983) Anatomical and electrophysiological studies on the reciprocal projections between the subthalamic nucleus and nucleus tegmenti pedunculopontinus in the rat. Neuroscience 9:41-52.

Hara K, Harris RA (2002) The anesthetic mechanism of urethane: the effects on neurotransmitter-gated ion channels. Anesth Analg 94:313-318.

Hardman CD, Henderson JM, Finkelstein DI, Horne MK, Paxinos G, Halliday GM (2002) Comparison of the basal ganglia in rats, marmosets, macaques, baboons, and humans: volume and neuronal number for the output, internal relay, and striatal modulating nuclei. J Comp Neurol 445:238-255.

Haslinger B, Kalteis K, Boecker H, Alesch F, Ceballos-Baumann AO (2005) Frequency-correlated decreases of motor cortex activity associated with subthalamic nucleus stimulation in Parkinson's disease. NeuroImage 28:598-606.

Hassani OK, Mouroux M, Feger J (1996) Increased subthalamic neuronal activity after nigral dopaminergic lesion independent of disinhibition via the globus pallidus. Neuroscience 72:105-115.

Hattori T, Takada M, Moriizumi T, Van der Kooy, D (1991) Single dopaminergic nigrostriatal neurons form two chemically distinct synaptic types: possible transmitter segregation within neurons. J Comp Neurol 309:391-401.

Hausdorff JM, Balash J, Giladi N (2003a) Effects of cognitive challenge on gait variability in patients with Parkinson's disease. J Geriatr Psychiatry Neurol 16:53-58.

Hausdorff JM, Cudkowicz ME, Firtion R, Wei JY, Goldberger AL (1998) Gait variability and basal ganglia disorders: stride-to-stride variations of gait cycle timing in Parkinson's disease and Huntington's disease. Mov Disord 13:428-437.

Hausdorff JM, Edelberg HK, Cudkowicz ME, Singh MA, Wei JY (1997) The relationship between gait changes and falls. J Am Geriatr Soc 45:1406.

Hausdorff JM, Schaafsma JD, Balash Y, Bartels AL, Gurevich T, Giladi N (2003b) Impaired regulation of stride variability in Parkinson's disease subjects with freezing of gait. Exp Brain Res 149:187-194.

Hazrati LN, Parent A (1992a) Differential patterns of arborization of striatal and subthalamic fibers in the two pallidal segments in primates. Brain Res 598:311-315.

Hazrati LN, Parent A (1992b) Projection from the deep cerebellar nuclei to the pedunculopontine nucleus in the squirrel monkey. Brain Res 585:267-271.

Hazrati LN, Parent A (1991) Contralateral pallidothalamic and pallidotegmental projections in primates: an anterograde and retrograde labeling study. Brain Res 567:212-223.

Hazrati LN, Parent A, Mitchell S, Haber SN (1990) Evidence for interconnections between the two segments of the globus pallidus in primates: a PHA-L anterograde tracing study. Brain Res 533:171-175.

Hedreen JC, DeLong MR (1991) Organization of striatopallidal, striatonigral, and nigrostriatal projections in the macaque. J Comp Neurol 304:569-595.

Heise CE, Mitrofanis J (2006) Fos immunoreactivity in some locomotor neural centres of 6OHDA-lesioned rats. Anat Embryol (Berl) 211:659-671.

Helmich RC, Siebner HR, Bakker M, Munchau A, Bloem BR (2006) Repetitive transcranial magnetic stimulation to improve mood and motor function in Parkinson's disease. J Neurol Sci. 248:84-96.

Herkenham M (1979) The afferent and efferent connections of the ventromedial thalamic nucleus in the rat. J Comp Neurol 183:487-517.

Hirsch EC, Graybiel AM, Duyckaerts C, Javoy-Agid F (1987) Neuronal loss in the pedunculopontine tegmental nucleus in Parkinson disease and in progressive supranuclear palsy. Proc Natl Acad Sci U S A 84:5976-5980.

Hollerman JR, Grace AA (1992) Subthalamic nucleus cell firing in the 6-OHDA-treated rat: basal activity and response to haloperidol. Brain Res 590:291-299.

Hosey T, Williams G, Ansorge R (2005) Inference of multiple fiber orientations in high angular resolution diffusion imaging. Magn Reson Med 54:1480-1489.

Inase M, Tokuno H, Nambu A, Akazawa T, Takada M (1999) Corticostriatal and corticosubthalamic input zones from the presupplementary motor area in the macaque monkey: comparison with the input zones from the supplementary motor area. Brain Res 833:191-201.

Ingham CA, Hood SH, Arbuthnott GW (1989) Spine density on neostriatal neurones changes with 6-hydroxydopamine lesions and with age. Brain Res 503:334-338.

Ingham CA, Hood SH, Taggart P, Arbuthnott GW (1998) Plasticity of synapses in the rat neostriatum after unilateral lesion of the nigrostriatal dopaminergic pathway. J Neurosci 18:4732-4743.

Ingham CA, Hood SH, van Maldegem B, Weenink A, Arbuthnott GW (1993) Morphological changes in the rat neostriatum after unilateral 6-hydroxydopamine injections into the nigrostriatal pathway. Exp Brain Res 93:17-27.

Inglis WL, Olmstead MC, Robbins TW (2001) Selective deficits in attentional performance on the 5-choice serial reaction time task following pedunculopontine tegmental nucleus lesions. Behav Brain Res 123:117-131.

Inglis WL, Winn P (1995) The pedunculopontine tegmental nucleus: where the striatum meets the reticular formation. Prog Neurobiol 47:1-29.

Jackson A, Crossman AR (1981a) Subthalamic nucleus efferent projection to the cerebral cortex. Neuroscience 6:2367-2377.

Jackson A, Crossman AR (1981b) Subthalamic projection to nucleus tegmenti pedunculopontinus in the rat. Neurosci Lett 22:17-22.

Jackson A, Crossman AR (1983) Nucleus tegmenti pedunculopontinus: efferent connections with special reference to the basal ganglia, studied in the rat by anterograde and retrograde transport of horseradish peroxidase. Neuroscience 10:725-765.

Jenkinson N, Nandi D, Miall RC, Stein JF, Aziz TZ (2004) Pedunculopontine nucleus stimulation improves akinesia in a Parkinsonian monkey. NeuroReport 15:2621-2624.

Jenkinson N, Nandi D, Oram R, Stein JF, Aziz TZ (2006) Pedunculopontine nucleus electric stimulation alleviates akinesia independently of dopaminergic mechanisms. NeuroReport 17:639-641.

Jeon MF, Ha Y, Cho YH, Lee BH, Park YG, Chang JW (2003) Effect of ipsilateral subthalamic nucleus lesioning in a rat parkinsonian model: study of behavior correlated with neuronal activity in the pedunculopontine nucleus. J Neurosurg 99:762-767.

Joel D, Weiner I (1997) The connections of the primate subthalamic nucleus: indirect pathways and the open-interconnected scheme of basal ganglia-thalamocortical circuitry. Brain Res Rev 23:62-78.

Joel D, Weiner I (2000) The connections of the dopaminergic system with the striatum in rats and primates: an analysis with respect to the functional and compartmental organization of the striatum. Neuroscience 96:451-474.

Johansen-Berg H, Behrens TEJ, Sillery E, Ciccarelli O, Thompson AJ, Smith SM, Matthews PM (2005) Functional-anatomical validation and individual variation of diffusion tractography-based segmentation of the human thalamus. Cereb Cortex 15:31-39.

Jurgens U (1984) The efferent and afferent connections of the supplementary motor area. Brain Res 300:63-81.

Kaiya H, Namba M (1981) Two types of dopaminergic nerve terminals in the rat neostriatum. An ultrastructural study. Neurosci Lett 25:251-256.

Kang Y, Kitai ST (1990) Electrophysiological properties of pedunculopontine neurons and their postsynaptic responses following stimulation of substantia nigra reticulata. Brain Res 535:79-95.

Karle EJ, Anderson KD, Reiner A (1994) Dopaminergic terminals form synaptic contacts with enkephalinergic striatal neurons in pigeons: an electron microscopic study. Brain Res 646:149-156.

Karmon B, Bergman H (1993) Detection of neuronal periodic oscillations in the basal ganglia of normal and parkinsonian monkeys. Isr J Med Sci 29:570-579.

Kaufman KR, Sutherland DH (2006) Kinematics of normal human walking. In: Human Walking (Rose J, Gamble JG, eds), pp 33-52. Philadelphia, PA, USA: Lippincott Williams & Wilkins.

Kelly RM, Strick PL (2000) Rabies as a transneuronal tracer of circuits in the central nervous system. J Neurosci Methods 103:63-71.

Kelly VE, Hyngstrom AS, Rundle MM, Bastian AJ (2002) Interaction of levodopa and cues on voluntary reaching in Parkinson's disease. Mov Disord 17:38-44.

Kemp JM, Powell TP (1971) The connexions of the striatum and globus pallidus: synthesis and speculation. Philos Trans R Soc Lond B Biol Sci 262:441-457.

Kempf F, Kuhn A, Kupsch A, Brucke C, Weise L, Schneider GH, Brown P (2007) Premovement activities in the subthalamic area of patients with Parkinson's disease and their dependence on task. Eur J Neurosci 25:3137-3145.

Kim JS (1979) Studies on the transmitters of the afferent and efferent pathways of the striatum and their interaction in the baboon, cat and rat. Appl Neurophysiol 42:62-64.

Kim JS (1978) Transmitters for the afferent and efferent systems of the neostriatum and their possible interactions. Adv Biochem Psychopharmacol 19:217-233.

Kim R, Nakano K, Jayaraman A, Carpenter MB (1976) Projections of the globus pallidus and adjacent structures: an autoradiographic study in the monkey. J Comp Neurol 169:263-290.

Kita H, Kitai ST (1987) Efferent projections of the subthalamic nucleus in the rat: light and electron microscopic analysis with the PHA-L method. J Comp Neurol 260:435-452.

Kitai ST (1981) Anatomy and physiology of the neostriatum. Adv Biochem Psychopharmacol 30:1-21.

Kleiner-Fisman G, Fisman DN, Sime E, Saint-Cyr JA, Lozano AM, Lang AE (2003) Long-term follow up of bilateral deep brain stimulation of the subthalamic nucleus in patients with advanced Parkinson disease. J Neurosurg 99:489-495.

Klimesch W, Doppelmayr M, Schimke H, Pachinger T (1996) Alpha frequency, reaction time, and the speed of processing information. J Clin Neurophysiol 13:511-518.

Klimesch W, Schimke H, Pfurtscheller G (1993) Alpha frequency, cognitive load and memory performance. Brain Topogr 5:241-251.

Klostermann F, Nikulin VV, Kuhn AA, Marzinzik F, Wahl M, Pogosyan A, Kupsch A, Schneider GH, Brown P, Curio G (2007) Task-related differential dynamics of EEG alpha- and beta-band synchronization in cortico-basal motor structures. Eur J Neurosci 25:1604-1615.

Kobayashi Y, Inoue Y, Yamamoto M, Isa T, Aizawa H (2002) Contribution of pedunculopontine tegmental nucleus neurons to performance of visually guided saccade tasks in monkeys. J Neurophysiol 88:715-731.

Kojima J, Yamaji Y, Matsumura M, Nambu A, Inase M, Tokuno H, Takada M, Imai H (1997) Excitotoxic lesions of the pedunculopontine tegmental nucleus produce contralateral hemiparkinsonism in the monkey. Neurosci Lett 226:111-114.

Kozak R, Bowman EM, Latimer MP, Rostron CL, Winn P (2005) Excitotoxic lesions of the pedunculopontine tegmental nucleus in rats impair performance on a test of sustained attention. Exp Brain Res 162:257-264.

Krack P, Batir A, Van Blercom N, Chabardes S, Fraix V, Ardouin C, Koudsie A, Limousin PD, Benazzouz A, LeBas JF, Benabid AL, Pollak P (2003) Five-year follow-up of bilateral stimulation of the subthalamic nucleus in advanced Parkinson's disease. N Engl J Med 349:1925-1934.

Krack P, Limousin P, Benabid AL, Pollak P (1997a) Chronic stimulation of subthalamic nucleus improves levodopa-induced dyskinesias in Parkinson's disease. Lancet 350:1676.

Krack P, Pollak P, Limousin P, Benazzouz A, Benabid AL (1997b) Stimulation of subthalamic nucleus alleviates tremor in Parkinson's disease. Lancet 350:1675.

Krause M, Fogel W, Heck A, Hacke W, Bonsanto M, Trenkwalder C, Tronnier V (2001) Deep brain stimulation for the treatment of Parkinson's disease: subthalamic nucleus versus globus pallidus internus. J Neurol Neurosurg Psychiatry 70:464-470.

Kringelbach ML, Jenkinson N, Owen SL, Aziz TZ (2007) Translational principles of deep brain stimulation. Nat Rev Neurosci 8:623-635.

Krystkowiak P, Blatt JL, Bourriez JL, Duhamel A, Perina M, Blond S, Guieu JD, Destee A, Defebvre L (2003) Effects of subthalamic nucleus stimulation and levodopa treatment on gait abnormalities in Parkinson disease. Arch Neurol 60:80-84.

Kubo M, Holt KG, Saltzman E, Wagenaar RC (2006) Changes in axial stiffness of the trunk as a function of walking speed. J Biomech 39:750-757.

Kuhn AA, Doyle L, Pogosyan A, Yarrow K, Kupsch A, Schneider GH, Hariz MI, Trottenberg T, Brown P (2006) Modulation of beta oscillations in the subthalamic area during motor imagery in Parkinson's disease. Brain 129:695-706.

Kuhn AA, Trottenberg T, Kivi A, Kupsch A, Schneider GH, Brown P (2005) The relationship between local field potential and neuronal discharge in the subthalamic nucleus of patients with Parkinson's disease. Exp Neurol 194:212-220.

Kuhn AA, Williams D, Kupsch A, Limousin P, Hariz M, Schneider GH, Yarrow K, Brown P (2004) Event-related beta desynchronization in human subthalamic nucleus correlates with motor performance. Brain 127:735-746.

Kumar R, Lozano AM, Kim YJ, Hutchison WD, Sime E, Halket E, Lang AE (1998) Double-blind evaluation of subthalamic nucleus deep brain stimulation in advanced Parkinson's disease. Neurology 51:850-855.

Kuo PL, Lee DL, Jindrich DL, Dennerlein JT (2006) Finger joint coordination during tapping. J Biomech 39:2934-2942.

Laitinen LV, Bergenheim AT, Hariz MI (1992) Leksell's posteroventral pallidotomy in the treatment of Parkinson's disease. J Neurosurg 76:53-61.

Lanotte MM, Rizzone M, Bergamasco B, Faccani G, Melcarne A, Lopiano L (2002) Deep brain stimulation of the subthalamic nucleus: anatomical, neurophysiological, and outcome correlations with the effects of stimulation. J Neurol Neurosurg Psychiatry 72:53-58.

Lapper SR, Bolam JP (1992) Input from the frontal cortex and the parafascicular nucleus to cholinergic interneurons in the dorsal striatum of the rat. Neuroscience 51:533-545.

Lavoie B, Parent A (1994a) Pedunculopontine nucleus in the squirrel monkey: cholinergic and glutamatergic projections to the substantia nigra. J Comp Neurol 344:232-241.

Lavoie B, Parent A (1994b) Pedunculopontine nucleus in the squirrel monkey: distribution of cholinergic and monoaminergic neurons in the mesopontine tegmentum with evidence for the presence of glutamate in cholinergic neurons. J Comp Neurol 344:190-209.

Lavoie B, Parent A (1994c) Pedunculopontine nucleus in the squirrel monkey: projections to the basal ganglia as revealed by anterograde tract-tracing methods. J Comp Neurol 344:210-231.

Le Bihan D, Poupon C, Amadon A, Lethimonnier F (2006) Artifacts and pitfalls in diffusion MRI. J Magn Reson Imaging 24:478-488.

Leblois A, Boraud T, Meissner W, Bergman H, Hansel D (2006) Competition between feedback loops underlies normal and pathological dynamics in the basal ganglia. J Neurosci 26:3567-3583.

Lee MS, Rinne JO, Marsden CD (2000) The pedunculopontine nucleus: its role in the genesis of movement disorders. Yonsei Med J 41:167-184.

Levy R, Ashby P, Hutchison WD, Lang AE, Lozano AM, Dostrovsky JO (2002) Dependence of subthalamic nucleus oscillations on movement and dopamine in Parkinson's disease. Brain 125:1196-1209.

Levy R, Hutchison WD, Lozano AM, Dostrovsky JO (2000) High-frequency synchronization of neuronal activity in the subthalamic nucleus of parkinsonian patients with limb tremor. J Neurosci 20:7766-7775.

Limousin P, Krack P, Pollak P, Benazzouz A, Ardouin C, Hoffmann D, Benabid AL (1998) Electrical stimulation of the subthalamic nucleus in advanced Parkinson's disease. N Engl J Med 339:1105-1111.

Limousin P, Pollak P, Benazzouz A, Hoffmann D, Le Bas JF, Broussolle E, Perret JE, Benabid AL (1995) Effect of parkinsonian signs and symptoms of bilateral subthalamic nucleus stimulation. Lancet 345:91-95.

Liu X (2003) What can be learned from recording local field potentials from the brain via implanted electrodes used to treat patients with movement disorders? Curr Med Lit: Neurology 19:1-6.

Liu X, Ford-Dunn HL, Hayward GN, Nandi D, Miall RC, Aziz TZ, Stein JF (2002) The oscillatory activity in the Parkinsonian subthalamic nucleus investigated using the macro-electrodes for deep brain stimulation. Clin Neurophysiol 113:1667-1672.

Liu X, Rowe J, Nandi D, Hayward G, Parkin S, Stein J, Aziz T (2001) Localisation of the subthalamic nucleus using Radionics Image Fusion and Stereoplan combined with field potential recording. A technical note. Stereotact Funct Neurosurg 76:63-73.

Loukas C, Brown P (2004) Online prediction of self-paced hand-movements from subthalamic activity using neural networks in Parkinson's disease. J Neurosci Methods 137:193-205.

Luginger E, Wenning GK, Bosch S, Poewe W (2000) Beneficial effects of amantadine on L-dopa-induced dyskinesias in Parkinson's disease. Mov Disord 15:873-878.

Lynd-Balta E, Haber SN (1994) Primate striatonigral projections: a comparison of the sensorimotor-related striatum and the ventral striatum. J Comp Neurol 345:562-578.

MacKay WA, Mendonca AJ (1995) Field potential oscillatory bursts in parietal cortex before and during reach. Brain Res 704:167-174.

MacLeod NK, Ryman A, Arbuthnott GW (1990) Electrophysiological properties of nigrothalamic neurons after 6-hydroxydopamine lesions in the rat. Neuroscience 38:447-456.

Magill PJ, Bolam JP, Bevan MD (2000) Relationship of activity in the subthalamic nucleus-globus pallidus network to cortical electroencephalogram. J Neurosci 20:820-833.

Magill PJ, Bolam JP, Bevan MD (2001) Dopamine regulates the impact of the cerebral cortex on the subthalamic nucleus-globus pallidus network. Neuroscience 106:313-330.

Majsak MJ, Kaminski T, Gentile AM, Flanagan JR (1998) The reaching movements of patients with Parkinson's disease under self-determined maximal speed and visually cued conditions. Brain 121 (Pt 4):755-766.

Mallet N, Ballion B, Le Moine C, Gonon F (2006) Cortical inputs and GABA interneurons imbalance projection neurons in the striatum of parkinsonian rats. J Neurosci 26:3875-3884.

Mallet N, Le Moine C, Charpier S, Gonon F (2005) Feedforward inhibition of projection neurons by fast-spiking GABA interneurons in the rat striatum *in vivo*. J Neurosci 25:3857-3869.

Marple SL (1999) Computing the discrete-time analytic signal via FFT. IEEE Trans Signal Processing 47:2600-2603.

Martin RF, Bowden DM (2000) Primate Brain Maps: Structure of the Macaque Brain, A Laboratory Guide with Original Brain Sections, Printed Atlas and Electronic Templates for Data and Schematics. Amsterdam: Elsevier.

Masdeu JC, Alampur U, Cavaliere R, Tavoulareas G (1994) Astasia and gait failure with damage of the pontomesencephalic locomotor region. Ann Neurol 35:619-621.

Matsumura M, Kojima J (2001) The role of the pedunculopontine tegmental nucleus in experimental parkinsonism in primates. Stereotact Funct Neurosurg 77:108-115.

Matsumura M, Nambu A, Yamaji Y, Watanabe K, Imai H, Inase M, Tokuno H, Takada M (2000) Organization of somatic motor inputs from the frontal lobe to the pedunculopontine tegmental nucleus in the macaque monkey. Neuroscience 98:97-110.

Mazzone P, Lozano A, Stanzione P, Galati S, Scarnati E, Peppe A, Stefani A (2005) Implantation of human pedunculopontine nucleus: a safe and clinically relevant target in Parkinson's disease. NeuroReport 16:1877-1881.

McAllister AK (2000) Cellular and molecular mechanisms of dendrite growth. Cereb Cortex 10:963-973.

Mena-Segovia J, Bolam JP, Magill PJ (2004) Pedunculopontine nucleus and basal ganglia: distant relatives or part of the same family? Trends Neurosci 27:585-588.

Mena-Segovia J, Ross HM, Magill PJ, Bolam JP (2005) The pedunculopontine nucleus: towards a functional integration with the basal ganglia. In: The Basal Ganglia VIII (Bolam JP, Ingham CA, Magill PJ, eds), pp 523-532. New York, NY, USA: Springer Science+Business Media, Inc.

Milner KL, Mogenson GJ (1988) Electrical and chemical activation of the mesencephalic and subthalamic locomotor regions in freely moving rats. Brain Res 452:273-285.

Mink JW (1996) The basal ganglia: focused selection and inhibition of competing motor programs. Prog Neurobiol 50:381-425.

Mitchell IJ, Clarke CE, Boyce S, Robertson RG, Peggs D, Sambrook MA, Crossman AR (1989) Neural mechanisms underlying parkinsonian symptoms based upon regional uptake of 2-deoxyglucose in monkeys exposed to 1-methyl-4-phenyl-1,2,3,6-tetrahydropyridine. Neuroscience 32:213-226.

Moran A, Bar-Gad I, Bergman H, Israel Z (2006) Real-time refinement of subthalamic nucleus targeting using Bayesian decision-making on the root mean square measure. Mov Disord 21:1425-1431.

Morris M, Iansek R, Matyas T, Summers J (1998) Abnormalities in the stride length-cadence relation in parkinsonian gait. Mov Disord 13:61-69.

Morris M, Iansek R, Smithson F, Huxham F (2000) Postural instability in Parkinson's disease: a comparison with and without a concurrent task. Gait Posture 12:205-216.

Morris ME, Huxham F, McGinley J, Dodd K, Iansek R (2001) The biomechanics and motor control of gait in Parkinson disease. Clin Biomech 16:459-470.

Morris ME, Iansek R, Matyas TA, Summers JJ (1994) The pathogenesis of gait hypokinesia in Parkinson's disease. Brain 117 (Pt 5):1169-1181.

Morris ME, Iansek R, Matyas TA, Summers JJ (1996) Stride length regulation in Parkinson's disease. Normalization strategies and underlying mechanisms. Brain 119 (Pt 2):551-568.

Munro-Davies LE, Winter J, Aziz TZ, Stein JF (1999) The role of the pedunculopontine region in basal-ganglia mechanisms of akinesia. Exp Brain Res 129:511-517.

Murer MG, Riquelme LA, Tseng KY, Pazo JH (1997) Substantia nigra pars reticulata single unit activity in normal and 6-OHDA-lesioned rats: effects of intrastriatal apomorphine and subthalamic lesions. Synapse 27:278-293.

Murer MG, Tseng KY, Kasanetz F, Belluscio M, Riquelme LA (2002) Brain oscillations, medium spiny neurons, and dopamine. Cell Mol Neurobiol 22:611-632.

Murray MP, Sepic SB, Gardner GM, Downs WJ (1978) Walking patterns of men with parkinsonism. Am J Phys Med 57:278-294.

Murthy VN, Fetz EE (1996a) Synchronization of neurons during local field potential oscillations in sensorimotor cortex of awake monkeys. J Neurophysiol 76:3968-3982.

Murthy VN, Fetz EE (1996b) Oscillatory activity in sensorimotor cortex of awake monkeys: synchronization of local field potentials and relation to behavior. J Neurophysiol 76:3949-3967.

Musizza B, Stefanovska A, McClintock PV, Palus M, Petrovcic J, Ribaric S, Bajrovic FF (2007) Interactions between cardiac, respiratory and EEG-delta oscillations in rats during anaesthesia. J Physiol 580:315-326.

Muthusamy KA, Aravamuthan BR, Kringelbach ML, Jenkinson N, Voets NL, Johansen-Berg H, Stein JF, Aziz TZ (2007) Connectivity of the human pedunculopontine nucleus region and diffusion tensor imaging in surgical targeting. J Neurosurg 107:814-820.

Nambu A, Takada M, Inase M, Tokuno H (1996) Dual somatotopical representations in the primate subthalamic nucleus: evidence for ordered but reversed body-map transformations from the primary motor cortex and the supplementary motor area. J Neurosci 16:2671-2683.

Nambu A, Tokuno H, Hamada I, Kita H, Imanishi M, Akazawa T, Ikeuchi Y, Hasegawa N (2000) Excitatory cortical inputs to pallidal neurons via the subthalamic nucleus in the monkey. J Neurophysiol 84:289-300.

Nambu A, Tokuno H, Inase M, Takada M (1997) Corticosubthalamic input zones from forelimb representations of the dorsal and ventral divisions of the premotor cortex in the macaque monkey: comparison with the input zones from the primary motor cortex and the supplementary motor area. Neurosci Lett 239:13-16.

Nambu A, Tokuno H, Takada M (2002) Functional significance of the cortico-subthalamo-pallidal 'hyperdirect' pathway. Neurosci Res 43:111-117.

Nandi D, Aziz TZ, Giladi N, Winter J, Stein JF (2002a) Reversal of akinesia in experimental parkinsonism by GABA antagonist microinjections in the pedunculopontine nucleus. Brain 125:2418-2430.

Nandi D, Liu X, Winter JL, Aziz TZ, Stein JF (2002b) Deep brain stimulation of the pedunculopontine region in the normal non-human primate. J Clin Neurosci 9:170-174.

Netter FH, Craig JA, Perkins J, Hansen JT, Koeppen BM (2002) Atlas of Neuroanatomy and Neurophysiology. Selections from the Netter Collection of Medical Illustrations. Teterboro, NJ: Icon Custom Communications.

Neuper C, Pfurtscheller G (2001) Event-related dynamics of cortical rhythms: frequency-specific features and functional correlates. Int J Psychophysiol 43:41-58.

Ni ZG, Bouali-Benazzouz R, Gao DM, Benabid AL, Benazzouz A (2001) Time-course of changes in firing rates and firing patterns of subthalamic nucleus neuronal activity after 6-OHDA-induced dopamine depletion in rats. Brain Res 899:142-147.

Niewenhuys R, Voogd J, van Huijzen C (1988) The human central nervous system. A synopsis and atlas. Berlin: Springer-Verlag.

Nisenbaum ES, Wilson CJ (1995) Potassium currents responsible for inward and outward rectification in rat neostriatal spiny projection neurons. J Neurosci 15:4449-4463.

Nisenbaum ES, Wilson CJ, Foehring RC, Surmeier DJ (1996) Isolation and characterization of a persistent potassium current in neostriatal neurons. J Neurophysiol 76:1180-1194.

Nisenbaum ES, Xu ZC, Wilson CJ (1994) Contribution of a slowly inactivating potassium current to the transition to firing of neostriatal spiny projection neurons. J Neurophysiol 71:1174-1189.

Obeso JA, Rodriguez-Oroz MC, Rodriguez M, Macias R, Alvarez L, Guridi J, Vitek J, DeLong MR (2000) Pathophysiologic basis of surgery for Parkinson's disease. Neurology 55:S7-12.

Olsson M, Nikkhah G, Bentlage C, Bjorklund A (1995) Forelimb akinesia in the rat Parkinson model: differential effects of dopamine agonists and nigral transplants as assessed by a new stepping test. J Neurosci 15:3863-3875.

Oppenheim AV, Schafer RW (1998) Discrete-Time Signal Processing. Upper Saddle River, NJ: Prentice-Hall.

Oster PJ, Stern JA (1980) Measurement of eye movement. In: Techniques in Psychology (Martin I, Venables PH, eds), pp 275-309. Chichester: John Wiley & Sons.

Pahapill PA, Lozano AM (2000) The pedunculopontine nucleus and Parkinson's disease. Brain 123 (Pt 9):1767-1783.

Pahwa R, Factor SA, Lyons KE, Ondo WG, Gronseth G, Bronte-Stewart H, Hallett M, Miyasaki J, Stevens J, Weiner WJ (2006) Practice Parameter: treatment of Parkinson disease with motor fluctuations and dyskinesia (an evidence-based review): report of the Quality Standards Subcommittee of the American Academy of Neurology. Neurology 66:983-995.

Palombo E, Porrino LJ, Bankiewicz KS, Crane AM, Kopin IJ, Sokoloff L (1988) Administration of MPTP acutely increases glucose utilization in the substantia nigra of primates. Brain Res 453:227-234.

Pan WX, Hyland BI (2005) Pedunculopontine tegmental nucleus controls conditioned responses of midbrain dopamine neurons in behaving rats. J Neurosci 25:4725-4732.

Papa SM, Boldry RC, Engber TM, Kask AM, Chase TN (1995) Reversal of levodopa-induced motor fluctuations in experimental parkinsonism by NMDA receptor blockade. Brain Res 701:13-18.

Papa SM, Chase TN (1996) Levodopa-induced dyskinesias improved by a glutamate antagonist in Parkinsonian monkeys. Ann Neurol 39:574-578.

Paradiso G, Saint-Cyr JA, Lozano AM, Lang AE, Chen R (2003) Involvement of the human subthalamic nucleus in movement preparation. Neurology 61:1538-1545.

Parent A, De Bellefeuille L (1982) Organization of efferent projections from the internal segment of globus pallidus in primate as revealed by fluorescence retrograde labeling method. Brain Res 245:201-213.

Parent A, Hazrati LN (1995b) Functional anatomy of the basal ganglia. II. The place of subthalamic nucleus and external pallidum in basal ganglia circuitry. Brain Res Rev 20:128-154.

Parent A, Hazrati LN (1995a) Functional anatomy of the basal ganglia. I. The cortico-basal ganglia-thalamo-cortical loop. Brain Res Rev 20:91-127.

Parent A, Levesque M, Parent M (2001) A re-evaluation of the current model of the basal ganglia. Parkinsonism Relat Disord 7:193-198.

Parker GJ, Alexander DC (2005) Probabilistic anatomical connectivity derived from the microscopic persistent angular structure of cerebral tissue. Philos Trans R Soc Lond B Biol Sci 360:893-902.

Parker GJ, Haroon HA, Wheeler-Kingshott CA (2003) A framework for a streamline-based probabilistic index of connectivity (PICo) using a structural interpretation of MRI diffusion measurements. J Magn Reson Imaging 18:242-254.

Parkinson J (2002) An essay on the shaking palsy. 1817. J Neuropsychiatry Clin Neurosci 14:223-236.

Parr-Brownlie LC, Poloskey SL, Flanagan KK, Eisenhofer G, Bergstrom DA, Walters JR (2007) Dopamine lesion-induced changes in subthalamic nucleus activity are not associated with

alterations in firing rate or pattern in layer V neurons of the anterior cingulate cortex in anesthetized rats. Eur J Neurosci 26:1925-1939.

Paxinos G, Watson C (1986) The Rat Brain in Stereotaxic Coordinates. San Diego, CA: Academic Press Inc.

Percheron G, Filion M (1991) Parallel processing in the basal ganglia: up to a point. Trends Neurosci 14:55-59.

Perier C, Agid Y, Hirsch EC, Feger J (2000) Ipsilateral and contralateral subthalamic activity after unilateral dopaminergic lesion. NeuroReport 11:3275-3278.

Perier C, Tremblay L, Feger J, Hirsch EC (2002) Behavioral consequences of bicuculline injection in the subthalamic nucleus and the zona incerta in rat. J Neurosci 22:8711-8719.

Perry J (1992) Gait Analysis: Normal and Pathological Function. New York, NY, USA: McGraw-Hill, Inc.

Pfefferbaum A, Sullivan EV, Adalsteinsson E, Garrick T, Harper C (2004) Postmortem MR imaging of formalin-fixed human brain. NeuroImage 21:1585-1595.

Pfurtscheller G (2001) Functional brain imaging based on ERD/ERS. Vision Res 41:1257-1260.

Pfurtscheller G, Lopes da Silva FH (1999) Event-related EEG/MEG synchronization and desynchronization: basic principles. Clin Neurophysiol 110:1842-1857.

Pfurtscheller G, Neuper C (1994) Event-related synchronization of mu rhythm in the EEG over the cortical hand area in man. Neurosci Lett 174:93-96.

Pfurtscheller G, Neuper C, Flotzinger D, Pregenzer M (1997) EEG-based discrimination between imagination of right and left hand movement. Electroencephalogr Clin Neurophysiol 103:642-651.

Pfurtscheller G, Neuper C, Krausz G (2000) Functional dissociation of lower and upper frequency mu rhythms in relation to voluntary limb movement. Clin Neurophysiol 111:1873-1879.

Plaha P, Gill SS (2005) Bilateral deep brain stimulation of the pedunculopontine nucleus for Parkinson's disease. NeuroReport 16:1883-1887.

Plotkin JL, Wu N, Chesselet MF, Levine MS (2005) Functional and molecular development of striatal fast-spiking GABAergic interneurons and their cortical inputs. Eur J Neurosci 22:1097-1108.

Priori A, Foffani G, Pesenti A, Bianchi A, Chiesa V, Baselli G, Caputo E, Tamma F, Rampini P, Egidi M, Locatelli M, Barbieri S, Scarlato G (2002) Movement-related modulation of neural activity in human basal ganglia and its L-DOPA dependency: recordings from deep brain stimulation electrodes in patients with Parkinson's disease. Neurol Sci 23 Suppl 2:S101-S102.

Priori A, Foffani G, Pesenti A, Tamma F, Bianchi AM, Pellegrini M, Locatelli M, Moxon KA, Villani RM (2004) Rhythm-specific pharmacological modulation of subthalamic activity in Parkinson's disease. Exp Neurol 189:369-379.

Rasch MJ, Gretton A, Murayama Y, Maass W, Logothetis NK (2008) Inferring spike trains from local field potentials. J Neurophysiol 99:1461-1476.

Raz A, Vaadia E, Bergman H (2000) Firing patterns and correlations of spontaneous discharge of pallidal neurons in the normal and the tremulous 1-methyl-4-phenyl-1,2,3,6-tetrahydropyridine vervet model of parkinsonism. J Neurosci 20:8559-8571.

Reese NB, Garcia-Rill E, Skinner RD (1995) The pedunculopontine nucleus--auditory input, arousal and pathophysiology. Prog Neurobiol 47:105-133.

Reiner A, Veenman CL, Medina L, Jiao Y, Del Mar N, Honig MG (2000) Pathway tracing using biotinylated dextran amines. J Neurosci Methods 103:23-37.

Rochester L, Nieuwboer A, Baker K, Hetherington V, Willems AM, Chavret F, Kwakkel G, Van Wegen E, Lim I, Jones D (2007) The attentional cost of external rhythmical cues and their impact on gait in Parkinson's disease: effect of cue modality and task complexity. J Neural Transm 114:1243-1248.

Rodriguez-Oroz MC, Obeso JA, Lang AE, Houeto JL, Pollak P, Rehncrona S, Kulisevsky J, Albanese A, Volkmann J, Hariz MI, Quinn NP, Speelman JD, Guridi J, Zamarbide I, Gironell A, Molet J, Pascual-Sedano B, Pidoux B, Bonnet AM, Agid Y, Xie J, Benabid AL, Lozano AM, Saint-Cyr J, Romito L, Contarino MF, Scerrati M, Fraix V, Van Blercom N (2005) Bilateral deep brain stimulation in Parkinson's disease: a multicentre study with 4 years follow-up. Brain 128:2240-2249.

Rohlfs A, Nikkhah G, Rosenthal C, Rundfeldt C, Brandis A, Samii M, Loscher W (1997) Hemispheric asymmetries in spontaneous firing characteristics of substantia nigra pars reticulata neurons following a unilateral 6-hydroxydopamine lesion of the rat nigrostriatal pathway. Brain Res 761:352-356.

Rolland AS, Herrero MT, Garcia-Martinez V, Ruberg M, Hirsch EC, Francois C (2007) Metabolic activity of cerebellar and basal ganglia-thalamic neurons is reduced in parkinsonism. Brain 130:265-275.

Romanelli P, Bronte-Stewart H, Heit G, Schaal DW, Esposito V (2004) The functional organization of the sensorimotor region of the subthalamic nucleus. Stereotact Funct Neurosurg 82:222-229.

Rosenberg JR, Amjad AM, Breeze P, Brillinger DR, Halliday DM (1989) The Fourier approach to the identification of functional coupling between neuronal spike trains. Prog Biophys Mol Biol 53:1-31.

Rouzaire-Dubois B, Scarnati E (1987) Pharmacological study of the cortical-induced excitation of subthalamic nucleus neurons in the rat: evidence for amino acids as putative neurotransmitters. Neuroscience 21:429-440.

Rudolph U, Antkowiak B (2004) Molecular and neuronal substrates for general anaesthetics. Nat Rev Neurosci 5:709-720.

Ruskin DN, Bergstrom DA, Kaneoke Y, Patel BN, Twery MJ, Walters JR (1999) Multisecond oscillations in firing rate in the basal ganglia: robust modulation by dopamine receptor activation and anesthesia. J Neurophysiol 81:2046-2055.

Ruskin DN, Bergstrom DA, Tierney PL, Walters JR (2003) Correlated multisecond oscillations in firing rate in the basal ganglia: modulation by dopamine and the subthalamic nucleus. Neuroscience 117:427-438.

Rye DB, Saper CB, Lee HJ, Wainer BH (1987) Pedunculopontine tegmental nucleus of the rat: cytoarchitecture, cytochemistry, and some extrapyramidal connections of the mesopontine tegmentum. J Comp Neurol 259:483-528.

Sadikot AF, Parent A, Francois C (1992a) Efferent connections of the centromedian and parafascicular thalamic nuclei in the squirrel monkey: a PHA-L study of subcortical projections. J Comp Neurol 315:137-159.

Sadikot AF, Parent A, Smith Y, Bolam JP (1992b) Efferent connections of the centromedian and parafascicular thalamic nuclei in the squirrel monkey: a light and electron microscopic

study of the thalamostriatal projection in relation to striatal heterogeneity. J Comp Neurol 320:228-242.

Saint-Cyr JA, Trepanier LL, Kumar R, Lozano AM, Lang AE (2000) Neuropsychological consequences of chronic bilateral stimulation of the subthalamic nucleus in Parkinson's disease. Brain 123 (Pt 10):2091-2108.

Saka E, Iadarola M, Fitzgerald DJ, Graybiel AM (2002) Local circuit neurons in the striatum regulate neural and behavioral responses to dopaminergic stimulation. Proc Natl Acad Sci U S A 99:9004-9009.

Sakai ST, Smith A (1992) Distribution of nigrothalamic projections in the dog. J Comp Neurol 318:83-92.

Salinas E, Sejnowski TJ (2001) Correlated neuronal activity and the flow of neural information. Nat Rev Neurosci 2:539-550.

Sanchez R, Leonard CS (1994) NMDA receptor-mediated synaptic input to nitric oxide synthase-containing neurons of the guinea pig mesopontine tegmentum *in vitro*. Neurosci Lett 179:141-144.

Sanderson P, Mavoungou R, Albe-Fessard D (1986) Changes in substantia nigra pars reticulata activity following lesions of the substantia nigra pars compacta. Neurosci Lett 67:25-30.

Sanes JN, Donoghue JP (1993) Oscillations in local field potentials of the primate motor cortex during voluntary movement. Proc Natl Acad Sci U S A 90:4470-4474.

Scarnati E, Campana E, Pacitti C (1984) Pedunculopontine-evoked excitation of substantia nigra neurons in the rat. Brain Res 304:351-361.

Scarnati E, Di Loreto S, Proia A, Gallie G (1988) The functional role of the pedunculopontine nucleus in the regulation of the electrical activity of entopeduncular neurons in the rat. Arch Ital Biol 126:145-163.

Scarnati E, Proia A, Campana E, Pacitti C (1986) A microiontophoretic study on the nature of the putative synaptic neurotransmitter involved in the pedunculopontine-substantia nigra pars compacta excitatory pathway of the rat. Exp Brain Res 62:470-478.

Sceniak MP, Maciver MB (2006) Cellular actions of urethane on rat visual cortical neurons *in vitro*. J Neurophysiol 95:3865-3874.

Schmiedt C, Meistrowitz A, Schwendemann G, Herrmann M, Basar-Eroglu C (2005) Theta and alpha oscillations reflect differences in memory strategy and visual discrimination performance in patients with Parkinson's disease. Neurosci Lett 388:138-143.

Schnitzler A, Gross J (2005) Normal and pathological oscillatory communication in the brain. Nat Rev Neurosci 6:285-296.

Schwartzman RJ, Alexander GM, Ferraro TN, Grothusen JR, Stahl SM (1988) Cerebral metabolism of parkinsonian primates 21 days after MPTP. Exp Neurol 102:307-313.

Semba K, Fibiger HC (1992) Afferent connections of the laterodorsal and the pedunculopontine tegmental nuclei in the rat: a retro- and antero-grade transport and immunohistochemical study. J Comp Neurol 323:387-410.

Semba K, Fibiger HC, Vincent SR (1987) Neurotransmitters in the mammalian striatum: neuronal circuits and heterogeneity. Can J Neurol Sci 14:386-394.

Sharott A, Magill PJ, Bolam JP, Brown P (2005a) Directional analysis of coherent oscillatory field potentials in the cerebral cortex and basal ganglia of the rat. J Physiol 562:951-963.

Sharott A, Magill PJ, Harnack D, Kupsch A, Meissner W, Brown P (2005b) Dopamine depletion increases the power and coherence of beta-oscillations in the cerebral cortex and subthalamic nucleus of the awake rat. Eur J Neurosci 21:1413-1422.

Sheridan MR, Flowers KA (1990) Movement variability and bradykinesia in Parkinson's disease. Brain 113 (Pt 4):1149-1161.

Sheridan MR, Flowers KA, Hurrell J (1987) Programming and execution of movement in Parkinson's disease. Brain 110 (Pt 5):1247-1271.

Shink E, Bevan MD, Bolam JP, Smith Y (1996) The subthalamic nucleus and the external pallidum: two tightly interconnected structures that control the output of the basal ganglia in the monkey. Neuroscience 73:335-357.

Shink E, Sidibe M, Smith Y (1997) Efferent connections of the internal globus pallidus in the squirrel monkey: II. Topography and synaptic organization of pallidal efferents to the pedunculopontine nucleus. J Comp Neurol 382:348-363.

Shumway-Cook A, Baldwin M, Polissar NL, Gruber W (1997) Predicting the probability for falls in community-dwelling older adults. Phys Ther 77:812-819.

Siegfried J, Lippitz B (1994) Chronic electrical stimulation of the VL-VPL complex and of the pallidum in the treatment of movement disorders: personal experience since 1982. Stereotact Funct Neurosurg 62:71-75.

Sillery E, Bittar RG, Robson MD, Behrens TEJ, Stein J, Aziz TZ, Johansen-Berg H (2005) Connectivity of the human periventricular-periaqueductal gray region. J Neurosurg 103:1030-1034.

Smith ID, Grace AA (1992) Role of the subthalamic nucleus in the regulation of nigral dopamine neuron activity. Synapse 12:287-303.

Smith SM, Jenkinson M, Woolrich MW, Beckmann CF, Behrens TEJ, Johansen-Berg H, Bannister PR, De Luca M, Drobnjak I, Flitney DE, Niazy RK, Saunders J, Vickers J, Zhang Y, De Stefano N, Brady JM, Matthews PM (2004) Advances in functional and structural MR image analysis and implementation as FSL. NeuroImage 23 Suppl 1:S208-S219.

Smith Y, Bennett BD, Bolam JP, Parent A, Sadikot AF (1994a) Synaptic relationships between dopaminergic afferents and cortical or thalamic input in the sensorimotor territory of the striatum in monkey. J Comp Neurol 344:1-19.

Smith Y, Hazrati LN, Parent A (1990) Efferent projections of the subthalamic nucleus in the squirrel monkey as studied by the PHA-L anterograde tracing method. J Comp Neurol 294:306-323.

Smith Y, Wichmann T, DeLong MR (1994b) Synaptic innervation of neurones in the internal pallidal segment by the subthalamic nucleus and the external pallidum in monkeys. J Comp Neurol 343:297-318.

Soares J, Kliem MA, Betarbet R, Greenamyre JT, Yamamoto B, Wichmann T (2004) Role of external pallidal segment in primate parkinsonism: comparison of the effects of 1-methyl-4-phenyl-1,2,3,6-tetrahydropyridine-induced parkinsonism and lesions of the external pallidal segment. J Neurosci 24:6417-6426.

Solis O, Limon DI, Flores-Hernandez J, Flores G (2007) Alterations in dendritic morphology of the prefrontal cortical and striatum neurons in the unilateral 6-OHDA-rat model of Parkinson's disease. Synapse 61:450-458.

Somogyi P, Bolam JP, Smith AD (1981) Monosynaptic cortical input and local axon collaterals of identified striatonigral neurons. A light and electron microscopic study using the Golgi-peroxidase transport-degeneration procedure. J Comp Neurol 195:567-584.

Spann BM, Grofova I (1989) Origin of ascending and spinal pathways from the nucleus tegmenti pedunculopontinus in the rat. J Comp Neurol 283:13-27.

Spann BM, Grofova I (1991) Nigropedunculopontine projection in the rat: an anterograde tracing study with phaseolus vulgaris-leucoagglutinin (PHA-L). J Comp Neurol 311:375-388.

Spann BM, Grofova I (1992) Cholinergic and non-cholinergic neurons in the rat pedunculopontine tegmental nucleus. Anat Embryol (Berl) 186:215-227.

Springer S, Giladi N, Peretz C, Yogev G, Simon ES, Hausdorff JM (2006) Dual-tasking effects on gait variability: the role of aging, falls, and executive function. Mov Disord 21:950-957.

Stefani A, Lozano AM, Peppe A, Stanzione P, Galati S, Tropepi D, Pierantozzi M, Brusa L, Scarnati E, Mazzone P (2007) Bilateral deep brain stimulation of the pedunculopontine and subthalamic nuclei in severe Parkinson's disease. Brain 130:1596-1607.

Steininger TL, Rye DB, Wainer BH (1992) Afferent projections to the cholinergic pedunculopontine tegmental nucleus and adjacent midbrain extrapyramidal area in the albino rat. I. Retrograde tracing studies. J Comp Neurol 321:515-543.

Steriade M, Nunez A, Amzica F (1993) A novel slow (< 1 Hz) oscillation of neocortical neurons *in vivo*: depolarizing and hyperpolarizing components. J Neurosci 13:3252-3265.

Stieltjes B, Kaufmann WE, van Zijl PCM, Fredericksen K, Pearlson GD, Solaiyappan M, Mori S (2001) Diffusion tensor imaging and axonal tracking in the human brainstem. NeuroImage 14:723-735.

Stolze H, Klebe S, Poepping M, Lorenz D, Herzog J, Hamel W, Schrader B, Raethjen J, Wenzelburger R, Mehdorn HM, Deuschl G, Krack P (2001) Effects of bilateral subthalamic nucleus stimulation on parkinsonian gait. Neurology 57:144-146.

Sugimoto T, Hattori T (1983) Confirmation of thalamosubthalamic projections by electron microscopic autoradiography. Brain Res 267:335-339.

Sugimoto T, Hattori T, Mizuno N, Itoh K, Sato M (1983) Direct projections from the centre median-parafascicular complex to the subthalamic nucleus in the cat and rat. J Comp Neurol 214:209-216.

Sun SW, Neil JJ, Song SK (2003) Relative indices of water diffusion anisotropy are equivalent in live and formalin-fixed mouse brains. Magn Reson Med 50:743-748.

Tai CH, Boraud T, Bezard E, Bioulac B, Gross C, Benazzouz A (2003) Electrophysiological and metabolic evidence that high-frequency stimulation of the subthalamic nucleus bridles neuronal activity in the subthalamic nucleus and the substantia nigra reticulata. FASEB J 17:1820-1830.

Takada M, Tokuno H, Ikai Y, Mizuno N (1994) Direct projections from the entopeduncular nucleus to the lower brainstem in the rat. J Comp Neurol 342:409-429.

Takakusaki K, Kitai ST (1997) Ionic mechanisms involved in the spontaneous firing of tegmental pedunculopontine nucleus neurons of the rat. Neuroscience 78:771-794.

Takeshita S, Kurisu K, Trop L, Arita K, Akimitsu T, Verhoeff NP (2005) Effect of subthalamic stimulation on mood state in Parkinson's disease: evaluation of previous facts and problems. Neurosurg Rev 28:179-186.

Taylor Tavares AL, Jefferis GS, Koop M, Hill BC, Hastie T, Heit G, Bronte-Stewart HM (2005) Quantitative measurements of alternating finger tapping in Parkinson's disease correlate with UPDRS motor disability and reveal the improvement in fine motor control from medication and deep brain stimulation. Mov Disord 20:1286-1298.

Temel Y, Blokland A, Steinbusch HW, Visser-Vandewalle V (2005) The functional role of the subthalamic nucleus in cognitive and limbic circuits. Prog Neurobiol 76:393-413.

Temel Y, Kessels A, Tan S, Topdag A, Boon P, Visser-Vandewalle V (2006) Behavioural changes after bilateral subthalamic stimulation in advanced Parkinson disease: a systematic review. Parkinsonism Relat Disord 12:265-272.

Tepper JM, Koos T, Wilson CJ (2004) GABAergic microcircuits in the neostriatum. Trends Neurosci 27:662-669.

Thaut MH, McIntosh GC, Rice RR, Miller RA, Rathbun J, Brault JM (1996) Rhythmic auditory stimulation in gait training for Parkinson's disease patients. Mov Disord 11:193-200.

Tisch S, Silberstein P, Limousin-Dowsey P, Jahanshahi M (2004) The basal ganglia: anatomy, physiology, and pharmacology. Psychiatr Clin North Am 27:757-799.

Trottenberg T, Fogelson N, Kuhn AA, Kivi A, Kupsch A, Schneider GH, Brown P (2006) Subthalamic gamma activity in patients with Parkinson's disease. Exp Neurol 200:56-65.

Tseng KY, Kasanetz F, Kargieman L, Pazo JH, Murer MG, Riquelme LA (2001a) Subthalamic nucleus lesions reduce low frequency oscillatory firing of substantia nigra pars reticulata neurons in a rat model of Parkinson's disease. Brain Res 904:93-103.

Tseng KY, Kasanetz F, Kargieman L, Riquelme LA, Murer MG (2001b) Cortical slow oscillatory activity is reflected in the membrane potential and spike trains of striatal neurons in rats with chronic nigrostriatal lesions. J Neurosci 21:6430-6439.

Tseng KY, Riquelme LA, Belforte JE, Pazo JH, Murer MG (2000) Substantia nigra pars reticulata units in 6-hydroxydopamine-lesioned rats: responses to striatal D2 dopamine receptor stimulation and subthalamic lesions. Eur J Neurosci 12:247-256.

Turner MS, Lavin A, Grace AA, Napier TC (2001) Regulation of limbic information outflow by the subthalamic nucleus: excitatory amino acid projections to the ventral pallidum. J Neurosci 21:2820-2832.

Van der Kooy D, Carter DA (1981) The organization of the efferent projections and striatal afferents of the entopeduncular nucleus and adjacent areas in the rat. Brain Res 211:15-36.

Vercelli A, Repici M, Garbossa D, Grimaldi A (2000) Recent techniques for tracing pathways in the central nervous system of developing and adult mammals. Brain Res Bull 51:11-28.

Verhagen Metman L, Del Dotto P, van den Munckhof P, Fang J, Mouradian MM, Chase TN (1998) Amantadine as treatment for dyskinesias and motor fluctuations in Parkinson's disease. Neurology 50:1323-1326.

Vila M, Perier C, Feger J, Yelnik J, Faucheux B, Ruberg M, Raisman-Vozari R, Agid Y, Hirsch EC (2000) Evolution of changes in neuronal activity in the subthalamic nucleus of rats with unilateral lesion of the substantia nigra assessed by metabolic and electrophysiological measurements. Eur J Neurosci 12:337-344.

Voges J, Volkmann J, Allert N, Lehrke R, Koulousakis A, Freund HJ, Sturm V (2002) Bilateral high-frequency stimulation in the subthalamic nucleus for the treatment of Parkinson disease: correlation of therapeutic effect with anatomical electrode position. J Neurosurg 96:269-279.

Volkmann J (2004) Deep brain stimulation for the treatment of Parkinson's disease. J Clin Neurophysiol 21:6-17.

Walters JR, Hu D, Itoga CA, Parr-Brownlie LC, Bergstrom DA (2007) Phase relationships support a role for coordinated activity in the indirect pathway in organizing slow oscillations in basal ganglia output after loss of dopamine. Neuroscience 144:762-776.

Walters JR, Hu D, Itoga CA, Parr-Brownlie LC, Bergstrom DA (2005) Do local field potentials reflect synchronized spiking activity of neuronal populations in the basal ganglia? Studies in a rodent model of Parkinson's disease. In: The Basal Ganglia VIII (Bolam JP, Ingham CA, Magill PJ, eds), pp 37-46. New York, NY, USA: Springer Science+Business Media, INc.

Wheaton LA, Nolte G, Bohlhalter S, Fridman E, Hallett M (2005) Synchronization of parietal and premotor areas during preparation and execution of praxis hand movements. Clin Neurophysiol 116:1382-1390.

White LE, Hodges HD, Carnes KM, Price JL, Dubinsky JM (1994) Colocalization of excitatory and inhibitory neurotransmitter markers in striatal projection neurons in the rat. J Comp Neurol 339:328-340.

Whone AL, Moore RY, Piccini PP, Brooks DJ (2003) Plasticity of the nigropallidal pathway in Parkinson's disease. Ann Neurol 53:206-213.

Wichmann T, Bergman H, DeLong MR (1994a) The primate subthalamic nucleus. I. Functional properties in intact animals. J Neurophysiol 72:494-506.

Wichmann T, Bergman H, DeLong MR (1994b) The primate subthalamic nucleus. III. Changes in motor behavior and neuronal activity in the internal pallidum induced by subthalamic inactivation in the MPTP model of parkinsonism. J Neurophysiol 72:521-530.

Wichmann T, Bergman H, Starr PA, Subramanian T, Watts RL, DeLong MR (1999) Comparison of MPTP-induced changes in spontaneous neuronal discharge in the internal pallidal segment and in the substantia nigra pars reticulata in primates. Exp Brain Res 125:397-409.

Wichmann T, DeLong MR (2003) Functional neuroanatomy of the basal ganglia in Parkinson's disease. Adv Neurol 91:9-18.

Wichmann T, DeLong MR (2006) Deep brain stimulation for neurologic and neuropsychiatric disorders. Neuron 52:197-204.

Wichmann T, Kliem MA, Soares J (2002) Slow oscillatory discharge in the primate basal ganglia. J Neurophysiol 87:1145-1148.

Williams D, Kuhn A, Kupsch A, Tijssen M, van Bruggen G, Speelman H, Hotton G, Yarrow K, Brown P (2003) Behavioural cues are associated with modulations of synchronous oscillations in the human subthalamic nucleus. Brain 126:1975-1985.

Williams D, Kuhn A, Kupsch A, Tijssen M, van Bruggen G, Speelman H, Hotton G, Loukas C, Brown P (2005) The relationship between oscillatory activity and motor reaction time in the parkinsonian subthalamic nucleus. Eur J Neurosci 21:249-258.

Williams D, Tijssen M, van Bruggen G, Bosch A, Insola A, Di Lazarro V, Mazzone P, Oliviero A, Quartarone A, Speelman H, Brown P (2002) Dopamine-dependent changes in the functional connectivity between basal ganglia and cerebral cortex in humans. Brain 125:1558-1569.

Winn P (2006) How best to consider the structure and function of the pedunculopontine tegmental nucleus: evidence from animal studies. J Neurol Sci 248:234-250.

Wolff K, Winstock AR (2006) Ketamine : from medicine to misuse. CNS Drugs 20:199-218.

Woolf NJ, Butcher LL (1986) Cholinergic systems in the rat brain: III. Projections from the pontomesencephalic tegmentum to the thalamus, tectum, basal ganglia, and basal forebrain. Brain Res Bull 16:603-637.

Woollacott M, Shumway-Cook A (2002) Attention and the control of posture and gait: a review of an emerging area of research. Gait Posture 16:1-14.

Yelnik J (2007) PPN or PPD, what is the target for deep brain stimulation in Parkinson's disease? Brain 130:e79.

Yogev G, Giladi N, Peretz C, Springer S, Simon ES, Hausdorff JM (2005) Dual tasking, gait rhythmicity, and Parkinson's disease: which aspects of gait are attention demanding? Eur J Neurosci 22:1248-1256.

Yokoyama T, Sugiyama K, Nishizawa S, Yokota N, Ohta S, Uemura K (1999) Subthalamic nucleus stimulation for gait disturbance in Parkinson's disease. Neurosurgery 45:41-47.

Yong-Hing CJ, Obenaus A, Stryker R, Tong K, Sarty GE (2005) Magnetic resonance imaging and mathematical modeling of progressive formalin fixation of the human brain. Magn Reson Med 54:324-332.

Young LR, Sheena D (1975) Methods & designs: survey of eye movement recording methods. Behav Res Methods Instrum 7:397-429.

Zaidel A, Moran A, Marjan G, Bergman H, Israel Z (2008) Prior pallidotomy reduces and modifies neuronal activity in the subthalamic nucleus of Parkinson's disease patients. Eur J Neurosci 27:483-491.

Zold CL, Ballion B, Riquelme LA, Gonon F, Murer MG (2007) Nigrostriatal lesion induces D2-modulated phase-locked activity in the basal ganglia of rats. Eur J Neurosci 25:2131-2144.

Zrinzo L, Zrinzo LV, Hariz M (2007b) The pedunculopontine and peripeduncular nuclei: a tale of two structures. Brain 130:e73.

Zrinzo L, Zrinzo LV, Hariz M (2007a) The peripeduncular nucleus: a novel target for deep brain stimulation? NeuroReport 18:1301-1302.